Metamorphic evolution and its implication for tectonic process in the central Sør Rondane Mountains, East Antarctica

Tatsuro Adachi

A thesis submitted to the Graduate University for Advanced Studies

(Department of Polar Science, School of Multidisciplinary Sciences)

For the degree of Doctor of Philosophy (Science)

2010

Contents

Abstract

The Sør Rondane Mountains in the eastern Dronning Maud Land, East Antarctica is inferred to be situated within an orogen which is a collision boundary of Gondwana amalgamation at late Neoproterozoic to early Cambrian. The mountains have been recognized as the key area for the reconstruction of Gondwana super-continent and geological activity during the formation of super-continent. In this context, the author has carried out petrological and geochronological studies of the metamorphic rocks in the central Sør Rondane Mountains.

Metamorphic rocks in the central part of Sør Rondane Mountains are classified into at least three types based on petrological characteristics as follows: (1) Metamorphic rocks mainly from Austkampane area preserve ca. 800 °C and 0.4-0.5 GPa peak metamorphic condition followed by the decompression and subsequent isobaric cooling accompanying with hydration (A-type). (2) Rocks from the Brattnipene area preserve peak metamorphic temperature of ca. 800 °C similar-T with Austkampane but relatively higher pressure at 0.7-0.8 GPa. They also experienced compression after peak metamorphism and subsequent isobaric cooling with hydration (B-type). (3) Rocks in Lunckeryggen and couple of other areas preserve signatures of

prograde metamorphism and amphibolite-facies peak metamorphic condition (L-type).

Rutile exsolution in quartz was found from the retrograde hydrated gneisses widespread in central Sør Rondane Mountains. Recovered pre-exsolution Ti concentration in quartz combined with Ti-in-quartz thermometer indicates that >700-800 °C peak metamorphic conditions are pervasive in the NE terrane (Austkampane, Brattnipene and Menipa areas). On the other hand, <600 °C of the metamorphic condition is recognized in the SW terrane (mainly Lunckeryggen area).

U-Pb zircon SHRIMP and U-Th-Pb monazite EPMA datings suggest that ca. 640-600 Ma event is the timing of peak granulite-facies metamorphism for A- and B-type rocks and that ca. 570-550 Ma event is also detected which being interpreted as timing of hydration. Contact metamorphism locally recognized in A-type rocks occurs at ca. 500 Ma. Timing of amphibolite-facies metamorphism of L-type rocks is ca. 550 Ma. L-type rocks lack ca. 640-600 Ma events, indicating that A- and B-type rocks and L-type rocks share the geological event after 550 Ma.

L-type unit is structurally apparently overlain by B-type unit. The

boundary between B-type unit and L-type unit seems nearly-horizontal and parallel to the foliation observed in both units. This implies that nappe-like structure, A- and B-type units thrust up onto L-type unit, is essentially prevailing in the central Sør Rondane Mountains. Such nappe-like structure has been also proposed for EAAO related areas including Mozambique, central Dronning Maud Land and Sri Lanka, and nappe structure should be dominant tectonics in the EAAO region.

Chapter 1 Introduction

1.1. Significance of the Sør Rondane Mountains in the framework of the Gondwana reconstruction

The concept of “Gondwana” super-continent is proposed that it existed in the Paleozoic and broke apart in the Late Mesozoic as South America, Africa, India, Australia and East Antarctica on the bases of the observations in the present-day distribution of Permo-Carboniferous glacial sediments, plant fossils and other geological features (e.g. Wegener, 1966). Evidence for the birth of Gondwana and its nature of geological events during the formation of the super-continent have been provided by basement geology in the Gondwana fragments.

According to compilation of geochronological studies, basement rocks can be divided into the cratons of the Archean and Paleoproterozoic ages and mobile belts which were formed after 1600 Ma and united the cratons together (Fitzsimons, 2000). These mobile belts indicate three broad tectonic events; Grenville-age mobile belts (1400-900 Ma), Pan-African mobile belts (700-500 Ma) and Early Paleozoic tectonism (550-450 Ma) (e.g. Fitzsimons, 2000).

Several authors suggested a two-stage assembly of Gondwana based on paleomagnetic data and basement geology (e.g. McWilliams, 1981; Rogers

et al., 1995). In West Gondwana which is composed of South America and Africa, Pan-African mobile belts are abundant, whereas East Gondwana, which is composed of India, Australia and East Antarctica, appears to be dominated by Grenville-age mobile belts. Such difference of the age population of mobile belts have been interpreted as East Gondwana assembled at 1400-900 Ma and then combined with the West Gondwana at 700-500 Ma. The East African Orogen is generally assumed to be a collision boundary between East and West Gondwana (Stern, 1994).

In recent studies, two models for the assembly of East Gondwana have been proposed. Jacobs and Thomas (2002, 2004) considered that Pan-African event develops as a broad linear orogen from East Africa to southern East Antarctica (East Africa Antarctic Orogen (EAAO). On the other hand, Meert (2003) emphasized that two overlapping orogens, older East Africa Orogen and younger Kuunga Orogen, are recognized during the assembly of east Gondwana. These two models are based on two stages of Pan-African orogenesis, at 750-620 Ma and 570-530 Ma (Meert, 2003; Jacobs et al., 2003). However it is still unclear which model is more realistic.

Around East Antarctica, most of the high-grade metamorphism and

plutonic activity had been considered to occur 1400-900 Ma as the results of dating with whole rock Rb-Sr technique (Tingey, 1991 and references therein) and these ages were used as evidence for a Grenville-age mobile belt surrounding the coast of East Antarctica, so-called the Circum-East Antarctic mobile belt (Yoshida, 1995). Signature of Early Paleozoic tectonism had been limited mainly in the Ross orogen, situated in present-day Transantarctic Mountains (e.g. Adams, 1987; Tingey, 1991). Hoffman (1991) interpreted these early geochronological works as that the fragments of East Gondwana amalgamated along the Circum-East Antarctic mobile belt at 1400-900 Ma and then remained as a coherent block until the Gondwana breakup. However Shiraishi et al. (1994) reported 500-600 Ma of zircon U-Pb ages from East Antarctica. This shows, for the first time, the existence of a Cambrian orogenic belt within the East Antarctic Shield. After that, Fitzsimons (2000) emphasized that there are two Pan-African age mobile belts, Lützow-Holm Belt and Prydz Belt, cutting across the East Antarctica based on the accumulation of zircon U-Pb age data. When the East Antarctica was finally united is still in argument. Thus, although widespread geochronological works have been performed on the Dronning Maud Land, the timing of magmatic and metamorphic events have not

been sufficiently correlated with the formation of Gondwana.

The Sør Rondane Mountains, which is located in the eastern Dronning Maud Land, have been considered to be situated in the central part of the inferred orogens, therefore the mountains have been recognized as the key to clarify the reconstruction of Gondwana super-continent in the context described above. Investigation of tectonic evolution of the Sør Rondane Mountains should play an important role to build up precise tectonic process during formation of the super-continent.

1.2. Previous works on the Sør Rondane Mountains

The Sør Rondane Mountains were one of the large exposures in the Dronning Maud Land, East Antarctica (Fig. 1.2). The Mountains were found from the air in 1937 by Norwegian expedition, and then U.S. Navy Antarctic Expedition made a topographical map of 1:250,000 scale during 1946-1947 that was published by the Norwegian Polar Institute in 1957. Pioneer work for geological, glaciological and geomorphological studies was carried out by Belgian geological reconnaissance parties during 1958 to 1960 (Michot, 1961, 1962; Van Autenboer, 1964; Picciotto et al., 1964). On the basis of these investigations, a geological map was published in 1:500,000 scale by Van

Autenboer (1969).

On Japanese activity, the 25th Japanese Antarctic Research Expedition (JARE) started geological survey in the central part of the Sør Rondane Mountains in 1984 (Member of the Sør Rondane Reconnaissance Party, 1985). Field survey in the Sør Rondane Mountains was carried out by following seven expeditions (JARE-26 (1984-1985) to -32 (1990-1991)) covering the whole region of the mountains using Asuka Station. The results of these field investigations have already been published by National Institute of Polar Research, Japan, as the Antarctic Geological Map Series of Balchenfljella (Sheet 31: Asami et al., 1991), Widrøefjellet (Sheet 32: Shiraishi et al., 1992a), Bergersenfjella (Sheet 33: Ishizuka et al., 1993) and Brattnipene (Sheet 34: Osanai et al., 1996).

The Sør Rondane Mountains are composed of medium to high-grade metamorphic rocks with various intrusions of plutonic rocks and minor mafic dykes (e.g. Shiraishi et al, 1991, 1997a). The mountains are divided into Northeastern (NE) and Southwestern (SW) terranes by an inferred tectonic line, the Sør Rondane Suture (SRS: Osanai et al., 1992). The NE terrane is

characterized by the occurrence of granulite-facies metamorphic rocks, whereas the SW terrane is composed of amphibolite-facies and lower-grade metamorphic rocks. Syn- to post- orogenic plutonic rocks and dykes intrude metamorphic rocks in both terranes.

Metamorphic conditions of the NE terrane have been estimated (Shiraishi and Kojima 1987; Asami and Shiraishi, 1987; Grew et al., 1989; Ishizuka et al., 1995, Asami et al, 1990; 1992; 2007). The NE terrane was metamorphosed under granulite-facies conditions (800 °C and 0.7-0.8 GPa), with subsequent amphibolite-facies retrogression (530-580 °C and 0.55 GPa) within the kyanite stability field. In contrast, such high-T metamorphism has not been recognized in the SW terrane. Peak metamorphic conditions are estimated as up to amphibolite-facies conditions and followed by pervasive retrograde metamorphism accompanying mylonitization (Shiraishi and Kojima, 1987).

In 1960s, many Rb-Sr and K-Ar geochronological studies in both terranes have yielded ages younger than 500 Ma which is attributed to late thermal event associated with plutonic activity in the early Paleozoic (Picciotto et al., 1964, Takahashi et al., 1990, Grew et al., 1992, Shiraishi and Kagami, 1992, Shiraishi et al., 1997a). Shiraishi and Kagami (1992) reported older mineral and

whole-rock isochron ages. They considered the timing of granulite-facies metamorphism in the NE terrane to be *ca.*1000 Ma, on the basis of Sm-Nd and Rb-Sr whole-rock isochron ages from orthogneisses. In contrast, internal mineral isochrons yielded 560-620 Ma ages for Rb-Sr and Sm-Nd systems, which are attributed to a series of thermal events accompanying granitic intrusions. Asami et al. (1996, 1997, 2005) proposed different interpretation on the basis of dating of monazite and zircon with chemical Th-U-total Pb isochron method (CHIME) using electron micro probe analyzer (EPMA). Monazites in granulite facies metamorphic rocks yielded the age ranging from 550 to 510 Ma, and 1100-1200 Ma ages were obtained from the cores of zircons. The authors concluded that granulite-facies metamorphism and high-strain deformation took place at 540-530 Ma and 1100-1200 Ma ages should correspond to the formation of protoliths. Recently, Shiraishi et al. (2008) reported SHRIMP zircon U-Pb ages and compilation of Nd model ages for new and published data from the widespread area in the Sør Rondane Mountains. According to them, ca. 1130 Ma, 1000 Ma and 800 Ma magmatic activities are recognized as the ages obtained from the cores of zircon in both terranes. Abundant and widespread metamorphic growth at ca. 600 Ma was recognized in the NE terrane, whereas

in the SW terrane, ca. 600 Ma is lacking and ca. 550 Ma is common. Based on these age distributions, they concluded that 1000-1200 Ma and 700-800 Ma of magmatism and/or sedimentaion were recognized and the main metamorphism of the NE and the SW terranes should be *ca.*600-650Ma and ca. 550Ma, respectively.

1.3. Summary of the previous studies and targets of this study

Summary of previous works and unresolved scientific targets in the Sør Rondane Mountains are described as follows.

• Metamorphic evolution was proposed by Asami et al. (1992) as peak granulite-facies metamorphism (800 °C, 0.7-0.8 GPa) accompanied by decompression and later stage retrogression (530-580 °C and 0.55 GPa) and local heating associated with granite intrusion (Fig. 1.3).

However proposed P-T path is organized on the basis of the idea of that whole area of the Sør Rondane Mountains should be subjected to several thermal events as a single geological unit. However it is hard to confirm because of lack of the lithological continuity due to surface denudation by glacier. Therefore investigation for each area should be essential. Recent studies

indicate that different P-T paths within the NE terrane (Baba et al., 2008; Osanai et al., 2008; Hokada et al., 2008), which support the requirement of area-specific investigation. In Chapter 3, re-investigation of the difference of P-T paths for the area-scale is discussed.

• The mountains are divided into two terranes; the NE terrane where granulite-facies metamorphic rocks are distributed and the SW terrane which is composed up to amphibolite-facies rocks (e.g. Osanai et al., 1992).

Metamorphic rocks in the Sør Rondane Mountains are widely subjected to retrograde hydration, resulting in that initial metamorphic condition is modified to several extend. This overprinting makes it difficult to estimation the primary metamorphic condition in the Sør Rondane Mountains. Rutile exsolution is found in the retrograde rocks widespread throughout the NE terrane. T dependence of Ti solubility in quartz has been experimentally confirmed (Wark and Watson, 2006; Kawasaki and Osanai, 2008), indicating that the rutile exsolution in quartz should be records of prior high-grade metamorphic event. In the Chapter 4, assessment and application of Ti in quartz as the method for estimation of the metamorphic process of the retrogressed rocks is discussed.

• The ages obtained from the metamorphic rocks are clustered at ~1000 Ma, 700-800 Ma, 650-600 Ma and 570-550 Ma with several methods.

To build up precise tectonic process, comparison of the isochronal phenomena within the mountains is essential. Previous studies have clarified to cluster the ages at ~1000 Ma, 700-800 Ma, 650-600 Ma and 570-550 Ma. However interpretation of each age is still in argument (summarized in Table 1.1). The controversy suggests that the correspondence the ages to P-T conditions is required, i.e., age interpretation based on the precise petrography is necessary. In Chapter 5, dating with SHIRIMP zircon U-Pb method and monazite EPMA U-Th-total Pb method is performed on the rocks of which P-T processes are constrained in Chapters 3 and 4 and the age interpretations are discussed.

On the basis of the results of the preceding chapters and previous works, the possible tectonic process of the Sør Rondane Mountains is proposed in conclusion (Chapter 6).

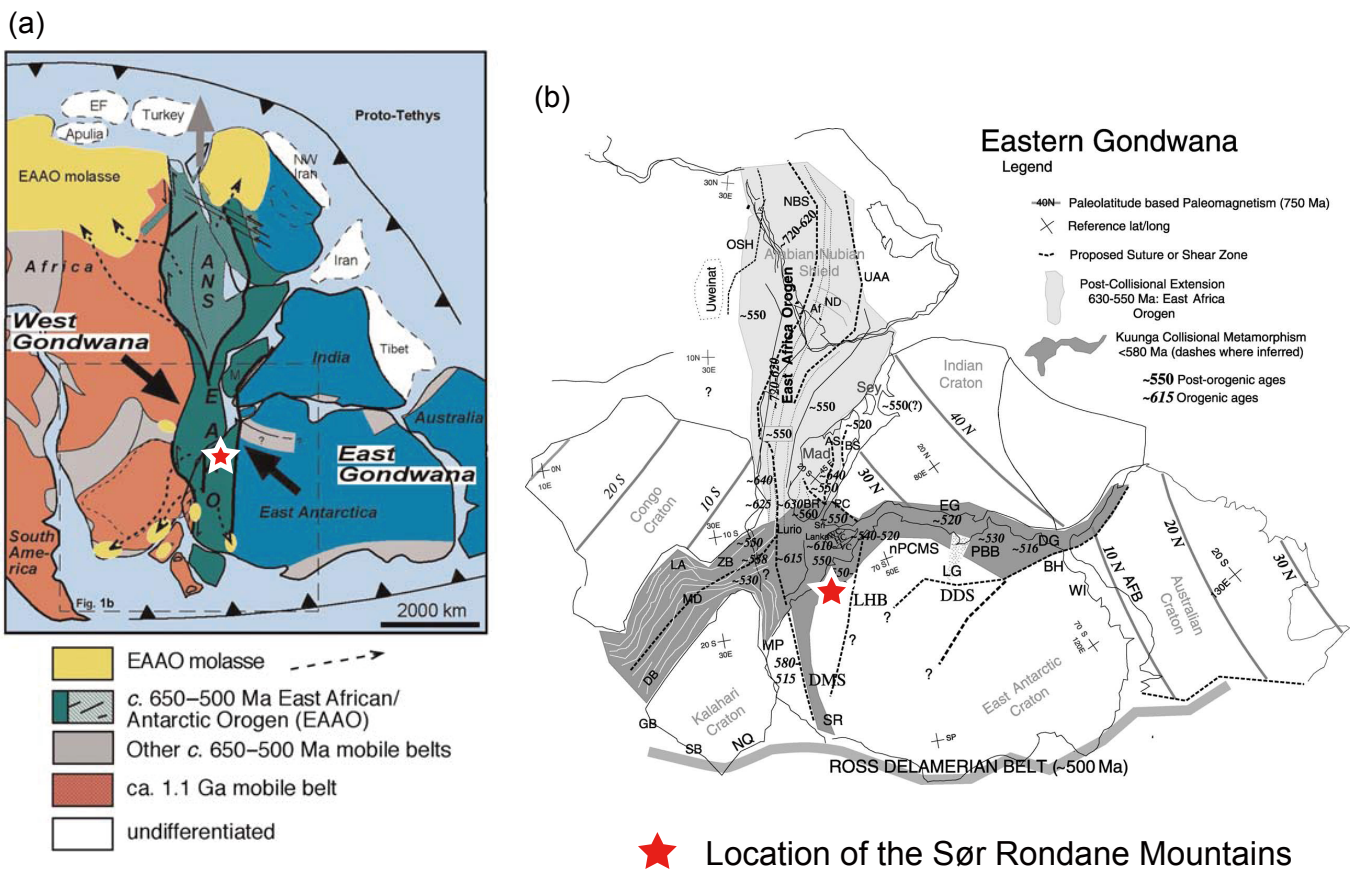

Fig. 1.1 Location of the Sør Rondane Mountains in the reconstructed Gondwana Super Continent. (a) Geological settings of the East African-Antarctic Orogen (EAAO). (modified after Jacobs & Thomas (2004)) (b) Geological relation of the East Africa Orogen and the Kuunga Orogen. (modified after Meert (2003)). Stars mark the location of the Sør Rondane Mountains.

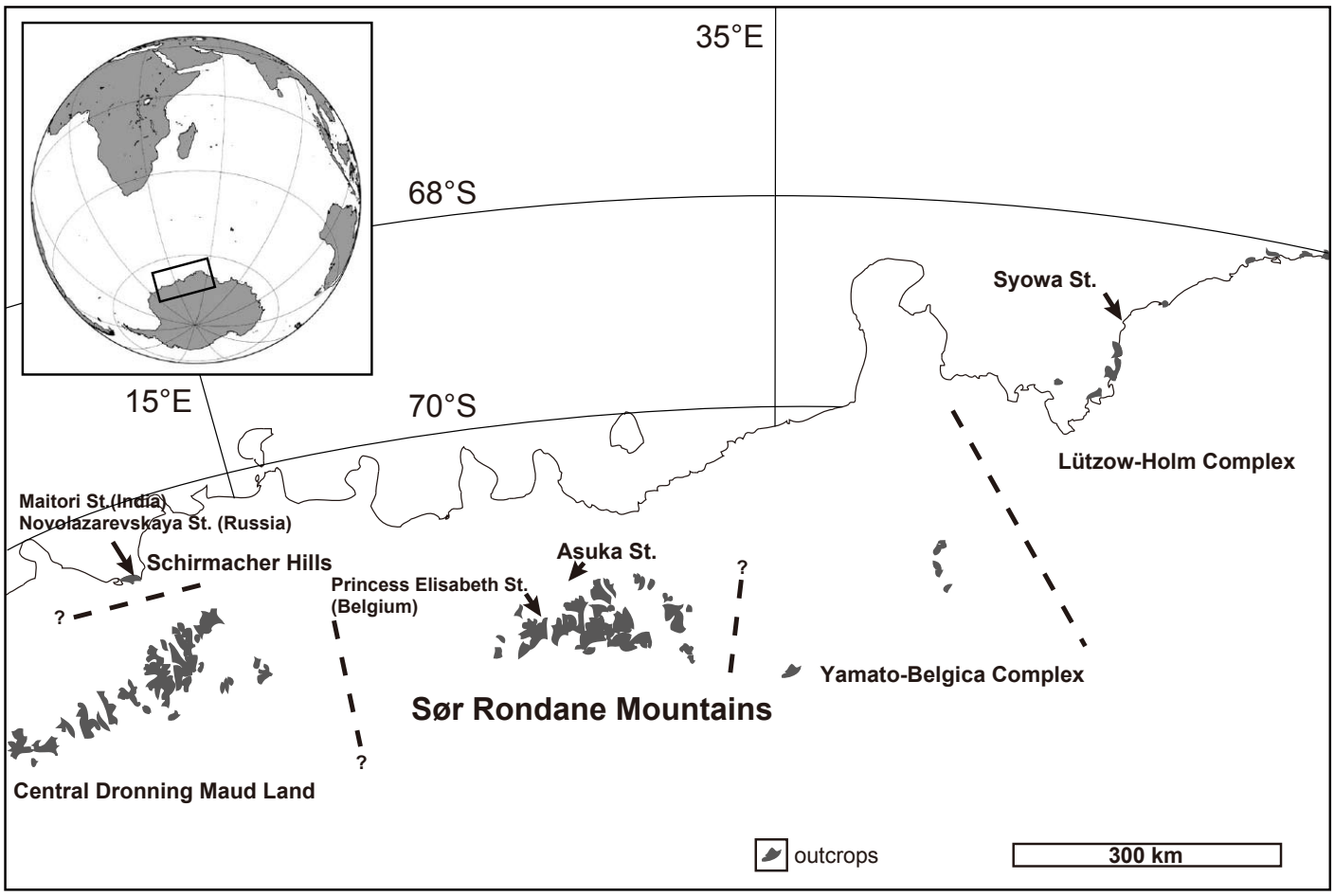

Fig. 1.2 Map of geological terranes in the Dronning Maud Land, East Antarctica.

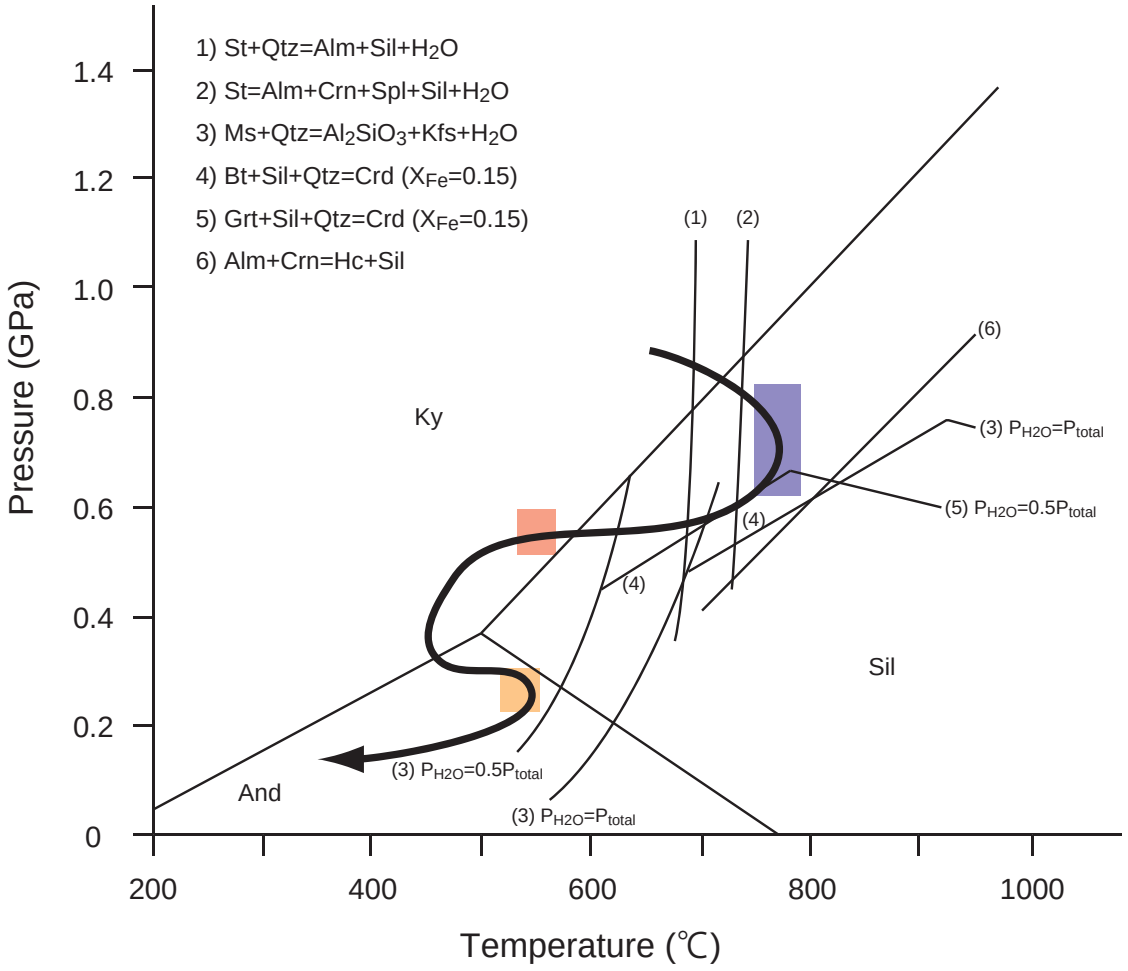

Fig. 1.3. P-T path of the Sør Rondane Mountains proposed by Asami et al. (1992).
P-T condition indicated by blue, red and orange rectangles were estimated with the rocks from Balchenfjella, Brattnipene and Austkampane areas, respectively.

Table 1.1. Comparison of proposed geochronological interpretation on the Sør Rondane Mountains.

Asami et al. (2005)	Shiraishi et al. (2008)	
	SW	NE
	515 metamorphism (Ttn), post-orogenic granite	
~530 Peak granulite facies metamorphism		
	ca.560 Metamorphism, Magmatism	
		ca.600-650 Peak granulite facies metamorphism
	ca.650 Magmatism	
		ca.800 Magmatism (det), Metamorphism?(det)
	ca.1000 Magmatism (prot+det)	
ca.1100-1200 Source rock generation of the protoliths of metamorphic rocks	**ca. 1130** Magmatism	
		ca. 1200, 3260 (det)
	0.9-1.0, 1.6 Ga Crustal inheritance(T_{DM})	

Bold numbers are SHRIMP zircon/titanite (Ttn) ages (inh: inherited, prot: protolith, det: detrital), Italic numbers are CHIME monazite/zircon ages, TDM: Depleted mantle model age (Ga)

Chapter 2 Geology of the Sør Rondane Mountains

2.1. General geology

The Sør Rondane Mountains is located between 22° to 28° E and 71.5° to 72.5° S in East Antarctica. The Sør Rondane Mountains comprise medium to high-grade metamorphic rocks with various intrusions of plutonic rocks and minor mafic dykes (e.g. Shiraishi et al, 1991, 1997). The mountains are considered to be divided into the NE and the SW terranes by an inferred tectonic line so-called the Sør Rondane Suture (Osanai et al., 1992) (Fig. 2.1). The NE terrane is considered to be mainly composed of granulite-facies metamorphic rocks of pelitic, psammitic and intermediate compositions, whereas the SW terrane is composed of amphibolite-facies and lower-grade metamorphic rocks of mainly intermediate composition, including large volume of meta-tonalite. Plutonic rocks and dykes of various sizes intrude metamorphic lithologies in both terranes, and composed of syn- to post-orogenic granite, syenite, diorite and alkaline mafic dykes.

Basic and intermediate igneous rocks in the central part of the mountains indicate that magmatic protoliths have geochemical affinities with oceanic, island arc, accretionary complex and continental margin arc settings in modern plate tectonics (Osanai et al., 1992). Ishizuka et al. (1996) reported that

ultramafic metamorphic rocks in the NE terrane suggested a MORB-like origin. Meta-tonalite from the SW terrane is characterized by relatively high Na_2O/K_2O, K/Rb. Sr/Y and $(La/Yb)_N$, low CaO/Na_2O and low initial Sr isotopic ratios, being attributed to originate from a hot subducting plate (Ikeda and Shiraishi, 1998).

Metamorphic P-T conditions of gneisses from the NE terrane have been estimated by several authors (Shiraishi and Kojima 1987; Asami and Shiraishi, 1987; Grew et al., 1989; Ishizuka et al., 1995, Asami et al, 1990; 1992; 2007). The NE terrane was metamorphosed under granulite-facies conditions (800°C and 0.7-0.8 GPa), with subsequent amphibolite-facies retrogression (530-580°C and 0.55 GPa) within the kyanite stability field. Subsequently, the rocks were recrystallized at lower pressures, as indicated by the presence of andalusite in several localities (Asami and Shiraishi, 1987; Asami et al., 1992, 1993). Recently, Asami et al. (2007) reported sapphirine+kyanite and spinel+kyanite composite inclusions in garnet from Balchenfjella. These inclusions indicate the peak conditions of granulite-facies metamorphism as 860-895 °C and 1.2 GPa (Asami et al., 2007). In contrast, such high-T metamorphism has not been recognized in the SW terrane. Peak metamorphic conditions of gneisses at Vengen ridge and northern Walnumfjelle have been estimated as upper amphibolite-facies. These

gneisses have experienced subsequent pervasive retrograde metamorphism accompanying mylonitization (Shiraishi and Kojima, 1987).

2.2. Structural geology

Structural evolution of the central part of the Sør Rondane Mountains is divided in to seven stages, from D1 to D7, based on their characteristics of deformation, metamorphism and igneous activity (Table 2.1, after Toyoshima et al., 1995). The deformations of three early stages (D2 to D4) are not regional. The metamorphic-deformation history is divided into three stages, prograde metamorphic peak stage (D1) related to flattening type deformation, retrograde metamorphic stage (D2 to D6) related to exhumation and mylonitization, and contact metamorphic stage (D7). The metamorphism of the former two stages has occurred not only related with ductile deformation but also with various magmatic intrusions.

Foliation of metamorphic rocks trends variously in the central part of the Sør Rondane Mountains as well as the eastern part where NE-SW and NW-SE trending folds develop (Ishizuka et al., 1993). In contrast, E-W to NE-SW trending and southward dipping foliation is the most prominent structure in the

western part of the Sør Rondane Mountains (Shiraishi et al., 1992a). Multiphase folding (D4 to D6) has been observed as various orientation of foliation in the central Sør Rondane Mountains (Toyoshima et al., 1995). Discontinuity of fold axes of WNW-ESE trending antiform and synform implies N-S trending fault in the Gjelbreen (Shiraishi et al., 1991).

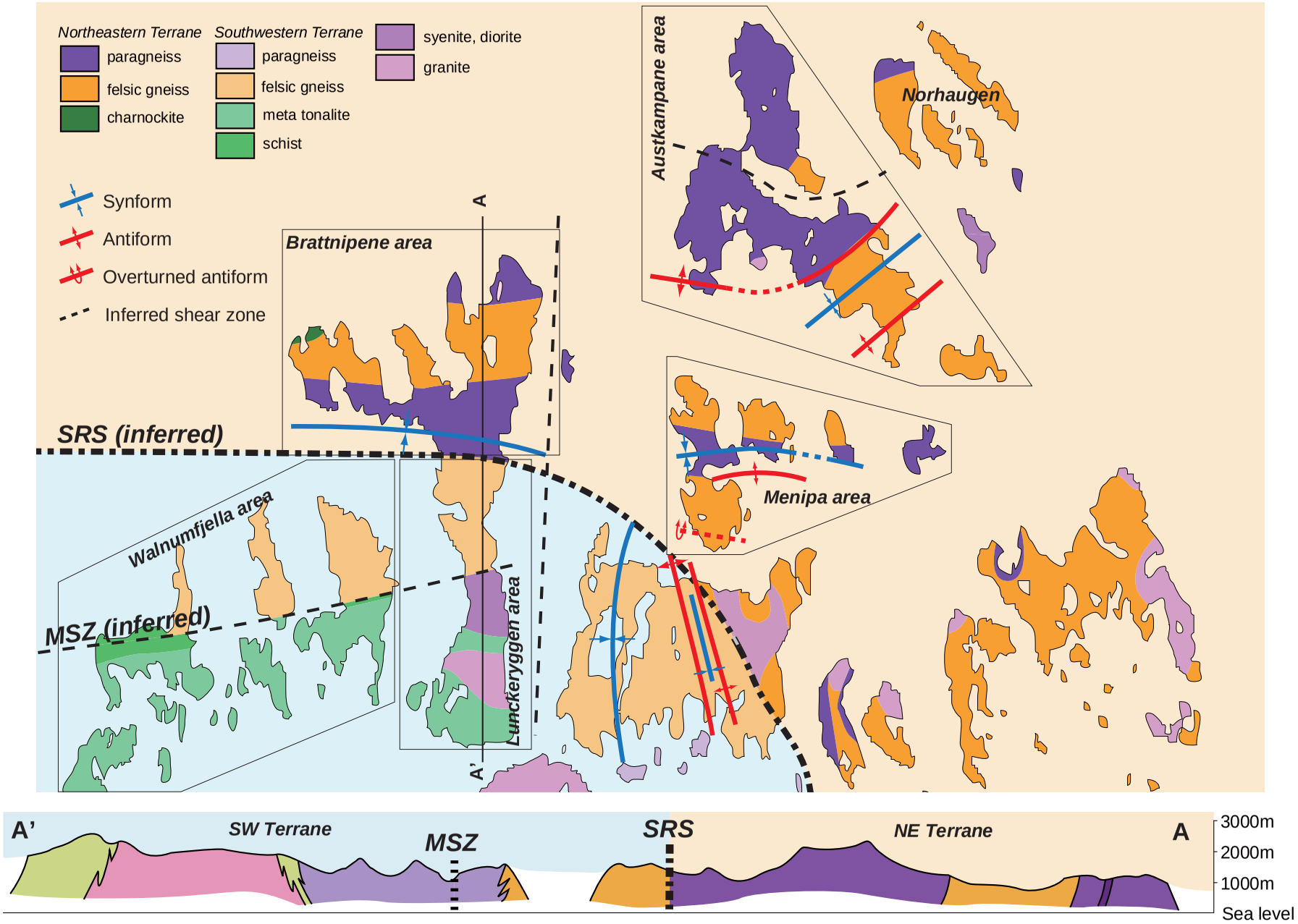

Fig. 2.1. Geological map and geological cross section of the central Sør Rondane Mountains (modified after Shiraishi et al., 1997). Investigated areas are also shown with polygons. MSZ: Main Shear Zone (Kojima&Shiraishi, 1986), SRS: Sør Rondane Suture (Osanai et al., 1992)

Table 2.1. Deformation and metamorphic history of the central Sør Rondane Mountains proposed by Toyoshima et al. (1995).

Deformation event	Structure	Magmatism	Metamorphism	Movement picture	Age (Ma)
D1	banding-parallel foliation (S1) with boudins, tight to isoclinal fold (B1)		Peak metamorphism? granulite to amphibolite facies?		1000
D2	fracture filled with tonalite and gabbro intrusives, mylonitic foliation (S2) and tight fold (B2)	tonalitic and gabrroic	amphibolite facies	top-to the SW to S displacement formation of the MSZ	950
D3	mylonitic foliation (S3), minor tight fold (B3) and major recumbent fold (B3)	pegmatite I and granitic	retrograde metamorphism	top-to the SE displacement formation of the SRS	
D4	WNW-ESE trending open to tight fold (B4), minor shear zone and fracture filled with intruded granitic rock	pegmatite II	greenschist facies	N-S trendign compression and northward thrusting?	
D5	N-S trending open to gentle fold (B5)			E-W trending compression	
D6	NE-SW trending gentle fold (B6)			NW-SE trending compression	
D7	fracture filled with intruded syenitic and granitic rocks	syenitic and granitic			500

Chapter 3. Petrology and metamorphism of the central Sør Rondane Mountains.

3.1. Introduction

Metamorphic evolution in the Sør Rondane Mountains was proposed by Asami et al. (1992). This P-T path is organized on the basis of the idea of that whole area of the Sør Rondane Mountains should be subjected to several thermal events as a single geological unit. However following regional characteristics based on petrography were pointed out; (1) orthopyroxene-bearing metamorphic rocks, indicating granulite-facies metamorphism, are distributed in the NE terrane, whereas such granulite-facies rocks are not found in the SW terrane (e.g. Osanai et al., 1992), (2) within the NE terrane, occurrence of the aluminosilicate minerals are different from each area, for example, prograde kyanite occurs in Balchenfjella, retrograde kyanite in Brattnipene and Menipa area and retrograde andalusite in Austkampane area (Ishizuka & Kojima, 1987; Asami & Shiraishi, 1987; Asami et al., 1989). Recent petrological studies support difference of P-T paths in each area. Baba et al. (2008) found sapphirine + spinel inclusion in garnet and orthopyroxene + sillimanite + quartz paragenesis in pelitic gneisses from Brattnipene area. These

parageneses imply pressure increase near the temperature peak condition. On the other hand, in Austkampane area, textures indicating decompression near peak conditions are reported as orthopyroxene + plagioclase symplectite after garnet + hornblende (Osanai et al., 2008), cordierite after garnet + sillimanite + quartz and Al zoning of orthoamphibole (Hokada et al., 2008). Such petrographical regionality implies that P-T path of each area could be different, and area-specific petrological analyses must be required.

In this chapter, petrography and mineral chemistry are described in each area, and then metamorphic conditions are estimated using geothermobarometers. Based on these results, P-T evolution for rocks in each area will be discussed.

Samples described in this study and their localities are shown in Fig.3.1. Distributions of the key minerals and textures are shown in Fig. 3.2.

3.2. Brattnipene area

3.2.1. Field relationship in Brattnipene area

Brattnipene area comprises mainly of felsic gneiss (hornblende-biotite gneiss, garnet-biotite gneiss, etc.) intercalated with pelitic gneiss

(garnet-orthopyroxene-biotite gneiss, garnet-biotite-sillimanite gneiss, garnet-corundum-biotite gneiss, etc.), marble and mafic gneiss (Fig. 3.4a-g). Orthopyroxene-bearing quartzofeldspathic gneiss and mafic granulites are dotted in the area, and these granulite-facies metamorphic rocks commonly surrounded by lower grade rocks. Metamorphic rocks are intruded by the undeformed pegmatite and granite striking NNE-SSW accompanying mylonite formation (Fig. 3.3a). Foliations and lithological boundaries are monotonously striking E-W and dipping S to SWS except the southern part. In the southern part of Brattnipene area, large-scale fold zone is developed (Fig. 3.3b).

3.2.2. Petrography of representative lithologies in Brattnipene area

Garnet-orthopyroxene-biotite gneiss (A07123001E, A07123001F, A07123001R)

This quartzofeldspathic rock is mainly composed of garnet, orthopyroxene, biotite, plagioclase, K-feldspar and quartz with minor amount of ilmenite, magnetite, apatite and zircon (Fig. 3.5a,b). This rock type is found in the northern part of the area.

Garnet has commonly rutile exsolution texture (Fig. 3.5d). Rutile needles

are oriented in three directions. Garnet in this rock type shows no clear replacement texture. Orthopyroxene occurs in matrix. Occasionally rim of orthopyroxene is replaced by fine-grained biotite and quartz (Fig. 3.5e). Biotite occurs in the matrix and is random oriented. The grain in the matrix is relatively large and commonly contains ilmenite needles oriented in three directions. Apatite in this rock type commonly contains monazite needles oriented in one direction (Fig. 3.5c).

Garnet-biotite-corundum gneiss (A07123001P, BC08010302B)

This pelitic rock occurs as thin layer in the host pelitic rocks. This rock type is composed of garnet, biotite, corundum, sillimanite, spinel, K-feldspar and plagioclase with minor amount of magnetite, rutile, monazite and zircon. (Fig. 3.6a,b). Samples A07123001P and BC08010302B occur as thin layer intercalated with orthopyroxene bearing lithologies and garnet-sillimanite-biotite gneiss, respectively.

Quartz is typically absent. Spinel commonly occurs as inclusion in garnet and corundum (Fig. 3.6c,d). Minor amount of spinel is also present in the matrix. These spinel grains never have contact with sillimanite. Corundum commonly

has contact with garnet. Sillimanite is present in the domain where spinel is absent. Garnet does not contain rutile needles. Biotite is present both in matrix and as inclusions in garnet and corundum.

Orthopyroxene-hornblende mafic granulite (A07123001I, A07123001N)

These rocks are mainly composed of orthopyroxene, hornblende, garnet/clinopyroxene, biotite and plagioclase with minor magnetite, ilmenite and apatite (Fig 3.6e,f). Garnet is contained in sample A07123001I, and clinopyroxene is in sample A07123001N. These rocks show granoblastic texture and rare signatures indicating retrogression can be observed.

Garnet-biotite-sillimanite gneiss (07120402A, BC08010302C, BC08010401B, 84021904B, 85011511B)

These pelitic rocks are mainly composed of garnet, biotite, sillimanite, K-feldspar, plagioclase and quartz with minor amount of magnetite, rutile, apatite, monazite and zircon (Fig. 3.7a,c,f, Fig3 3.8a). This rock type mainly occurs in the southern part of the area. Sample 07120402A is collected at the northeastern part of the area, and the other samples are collected in the southern part.

Samples 84021904B and 85011511B were collected by JARE-25 and 26 parties.

Garnet contains spinel and sillimanite inclusions. Garnet is commonly replaced rim of grain by two-type aggregates: corona of biotite+plagioclase (Fig. 3.7b) or radial aggregate of biotite+sillimanite/kyanite (Fig. 3.7d,f). Kyanite bearing aggregate is found in samples 84021904B and 85011511B. Kyanite and sillimanite are observed in the same aggregate. There are no clear textures which identify anteroposterior relationship between kyanite and sillimanite (Fig. 3.7f). Sillimanite also occurs in matrix, commonly preferred oriented with biotite. Such sillimanite is certainly present at the peak condition. In the sample BC08010302C, andalusite occurs associated with clay minerals in the strongly altered portion (Fig. 3.8b). Spinel is present as inclusion in garnet. Biotite occurs in the matrix, as inclusions in garnet and as aggregates replacing rim of garnet grain.

Garnet-biotite gneiss (A07123001AF, BC08010302A, BC08010502B)

These quartzofeldspathic rocks are mainly composed of garnet, biotite, K-feldspar, plagioclase and quartz with minor magnetite, apatite and zircon. This rock type is commonly strongly deformed and includes porphyroclastic garnet

and plagioclase and ribbon of quartz. (Fig. 3.8c,d,f). This rock type is one of the widespread lithologies in this area. Sample A07123001AF is collected at the northern part, samples BC08010302A and BC08010502B are collected at the southern part of the area.

Garnet is commonly replaced its rim portion by biotite+plagioclase aggregate. Quartz in sample BC08010302A contains rutile exsolution. Rutile needles are oriented in three directions, interpreted as exsolution origin (Fig. 3.8e), however the grains in the other samples contain no needles.

Hornblende-biotite gneiss (A07123001AC, BC08010504A)

This felsic rock is composed mainly of hornblende, biotite, plagioclase and quartz and/or epidote with minor ilmenite, magnetite, allanite and zircon (Fig. 3.9a,c).

The sample A07123001AC is a layer from which this rock was collected apparently overlies the layers composed of orthopyroxene-bearing lithologies, for example, A07123001E, A07123001I, A07123001N and A07123001R. Rare replacement or alteration signatures can be observed. Hornblende and biotite are weakly aligned and form foliation.

The sample BC08010504A was collected at the southern part of Brattnipene. This rock has no clear texture indicating retrogression. Hornblende, epidote and biotite are random oriented. Epidote shows subhedral shape and has contact with other mafic minerals. These textures indicate minerals in matrix should coexist as peak assemblage.

3.2.3. Mineral chemistry in Brattnipene area

Garnet

Grains in felsic~pelitic samples escaping retrograde hydration commonly show slight increase of grossular component rimward. Grains in samples subjected to hydration commonly show the increase of almandine and spessartine components and decrease of pyrope component rimward (Fig. 3.14, 3.15). Grain in sample BC08010502B has different compositional characteristics from other samples: obviously high grossular (20 mol%) and spessartine (14 mol%) contents and low pyrope content (5 mol%).

Orthopyroxene, spinel, hornblende, biotite

Orthopyroxene in Brattnipene area have X_{Mg} ranging 0.58-0.63 and Al_2O_3 ranging 1.66-3.97 wt% (Fig. 3.16). The grains are compositionally

homogeneous in throughout the samples.

Spinel grains have X_{Mg} = 0.21-0.43 and ZnO = 5-12 wt%.

Hornblende grains occurring in the northern part of the area have X_{Mg} ranging 0.52-0.71. On the other hand, grain occurring in the southern part, which coexists with epidote (BC08010504A), has much lower X_{Mg} (0.30-0.32) (Fig. 3.17).

Biotite grains, which occur as inclusion and in matrix of the samples less affected by retrogression, have X_{Mg} of > 0.7. Grains in matrix of retrogressed rocks have X_{Mg} ranging 0.5-0.7. Biotite in the samples BC08010502B and BC08010504A shows much lower X_{Mg} value (0.34-0.37). Relation between X_{Mg} value, Ti, Al^{vi} and F contents is unclear (Fig. 3.18). Concentration of these elements in biotite could be controlled mainly by bulk composition.

3.2.4. Metamorphism and *P-T* estimation in Brattnipene area

In Brattnipene area, orthopyroxene-bearing rocks are recognized, suggesting granulite-facies metamorphism in this area. Garnet grains in garnet-orthopyroxene-biotite gneisses (e.g. A07123001E, A07123001R) have chemical zoning with increase of grossular content rimward. This chemical

variation qualitatively implies pressure increase near peak metamorphic conditions. Garnet-orthopyroxene thermometer (Harley, 1984) and garnet-orthopyroxene-plagioclase-quartz barometer (Newton & Perkins, 1982) give 750-770 °C, and 0.7-0.8 GPa using compositions of rim of garnet and homogeneous orthopyroxene and plagioclase. Two-pyroxene-bearing rocks (07121003A, A07123001N) also occur adjacent to garnet-orthopyroxene-biotite gneisses. Pairs of two-pyroxene yield 800-810 °C assuming 0.8 GPa with two-pyroxene thermometers (Wells, 1977; Taylor, 1998). These P-T conditions, 750-810 °C, and 0.7-0.8 GPa, are consistent with the orthopyroxene-bearing mineral parageneses which suggest granulite-facies metamorphism (Fig. 3.19).

Also in orthopyroxene-free lithologies, reaction texture indicating pressure increase near peak condition can be observed. Garnet-biotite-corundum gneiss (A07123001P, BC08010302B) has mineral paragenesis as garnet, corundum, spinel and sillimanite. Corundum commonly has contact with garnet. Spinel dominantly occurs as inclusion in garnet and corundum and small amount of spinel grains occurring in matrix never have contact with sillimanite. Additionally X_{Mg} value of garnet is equivalent to that of spinel inclusion in garnet (Fig. 3.16). These textual and chemical relationships

imply the reaction as follows;

spinel+sillimanite => garnet+corundum (1)

P-T condition of the reaction (1) above was confirmed experimentally by Shulters and Bohlen (1989). The reaction (1) curve using X_{Mg} values of the garnet and spinel in this area is shown in Fig. 3.19. It can be assumed that inclusions in garnet preserve chemical composition which was obtained at the reaction (1) because of equivalence of X_{Mg} values of the garnet and spinel inclusion in garnet (Fig. 3.16). Garnet-biotite thermometer (Holdaway, 2000) gives 750-770 °C using compositions of the core of garnet and biotite grain in matrix. Consequently, reaction (1) in Brattnipene area should occurs at ca. 750 °C and 0.7 GPa during compression process. This P-T condition is slightly lower P and T condition than estimated with orthopyroxene-bearing rocks, indicating that the reaction (1) should precede peak metamorphism.

Textures indicating several stages of retrograde metamorphism are recognized widely in the area. Radial aggregate with biotite and sillimanite/kyanite replacing garnet is found locally. This texture implies following hydration reaction;

garnet+K-feldspar+H_2O => biotite+sillimanite/kyanite+quartz (2)

P-T condition of the reaction (2) is experimentally reported (Breton & Thompson, 1988), and it intercepts sillimanite/kyanite transition around 720 °C, 0.85 GPa; shown in Fig. 3.19). There is rare texture which reveal anteroposterior relationship between kyanite and sillimanite, for example, cross-cut relation and replacement relation. In several aggregates, kyanite and sillimanite have contact with each other. Consequently kyanite and sillimanite could be interpreted to be formed around the same period. Since the intercept of reaction (2) and sillimanite/kyanite transition situates slightly lower-T side than peak condition of Brattnipene area, it suggests that local hydration (related to partial melting?) during isobaric cooling process after peak metamorphism.

Most widespread retrograde signature is corona of biotite and plagioclase replacing rim of garnet. P-T condition of the hydration is hard to be constrained, however, it might be a one of the product of lower-T stage retrogression.

Andalusite is also found with clay minerals in highly altered portion of garnet-sillimanite-biotite gneiss (BC08010302C). Occurrence of andalusite indicates that the rocks were finally subjected to hydration in the andalusite stability field (Fig. 3.19).

3.3. Menipa area

3.3.1. Field relationship in Menipa area

In Menipa area, felsic~intermediate orthogneiss, pelitic~psammitic gneiss and marble are dominantly distributed lithologies (Fig. 3.4n,o). In the northwestern part of this area, granite intrudes into metamorphic rocks. Foliation defined by lithological boundary is E-W strike and gently dipping synform is observed in the middle part of this area. Felsic orthogneiss is apparently overlain by pelitic~psammitic gneiss and marbles (Fig. 3.3d).

3.3.2. Petrography of representative lithologies in Menipa area

Garnet-biotite gneiss (AC08011301M)

This psammitic gneiss is mainly composed of garnet, biotite, plagioclase, K-feldspar and quartz with minor rutile, ilmenite and zircon. No obvious texture indicating retrogression can be observed (Fig. 3.12c).

Biotite is random-oriented. Garnet and quartz contain a large amount of rutile needles with shape-preferred orientations in three directions (Fig. 3.12 d,e). The needles occur throughout the host grains, are interpreted to be of exsolution origin.

Hornblende-biotite gneiss (AC08012001A)

This felsic gneiss is mainly composed of hornblende, biotite, plagioclase and quartz with minor magnetite, allanite, titanite, apatite and zircon (Fig. 3.12f). No clear texture indicating replacement or alteration can be observed in this rock. Hornblende is weakly elongated and defines foliation with biotite. Quartz contains small amount of rutile needles.

Biotite gneiss (AC08011601A)

This felsic gneiss is mainly composed of biotite, plagioclase, K-feldspar and quartz with minor magnetite, apatite and zircon. No clear texture indicating replacement or alteration can be observed in this rock. Biotite is random oriented. Quartz contains sparse mineral inclusions.

3.3.3. Mineral chemistry in Menipa area

Garnet

Garnet in sample AC08011301M shows slight increase of grossular component rimward (Fig. 3.14, 3.15)). It is similar trend to grains in Brattnipene. X_{Mg} value is ranging from 0.34 of the core to 0.32 of rim.

Biotite and hornblende

Biotite in sample AC08011301M has 0.58 of X_{Mg} and 0.67 of Al^{vi} (O=22). Grains in felsic rocks of AC08011601A and AC08012001A show lower X_{Mg} (0.38-0.39) and Al^{vi} (0.36) than that of sample AC08011301M. These values of felsic rocks are similar to the composition of the grain in Lunckeryggen area (see description below) (Fig. 3.18).

Hornblende in sample AC012001A has 0.38 of X_{Mg}, 0.66 pfu of Al^{vi} and 0.12 pfu of Ti (O=23). These concentrations are within the range of hornblende in Lunckeryggen area (see description below) (Fig. 3.17).

3.3.4. Metamorphism and *P-T* estimation in Menipa area

In the investigated samples in Menipa area, any obvious retrograde textures cannot be recognized.

The peak metamorphic assemblage of the garnet-biotite gneiss (AC08011301M) is garnet+biotite+plagioclase+K-feldspar+quartz.

Garnet shows increase in grossular content rimward. It qualitatively implies rise in pressure near peak condition. A pair of garnet rim, biotite and plagioclase in matrix yields 750 °C, 0.72 GPa using garnet-biotite thermometer (Holdaway,

2000) and garnet-biotite-plagioclase-quartz barometer (Wu et al., 2004).

On felsic gneisses (AC08011601A, AC08012001A), the peak assemblages are biotite±hornblende+plagioclase±K-feldspar+quartz.

A pair of hornblende and plagioclase in AC08012001A yields 620 °C using hornblende-plagioclase thermometer (Holland & Blundy, 1994) assuming at 0.7 GPa, interpreted as peak metamorphic condition. Estimated temperature condition is considerably lower than the peak condition of garnet-biotite gneiss occurs in this area. Consequently it is found that relatively low-grade metamorphic rocks (AC08011601A, AC08012001A) are apparently overlain by high-grade metamorphic rock (AC08011301M).

3.4. Austkampane area

3.4.1. Field relationship in Austkampane area

In Austkampane area, pelitic gneiss (garnet-cordierite-biotite gneiss, garnet-sillimanite-biotite gneiss and so on) is the dominant lithology. Marble and mafic rocks are intercalated with pelitic gneiss. Felsic gneisses (garnet-biotite gneiss, hornblende-biotite gneiss and so on) are also distributed mainly at the southern part of this area (Fig. 3.3c). Granitic intrusions are observed locally.

Foliation defined by lithological boundary is E-W~NE-SW strike and gently dipping N or S, which forms syn- and anti- form in the southern part of this area (Fig. 3.4h-m).

3.4.2. Petrography of representative lithologies in Austkampane area

Garnet-cordierite-biotite/orthoamphibole gneiss (AC07121303E, AC07121701C, AC07121801H, AC07121701M)

This pelitic rock is mainly composed of garnet, biotite, cordierite, sillimanite, plagioclase, K-feldspar and quartz with minor rutile, ilmenite, monazite, apatite and zircon (Fig. 3.10a-d).

Commonly garnet grains are surrounded by cordierite (Fig. 3.10a-c). In this case, garnet never has contact with sillimanite in matrix. Cordierite commonly has contact with garnet. Biotite occurs in matrix and as inclusion in garnet. Garnet and quartz contain exsolved rutile needles orientated in three directions (Fig. 3.11e,f).

Garnet-biotite-sillimanite gneiss (AC07121302B, BC07122801D, BC07122804A)

This pelitic rock is composed of garnet, sillimanite, biotite, plagioclase, K-feldspar and quartz with minor ilmenite, rutile, monazite, apatite and zircon (Fig. 3.a,c). In this rock type, foliation defined by oriented biotite and sillimanite is well-developed.

Garnet contains spinel and sillimanite inclusions, and a large amount of exsolved rutile needles. Garnet is commonly replaced rim of grain by two-type aggregates: corona of biotite+plagioclase or radial aggregate of biotite+sillimanite (Fig. 3.11b). Kyanite is not found in the aggregate. Occasionally andalusite is present in matrix. Andalusite includes sillimanite, indicating transition from sillimanite (Fig. 3.11d). Quartz contains exsolved rutile needles orientated in three directions.

Garnet-corundum-spinel/sillimanite gneiss (AC07121702B)

This aluminous rock occurs as thin layer in the host pelitic rocks. This rock type is composed of garnet, biotite, corundum, sillimanite, spinel, K-feldspar and plagioclase with minor amount of magnetite, rutile, monazite and zircon (Fig.

3.10e,f). Quartz is absent. Garnet shows subhedral shape. The grains in this rock type show few replacement textures. Garnet includes biotite and spinel. Corundum commonly has contact with garnet. Spinel occurs in matrix and as inclusion in garnet and corundum (Fig. 3.10e,f). Spinel grains in matrix never have contact with sillimanite. Sillimanite is present in the domain where spinel is absent. Biotite is present both in matrix and as inclusions in garnet and corundum (Fig. 3.10e).

Hornblende-biotite gneiss (AC07121901A)

This felsic gneiss is mainly composed of hornblende, biotite, epidote, plagioclase, K-feldspar and quartz with minor magnetite, apatite and zircon (Fig. 3.12b). No obvious texture indicating retrogression can be observed.

Hornblende and biotite are random-oriented. Quartz contains sparse mineral inclusions. Epidote commonly has clear contact with biotite.

Garnet-biotite gneiss (BC07122805C)

This felsic gneiss contains dark-color enclaves and cuts across the foliation of surrounding gneisses in the field observation, which indicates

probably to be of syn-metamorphic intrusion. This rock is mainly composed of garnet, biotite, plagioclase, K-feldspar and quartz with minor ilmenite, apatite, monazite and zircon (Fig. 3.12a). This rock is characterized by the plagioclase elongated porphyroclast. Few retrograde signatures can be observed.

3.4.3. Mineral chemistry in Austkampane area

Garnet

Most garnet grains from Austkampane area show commonly increase of almandine and spessartine components and decrease of pyrope component (Fig. 3.14, 3.15).

Grain in sample BC07122805C, which is metamorphosed syn-metamorphic intrusion, has different compositional characteristics: obviously high grossular (20 mol%) and extremely low pyrope content (2 mol%).

Cordierite, spinel, biotite, hornblende

Cordierite in Austkampane area shows X_{Mg} values ranging 0.69-0.77 (Fig. 3.16).

Most spinel grains have X_{Mg} = 0.24-0.42 and ZnO = 2-13 wt%. Grains in

sample AC07121702B show much lower X_{Mg} value (0.07-0.15), and have ZnO = 4-5 wt%.

Hornblende is contained in felsic gneiss (AC07121901A), and has X_{Mg} = 0.39 (Fig. 3.17).

Biotite does not show clear relationship between chemical composition and mode of occurrence of the grains. Relation between X_{Mg} value, Ti, Al^{vi} and F contents is also unclear. Biotite in sample BC07122805C has obviously low X_{Mg} contents (0.12-0.14) (Fig. 3.18).

3.4.4. Metamorphism and *P-T* estimation in Austkampane area

Occurrence of cordierite in pelitic gneisses is a characteristic feature for rocks of Austkampane area. Cordierite commonly occurs associated with garnet. These garnet grains have never contact with sillimanite in matrix, indicating the reaction as follows;

garnet+sillimanite+quartz => cordierite (3)

X_{Mg} value of cordierite in the reaction (3) is a potential indicator of the pressure condition (Holdaway & Lee, 1977). According to Holdaway and Lee (1977), cordierite with 0.7 of X_{Mg}, which is representative value in Austkampane area, is

stable under 0.5-0.6 GPa assuming P_{H2O} = 0.4-1.0 P_{total} conditions. Pairs of coexisting garnet and cordierite in samples AC07121701C and AC07121801M yield 750-780 °C using garnet-cordierite thermometer (Perchuk & Lavrent'eva, 1983). Consequently, metamorphic rocks in Austkampane area probably experienced decompression around 750-780 °C, 0.5-0.6 GPa near peak condition (Fig. 3.19).

Textures indicating several stages of retrograde metamorphism are also recognized widely in the area. Radial aggregate with biotite and sillimanite replacing garnet is found locally, and this texture implies following hydration reaction;

garnet+K-feldspar+H_2O => biotite+sillimanite+quartz (2)

The reaction (2) curve locates slightly lower T side of peak metamorphic condition estimated above. It might imply that the radial aggregate of biotite and sillimanite was formed after peak metamorphism. This suggests local hydration near peak condition (Fig. 3.19).

Mineral paragenesis of garnet, corundum, spinel and sillimanite is also found in Austkampane area (AC07121702B). Textual and compositional relations are similar to those of Brattnipene area, and they imply the reaction as

follows;

spinel+sillimanite => garnet+corundum (1)

P-T condition of the reaction (1) using X_{Mg} values of the garnet (X_{Mg}=0.10) and spinel (X_{Mg}=0.07) in this area is shown in Fig. 3.19 (Shulters and Bohlen, 1989). Garnet-biotite thermometer (Holdaway, 2000) gives around ca. 600 °C using compositions of the core of garnet and biotite grain in matrix, which is considerably lower than peak T condition in this area. Combined with P-T condition of reaction (1) and T estimation, the reaction (1) in Austkampane area occurs at around 550-560 °C and 0.4-0.5 GPa. It is probably during isobaric cooling process (Fig. 3.19).

Most widespread retrograde signature is corona of biotite and plagioclase replacing rim of garnet in pelitic gneisses. It certainly is hydration reaction, implying a regional scale water supply. P-T condition of the hydration is not well-constrained, however it might be a product of lower-T conditions.

In Austkampane area, andalusite replacing sillimanite occurs in pelitic rocks which associated with granite intrusion. Andalusite commonly replaces sillimanite. This suggests such rocks are subjected to retrogression under the andalusite stability, probably related to heating by granite intrusion (Fig. 3.19).

3.5. Lunckeryggen area

3.5.1. Field relationship in Lunckeryggen area

In Lunckeryggen area, felsic~intermediate gneisses (garnet-hornblende-biotite gneiss, hornblende-epidote-biotite gneiss, etc.) are distributed (Fig. 3.3p-s). Syenite and granite interpreted as post-orogenic magmatism (e.g. Sakiyama et al., 1988) intrude into metamorphic rocks at the southern part of the area. In the northern part, folding of which axe steeply dipping is observed. In the middle part, foliations and lithological boundaries are dominantly striking E-W and dipping S to SWS (Fig. 3.3e).

3.5.2. Petrography of representative lithologies in Lunckeryggen area

Garnet-biotite gneiss (B08012201I, B08012203A, B08012204, B08012304C, B08012304E)

This felsic rock is composed of garnet, hornblende, biotite, plagioclase, quartz and/or hornblende, epidote with minor magnetite, ilmenite, apatite and zircon (Fig. 3.13a-d,f). The grains in this rock type are relatively finer than those in rocks occurring in other areas (most grains are 300 μm to 1 mm). Foliation defined by tabular biotite and elongated hornblende is clear. Garnet occasionally

shows zoning suggested by the change of color from transparent in the core to reddish in the rim. Epidote is present in matrix in samples B08012204, B08012304C, and hornblende is present in matrix in sample B08012201I, B08012204, B08012304E. Epidote shows subhedral shape and has contact with quartz.

Hornblende-biotite gneiss (B08012302A, B08012304D)

This intermediate~mafic rock is composed of hornblende, biotite, plagioclase, quartz and/or garnet, epidote with minor magnetite, titanite, apatite and zircon (Fig. 3.13e). Weak foliation defined by alignment of hornblende is observed. No clear reaction texture can be recognized. Epidote is present in matrix in sample B08012302A, and garnet is present in matrix in sample B08012304D. Epidote has contact with quartz.

3.5.3. Mineral chemistry in Lunckeryggen area

Garnet

Garnet in Lunckeryggen area has obviously high grossular (up to 29 mol%) than and spessartine (up to 40 mol%) contents and low pyrope content

(less than 13 mol%) compared with Brattnipene, Menipa and Austkampane areas (Fig. 3.14, 3.15). The trends of compositional variation are also different from other areas. Most garnet grains in felsic gneisses in Lunckeryggen area show considerable increase of grossular and spessartine components rimward with constant almandine and pyrope components. The grain in sample B08012304E increases with pyrope and almandine contents and decrease with spessartine content rimward, which indicate preservation of prograde condition.

Hornblende, biotite, epidote

Hornblende has X_{Mg} ranging 0.29-0.40. The grains in garnet-bearing samples show relatively higher Al^{vi} (0.74-0.85 pfu based on O = 23) than those in garnet-free samples (0.31-0.57 pfu). Ti content is ranging 0.06-0.1 pfu regardless of mineral paragenesis (Fig. 3.17).

Biotite grains show compositional unity compared with the other areas; X_{Mg} = 0.25-0.40, Ti = 0.25-0.39 pfu and Al^{vi} = 0.40-0.62 pfu (O=22) (Fig. 3.18).

Epidote has pistacite ($Ca_2Fe^{3+}Al_2Si_3O_{12}(OH)$) component ranging 78-87 mol%. Pistacite content is independent from mineral paragenesis.

3.5.4. Metamorphism and *P-T* estimation in Lunckeryggen area

In Lunckeryggen area, any obvious retrograde textures cannot be recognized, suggesting that the rocks preserve prograde or near peak condition. Peak metamorphic mineral assemblage in this area is garnet+hornblende+biotite±epidote+plagioclase+quartz.

Epidote+quartz paragenesis is recognized widely in the area. Liou (1973) and Liou et al. (1983) reported experimental study on epidote stability and suggest that epidote (+quartz) break down to garnet+plagioclase+magnetite+H_2O around 680 °C at 0.3 GPa and 750 °C at 0.5 GPa at hematite-magnetite buffer. Stability limit of epidote with 78-87 mol% of pistacite component, which is compositional range in Lunckeryggen area, is confirmed by Liou (1973) as shown in Fig.3.19. Presence of epidote+quartz paragenesis in the area indicates that peak metamorphic temperature should not be reached over 700 °C which is near upper T limit of the epidote break down reaction.

Garnet grains in this area have clear growth zoning showing bell-shape pattern of Mn content (Fig. 3.14), implying preservation of prograde metamorphic conditions. Common chemical variation of garnet is increase of grossular and

spessartine contents rimward, however almandine content is constant (Fig. 3.15). This possibly indicates that consumption of clinozoisite component in epidote involves garnet growth. Increase of pistacite component, i.e. decrease of clinozoisite component, in epidote makes epidote stability shift to higher T side (Liou, 1973), therefore it also can be interpreted as prograde signature in this area.

Garnet-hornblende thermometer (Graham & Powell, 1984), hornblende-plagioclase thermometer (Holland & Blundy, 1994) and garnet-hornblende-plagioclase-quartz barometer (Kohn & Spear, 1990) are applied to coexisting garnet-hornblende-plagioclase-quartz in sample B08012201I, B08012204 and B08012304E. Estimated P-T range is 550-700 °C and 5-8 kbar, being interpreted as peak metamorphic condition of this area. These conditions are consistent with presence of epidote+quartz paragenesis described above (Fig. 3.19).

3.6 Walnumfjella area

3.6.1. Field relationship in Walnumfjella area

Walnumfjella area is divided into the northern and the southern parts by

inferred shear zone (Main Shear Zone: MSZ, Kojima & Shiraishi, 1986). The northern part comprises mainly quartzofeldspathic gneisses (garnet-hornblende-biotite gneiss, etc.), whereas in the southern part, meta-tonalite are dominant. Mafic schist and marble are intercalated with such dominant lithologies (Fig. 3.4t,u). Foliations and lithological boundaries are monotonously striking E-W and steeply dipping S to SWS (Fig. 3.3f).

3.6.2. Petrography of representative lithologies in Walnumfjella area

Garnet-hornblende-biotite gneiss (BC08010604A, BC08010604E)

This quartzofeldspathic rock is collected from the northern part of this area. This rock type is composed of garnet, hornblende, biotite, plagioclase and quartz with minor magnetite, ilmenite, apatite and zircon. Mylonitic texture characterized by porphyroclastic garnet and plagioclase is recognized (Fig. 3.9d-f). Garnet is replaced by biotite and at rim portion. Apatite with monazite needles is included in garnet. Quartz contains small amount of rutile needles oriented in three directions. It can be interpreted as exsolution origin (Fig. 3.9f).

Garnet-biotite gneiss (BC08010602J)

This felsic rock is collected from the southern part of this area. This rock type is composed of garnet, biotite, epidote, plagioclase and quartz with minor magnetite, apatite and zircon (Fig. 3.9c). Foliation defined by biotite is clear. The grains in this rock type are relatively finer than those in rocks occurring in other areas (most grains are 300 μm to 1 mm). Quartz contains sparse mineral inclusions.

3.6.3. Mineral chemistry in Walnumfjella area

Garnet

Garnet grains in northern part of the area are characterized by increase of spessartine contents and decrease of pyrope and almandine contents rimward is also observed. Grossular content is constant (17-19 mol%). Grain in southern part of the area has similar trend to grains in Lunckeryggen, considerable grossular increase rimward (Fig. 3.14, 3.15).

Hornblende, biotite, epidote

Hornblende has X_{Mg} ranging 0.40-0.49. Values of Al^{vi} and Ti are due to

samples (Fig. 3.17).

Biotite shows clear relation between X_{Mg} 0.43-0.46. Values of Ti, Al^{vi} and F vary according to samples (Fig. 3.18).

Epidote has pistacite component ranging 23-25 mol%.

3.6.4. Metamorphism and *P-T* estimation in Walnumfjella area

In Walnumfjella area, petrographical characteristics differs northern part and southern part.

Rocks from northern part show retrograde hydration signature, for example, biotite replacing garnet. Additionally monazite exsolution in apatite and rutile exsolution in quartz are found, which are well-recognized in relatively high grade metamorphic rocks. A pair of rim of garnet and rim of hornblende yields 610 °C using garnet-hornblende thermometer (Graham & Powell, 1984), interpreted as condition of retrogression.

On the other hand, rocks from southern part have little retrograde signature and are resemble rocks from Lunckeryggen area in compositional variation of garnet and presence of epidote. Even though metamorphic condition of rocks from southern part is hard to estimate, rocks from each part in

Walnumfjella area might be formed under different condition.

3.7 Summary of the metamorphism in the central Sør Rondane Mountains

As pointed out by previous studies, P-T paths differ according to area in the Sør Rondane Mountains (Fig. 3.19). In Brattnipene area, peak metamorphic condition is estimated to attain 750-850 °C and 7-8 kbar with compression. Then rocks were subjected to retrograde hydration in kyanite stability field during isobaric cooling process. Even though P-T path is not well constrained, metamorphic temperature and compression near peak condition of pelitic~psamitic gneiss from Menipa area appears to be similar to that of Brattnipene. In Austkampane area, decompression near peak condition is recognized, and peak metamorphic condition is estimated as 750-800 °C and 4-5 kbar, of which pressure condition is lower than Brattnipene area. Rocks in Austkampane area probably experienced retrograde hydration during isobaric cooling process and finally were subjected contact metamorphism accompanying granite intrusion in andalusite stability. Even though mode of pressure change near peak condition is different between Austkampane area and Brattnipene and Menipa area, peak temperature condition and isobaric

cooling path after peak condition are common in these areas. Additionally garnet gains in pelitic gneisses from Brattnipene and Austkampane areas commonly include spinel with 5-12 wt% of ZnO and sillimanite inclusions. The combination of these mineral inclusions can be interpreted as the products of staurolite break down in the sillimanite stability field. This implies that prograde process might be also similar between Brattnipene area and Austkampane area.

Whereas metamorphic rocks in above areas show clear retrograde signature, rocks in Lunckeryggen area certainly preserve prograde condition in matrix minerals. Additionally peak metamorphic temperature, estimated as 550-700 °C, is obviously lower than the three areas. These differences imply a possibility that rocks in Lunckeryggen area probably have experienced different geological history from those in other areas.

Rocks which show relatively low peak temperature and have little retrograde signature, are also distributed locally in Brattnipene, Menipa and Austkampane areas. In the central Sør Rondane Mountains, retrograde hydration and deformation are pervasive in whole area. Therefore it is possible that such apparently low-grade metamorphic rocks would be intensely modified products during retrogression. To distinguish initially low-grade rocks from

re-equilibrated rocks during retrogression, it is required that metamorphic conditions are estimated with thermobarometers calibrated using an element and mineral which is insusceptible to retrogression. Metamorphic P-T conditions can be obtained limited lithologies using classical thermobarometers, therefore it is required to estimated with thermobarometers which are applicable much common minerals for putting constraint on regional distributions of metamorphic condition.

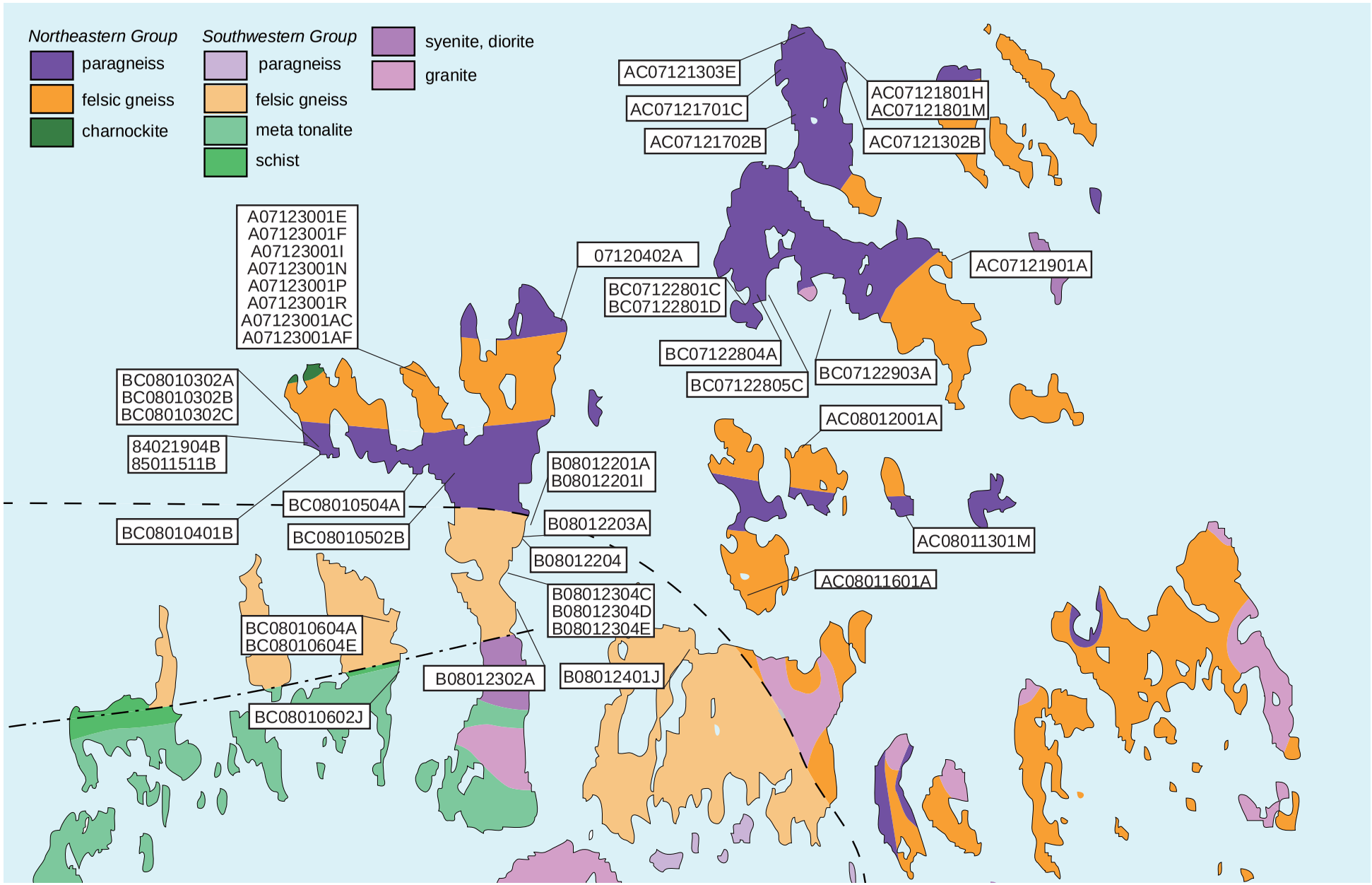

Fig. 3.1. Investigated rocks and their locality in the central Sør Rondane Mountains.

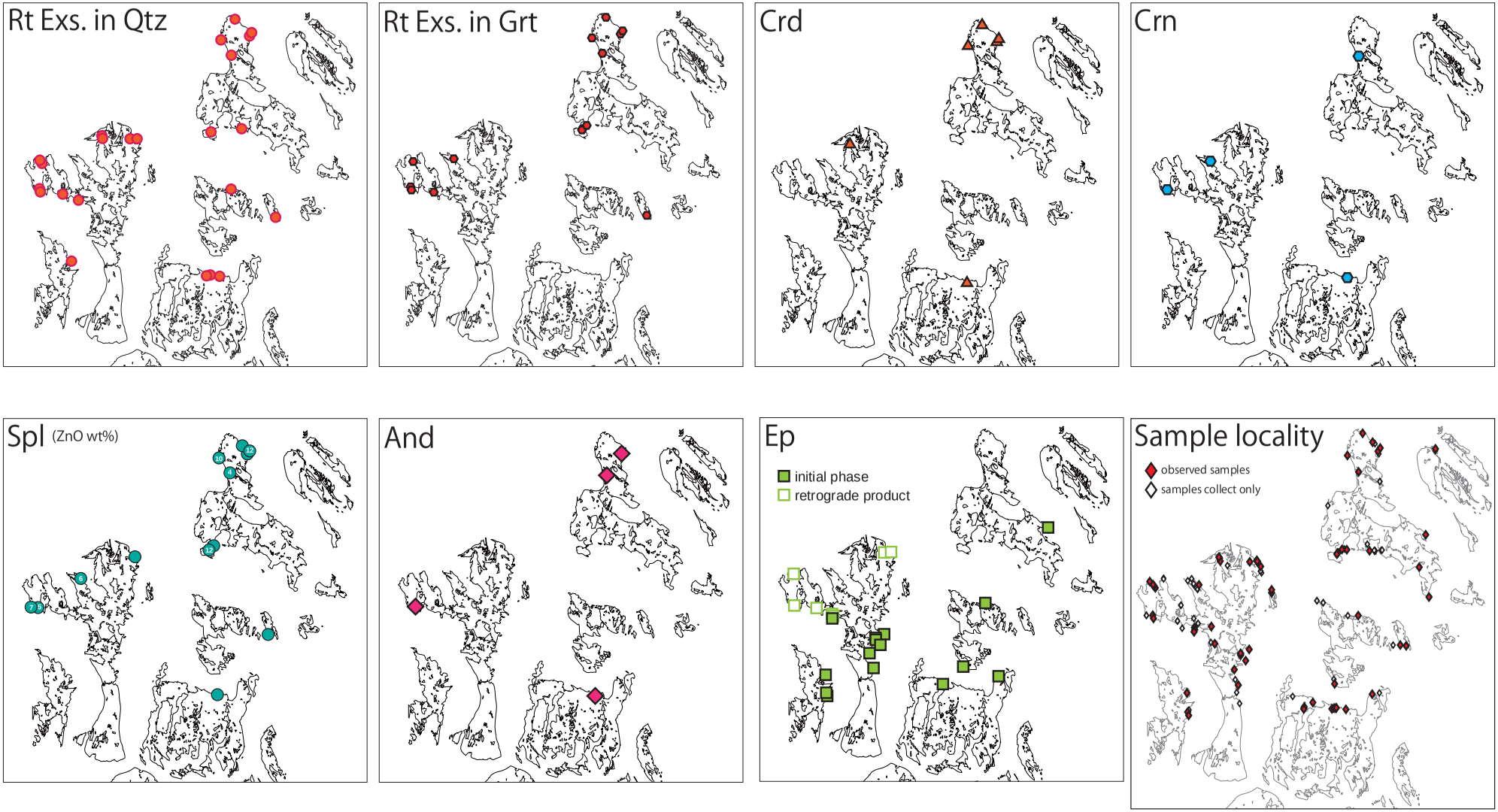

Fig. 3.2. Distributions of key minerals in the central Sør Rondane Mountains.

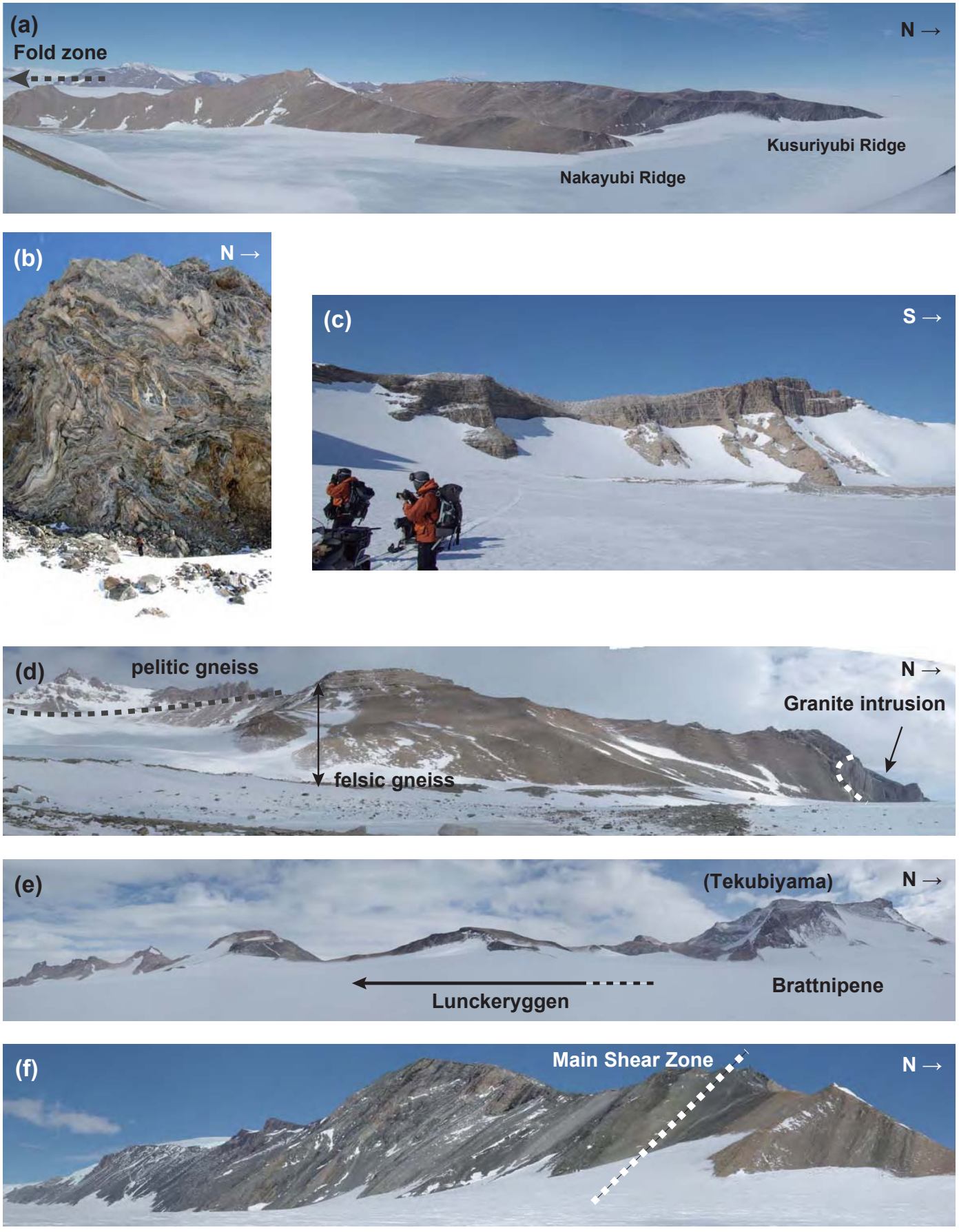

Fig. 3.3. Long-distance views of the central Sør Rondane Mountains. (a) Brattnipene area from Hitosashiyubi Ridge. The lithological boundary is monotonously dipping southward. (b) Large-scale fold in the southern part of Brattinilene. This indicates compression N-S direction. (c) The southern part of Austkampane area. The dipping of the foliation appears almost horizontal. (d) The northern part of Menipa area. The lithological boundary appears almost horizonrtal. (e) The view of Lunckeryggen area. The Sør Rondane Suture is inferred around between this area and Brattnipene area. (f) The view of Walnumfjellet area. The lithological boundary is relatively steeply dipping southward. The Main Shear Zone is condidered as the large tectonic boundary in the SW terrane.

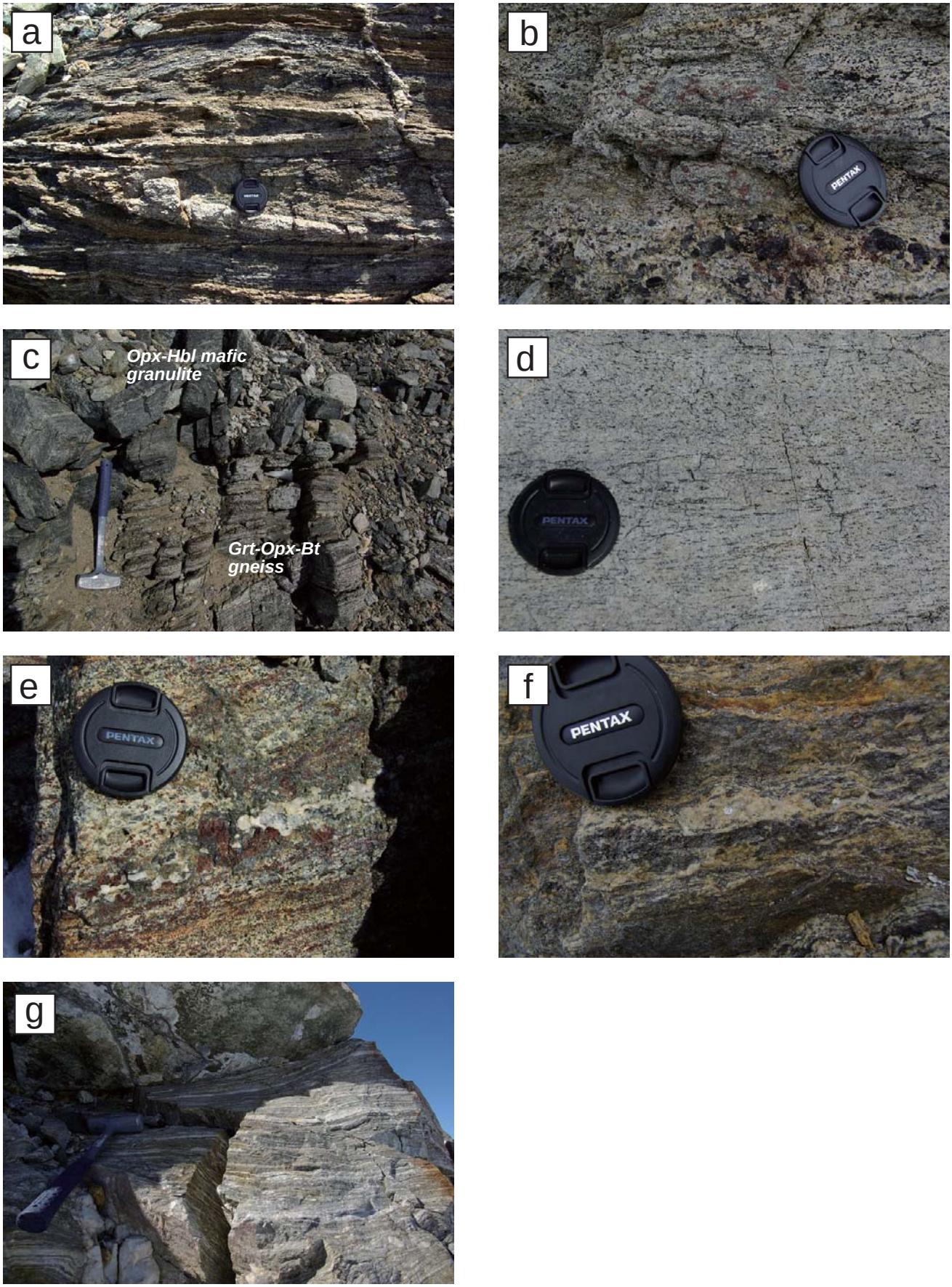

Fig. 3.4. Field occurrence of the metamorphic rocks in Brattnipene area. (a) Mode of occurrence of Grt-Sil-Bt gneisss (07120402A). (b) Mode of occurrence of Grt-Opx-Bt gneiss (A07123001E, A07123001F and A07123001R). (c) Field relation between Grt-opx-Bt gneiss and Opx-Hbl madic granulite (A07123001N). (d) Mode of occurrence of Hbl-Bt felsic gneiss (A07123001AC). This rock was located on apparently upper than the granulites. (e) Mode of occurrence of Grt-Bt gneiss (A07123001AF). This rock is highly deformed. (f) Mode of occurrence of Grt-Sil-Bt gneiss (BC08010302C) in the southern part of this area. (g) Mode of occurrence of Grt-Bt gneiss (BC08010502B) at the southern part of this area.

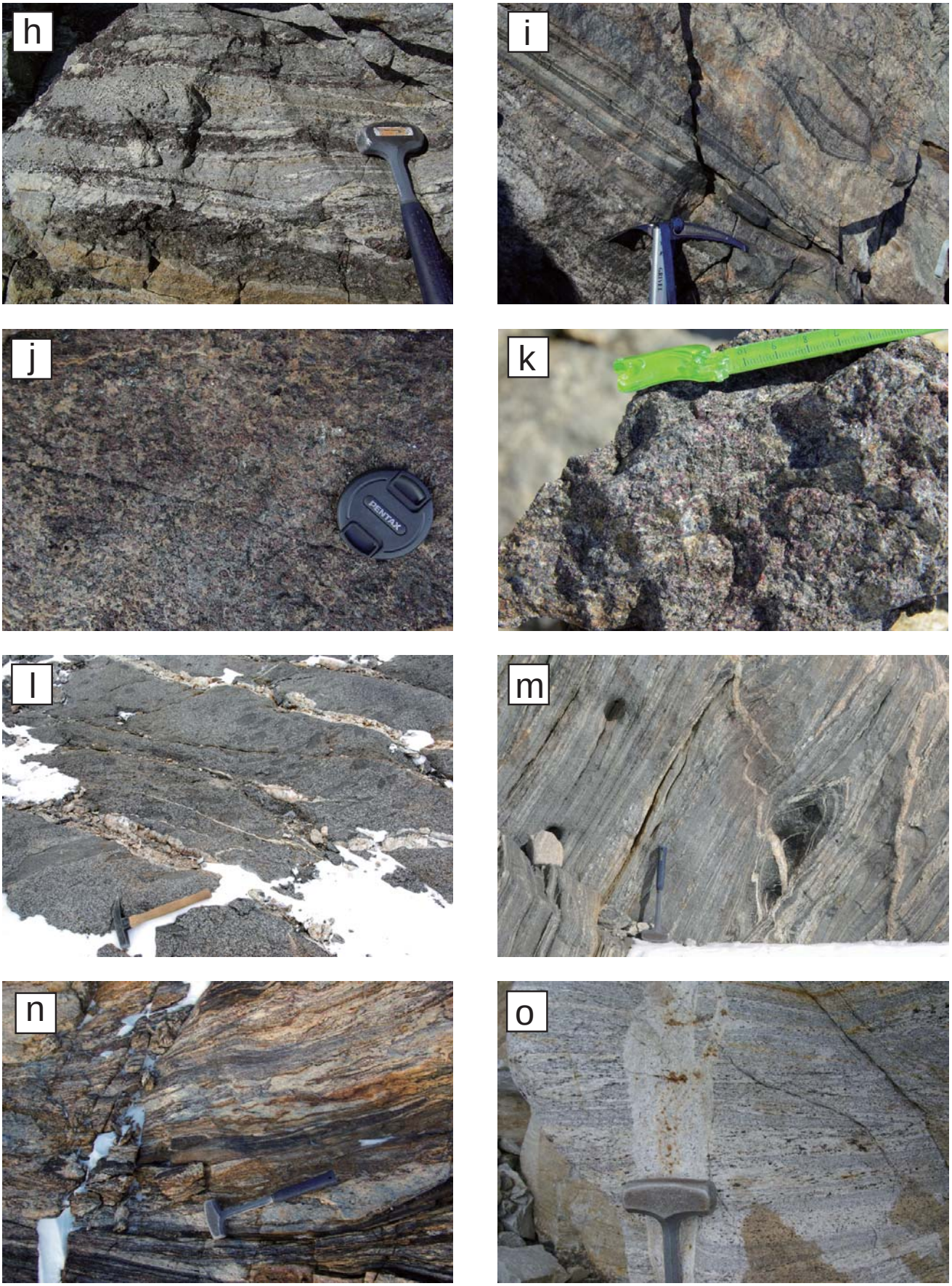

Fig. 3.4, continued. Field occurrence of the metamorphic rocks in Austkampane area and Menipa area. (h) Mode of occurrence of Grt-Crd-Bt gneisss (AC07121701C) in the northern part of Austkampane. (i) Mode of occurrence of Grt-Crn-Bt gneiss (AC07121702B) in the northern part of Austkampane. (j) Mode of occurrence of Grt-Crd-Oam gneiss (AC07121801M). (k) Close-up photograph of (j). (l) Mode of occurrence of Grt-Bt felsic gneiss (BC07122805C) in the southern part of Austkampane. This meta-intrusive rock truncates gneissose metamorphic rocks. (m) Mode of occurrence of Hbl-Bt gneiss (AC07121901A) in the southern part of Austkampane. (n) Mode of occurrence of Grt-Sil-Bt gneiss (AC08011301M) in Menipa. (o) Mode of occurrence of Hbl-Bt gneiss (AC08012001A2) in Menipa. This rock is apparently overlain by Grt-Sil-Bt gneiss.

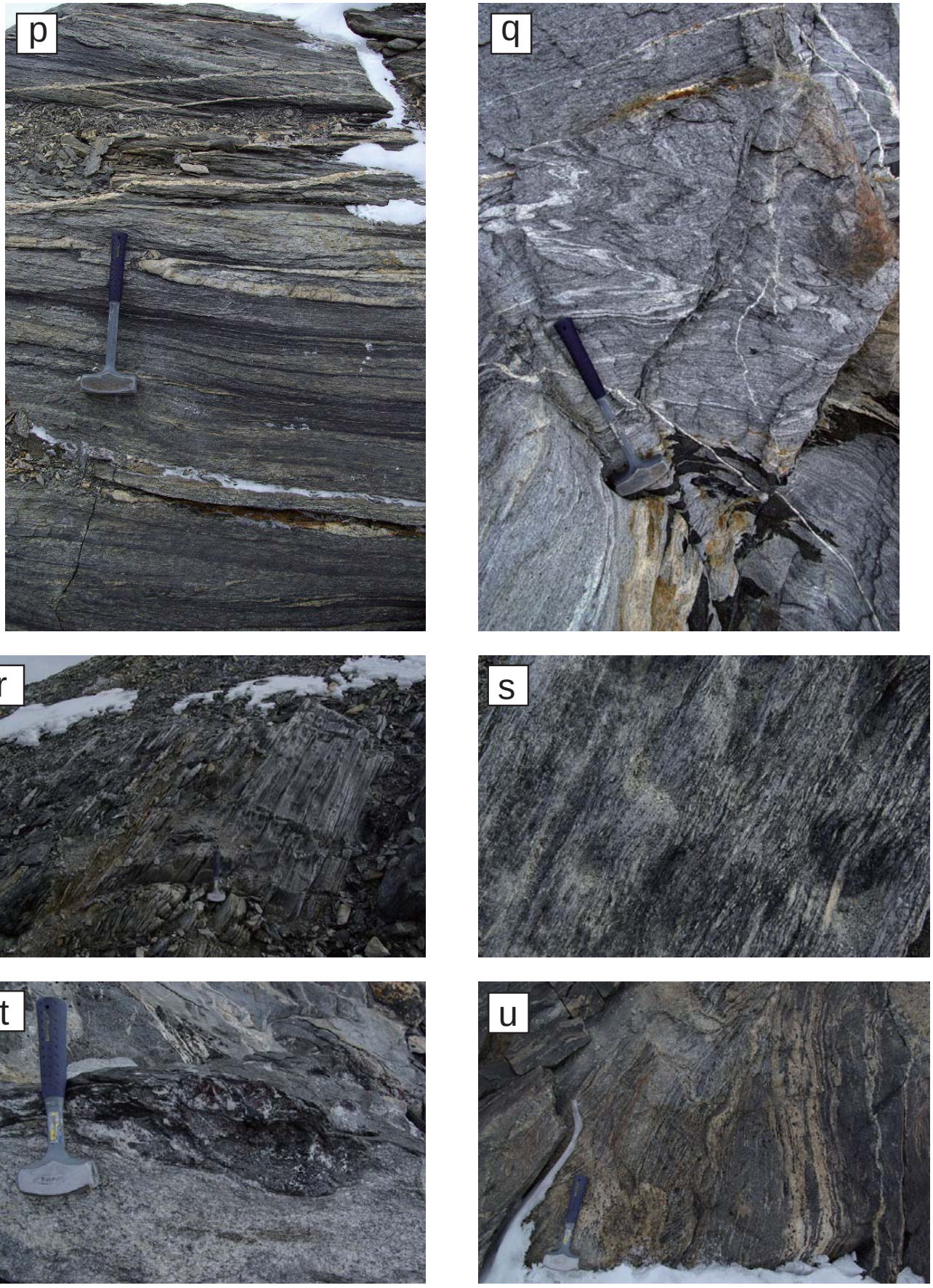

Fig. 3.4, continued. Field occurrence of the metamorphic rocks in lunckeryggen area and Walnumfjellet area. (p) Mode of occurrence of Grt-Hbl-Bt gneisss (B08012201I) in Lunckeryggen. (q) Mode of occurrence of Grt-Hbl-Bt gneiss (AC08012304E) in Lunckeryggen. (r) Mode of occurrence of Grt-Bt gneiss (BC08010602J) in the southern part of Walnumfjella. (s) Close-up photograph of (r). (t) Mode of occurrence of Grt-Bt felsic gneiss (BC08010604E) in the northern part of Walnufjella. This rocks is highly mylonitized and contains cm-order porphyroclastic Grt. (u) Mode of occurrence of Grt-Hbl-Bt gneiss (BC08010604A) in the northern part of Walnumfjella.

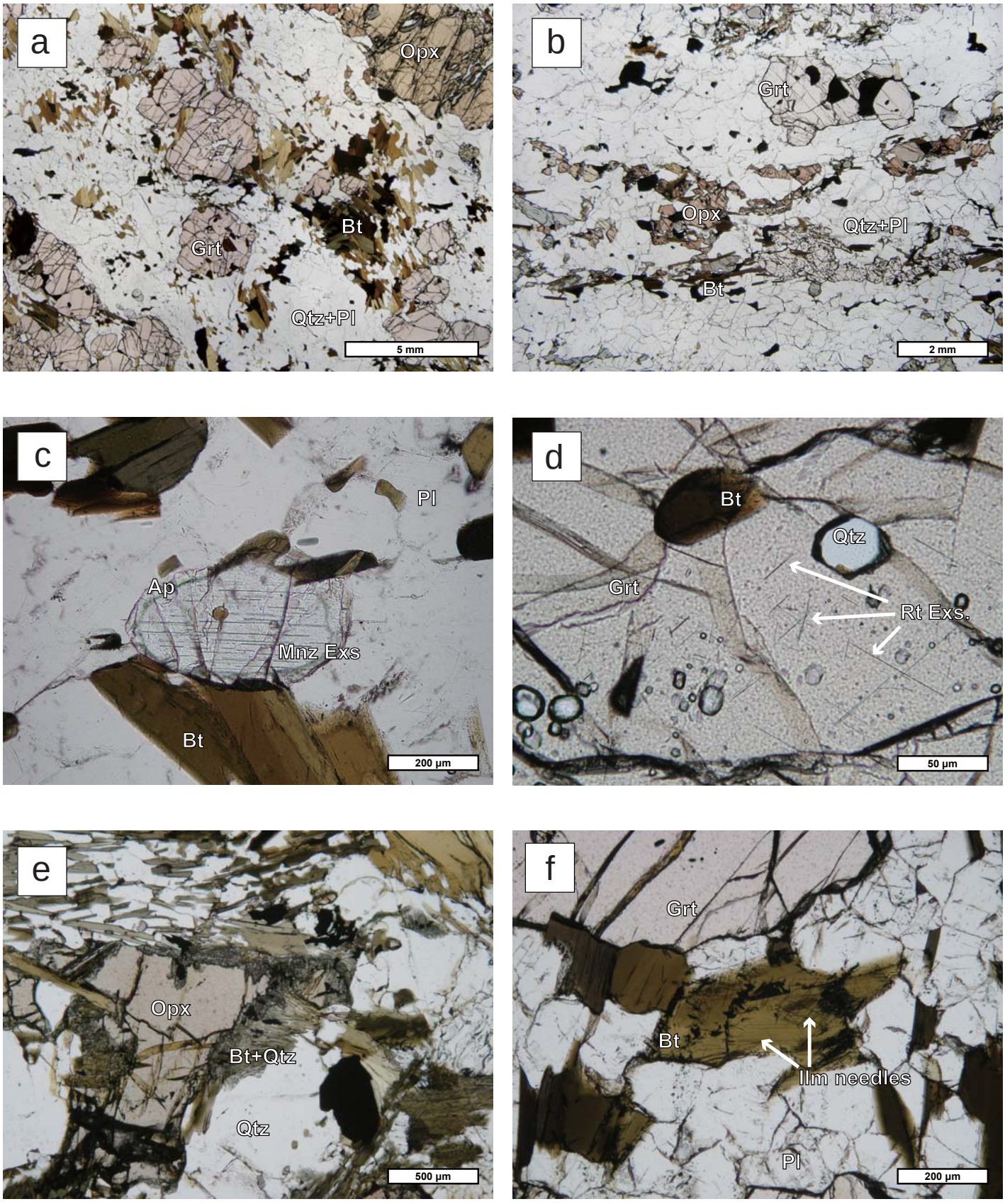

Fig. 3.5. Photomicrographs of metamorphic rocks in Brattnipene area. (a) Texture of Grt-Opx-Bt gneiss (A07123001E). Signature of retrogression is little recognized in this rock. (b) Texture of Grt-Opx-Bt felsic gneiss (A07123001R). (c) Mnz exsolution in Ap of Grt-Opx-Bt gneiss (A07123001E). Mnz needles are oriented in one direction. (d) Rt exsolution in Grt of Grt-Opx-Bt gneiss (A07122602F). Rutile needles areoriented in three directions. (e) Bt+Qtz aggregate replacing Opx (A07123001F). (f) Ilm needles in Bt occuring in matrix (A07123001E).

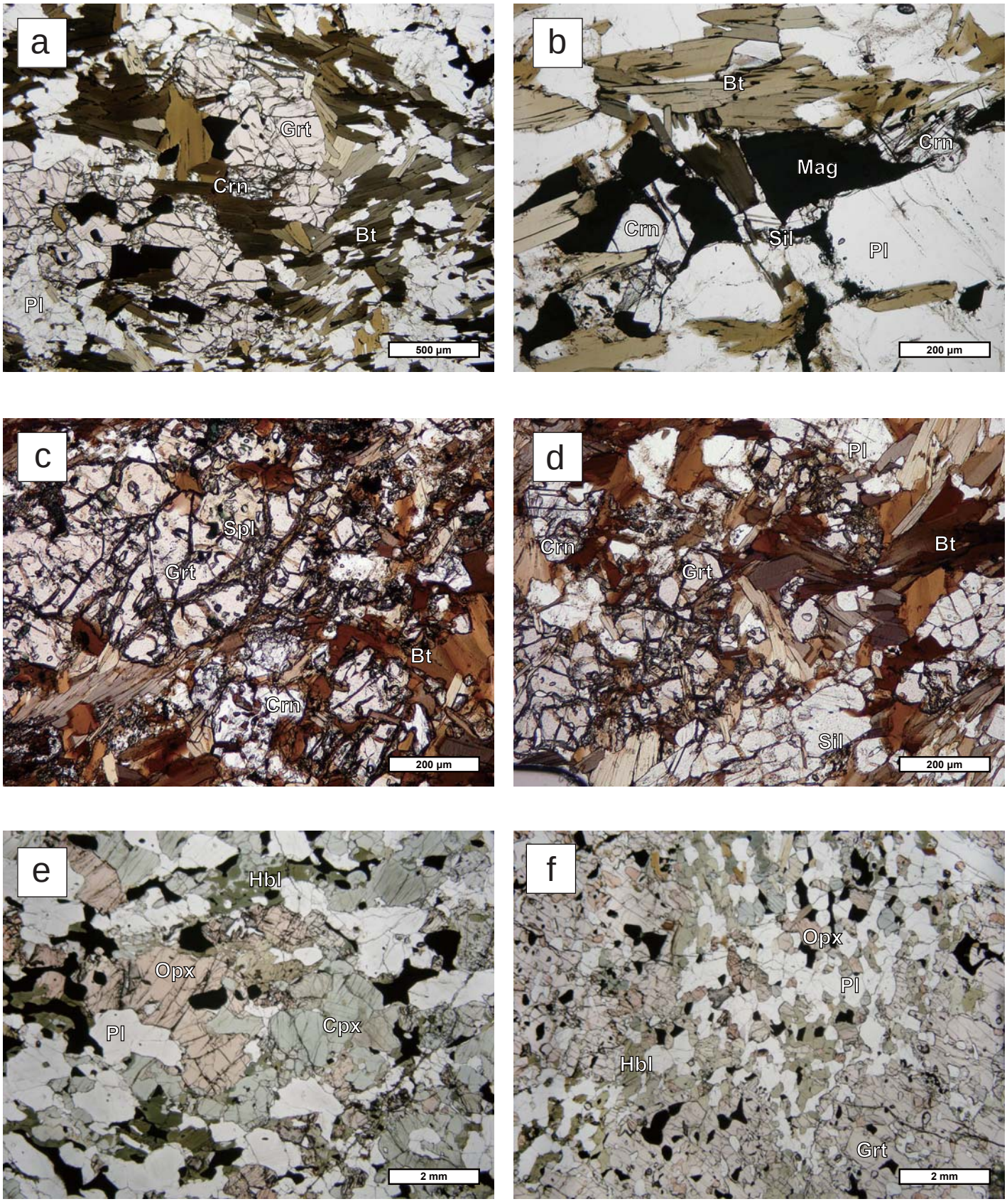

Fig. 3.6. Photomicrographs of metamorphic rocks in Brattnipene area. (a), (b) Texture of Grt-Crn-Bt gneiss (A07123001P). Crn occurs highly associated with Grt. Sil only occurs as inclusion in Grt. (c), (d) Texture of Grt-Crn-Bt gneiss (BC08010302B) in the southern part of Brattnipene. Spl occurs as mainly as inclusions in Grt and Crn. Spl and Sil never have contact with each other. (e), (f) Grt-Sil-Bt gneiss (BC08010302C) in the southern part of Brattnipene. In the highly altered portion in this rock, And occurs associated with clay mineral.

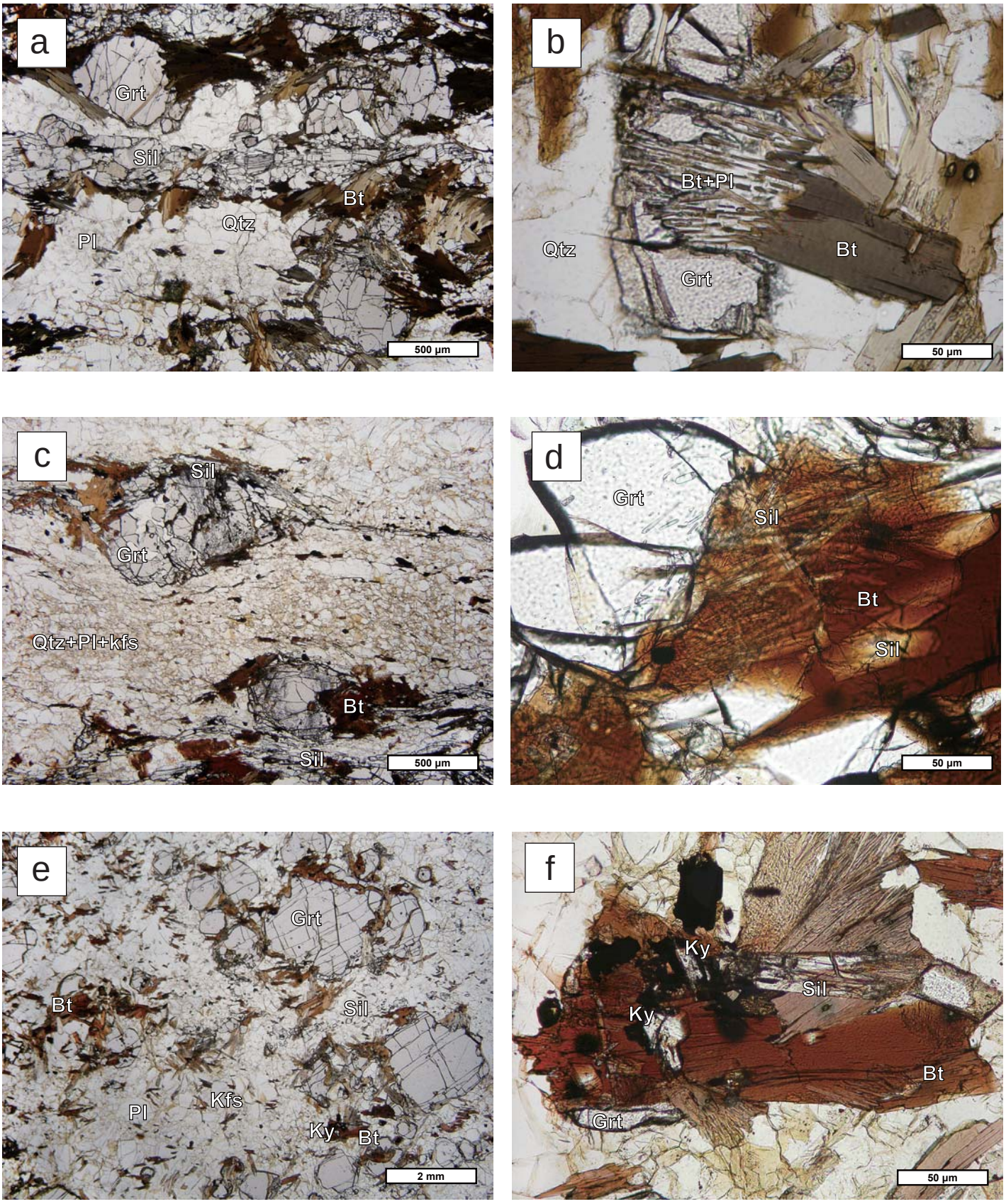

Fig. 3.7. Photomicrographs of Grt-Sil-Bt gneisses in Brattnipene area. (a) Texture of 07120402A. (b) Bt+Pl aggregate replacing the rim of Grt in 07120402A. (c) Texture of BC08010401B. (d) Bt+Sil aggregate replacing the rim of Grt. (e) Texture of 84021904B. (f) Bt+Ky/Sil aggregate replacing the rim of Grt. It is unclear which is the primary phase, kyanite or sillimanite.

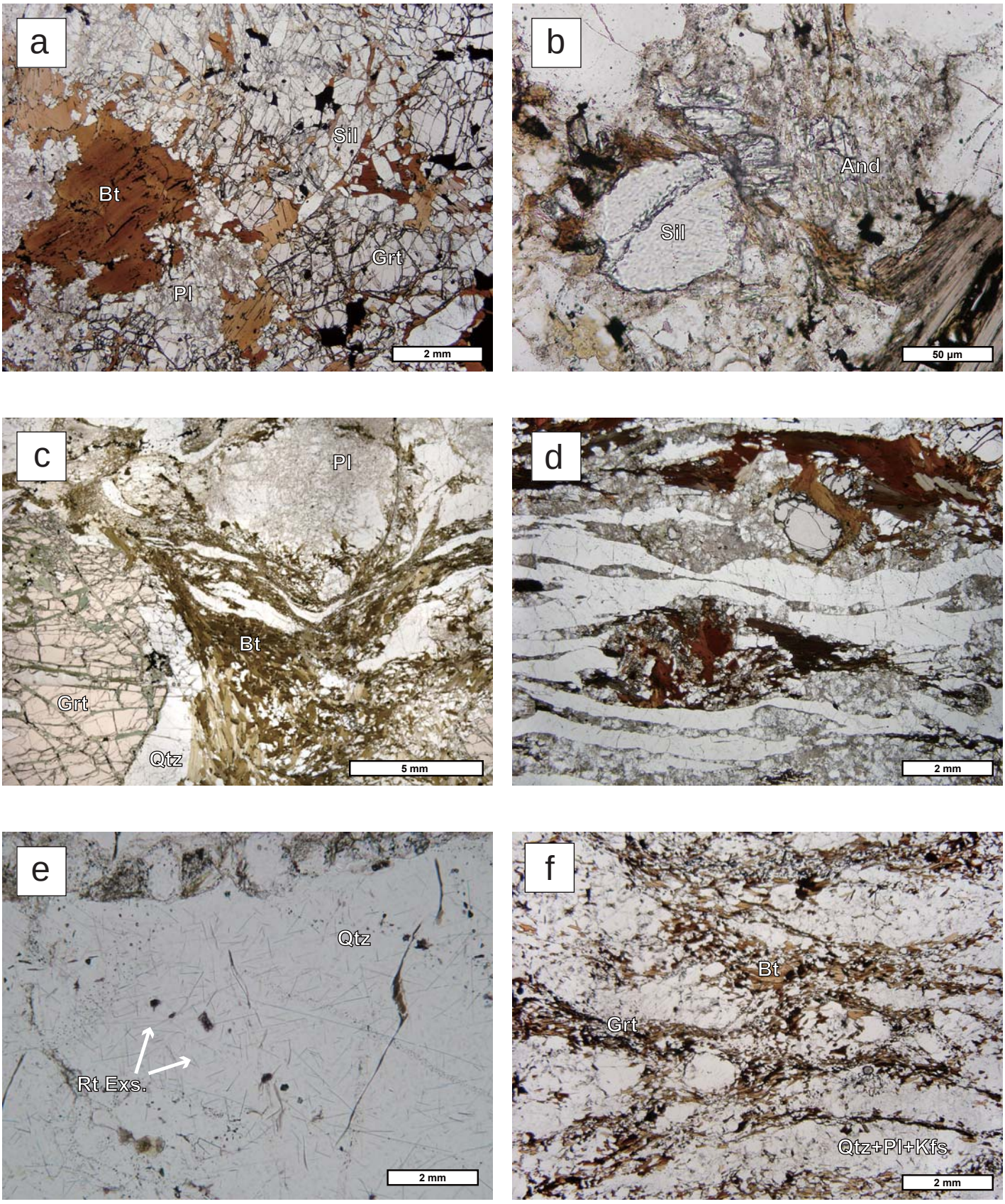

Fig. 3.8. Photomicrographs of metamorphic rocks in Brattnipene area. (a), (b) Grt-Sil-Bt gneiss (BC08010302C) in the southern part of Brattnipene. In the highly altered portion in this rock, And occurs associated with clay mineral. (c) Texture of Grt-Bt gneiss (A07123001AF). This rock is overlain by Opx-bearing lithologies and is highly deformed. (d) Texture of Grt-Bt gneiss (BC08010302A) in the southern part of Brattnipene. The rim of Grt is replaced by Bt+Pl. (e) Rt exsolution in Qtz (BC08010302A). Rt needles are oriented in three directions. (f) Grt-Bt gneiss (BC08010502B) in the southern part of Brattnipene. Porphyloclastic Pl is recognized.

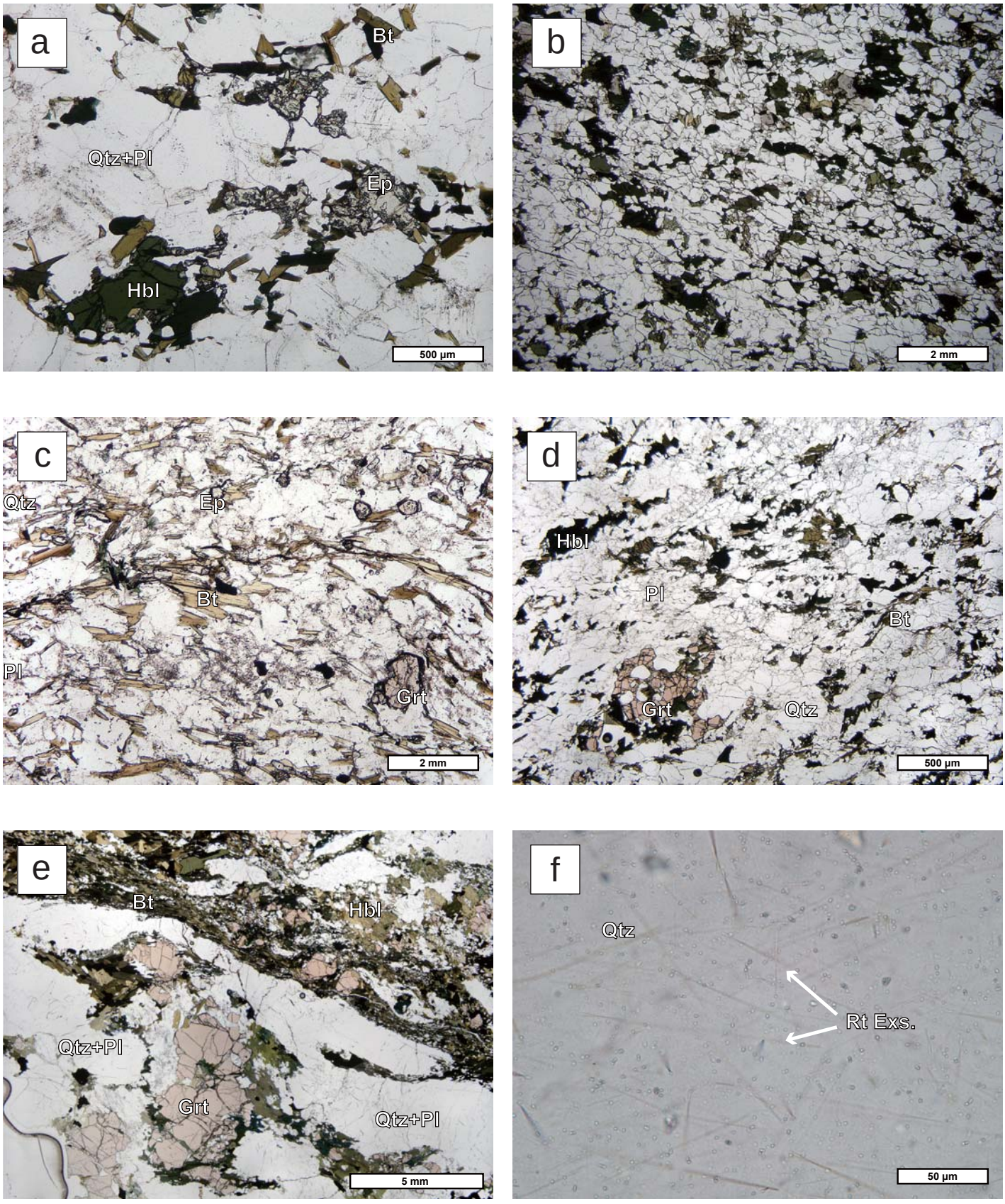

Fig. 3.9. Photomicrographs of metamorphic rocks in Brattnipene area and Walnumfjella area. (a) Texture of Hbl-Ep-Bt gneiss (BC08010504A) in the southern part of Brattnipene. (b) Texture of Hbl-Bt gneiss (A07123001AC). This rock occurs at the same outcrop as A07123001AF (Fig. 3.x (c), (d)). (c) Texture of Grt-Ep-Bt gneiss (BC08010602J). (d) Texture of Grt-Hbl-Bt gneiss (BC08010604A). (e) Texture of Grt-Hbl-Bt gneiss (BC08010604E). This rock shows mylonitic deformation texture. (f) Rt exsolution in Qtz in Grt-Hbl-Bt gneiss (BC08010604E).

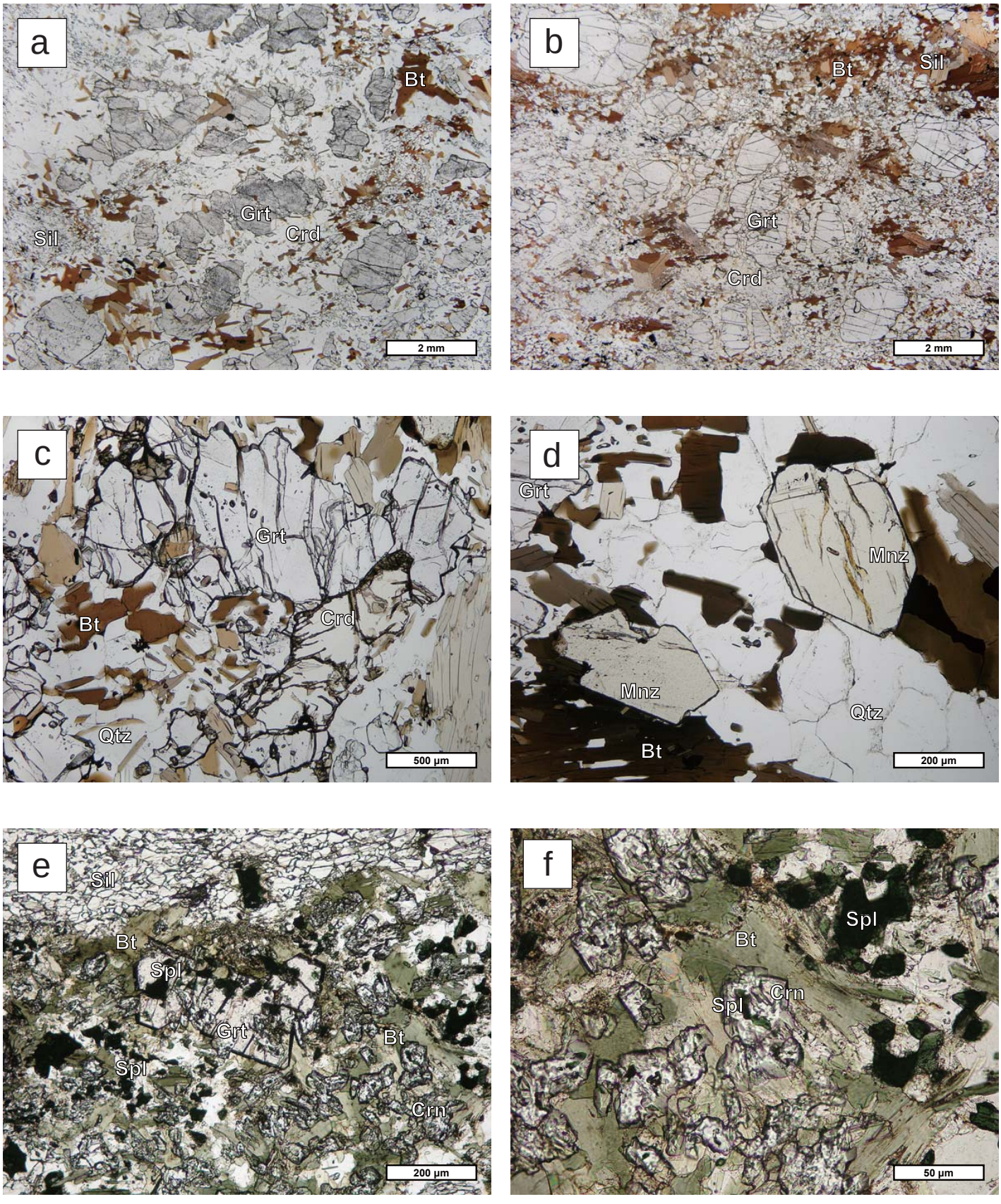

Fig. 3.10. Photomicrographs of metamorphic rocks in Austkampane area. (a) Texture of Grt-Crd-Bt gneiss (AC07121303E). Grt and Sil never have contact with each other. (b) Texture of Grt-Crd-Bt gneiss (AC07121801H). (c) Texture of Grt-Crd-Bt gneiss (AC07121701C). Sil is only observed as inclusion in Grt. (d) Euhedral Mnz in Grt-Crd-Bt gneiss (AC07121701C). (e) Texture of Grt-Crn-Bt gneiss (AC07121702B). Spl and Sil never have contact with each other. (f) Close-up photograph of (e). Spl is observed in Crn and Grt.

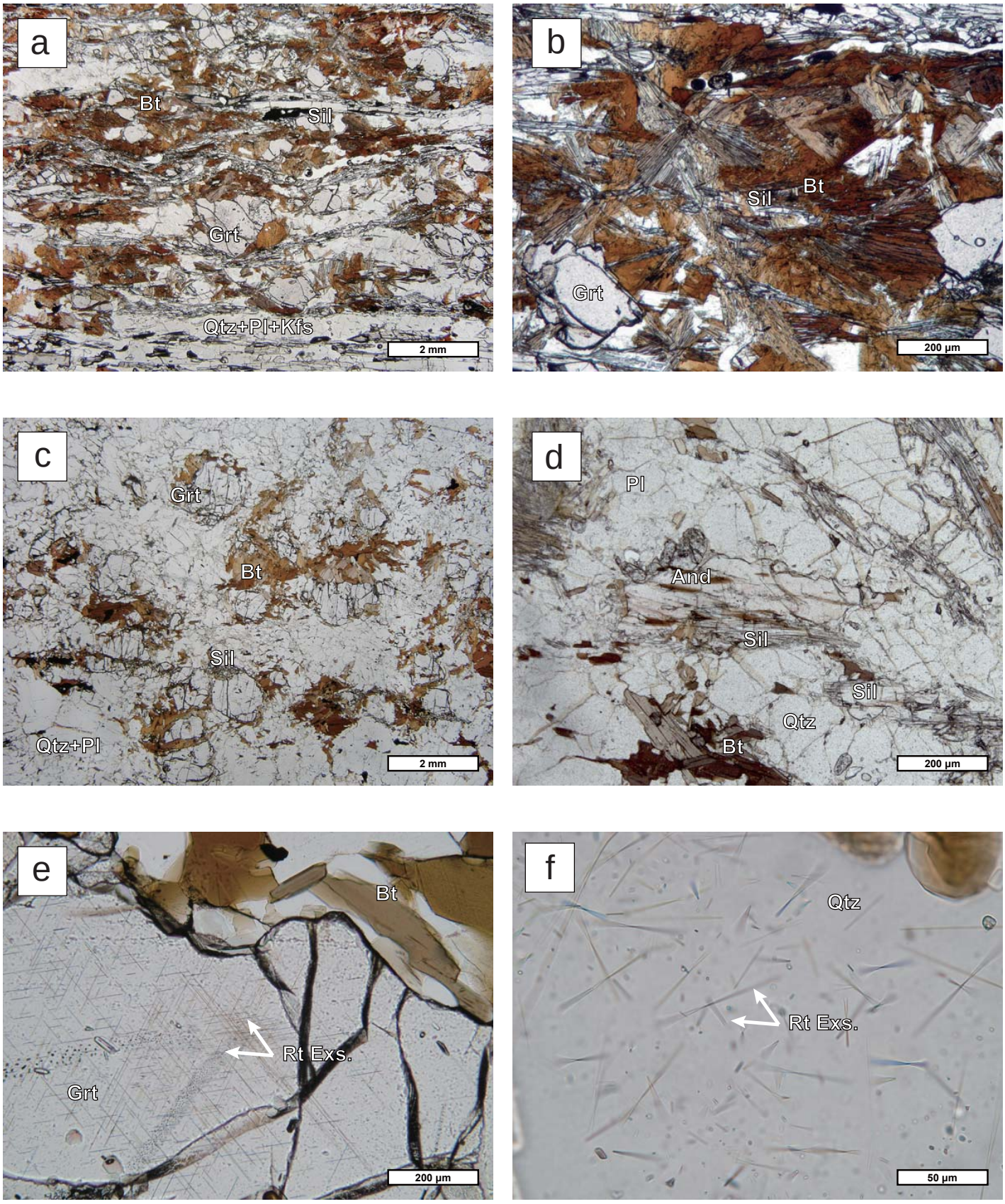

Fig. 3.11. Photomicrographs of metamorphic rocks in Austkampane area. (a) Texture of Grt-Sil-Bt gneiss (AC07121302B). (b) Close-up photograph of (a). The rim of Grt is replaced by random-oriented Bt+Sil. (c) Texture of Grt-Sil-Bt gneiss (BC07122801D) in the southern part of Austkampane. (d) Mode of occurrence of retrograde And in Grt-Sil-Bt gneiss (AC07121302A). (e) Rt exsolution in Grt in Grt-Crd-Bt gneiss (AC07121701C). (f) Rt exsolution in Qtz in Grt in Grt-Crd-Bt gneiss (AC07121701C).

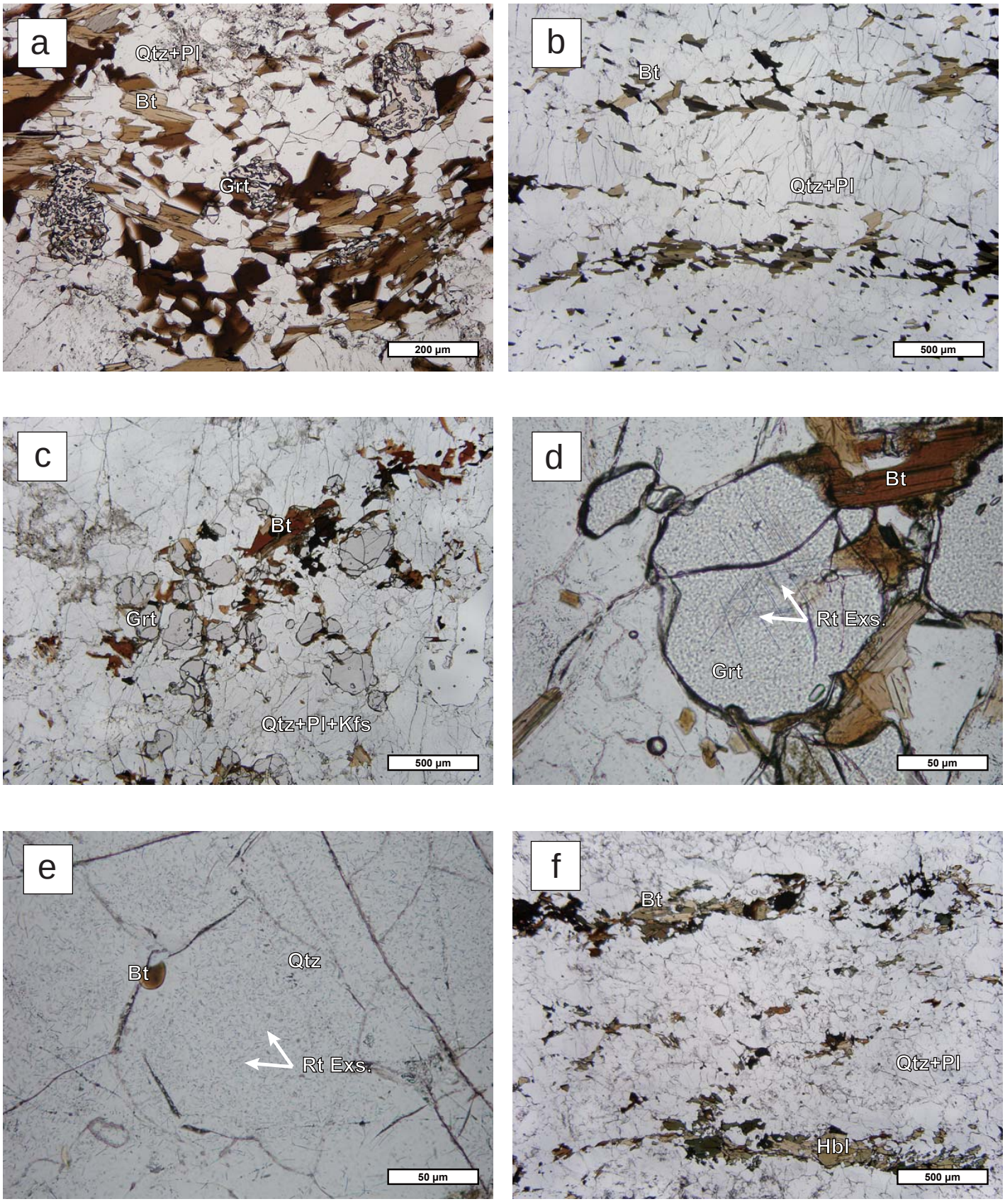

Fig. 3.12. Photomicrographs of metamorphic rocks in Austkampane area and Menipa area. (a) Texture of Grt-Bt gneiss (BC07122805C) in the southern part of Austkampane. Grt in this rock have relatively high Grs content (see text). (b) Texture of Hbl-Bt gneiss (AC07121901A) in the southern part of Austkampane. (d) Texture of Grt-Bt gneiss (AC08011301M) in Menipa area. (d) Rt exsolution in Grt in AC08011301M. Rt needles are oriented in three directions. (e) Rt exsoltion in Qtz in AC0801301M. Tiny Rt needles are oriented in three directions. (f) Texture of Hbl-Bt gneiss (AC07121901A) in Menipa area. Signatures of retrogression are little observed.

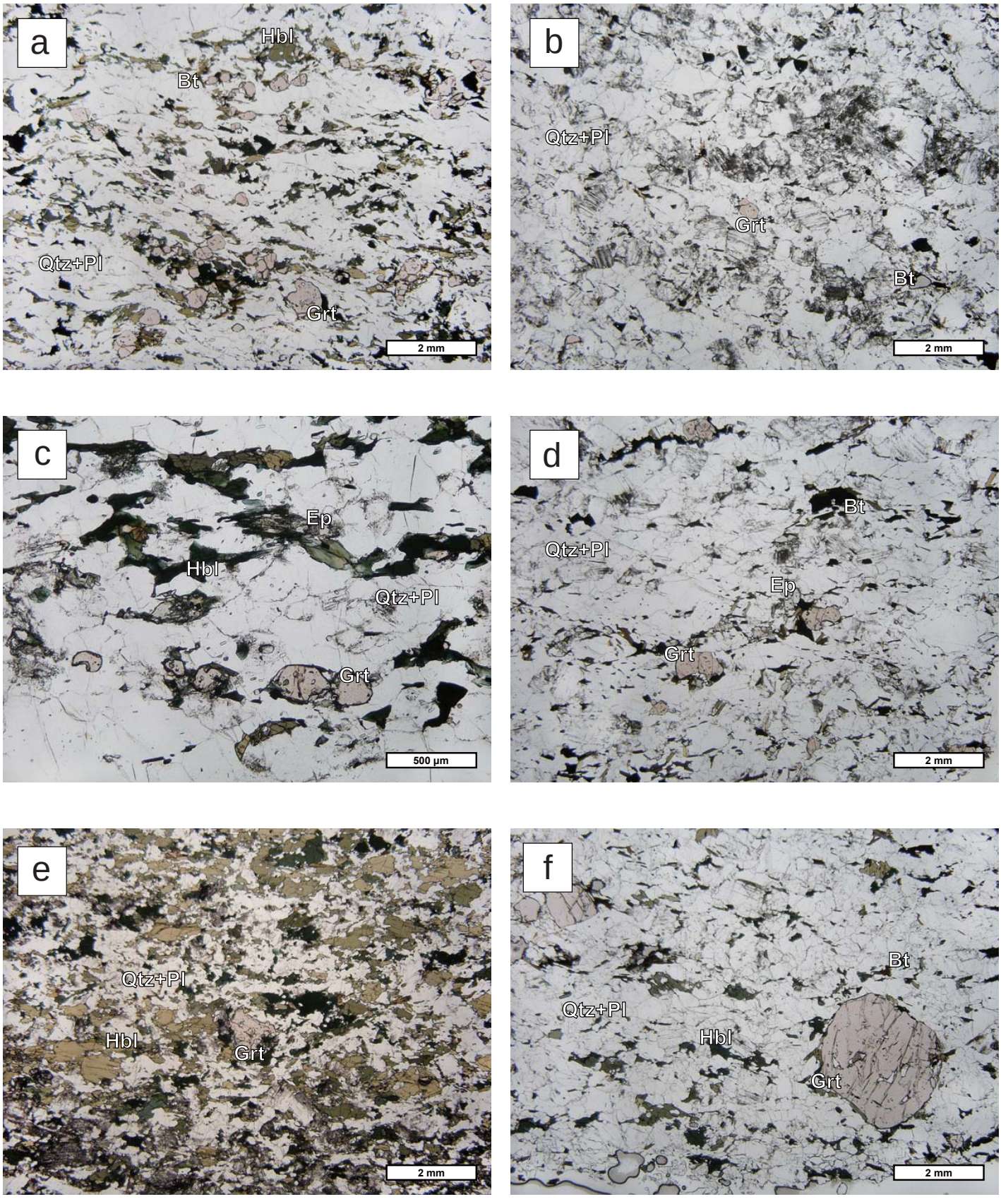

Fig. 3.13. Photomicrographs of metamorphic rocks in Lunckeryggen area. (a) Texture of Grt-Hbl-bt gneiss (B08012201I). (b) Texture of Grt-Bt gneiss (B08012203A). (c) Texture of Grt-Hbl-Ep gneiss (B08012204). (d) Texture of Grt-Ep-Bt gneiss (B08012304C). (e) Texture of Grt-Hbl gneiss (B08012304D). (f) Texture of Grt-Hbl-Bt gneiss (B08012304E).

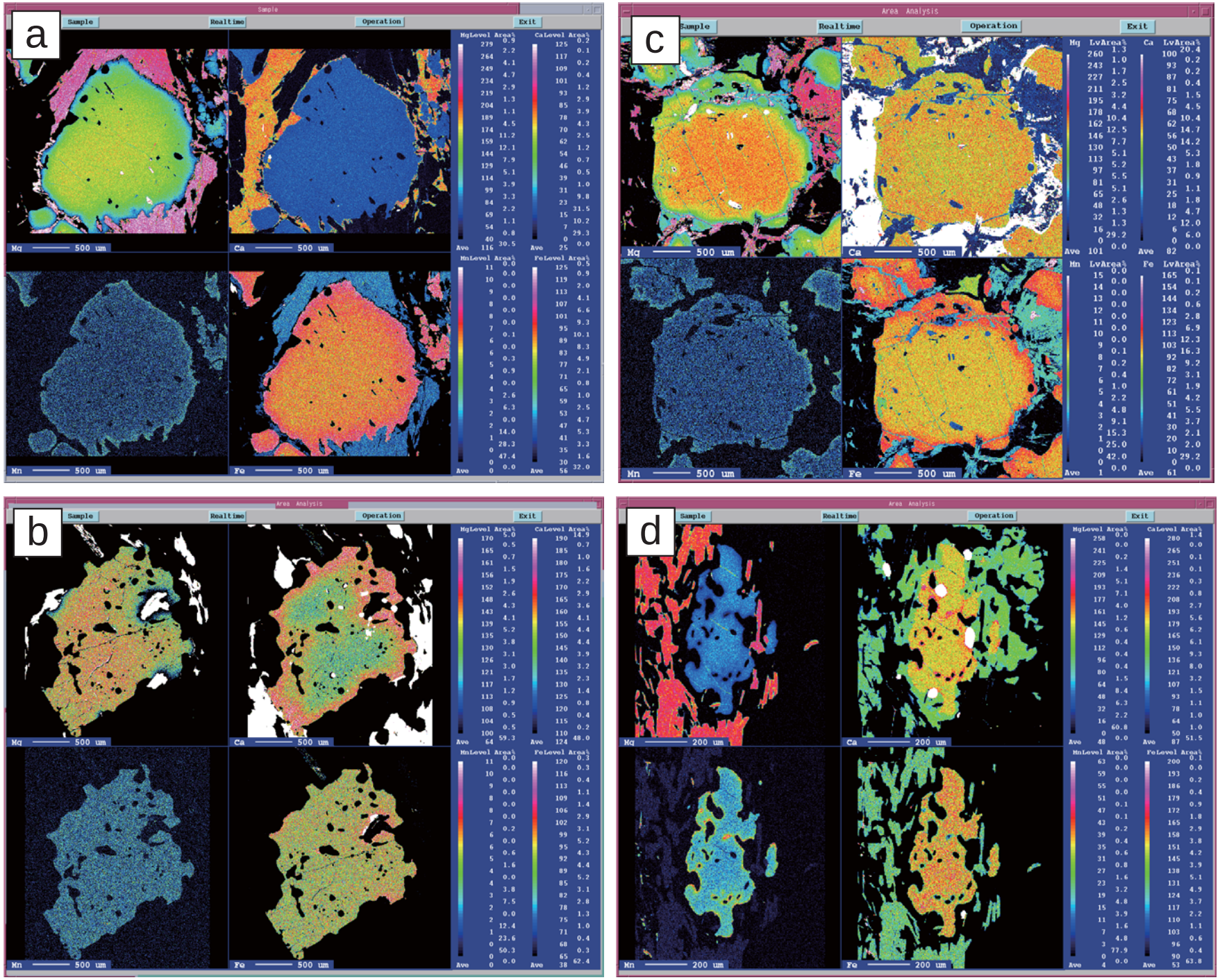

Fig. 3.14. X-ray elemental maps of Grt in the metamorphic rocks in Brattnipene area. (a) Grt of Grt-Sil-Bt gneiss (07120402A). (b) Grt of Grt-Opx-Bt gneiss (A07123001F). Grs content increases at the rim of the grain. (c) Grt of retrograde-Ky bearing Grt-Sil-Bt gneiss (84021905B). (d) Grt of Grt-Bt gneiss (BC08010502B).

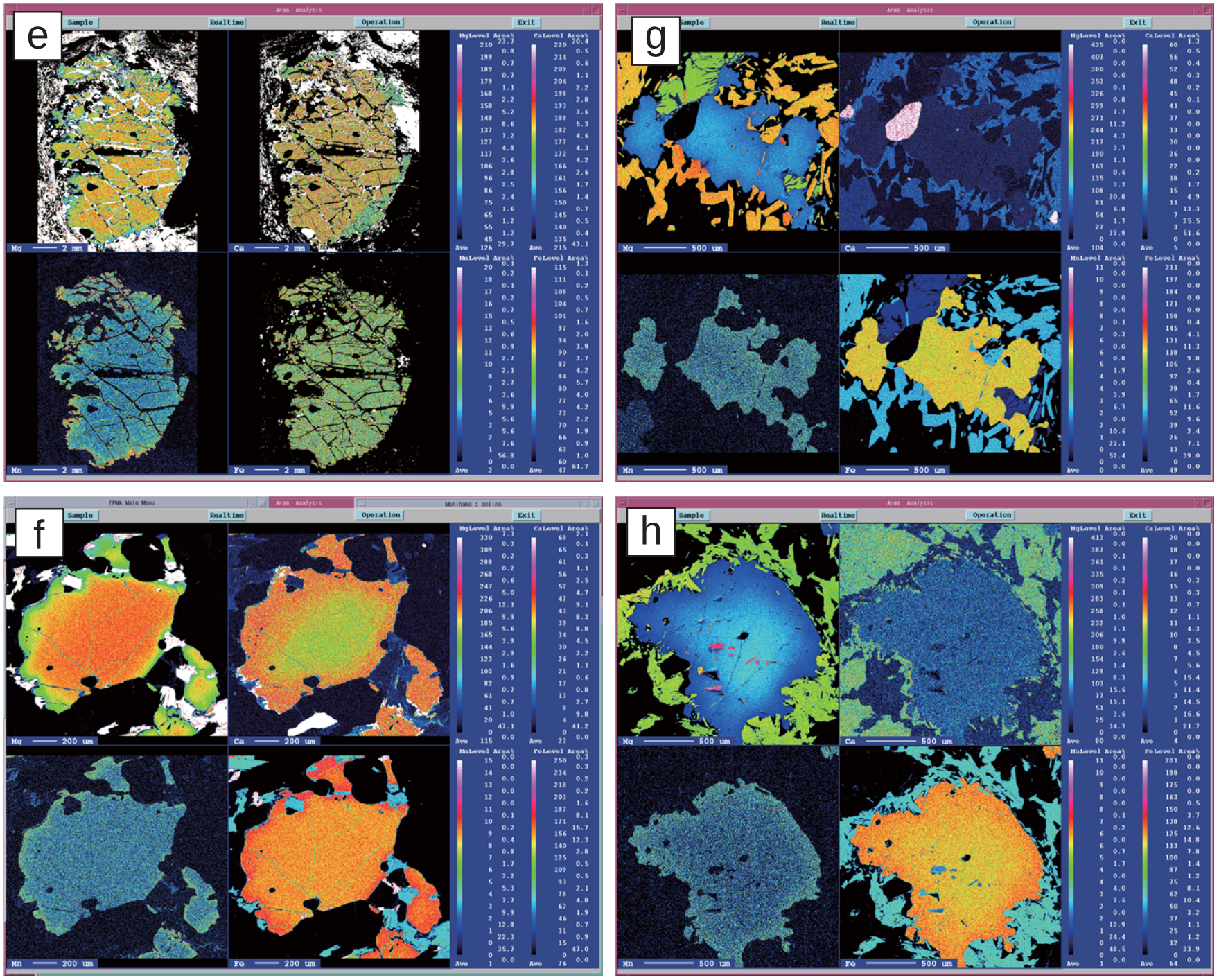

Fig. 3.14, continued. X-ray elemental maps of Grt in the metamorphic rocks. (e) Grt of Grt-Bt gneiss (A07123001AF) in Brattnipene area. (f) Grt of Grt-Bt gneiss (AC08011301M) in Menipa area. Grs content increases at the rim of the grain. (g) Grt of Grt-Crd-Bt gneiss (AC07121701C) in the northern part of Austkampane. (h) Grt of Grt-Sil-Bt gneiss (BC07122801D) in the southern part of Austkampane.

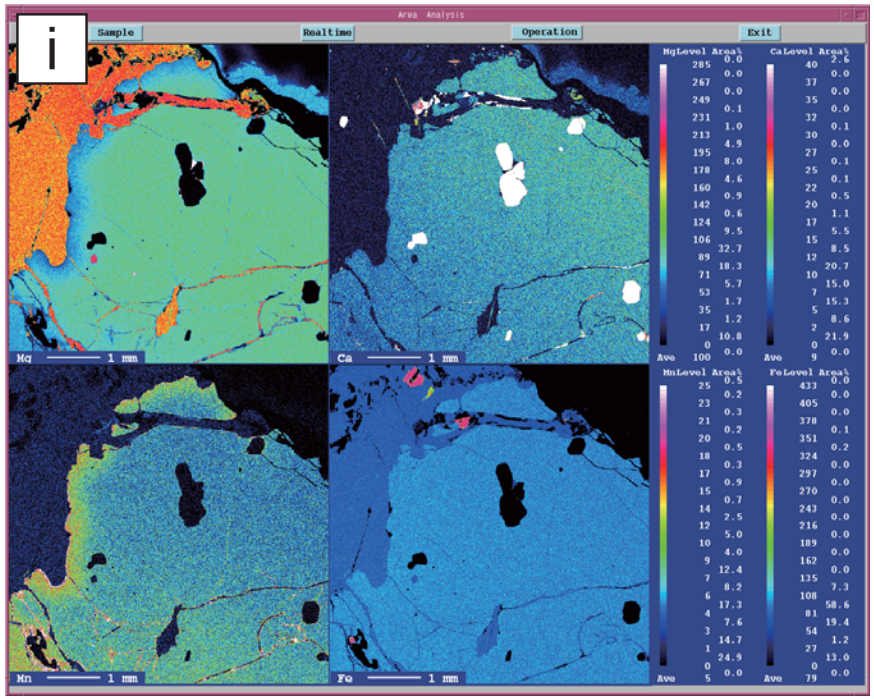

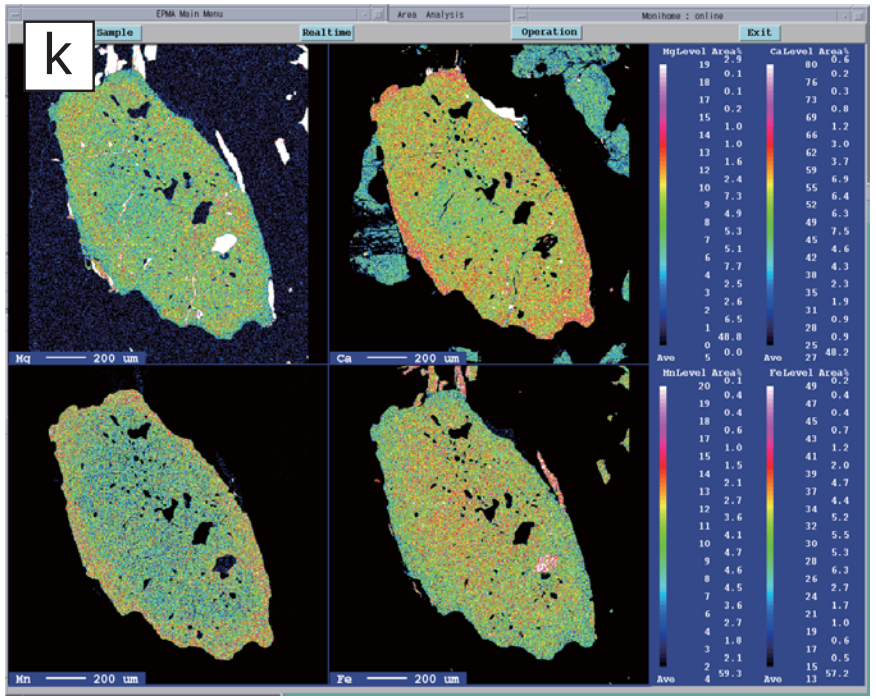

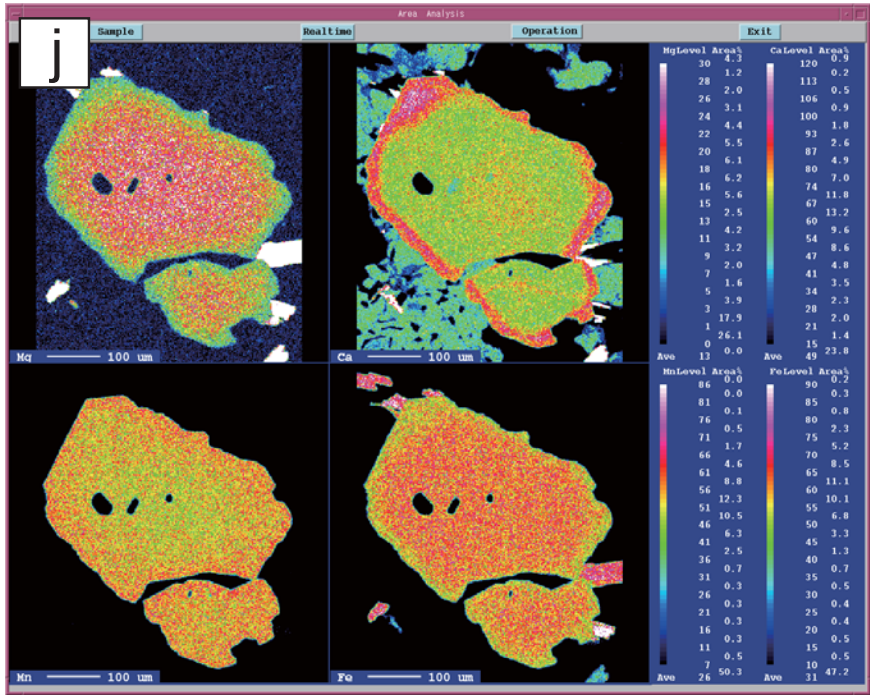

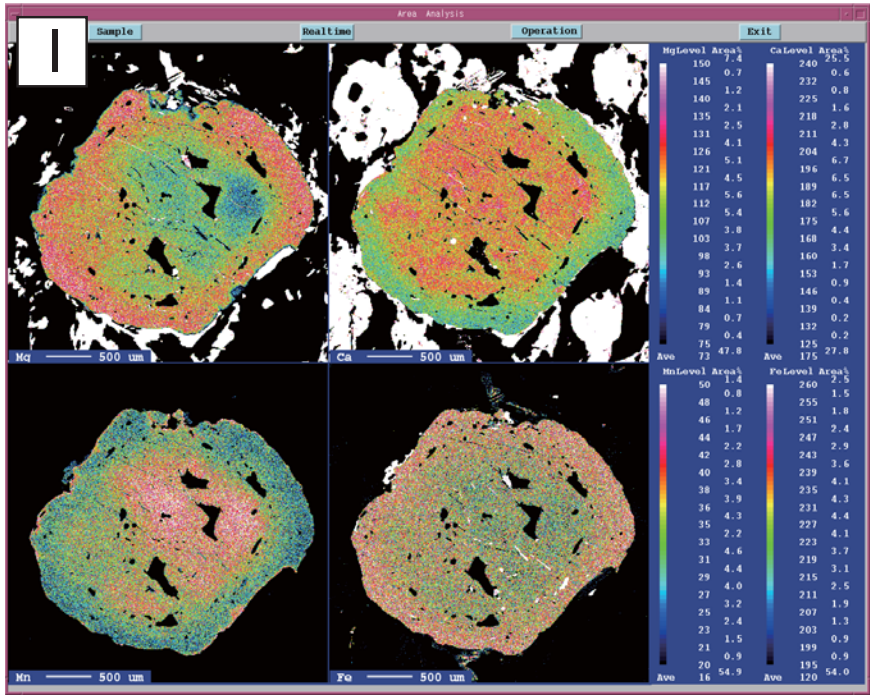

Fig. 3.14, continued. X-ray elemental maps of Grt in the metamorphic rocks. (i) Grt of Grt-Hbl-Bt gneiss (BC08010604E) in the northern part of Walnumfjella. (j) Grt of Grt-Hbl-Bt gneiss (B08012203A) in Lunckeryggen. (k) Grt of Grt-Hbl-Bt gneiss (B08012304C) in Lunckeryggen. (l) Grt of Grt-Hbl-Bt gneiss (BC08012304E) in Lunckeryggen.

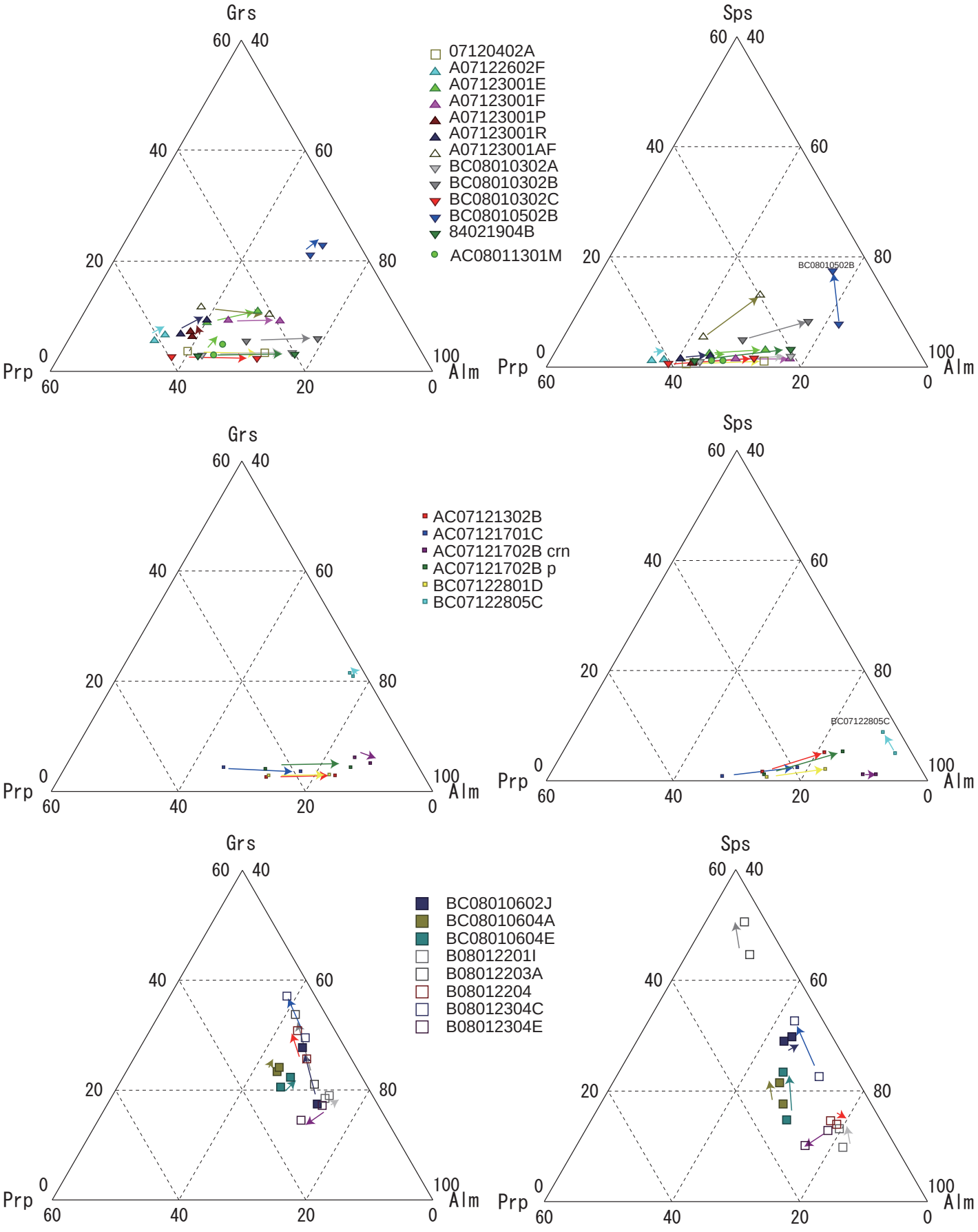

Fig. 3.15. Triangle plots of chemical composition of Grt in felsic and pelitic gneisses in the central Sør Rondane Mountains. Arrows indicate the chemical composition variation from the core to the rim.

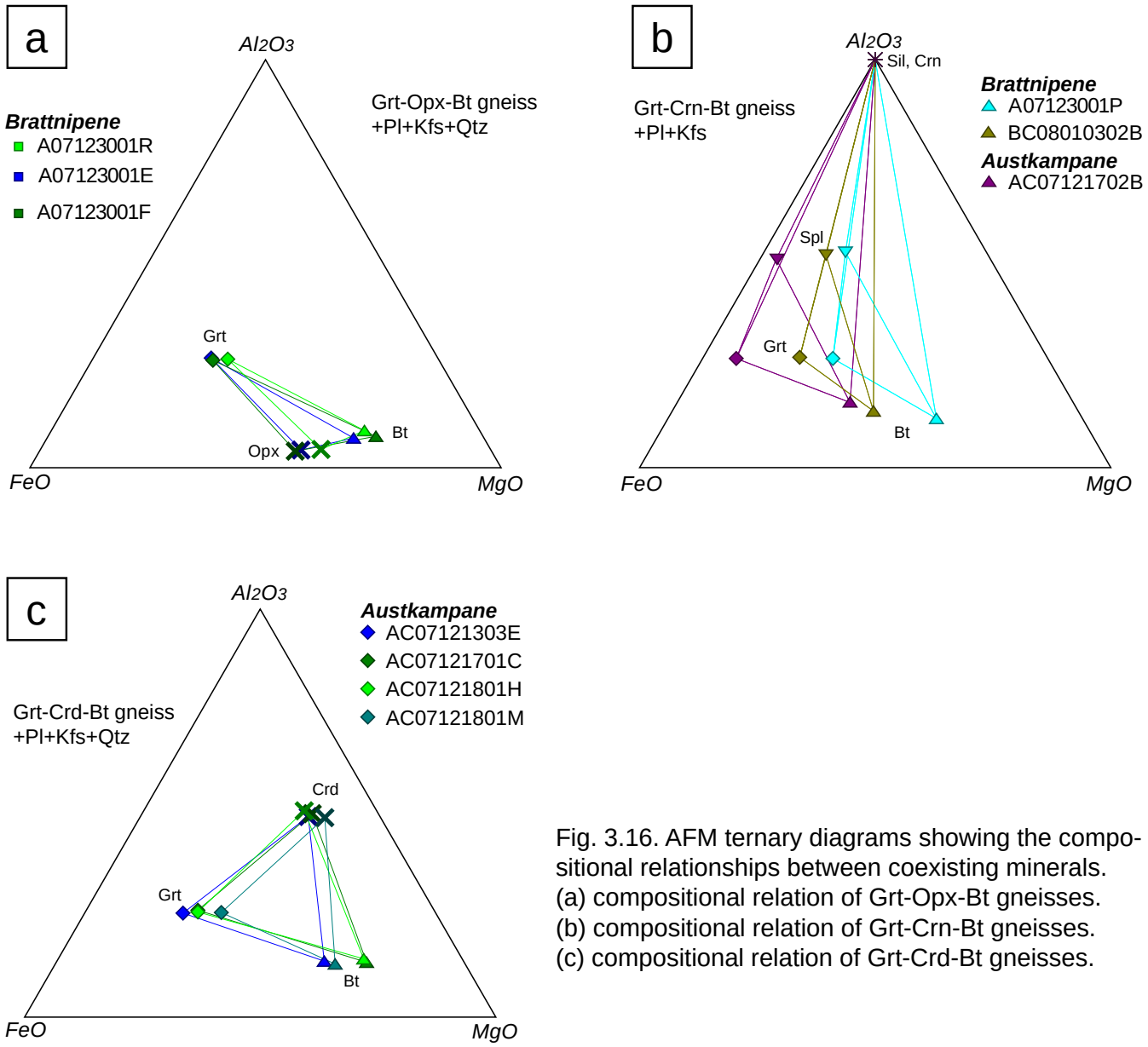

Fig. 3.16. AFM ternary diagrams showing the compositional relationships between coexisting minerals.
(a) compositional relation of Grt-Opx-Bt gneisses.
(b) compositional relation of Grt-Crn-Bt gneisses.
(c) compositional relation of Grt-Crd-Bt gneisses.

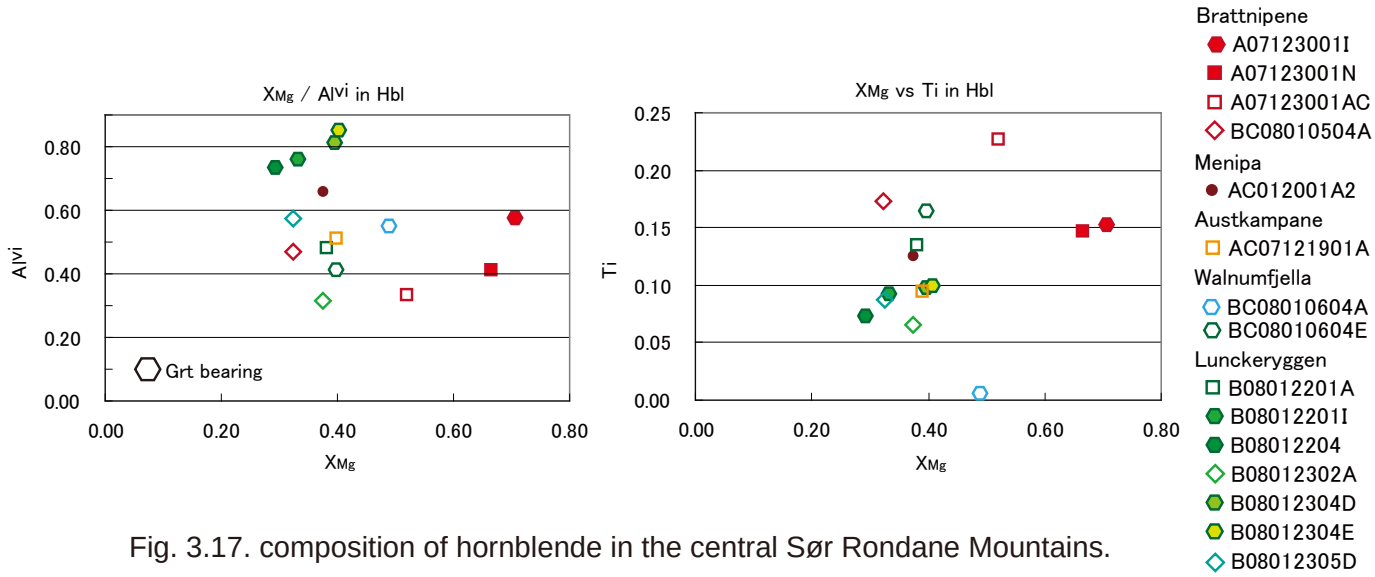

Fig. 3.17. composition of hornblende in the central Sør Rondane Mountains.

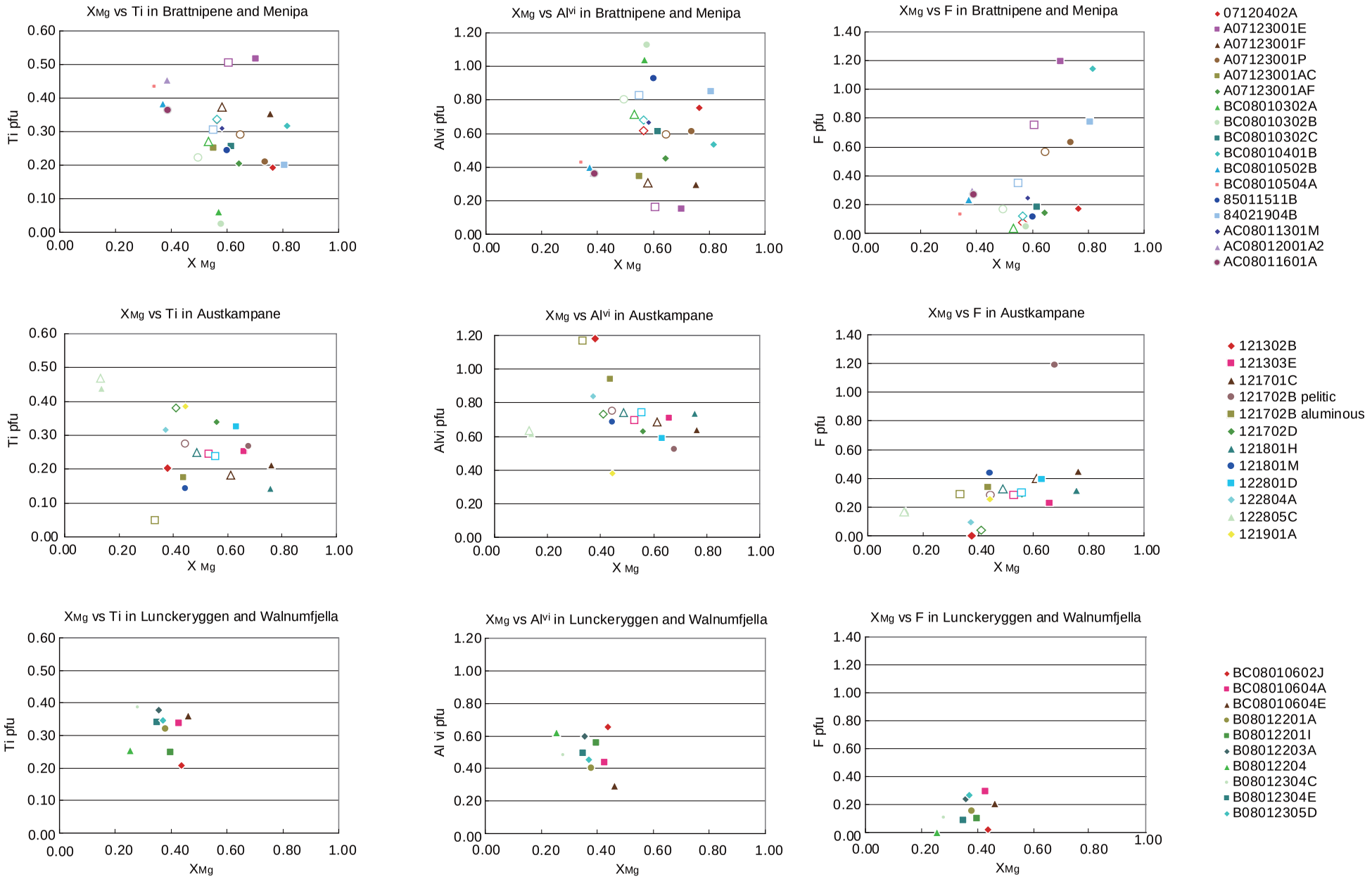

Fig. 3.18. Bt compositions in the central Sør Rondane Mountains in terms of Mg/(Mg+Fe) (X_{Mg}) ratio versus Ti, Al in octahedral site and F per 22-oxygen formula unit. Open-symbols indicate retrograde composition.

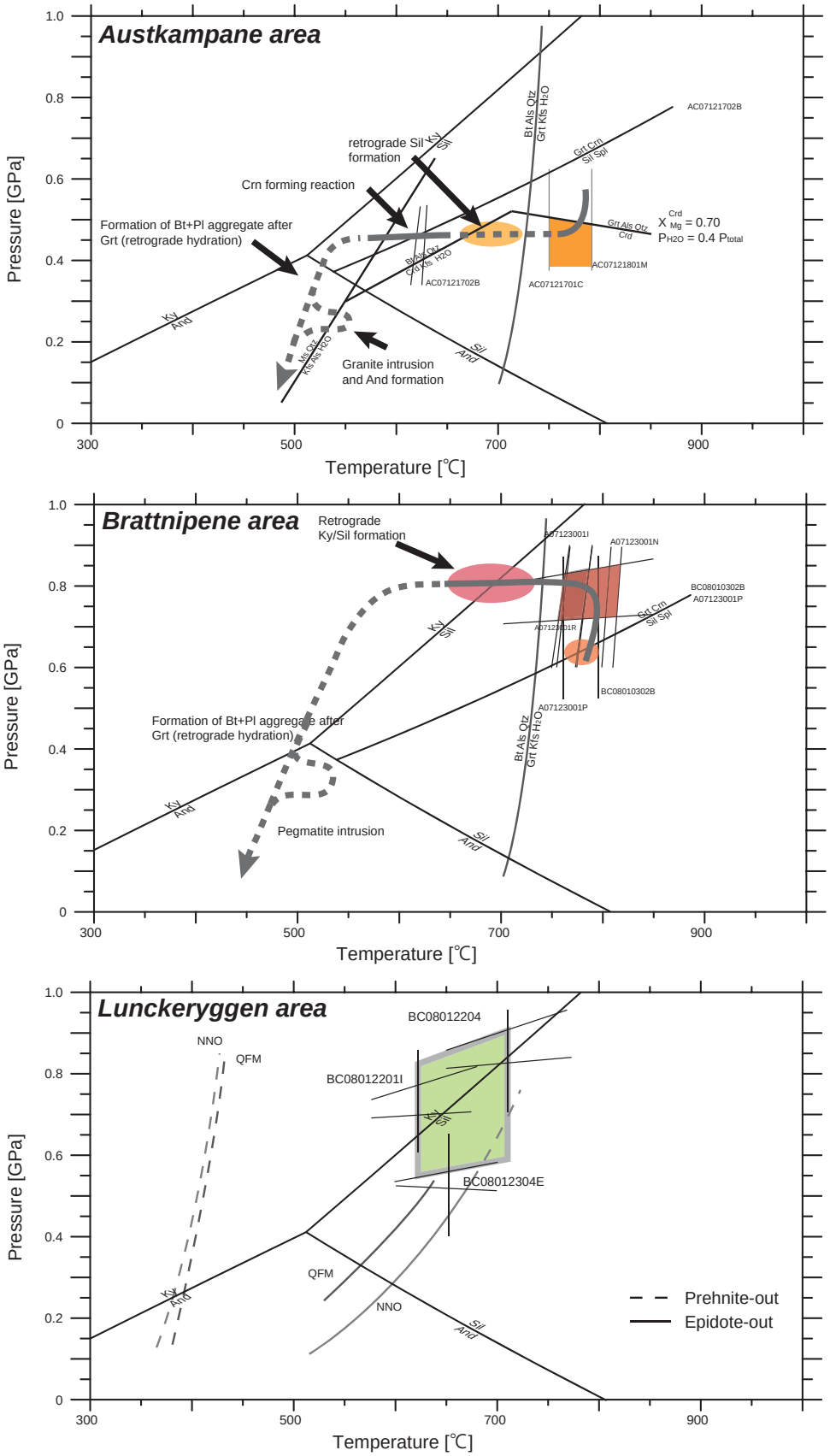

Fig. 3.19. P-T diagram showing P-T paths of the central Sør Rondane Mountains. (a) P-T path of Austkampane area. Crd (X_{Mg}=0.7) forming reactions are after Holdaway&Lee (1977). Crn forming reaction is calcurated after Shulter&Bohlen (1989). Bt dehydration reaction curve is after LeBreton&Thompson (1988). (b) P-T path of Brattnipene area. (c) P-T conditions of Lunchkeryggen. Prh and Ep-outreaction curves are after Liou (1973) and Liou et al. (1983).

Table 3.1. Mineral parageneses and textures of the investigated metamorphic rocks in the central Sør Rondane Mountains.

Area	sample No.	Mineral assemblage	Peak/prograde									Retrograde					Reaction texture	T (°C)	Method
			Grt	Opx	Cpx	Hbl	Bt	Sil	Crd	Ep	Other	And	Bt	Ms	Ep	Other			
Brattnipene	07120402A	Grt-Bt-Sil	○				○	○					○	○			Grt⇒Bt+Pl		
	07121003A	Opx-Cpx-Hbl-Bt		○	○	○	○										Opx+Pl ⇒Hbl+Bt+Qtz	850	OC
	07121003B	Hbl-Bt-Ep											○		○	Hbl		700	HP
	A07123001E	Grt-Opx-Bt	○	○			○											770	GO
	A07123001F	Grt-Opx-Bt	○	○			○												
	A07123001I	Grt-Opx-Hbl	○	○		○												750	GO
	A07123001N	Opx-Cpx-Hbl		○	○	○												810	OC
	A07123001P	Grt-Crn-Bt	○				○	○			Crn,Spl		○				Sil+Spl⇒Grt+Crn		
	A07123001R	Grt-Opx-Bt	○	○			○											750	GO
	A07123001AC	Hbl-Bt				○	○												
	A07123001AF	Grt-Bt	○				○						○				Grt⇒Bt+Pl	770	GB
	BC08010302A	Grt-Bt	○				○						○	○			Grt⇒Bt+Pl		
	BC08010302B	Grt-Crn-Bt	○				○	○			Crn,Spl						Sil+Spl⇒Grt+Crn	780	GB
	BC08010302C	Grt-Bt-Sil	○				○	○			Spl	○	○	○			Grt⇒Bt+Pl		
	BC08010401B	Grt-Bt-Sil	○				○	○					○				Grt⇒Bt+Pl		
	BC08010502B	Grt-Bt	○				○												
	BC08010504A	Hbl-Bt-Ep				○	○			○									
	84021904B	Grt-Bt-Sil	○				○	○			Spl		○			Ky/Sil	Grt⇒Bt+Ky/Sil		
	85011501B	Grt-Bt-Sil	○				○	○					○			Ky/Sil	Grt⇒Bt+Ky/Sil		
Menipa	AC08011301M	Grt-Bt	○				○											750	GB
	AC08011601A	Hbl-Bt				○	○												
	AC08012001A	Hbl-Bt				○	○											620	HP
Austkampane	AC07121302B	Grt-Bt-Sil	○				○	○			Spl		○	○			Grt⇒Bt+Sil		
	AC07121303E	Grt-Crd-Bt	○				○	○								Crd	Grt+Sil+Bt⇒Crd		
	AC07121701C	Grt-Crd-Bt	○				○		○		Spl							760	GCrd
	AC07121702B	Grt-Bt, Grt-Crn-Bt	○				○	○			Crn,Spl		○	○			Sil+Spl⇒Grt+Crn Grt⇒Bt+Pl	550	GB
	AC07121801H	Grt-Crd-Bt	○				○	○			Spl					Crd	Grt+Sil+Bt⇒Crd		
	AC07121801M	Grt-Crd-Oam	○				○		○		Oam							780	GCrd
	BC07122801C	Grt-Bt	○				○						○	○			Grt⇒Bt+Pl		
	BC07122801D	Grt-Bt-Sil	○				○	○			Spl		○	○			Grt⇒Bt+Pl	550	GB
	BC07122804A	Grt-Bt-Sil	○				○	○						○			Grt⇒Bt+Sil		
	BC07122805C	Grt-Bt	○				○												
	BC07122903A	Grt-Bt	○				○						○	○			Grt⇒Bt+Pl		
	AC07121901A	Hbl-Bt				○	○			○								700	HP
Walnumfjella	BC08010602J	Grt-Bt	○				○												
	BC08010604A	Grt-Hbl-Bt	○			○	○												
	BC08010604E	Grt-Hbl-Bt	○			○	○										Grt⇒Bt+Pl	610	GH
Lunckeryggen	B08012201I	Grt-Hbl-Bt	○			○	○											660-550	GH
	B08012203A	Grt-Bt	○				○												
	B08012204	Grt-Hbl-Bt	○			○	○			○								710-650	GH
	B08012302A	Hbl-Bt				○	○			○									
	B08012304C	Grt-Hbl-Bt	○			○	○			○									
	B08012304D	Grt-Hbl-Bt	○			○	○												
	B08012304E	Grt-Hbl-Bt	○			○	○											650-590	GH

T GB:Grt-Bt thermometer (Holldaway, 2000), GCrd: Grt-Crd thermometer (Perchuk&Lavrent'eva, 1983), GO: Grt-Opx thermomete

Table 3.2. Representative chemical composition of garnet in the central Sør Rondane Mountains.

Sample No.	AC07121302B	AC07121302B	AC07121303E	AC07121303E	AC07121701C	AC07121701C	AC07121702B p	AC07121702B p	AC07121702B a	AC07121702D	AC07121702D	AC07121801H	AC07121801H
Occurrence	core	rim	core	rim	core	rim	core	rim	core	core	rim	core	rim
Analysis No.	96	98	2	6	73	75	21	24	62	25	29	41	44
SiO_2	39.36	38.67	39.47	38.73	39.63	39.36	39.60	38.65	37.51	38.80	38.33	39.90	38.96
TiO_2	0.00	0.05	0.02	0.00	0.07	0.03	0.00	0.04	0.06	0.04	0.08	0.09	0.02
Al2O3	22.48	22.09	22.13	21.62	22.16	22.17	21.94	21.37	21.63	21.97	21.60	22.37	21.58
Cr_2O_3	0.00	0.01	0.02	0.03	0.04	0.08	0.07	0.00	0.03	0.00	0.01	0.00	0.01
FeO	33.09	34.81	32.79	36.04	29.88	34.23	32.78	36.27	37.69	35.17	38.99	30.84	35.47
MnO	0.74	2.16	0.40	0.67	0.37	1.04	0.66	2.26	0.46	0.34	0.70	0.88	1.73
MgO	6.35	3.23	7.11	3.96	7.93	4.69	6.07	2.63	2.26	5.09	2.74	8.22	3.12
CaO	0.93	0.93	0.86	1.39	1.54	1.23	1.35	1.51	1.99	1.02	0.79	0.92	1.21
Na_2O	0.05	0.00	0.03	0.01	0.00	0.04	0.01	0.02	0.01	0.00	0.01	0.00	0.00
K_2O	0.00	0.00	0.00	0.03	0.01	0.02	0.01	0.03	0.02	0.00	0.02	0.00	0.03
Total	103.00	101.95	102.82	102.47	101.62	102.88	102.56	102.78	101.66	102.43	103.26	103.23	102.14
Si	3.00	3.03	3.01	3.02	3.02	3.03	3.03	3.03	2.98	3.01	3.00	3.01	3.05
Ti	0.00	0.00	0.00	0.00	0.00	0.00	0.00	0.00	0.00	0.00	0.00	0.01	0.00
Al	2.02	2.04	1.99	1.99	1.99	2.01	1.98	1.98	2.03	2.01	2.00	1.99	1.99
Cr	0.00	0.00	0.00	0.00	0.00	0.00	0.00	0.00	0.00	0.00	0.00	0.00	0.00
Fe	2.11	2.28	2.09	2.35	1.91	2.20	2.10	2.38	2.51	2.28	2.56	1.94	2.32
Mn	0.05	0.14	0.03	0.04	0.02	0.07	0.04	0.15	0.03	0.02	0.05	0.06	0.11
Mg	0.72	0.38	0.81	0.46	0.90	0.54	0.69	0.31	0.27	0.59	0.32	0.92	0.36
Ca	0.08	0.08	0.07	0.12	0.13	0.10	0.11	0.13	0.17	0.08	0.07	0.07	0.10
Na	0.01	0.00	0.00	0.00	0.00	0.01	0.00	0.00	0.00	0.00	0.00	0.00	0.00
K	0.00	0.00	0.00	0.00	0.00	0.00	0.00	0.00	0.00	0.00	0.00	0.00	0.00
Total	7.99	7.95	8.00	7.99	7.98	7.97	7.97	7.98	8.00	7.99	7.99	8.00	7.95
XMg	0.25	0.14	0.28	0.16	0.32	0.20	0.25	0.11	0.10	0.21	0.11	0.32	0.14
Alm	0.71	0.79	0.70	0.79	0.64	0.76	0.71	0.80	0.84	0.77	0.86	0.65	0.80
Sps	0.02	0.05	0.01	0.01	0.01	0.02	0.01	0.05	0.01	0.01	0.02	0.02	0.04
Prp	0.24	0.13	0.27	0.15	0.30	0.18	0.24	0.10	0.09	0.20	0.11	0.31	0.13
Grs	0.03	0.03	0.02	0.04	0.04	0.03	0.04	0.04	0.06	0.03	0.02	0.02	0.03

Table 3.2. Continued

Sample No.	AC07121801M	AC07121801M	BC07122801D	BC07122801D	BC07122804A	BC07122804A	BC07122805C	BC07122805C	07120402A	07120402A	A07123001E	A07123001E	A07123001F
Occurrence	core	rim	core	rim	core	rim	core	rim	core	rim	core	rim	core
Analysis No.	1	4	80	81	53	88	25	27	15	30	18	23	64
SiO_2	40.43	40.00	39.75	39.11	39.02	38.03	38.95	38.78	39.94	38.79	40.10	39.06	39.54
TiO_2	0.00	0.06	0.00	0.00	0.10	0.02	0.02	0.02	0.02	0.03	0.02	0.05	0.04
Al2O3	22.51	22.07	22.14	21.70	22.42	21.78	21.00	21.12	22.77	21.17	22.62	22.34	22.04
Cr_2O_3	0.05	0.03	0.02	0.01	0.00	0.00	0.00	0.02	0.05	0.05	–	0.03	0.00
FeO	28.23	31.61	33.93	35.84	32.13	35.96	33.98	31.43	28.03	34.77	28.42	30.85	28.21
MnO	0.63	1.07	0.28	0.88	0.50	2.43	2.04	3.64	0.28	1.57	0.95	1.32	0.51
MgO	10.09	6.34	6.35	3.60	6.74	2.13	0.58	0.46	9.59	3.71	8.32	5.68	8.47
CaO	0.90	1.25	1.06	1.03	1.37	1.52	7.03	7.06	1.28	1.34	3.02	3.88	2.99
Na_2O	0.00	0.00	0.00	0.00	0.04	0.00	0.02	0.03	0.00	–	–	0.02	0.05
K_2O	0.00	0.01	0.00	0.00	0.00	0.00	0.00	0.01	–	0.02	–	–	0.02
Total	102.85	102.44	103.53	102.18	102.31	101.87	103.62	102.58	101.96	101.45	103.54	103.30	101.85
Si	3.02	3.05	3.02	3.05	2.99	3.01	3.04	3.05	3.00	3.05	3.00	2.98	3.00
Ti	0.00	0.00	0.00	0.00	0.01	0.00	0.00	0.00	0.00	0.00	0.00	0.00	0.00
Al	1.98	1.98	1.98	2.00	2.02	2.03	1.93	1.96	2.02	1.96	1.99	2.01	1.97
Cr	0.00	0.00	0.00	0.00	0.00	0.00	0.00	0.00	0.00	0.00	0.00	0.00	0.00
Fe	1.76	2.02	2.16	2.34	2.06	2.38	2.22	2.07	1.76	2.29	1.78	1.97	1.79
Mn	0.04	0.07	0.02	0.06	0.03	0.16	0.14	0.24	0.02	0.10	0.06	0.09	0.03
Mg	1.12	0.72	0.72	0.42	0.77	0.25	0.07	0.05	1.07	0.44	0.93	0.65	0.96
Ca	0.07	0.10	0.09	0.09	0.11	0.13	0.59	0.60	0.10	0.11	0.24	0.32	0.24
Na	0.00	0.00	0.00	0.00	0.01	0.00	0.00	0.00	0.00	0.00	0.00	0.00	0.01
K	0.00	0.00	0.00	0.00	0.00	0.00	0.00	0.00	0.00	0.00	0.00	0.00	0.00
Total	7.99	7.95	7.99	7.95	8.00	7.97	7.99	7.97	7.99	7.96	8.00	8.01	8.01
XMg	0.39	0.26	0.25	0.15	0.27	0.10	0.03	0.03	0.38	0.16	0.34	0.25	0.35
Alm	0.59	0.69	0.72	0.81	0.69	0.81	0.74	0.70	0.60	0.78	0.59	0.65	0.59
Sps	0.01	0.02	0.01	0.02	0.01	0.06	0.04	0.08	0.01	0.04	0.02	0.03	0.01
Prp	0.37	0.25	0.24	0.14	0.26	0.09	0.02	0.02	0.36	0.15	0.31	0.21	0.32
Grs	0.02	0.04	0.03	0.03	0.04	0.04	0.20	0.20	0.03	0.04	0.08	0.11	0.08

Table 3.2. Continued

Sample No.	A07123001F	A07123001I	A07123001I	A07123001P	A07123001R	A07123001R	A07123001AF	A07123001AF	BC08010302A	BC08010302A	BC08010302B	BC08010302B	BC08010302C
Occurrence	rim	core	rim	core	core	rim	core	rim	core	rim	core	rim	core
Analysis No.	15	107	123	70	20	13	59	63	73	59	52	53	23
SiO_2	38.63	40.33	40.12	40.05	39.50	40.11	38.95	38.46	39.07	37.66	39.75	38.90	39.96
TiO_2	0.05	0.00	0.00	0.02	0.01	0.02	0.05	0.00	0.01	0.01	0.08	0.00	0.00
Al2O3	21.07	22.47	22.80	22.96	22.39	22.02	21.33	20.62	22.48	21.37	22.41	22.21	22.09
Cr_2O_3	0.04	0.08	0.00	0.00	0.04	0.05	0.01	0.00	0.19	0.02	0.02	0.07	0.06
FeO	33.25	24.51	25.39	27.51	26.46	28.02	25.92	28.42	29.21	34.80	30.64	33.06	28.23
MnO	0.81	1.64	1.50	0.38	0.77	0.85	2.52	5.66	0.51	1.96	2.26	3.58	0.50
MgO	4.53	9.40	8.67	9.34	9.56	8.08	7.64	4.61	9.00	3.63	6.69	3.51	10.58
CaO	2.83	4.47	5.30	2.63	2.93	3.37	4.03	3.45	1.16	1.57	1.94	1.94	1.12
Na_2O	0.01	0.01	0.03	0.00	0.01	0.00	0.00	0.01	0.04	0.01	0.00	0.02	0.01
K_2O	0.03	0.00	0.00	0.00	0.02	0.00	0.00	0.00	0.01	0.02	0.00	0.04	0.01
Total	101.25	102.97	103.81	102.91	101.69	102.51	100.44	101.22	101.68	101.03	103.82	103.31	102.55
Si	3.03	3.00	2.98	2.99	2.98	3.03	3.01	3.03	2.97	2.99	3.00	3.01	3.00
Ti	0.00	0.00	0.00	0.00	0.00	0.00	0.00	0.00	0.00	0.00	0.00	0.00	0.00
Al	1.95	1.97	1.99	2.02	1.99	1.96	1.94	1.91	2.02	2.00	2.00	2.02	1.95
Cr	0.00	0.00	0.00	0.00	0.00	0.00	0.00	0.00	0.01	0.00	0.00	0.00	0.00
Fe	2.18	1.53	1.58	1.72	1.67	1.77	1.68	1.87	1.86	2.31	1.94	2.14	1.77
Mn	0.05	0.10	0.09	0.02	0.05	0.05	0.17	0.38	0.03	0.13	0.14	0.23	0.03
Mg	0.53	1.04	0.96	1.04	1.08	0.91	0.88	0.54	1.02	0.43	0.75	0.40	1.18
Ca	0.24	0.36	0.42	0.21	0.24	0.27	0.33	0.29	0.09	0.13	0.16	0.16	0.09
Na	0.00	0.00	0.00	0.00	0.00	0.00	0.00	0.00	0.01	0.00	0.00	0.00	0.00
K	0.00	0.00	0.00	0.00	0.00	0.00	0.00	0.00	0.00	0.00	0.00	0.00	0.00
Total	7.99	8.01	8.03	8.00	8.02	7.99	8.01	8.02	8.02	8.01	7.99	7.98	8.03
XMg	0.20	0.41	0.38	0.38	0.39	0.34	0.34	0.22	0.35	0.16	0.28	0.16	0.40
Alm	0.73	0.50	0.52	0.57	0.55	0.59	0.55	0.61	0.62	0.77	0.65	0.73	0.58
Sps	0.02	0.03	0.03	0.01	0.02	0.02	0.05	0.12	0.01	0.04	0.05	0.08	0.01
Prp	0.18	0.34	0.31	0.35	0.35	0.30	0.29	0.18	0.34	0.14	0.25	0.14	0.38
Grs	0.08	0.12	0.14	0.07	0.08	0.09	0.11	0.09	0.03	0.04	0.05	0.05	0.03

Table 3.2. Continued

Sample No.	BC08010502B	BC08010502B	85011511B	85011511B	84021904B	84021904B	B08012201I	B08012201I	B08012203A	B08012203A	B08B012204	B08B012204	B08012304C
Occurrence	core	rim	core	rim	core	rim	core	rim	core	rim	core	rim	core
Analysis No.	154	159	56	74	78	81	87	89	4	1	240	245	131
SiO_2	38.16	38.23	39.21	37.41	40.09	38.52	37.99	37.67	37.71	37.68	38.73	38.76	37.93
TiO_2	0.05	0.05	0.01	0.04	0.02	0.00	0.07	0.03	0.04	0.09	0.02	0.18	0.10
Al2O3	21.35	21.15	22.36	21.71	22.63	21.90	21.27	20.98	21.29	20.58	21.17	20.51	20.61
Cr_2O_3	0.00	0.00	0.08	0.04	0.02	0.00	0.01	0.03	0.00	0.00	0.00	0.00	0.00
FeO	27.95	29.46	30.66	35.64	28.89	35.10	32.03	31.66	19.66	16.81	26.49	25.98	25.08
MnO	6.40	3.02	0.67	1.41	0.70	1.39	3.07	3.38	17.07	18.02	5.00	5.08	7.75
MgO	1.27	2.05	8.37	3.60	9.70	4.79	2.40	1.73	1.40	0.71	1.51	1.16	1.11
CaO	7.02	6.93	1.14	1.09	1.09	1.01	5.29	6.39	4.85	7.17	8.65	10.57	8.85
Na_2O	0.03	0.01	0.00	0.00	0.00	0.03	0.01	0.00	0.09	0.04	0.00	0.04	0.00
K_2O	0.01	0.02	0.00	0.00	0.00	0.01	0.01	0.01	0.00	0.00	0.00	0.00	0.00
Total	102.23	100.91	102.49	100.94	103.23	102.74	102.15	101.87	102.10	101.09	101.56	102.28	101.42
Si	3.00	3.03	2.98	2.98	2.99	2.99	2.99	2.99	2.99	3.01	3.04	3.04	3.01
Ti	0.00	0.00	0.00	0.00	0.00	0.00	0.00	0.00	0.00	0.01	0.00	0.01	0.01
Al	1.98	1.97	2.00	2.04	1.99	2.00	1.97	1.96	1.99	1.94	1.96	1.89	1.93
Cr	0.00	0.00	0.00	0.00	0.00	0.00	0.00	0.00	0.00	0.00	0.00	0.00	0.00
Fe	1.84	1.95	1.95	2.37	1.80	2.28	2.11	2.10	1.30	1.12	1.74	1.70	1.67
Mn	0.43	0.20	0.04	0.09	0.04	0.09	0.20	0.23	1.15	1.22	0.33	0.34	0.52
Mg	0.15	0.24	0.95	0.43	1.08	0.55	0.28	0.20	0.17	0.08	0.18	0.14	0.13
Ca	0.59	0.59	0.09	0.09	0.09	0.08	0.45	0.54	0.41	0.61	0.73	0.89	0.75
Na	0.00	0.00	0.00	0.00	0.00	0.00	0.00	0.00	0.01	0.01	0.00	0.01	0.00
K	0.00	0.00	0.00	0.00	0.00	0.00	0.00	0.00	0.00	0.00	0.00	0.00	0.00
Total	8.00	7.99	8.02	8.00	8.00	8.01	8.02	8.03	8.02	8.01	7.98	8.01	8.02
XMg	0.07	0.11	0.33	0.15	0.37	0.20	0.12	0.09	0.11	0.07	0.09	0.07	0.07
Alm	0.61	0.65	0.64	0.79	0.60	0.76	0.69	0.68	0.43	0.37	0.58	0.56	0.54
Sps	0.14	0.07	0.01	0.03	0.01	0.03	0.07	0.07	0.38	0.40	0.11	0.11	0.17
Prp	0.05	0.08	0.31	0.14	0.36	0.18	0.09	0.07	0.05	0.03	0.06	0.04	0.04
Grs	0.20	0.20	0.03	0.03	0.03	0.03	0.15	0.18	0.14	0.20	0.24	0.29	0.25

Table 3.2. Continued

Sample No.	B08012304C	B08012304D	B08012304D	B08012304E	B08012304E	AC08011301M	AC08011301M	BC08010602J	BC08010602J	BC08010604A	BC08010604A	BC08010604E	BC08010604E
Occurrence	rim	core	rim	core	rim	core	rim	core	rim	core	rim	core	rim
Analysis No.	127	19	30	21	22	1	5	39	36	28	32	73	68
SiO_2	37.28	38.07	38.33	38.54	38.70	39.68	40.27	38.41	38.90	38.22	38.12	38.14	38.20
TiO_2	0.05	0.05	0.05	0.02	0.00	0.02	0.00	0.01	0.00	0.01	0.08	0.05	0.02
Al2O3	20.34	21.91	21.37	21.57	21.48	22.54	22.39	20.96	21.20	20.56	20.86	20.78	20.43
Cr_2O_3	0.01	0.00	0.03	0.00	0.00	0.00	0.04	0.00	0.00	0.00	0.00	0.03	0.02
FeO	22.64	31.21	30.23	29.52	30.11	28.13	30.60	24.50	22.36	25.99	25.01	28.24	24.81
MnO	10.71	3.41	2.97	4.77	3.92	0.63	0.51	11.98	10.16	6.03	8.08	4.09	9.35
MgO	0.86	2.47	3.19	1.95	3.13	8.27	8.17	1.81	1.27	2.80	1.97	3.42	2.13
CaO	8.87	5.20	5.02	5.31	4.67	1.25	1.68	4.99	7.44	6.64	6.94	5.98	6.17
Na_2O	0.04	0.03	0.00	0.00	0.04	0.01	0.03	0.00	0.86	0.02	0.01	0.03	0.00
K_2O	0.05	0.01	0.00	0.00	0.00	0.00	0.01	0.00	0.00	0.00	0.01	0.00	0.00
Total	100.84	102.36	101.20	101.67	102.04	100.54	103.70	102.66	102.21	100.27	101.08	100.76	101.13
Si	2.99	2.98	3.02	3.03	3.02	3.03	3.02	3.02	3.05	3.04	3.02	3.02	3.04
Ti	0.00	0.00	0.00	0.00	0.00	0.00	0.00	0.00	0.00	0.00	0.01	0.00	0.00
Al	1.92	2.02	1.98	2.00	1.98	2.03	1.98	1.94	1.96	1.93	1.95	1.94	1.91
Cr	0.00	0.00	0.00	0.00	0.00	0.00	0.00	0.00	0.00	0.00	0.00	0.00	0.00
Fe	1.52	2.04	1.99	1.94	1.97	1.80	1.92	1.61	1.46	1.73	1.66	1.87	1.65
Mn	0.73	0.23	0.20	0.32	0.26	0.04	0.03	0.80	0.67	0.41	0.54	0.27	0.63
Mg	0.10	0.29	0.37	0.23	0.36	0.94	0.91	0.21	0.15	0.33	0.23	0.40	0.25
Ca	0.76	0.44	0.42	0.45	0.39	0.10	0.13	0.42	0.62	0.57	0.59	0.51	0.53
Na	0.01	0.00	0.00	0.00	0.01	0.00	0.00	0.00	0.13	0.00	0.00	0.00	0.00
K	0.00	0.00	0.00	0.00	0.00	0.00	0.00	0.00	0.00	0.00	0.00	0.00	0.00
Total	8.05	8.01	7.99	7.97	7.99	7.95	8.00	8.01	8.05	8.00	8.00	8.01	8.02
XMg	0.06	0.12	0.16	0.11	0.16	0.34	0.32	0.12	0.09	0.16	0.12	0.18	0.13
Alm	0.49	0.68	0.67	0.66	0.66	0.62	0.64	0.53	0.50	0.57	0.55	0.61	0.54
Sps	0.23	0.08	0.07	0.11	0.09	0.01	0.01	0.26	0.23	0.13	0.18	0.09	0.21
Prp	0.03	0.10	0.13	0.08	0.12	0.33	0.30	0.07	0.05	0.11	0.08	0.13	0.08
Grs	0.25	0.15	0.14	0.15	0.13	0.04	0.05	0.14	0.21	0.19	0.19	0.17	0.17

Table 3.3. Representative chemical compositions of pyroxene in the central Sør Rondane Mountains.

Sample No.	A07123001E	A07123001F	A07123001I	A07123001N	A07123001R	A07123001N
Mineral	Opx	Opx	Opx	Opx	Opx	Cpx
Analysis No.	77	143	90	149	23	148
SiO2	51.41	50.55	51.61	52.57	51.35	51.94
TiO2	0.09	0.03	0.16	0.09	0.01	0.33
Al2O3	3.97	3.68	3.86	1.66	3.98	3.08
Cr2O3	0.01	0.02	0.04	0.03	0.00	0.02
FeO	25.57	26.64	22.93	24.22	22.51	9.46
MnO	0.39	0.23	0.62	1.28	0.21	0.50
MgO	19.71	19.45	21.67	20.03	20.87	12.54
CaO	0.41	0.23	0.34	0.51	0.15	22.60
Na2O	0.00	0.00	0.02	0.02	0.02	0.43
K2O	0.00	0.02	0.00	0.00	0.00	0.00
Total	101.67	100.85	101.26	100.50	99.10	100.94
Si	1.91	1.90	1.90	1.97	1.93	1.93
Ti	0.00	0.00	0.00	0.00	0.00	0.01
Al	0.17	0.16	0.17	0.07	0.18	0.14
Cr	0.00	0.00	0.00	0.00	0.00	0.00
Fe	0.79	0.84	0.71	0.76	0.71	0.29
Mn	0.01	0.01	0.02	0.04	0.01	0.02
Mg	1.09	1.09	1.19	1.12	1.17	0.69
Ca	0.02	0.01	0.01	0.02	0.01	0.90
Na	0.00	0.00	0.00	0.00	0.00	0.03
K	0.00	0.00	0.00	0.00	0.00	0.00
Total	4.00	4.02	4.01	3.99	3.99	4.01
XMg	0.58	0.57	0.63	0.60	0.62	0.70
En	0.57	0.56	0.62	0.59	0.62	0.36
Fs	0.42	0.43	0.37	0.40	0.38	0.15
Wo	0.01	0.00	0.01	0.01	0.00	0.47
Jd	0.00	0.00	0.00	0.00	0.00	0.02

Table 3.4. Representative chemical composition of amphibobles in the central Sør Rondane Mountains.

Sample No.	AC07121901A	A07123001I	A07123001N	A07123001AC	A07123001AC	BC08010504A	BC08010504A	AC08012001A	AC08012001A	BC08010604A	BC08010604E	B08012201A	B08012201I
occurrence	matrix	matrix	matrix	core	rim	core	rim	core	rim	matrix	core	matrix	matrix
Analysis No.	40	85	145	1	3	175	159	21	24	45	45	3	80
SiO_2	40.69	43.66	44.31	42.51	42.25	41.48	40.09	43.49	42.77	42.577	41.16	39.85	41.10
TiO_2	0.81	1.41	1.35	2.01	1.87	1.50	0.42	1.08	2.61	0.056	1.43	1.15	0.80
Al_2O_3	11.65	13.40	11.25	10.99	11.47	11.53	13.52	11.12	10.97	11.443	11.58	12.48	14.13
Cr_2O_3	0.00	0.06	0.00	0.05	0.01	0.03	0.03	0.00	0.00	0	0.00	0.04	0.03
FeO^{total}	21.40	14.01	14.47	18.26	19.01	23.44	25.95	20.24	21.82	19.976	21.61	22.40	23.02
MnO	0.54	0.08	0.29	0.52	0.55	0.47	0.55	0.31	0.28	0.77	0.79	0.88	0.30
MgO	6.74	12.54	12.44	9.70	8.73	5.84	4.85	7.00	6.74	8.284	7.00	6.07	5.62
CaO	11.48	11.19	11.70	11.03	10.89	11.33	11.34	12.01	11.40	11.033	11.42	11.39	11.17
Na_2O	1.19	1.14	1.42	1.79	1.64	1.34	1.29	0.93	1.52	1.395	1.28	0.91	1.59
K_2O	1.52	1.19	0.98	1.30	1.33	1.67	1.71	1.34	1.69	0.755	1.75	1.58	0.84
Total	96.01	99.23	98.73	98.17	97.75	98.63	99.73	97.51	99.80	96.289	98.02	96.86	98.58
Si	6.36	6.30	6.48	6.39	6.40	6.38	6.11	6.65	6.48	6.50	6.32	6.19	6.24
Ti	0.09	0.15	0.15	0.23	0.21	0.17	0.05	0.12	0.30	0.01	0.17	0.13	0.09
Al	2.15	2.28	1.94	1.95	2.05	2.09	2.43	2.01	1.96	2.06	2.09	2.29	2.53
Cr	0.00	0.01	0.00	0.01	0.00	0.00	0.00	0.00	0.00	–	0.00	0.00	0.00
Fe2+	2.43	1.12	1.36	2.02	2.17	2.80	2.61	2.65	2.91	1.96	2.43	2.33	2.54
Fe3+	0.37	0.57	0.41	0.28	0.24	0.21	0.70	–	–	0.59	0.35	0.58	0.38
Mn	0.07	0.01	0.04	0.07	0.07	0.06	0.07	0.04	0.04	0.10	0.10	0.12	0.04
Mg	1.57	2.70	2.71	2.17	1.97	1.34	1.10	1.60	1.52	1.88	1.60	1.41	1.27
Ca	1.92	1.73	1.83	1.78	1.77	1.87	1.85	1.97	1.85	1.80	1.88	1.90	1.82
Na	0.36	0.32	0.40	0.52	0.48	0.40	0.38	0.28	0.45	0.41	0.38	0.27	0.47
K	0.30	0.22	0.18	0.25	0.26	0.33	0.33	0.26	0.33	0.15	0.34	0.31	0.16
Total	15.62	15.39	15.50	15.65	15.61	15.66	15.63	15.58	15.84	15.45	15.66	15.53	15.53
X Mg	0.39	0.71	0.67	0.52	0.48	0.32	0.30	0.38	0.34	0.49	0.40	0.38	0.33
Al vi	0.50	0.57	0.41	0.34	0.45	0.47	0.54	0.66	0.44	0.55	0.41	0.48	0.76

Table 3.4. Continued

Sample No.	B08012204	B08012302A	B08012302A	B08012304D	B08012304D	B08012304E	B08012304E	B08012305D	AC07121801M
occurrence	matrix	core	rim	core	rim	core	rim	matrix	matrix
Analysis No.	255	104	87	9	18	28	35	14	5
SiO_2	40.15	42.04	40.71	41.42	40.41	42.25	41.07	39.91	54.65
TiO_2	0.64	0.57	0.29	0.86	0.44	0.88	0.64	0.76	0.02
Al_2O_3	14.37	10.49	11.08	13.85	15.89	13.92	15.34	12.98	2.52
Cr_2O_3	0.00	0.00	0.01	0.00	0.03	0.01	0.00	0.01	0.00
FeO^{total}	24.14	24.17	24.40	19.97	21.25	20.05	21.34	23.45	22.14
MnO	0.69	0.34	0.30	0.49	0.37	0.28	0.33	0.71	0.24
MgO	4.64	6.83	6.22	6.69	4.96	6.90	6.09	5.35	19.37
CaO	11.58	11.33	11.24	11.63	11.43	11.42	11.20	11.51	0.26
Na_2O	1.08	1.67	1.71	1.31	1.26	1.26	1.28	1.31	0.18
K_2O	1.22	1.46	1.75	0.89	1.08	0.72	0.83	1.42	0.01
Total	98.51	98.90	97.72	97.11	97.11	97.69	98.10	97.44	99.38
Si	6.14	6.42	6.33	6.32	6.21	6.38	6.19	6.20	7.76
Ti	0.07	0.06	0.03	0.10	0.05	0.10	0.07	0.09	0.00
Al	2.59	1.89	2.03	2.49	2.88	2.48	2.73	2.38	0.42
Cr	0.00	0.00	0.00	0.00	0.00	0.00	0.00	0.00	0.00
Fe2+	2.57	2.58	2.67	2.34	2.59	2.30	2.27	2.58	2.57
Fe3+	0.52	0.51	0.50	0.21	0.14	0.23	0.42	0.47	0.06
Mn	0.09	0.04	0.04	0.06	0.05	0.04	0.04	0.09	0.03
Mg	1.06	1.56	1.44	1.52	1.14	1.55	1.37	1.24	4.10
Ca	1.90	1.85	1.87	1.90	1.88	1.85	1.81	1.92	0.04
Na	0.32	0.50	0.52	0.39	0.38	0.37	0.37	0.39	0.05
K	0.24	0.29	0.35	0.17	0.21	0.14	0.16	0.28	0.00
Total	15.50	15.70	15.80	15.51	15.52	15.42	15.43	15.63	15.03
X Mg	0.29	0.38	0.35	0.39	0.30	0.40	0.38	0.32	0.61
Al vi	0.74	0.31	0.37	0.81	1.09	0.85	0.92	0.57	0.18

Table 3.5. Representative chemical composition of biotite in the central Sør Rondane Mountains.

Sample No.	AC07121302B	AC07121303E	AC07121303E	AC07121701C	AC07121701C	AC07121702B p	AC07121702B p	AC07121702B a	AC07121702B a	AC07121702D	AC07121702D	AC07121801H	AC07121801H
Occurrence	martix	martix	inclusion	inclusion	martix	martix	inclusion	inclusion	martix	inclusion	martix	inclusion	martix
Analysis No.	100	12	16	70	77	26	43	1	65	34	32	40	45
SiO2	35.88	36.44	37.68	38.78	38.05	36.35	38.15	35.58	34.83	36.04	34.88	37.75	35.57
TiO2	1.81	2.16	2.32	2.01	1.66	2.43	2.44	1.55	0.41	3.01	3.30	1.30	2.19
Al2O3	21.95	17.95	18.52	19.01	18.17	18.58	17.18	20.44	21.10	18.20	18.78	18.33	18.61
Cr2O3	0.01	0.05	0.16	0.11	0.12	0.05	0.07	0.00	0.07	0.05	0.04	0.02	0.00
FeO	20.77	18.05	13.30	10.04	15.63	20.50	13.03	20.67	23.36	16.63	20.63	9.85	19.16
MnO	0.11	0.00	0.00	0.07	0.00	0.08	0.00	0.11	0.00	0.00	0.00	0.03	0.00
MgO	7.07	11.44	14.35	17.90	13.84	9.22	15.39	9.00	6.58	11.85	8.06	17.10	10.24
CaO	0.00	0.06	0.01	0.02	0.01	0.05	0.01	0.01	0.07	0.01	0.00	0.02	0.02
Na2O	0.14	0.26	0.31	0.66	0.35	0.06	0.28	0.23	0.19	0.10	0.07	0.65	0.29
K2O	10.01	8.44	8.97	9.00	8.99	9.56	9.66	9.69	9.34	9.48	9.93	8.09	9.16
F	0.00	0.60	0.50	1.03	0.89	0.60	2.72	0.73	0.60	0.61	0.08	0.69	0.70
Cl	0.00	0.23	0.20	0.04	0.05	0.13	0.15	0.07	0.08	0.13	0.00	0.31	0.36
Total	97.89	95.36	96.06	98.21	97.37	97.35	97.91	97.76	96.36	95.83	95.74	93.79	95.90
Si	5.34	5.50	5.51	5.47	5.56	5.46	5.57	5.33	5.35	5.41	5.34	5.56	5.41
Ti	0.20	0.24	0.26	0.21	0.18	0.27	0.27	0.18	0.05	0.34	0.38	0.14	0.25
Al	3.85	3.19	3.19	3.16	3.13	3.29	2.96	3.61	3.82	3.22	3.39	3.18	3.33
Cr	0.00	0.01	0.02	0.01	0.01	0.01	0.01	0.00	0.01	0.01	0.00	0.00	0.00
Fe	2.58	2.28	1.63	1.18	1.91	2.57	1.59	2.59	3.00	2.09	2.64	1.21	2.43
Mn	0.01	0.00	0.00	0.01	0.00	0.01	0.00	0.01	0.00	0.00	0.00	0.00	0.00
Mg	1.57	2.57	3.13	3.77	3.01	2.07	3.35	2.01	1.51	2.65	1.84	3.75	2.32
Ca	0.00	0.01	0.00	0.00	0.00	0.01	0.00	0.00	0.01	0.00	0.00	0.00	0.00
Na	0.04	0.08	0.09	0.18	0.10	0.02	0.08	0.07	0.06	0.03	0.02	0.19	0.09
K	1.90	1.63	1.67	1.62	1.68	1.83	1.80	1.85	1.83	1.82	1.94	1.52	1.78
F	0.00	0.28	0.23	0.45	0.40	0.28	1.19	0.34	0.29	0.29	0.04	0.32	0.33
Cl	0.00	0.06	0.05	0.01	0.01	0.03	0.03	0.02	0.02	0.03	0.00	0.08	0.09
Total	15.49	15.17	15.23	15.17	15.16	15.23	14.40	15.29	15.33	15.24	15.52	15.17	15.19
XMg	0.38	0.53	0.66	0.76	0.61	0.45	0.68	0.44	0.33	0.56	0.41	0.76	0.49
Al vi	1.18	0.69	0.71	0.64	0.68	0.75	0.52	0.94	1.17	0.63	0.73	0.74	0.74

Table 3.5. Continued

Sample No.	AC07121801M	BC07122801D	BC07122801D	BC07122804A	BC07122805C	BC07122805C	AC07121901A	07120402A	07120402A	A07123001E	A07123001E	A07123001F	A07123001F
Occurrence	martix	inclusion	martix	martix	martix	martix	martix	martix	inclusion	martix	inclusion	martix	inclusion
Analysis No.	9	76	84	58	60	61	64	78	77	27	30	16	36
SiO2	39.55	37.94	37.62	34.90	34.93	34.44	38.00	37.11	38.90	37.07	37.98	37.21	38.60
TiO2	1.33	2.97	2.18	2.75	3.78	3.98	3.44	3.03	1.82	4.52	4.74	3.33	3.23
Al2O3	17.97	17.90	19.06	19.60	17.64	17.56	15.35	18.53	19.84	15.06	15.36	15.78	15.70
Cr2O3	0.00	0.07	0.03	0.03	0.00	0.00	0.00	0.12	0.08	0.00	0.02	0.05	0.00
FeO	13.37	14.42	17.24	22.08	30.00	29.39	21.71	16.86	9.81	15.84	12.27	17.09	10.37
MnO	0.05	0.06	0.01	0.03	0.25	0.12	0.36	0.00	0.00	0.04	0.01	0.00	0.00
MgO	16.16	13.83	12.15	7.33	2.66	2.49	9.69	12.21	17.72	13.67	16.23	13.31	17.80
CaO	0.03	0.00	0.00	0.00	0.00	0.00	0.00	0.00	0.02	0.00	0.01	0.00	0.03
Na2O	0.33	0.29	0.09	0.16	0.05	0.06	0.04	0.16	0.31	0.06	0.32	0.02	0.10
K2O	8.30	9.61	9.74	9.64	9.77	9.61	9.42	9.97	9.18	10.24	9.96	9.92	9.89
F	0.99	0.88	0.66	0.20	0.36	0.34	0.55	0.16	0.38	1.65	2.76	0.00	0.00
Cl	0.11	0.30	0.12	0.11	0.13	0.14	0.10	0.21	0.02	0.18	0.22	0.00	0.00
Total	97.73	97.87	98.75	96.71	99.38	97.95	98.40	98.25	97.91	97.61	98.69	96.69	95.71
Si	5.66	5.52	5.47	5.32	5.40	5.39	5.68	5.42	5.47	5.52	5.52	5.54	5.61
Ti	0.14	0.33	0.24	0.32	0.44	0.47	0.39	0.33	0.19	0.51	0.52	0.37	0.35
Al	3.03	3.07	3.27	3.52	3.21	3.24	2.70	3.19	3.29	2.64	2.63	2.77	2.69
Cr	0.00	0.01	0.00	0.00	0.00	0.00	0.00	0.01	0.01	0.00	0.00	0.01	0.00
Fe	1.60	1.75	2.10	2.81	3.88	3.85	2.71	2.06	1.15	1.97	1.49	2.13	1.26
Mn	0.01	0.01	0.00	0.00	0.03	0.02	0.05	0.00	0.00	0.00	0.00	0.00	0.00
Mg	3.44	3.00	2.63	1.67	0.61	0.58	2.16	2.66	3.71	3.03	3.51	2.95	3.85
Ca	0.00	0.00	0.00	0.00	0.00	0.00	0.00	0.00	0.00	0.00	0.00	0.00	0.00
Na	0.09	0.08	0.03	0.05	0.02	0.02	0.01	0.04	0.08	0.02	0.09	0.00	0.03
K	1.52	1.78	1.81	1.88	1.93	1.92	1.79	1.86	1.65	1.94	1.85	1.88	1.83
F	0.44	0.39	0.30	0.09	0.17	0.17	0.26	0.07	0.17	0.75	1.19	0.00	0.00
Cl	0.03	0.07	0.03	0.03	0.03	0.04	0.02	0.05	0.01	0.04	0.05	0.00	0.00
Total	15.03	15.08	15.23	15.44	15.32	15.28	15.21	15.47	15.38	14.84	14.37	15.65	15.63
XMg	0.44	0.63	0.56	0.37	0.14	0.13	0.44	0.56	0.76	0.61	0.70	0.58	0.75
Al vi	0.69	0.59	0.74	0.84	0.62	0.63	0.38	0.62	0.76	0.16	0.15	0.30	0.29

Table 3.5. Continued

Sample No.	A07123001I	A07123001I	A07123001P	A07123001P	A07123001R	A07123001R	A07123001AC	A07123001AF	BC08010302A	BC08010302A	BC08010302B	BC08010302B	BC08010302C
Occurrence	martix	martix	inclusion	martix	martix	martix	martix	martix	martix	martix	inclusion	martix	martix
Analysis No.	88	128	63	45	30	4	89	65	60	56	56	54	17
SiO2	38.58	39.15	37.95	36.73	38.06	39.17	37.59	38.09	36.14	36.02	36.81	36.72	37.57
TiO2	2.31	2.79	1.92	2.60	3.03	2.60	2.20	1.85	0.55	2.40	2.00	0.23	2.32
Al2O3	15.78	16.04	18.36	18.07	15.79	16.15	14.80	16.39	20.58	18.64	19.54	21.72	17.72
Cr2O3	0.04	0.00	0.02	0.00	0.03	0.08	0.01	0.04	0.00	0.04	0.00	0.11	0.03
FeO	12.41	11.28	10.87	13.92	12.79	11.84	18.26	15.09	15.99	17.60	19.15	15.77	15.26
MnO	0.00	0.00	0.00	0.00	0.14	0.00	0.23	0.03	0.07	0.08	0.06	0.11	0.08
MgO	16.60	17.72	17.12	14.31	16.04	18.10	12.56	15.25	11.82	11.22	10.55	12.10	13.68
CaO	0.00	0.02	0.01	0.00	0.00	0.06	0.01	0.00	0.00	0.00	0.05	0.02	0.07
Na2O	0.19	0.28	0.40	0.18	0.17	0.15	0.02	0.19	0.08	0.09	0.12	0.13	0.15
K2O	9.27	9.27	9.36	9.64	9.09	9.16	9.78	9.18	10.03	9.57	10.05	10.17	9.21
F	1.35	1.50	1.42	1.23	0.00	0.83	0.00	0.76	0.00	0.32	0.44	0.67	0.40
Cl	0.22	0.16	0.10	0.11	0.00	0.11	0.00	0.59	0.00	0.14	0.68	0.20	0.31
Total	96.12	97.58	96.90	96.23	95.14	97.88	95.44	97.01	95.25	95.96	99.09	97.60	96.57
Si	5.67	5.63	5.48	5.44	5.61	5.60	5.70	5.61	5.41	5.41	5.42	5.38	5.54
Ti	0.25	0.30	0.21	0.29	0.34	0.28	0.25	0.21	0.06	0.27	0.22	0.02	0.26
Al	2.73	2.72	3.13	3.15	2.74	2.72	2.64	2.85	3.63	3.30	3.39	3.75	3.08
Cr	0.00	0.00	0.00	0.00	0.00	0.01	0.00	0.00	0.00	0.00	0.00	0.01	0.00
Fe	1.52	1.36	1.31	1.72	1.58	1.42	2.31	1.86	2.00	2.21	2.36	1.93	1.88
Mn	0.00	0.00	0.00	0.00	0.02	0.00	0.03	0.00	0.01	0.01	0.01	0.01	0.01
Mg	3.63	3.80	3.69	3.16	3.52	3.86	2.84	3.35	2.64	2.51	2.31	2.64	3.01
Ca	0.00	0.00	0.00	0.00	0.00	0.01	0.00	0.00	0.00	0.00	0.01	0.00	0.01
Na	0.05	0.08	0.11	0.05	0.05	0.04	0.01	0.05	0.02	0.03	0.03	0.04	0.04
K	1.74	1.70	1.72	1.82	1.71	1.67	1.89	1.72	1.92	1.84	1.89	1.90	1.73
F	0.61	0.66	0.63	0.56	0.00	0.37	0.00	0.34	0.00	0.15	0.20	0.31	0.18
Cl	0.05	0.04	0.02	0.03	0.00	0.03	0.00	0.14	0.00	0.04	0.17	0.05	0.08
Total	14.95	14.90	15.01	15.05	15.56	15.22	15.68	15.16	15.69	15.40	15.26	15.33	15.29
XMg	0.70	0.74	0.74	0.65	0.69	0.73	0.55	0.64	0.57	0.53	0.50	0.58	0.62
Al vi	0.40	0.35	0.61	0.59	0.35	0.32	0.34	0.45	1.04	0.72	0.80	1.13	0.61

Table 3.5. Continued

Sample No.	BC08010401B	BC08010401B	BC08010502B	BC08010504A	85011511B	84021904B	84021904B	AC08011301M	AC08012001A	AC08011601A	BC08010602J	BC08010604A	BC08010604E
Occurrence	inclusion	martix	martix	martix	martix	inclusion	martix	martix	martix	martix	martix	martix	martix
Analysis No.	70	64	52	48	61	70	74	8	31	33	30	44	41
SiO2	39.82	36.21	36.54	36.94	37.83	40.79	37.16	37.16	36.75	36.40	35.39	35.92	37.06
TiO2	2.96	2.99	3.32	3.82	2.25	1.93	2.71	2.81	3.99	3.12	1.80	2.91	3.21
Al2O3	16.99	18.33	15.46	15.99	20.14	19.67	18.66	18.45	15.72	14.83	17.84	16.19	15.57
Cr2O3	0.00	0.06	0.02	0.02	0.06	0.08	0.06	0.20	0.02	0.00	0.00	0.02	0.04
FeO	7.43	16.17	23.73	24.54	14.85	7.95	15.77	15.81	23.20	22.72	21.76	21.84	21.81
MnO	0.00	0.04	0.29	0.38	0.00	0.00	0.04	0.03	0.21	0.84	0.19	0.50	0.71
MgO	18.36	11.74	7.83	7.11	12.57	18.48	10.86	12.41	8.10	8.10	9.49	9.15	10.46
CaO	0.01	0.05	0.00	0.00	0.05	0.01	0.02	0.04	0.00	0.00	0.02	0.01	0.00
Na2O	0.34	0.17	0.03	0.07	0.12	0.27	0.10	0.20	0.00	0.06	0.10	0.09	0.13
K2O	9.73	9.24	9.78	9.77	8.94	8.18	10.10	9.63	10.15	9.83	9.08	9.55	9.32
F	2.68	0.25	0.48	0.28	0.25	1.84	0.75	0.53	0.63	0.55	0.05	0.61	0.44
Cl	0.14	0.04	0.09	0.21	0.03	0.44	0.06	0.29	0.09	0.12	0.05	0.19	0.20
Total	97.29	95.18	97.34	98.95	96.96	98.78	95.95	97.27	98.56	96.31	95.72	96.67	98.72
Si	5.68	5.44	5.60	5.58	5.49	5.64	5.55	5.47	5.56	5.65	5.43	5.51	5.55
Ti	0.32	0.34	0.38	0.43	0.25	0.20	0.30	0.31	0.45	0.36	0.21	0.34	0.36
Al	2.86	3.24	2.79	2.85	3.44	3.21	3.28	3.20	2.80	2.71	3.23	2.93	2.75
Cr	0.00	0.01	0.00	0.00	0.01	0.01	0.01	0.02	0.00	0.00	0.00	0.00	0.00
Fe	0.89	2.03	3.04	3.10	1.80	0.92	1.97	1.95	2.93	2.95	2.79	2.80	2.73
Mn	0.00	0.01	0.04	0.05	0.00	0.00	0.00	0.00	0.03	0.11	0.02	0.06	0.09
Mg	3.90	2.63	1.79	1.60	2.72	3.81	2.42	2.72	1.83	1.87	2.17	2.09	2.33
Ca	0.00	0.01	0.00	0.00	0.01	0.00	0.00	0.01	0.00	0.00	0.00	0.00	0.00
Na	0.09	0.05	0.01	0.02	0.03	0.07	0.03	0.06	0.00	0.02	0.03	0.03	0.04
K	1.77	1.77	1.91	1.88	0.00	1.44	1.92	1.81	1.96	1.95	1.78	1.87	1.78
F	1.14	0.12	0.23	0.13	0.12	0.77	0.35	0.24	0.30	0.27	0.02	0.29	0.21
Cl	0.03	0.01	0.02	0.05	0.01	0.10	0.01	0.07	0.02	0.03	0.01	0.05	0.05
Total	14.34	15.38	15.32	15.33	13.62	14.43	15.12	15.23	15.25	15.32	15.62	15.30	15.37
XMg	0.81	0.56	0.37	0.34	0.60	0.81	0.55	0.58	0.38	0.39	0.44	0.43	0.46
Al vi	0.54	0.68	0.40	0.43	0.93	0.85	0.83	0.67	0.36	0.36	0.65	0.44	0.29

Table 3.5. Continued

Sample No.	B08012201A	B08012201I	B08012203A	B08012204	B08012304C	B08012304E	B08012304E	B08012305D
Occurrence	martix	martix	martix	martix	martix	martix	martix	martix
Analysis No.	1	21	19	252	8	4	4	11
SiO2	34.99	35.93	36.54	34.59	36.00	35.43	35.43	35.41
TiO2	2.75	2.14	3.29	2.15	3.35	2.95	2.95	2.94
Al2O3	16.09	16.73	16.78	17.24	16.31	16.94	16.94	15.98
Cr2O3	0.03	0.01	0.00	0.04	0.00	0.00	0.00	0.05
FeO	23.50	23.42	22.64	27.61	26.34	25.05	25.05	23.18
MnO	0.69	0.15	0.66	0.36	0.64	0.01	0.01	0.53
MgO	8.07	8.64	7.03	5.29	5.72	7.51	7.51	7.67
CaO	0.00	0.12	0.00	0.00	0.00	0.00	0.00	0.01
Na2O	0.08	0.12	0.05	0.03	0.09	0.15	0.15	0.05
K2O	9.98	8.68	10.07	9.30	9.60	9.35	9.35	9.83
F	0.32	0.21	0.50	0.00	0.22	0.19	0.19	0.55
Cl	0.03	0.15	0.04	0.00	0.08	0.04	0.04	0.02
Total	96.37	96.19	97.37	96.61	98.25	97.53	97.53	95.99
Si	5.45	5.53	5.58	5.43	5.53	5.43	5.43	5.52
Ti	0.32	0.25	0.38	0.25	0.39	0.34	0.34	0.34
Al	2.95	3.03	3.02	3.19	2.95	3.06	3.06	2.94
Cr	0.00	0.00	0.00	0.01	0.00	0.00	0.00	0.01
Fe	3.06	3.01	2.89	3.62	3.38	3.21	3.21	3.02
Mn	0.09	0.02	0.08	0.05	0.08	0.00	0.00	0.07
Mg	1.87	1.98	1.60	1.24	1.31	1.71	1.71	1.78
Ca	0.00	0.02	0.00	0.00	0.00	0.00	0.00	0.00
Na	0.02	0.04	0.02	0.01	0.03	0.05	0.05	0.02
K	1.98	1.70	1.96	1.86	1.88	1.83	1.83	1.96
F	0.16	0.10	0.24	0.00	0.11	0.09	0.09	0.27
Cl	0.01	0.04	0.01	0.00	0.02	0.01	0.01	0.01
Total	15.59	15.44	15.28	15.66	15.43	15.54	15.54	15.38
XMg	0.38	0.40	0.36	0.25	0.28	0.35	0.35	0.37
Al vi	0.40	0.56	0.60	0.62	0.48	0.49	0.49	0.45

Table 3.6. Representative chemical composition of spinel in the central Sør Rondane Mountains.

Sample No.	AC07121302B	AC07121701C	AC07121702B p	AC07121702B a	AC07121702B a	AC07121702D	AC07121801H	BC07122801D	A07123001P	BC08010302B	BC08010302B	BC08010302C	84021904B
Occurrence	inclusion	inclusion	inclusion	inclusion	matrix	inclusion	inclusion	inclusion	inclusion	inclusion	matrix	inclusion	inclusion
Analysis No.	93	68	17	59	50	23	39	72	39	47	39	8	73
SiO2	0.04	0.04	0.00	0.00	0.00	0.00	0.00	0.02	0.03	0.00	0.01	0.07	0.01
TiO2	0.02	0.00	0.00	0.00	0.00	0.03	0.00	0.00	0.01	0.01	0.00	0.01	0.01
Al2O3	62.83	62.31	59.01	57.83	57.70	61.05	63.56	62.22	62.54	60.91	60.75	58.23	63.33
Cr2O3	0.21	0.30	0.25	0.00	0.06	0.61	0.22	0.61	0.02	0.47	0.24	2.84	0.61
FeO	20.16	26.47	32.50	36.34	36.14	30.02	25.15	25.37	24.95	28.26	26.50	23.70	23.05
MnO	0.00	0.19	0.09	0.05	0.07	0.00	0.00	0.01	0.00	0.00	0.29	0.00	0.03
MgO	6.56	4.81	3.23	1.47	1.56	6.24	10.23	4.17	8.08	6.24	3.87	9.88	8.79
CaO	0.00	0.00	0.00	0.00	0.02	0.01	0.00	0.01	0.01	0.01	0.00	0.00	0.01
Na2O	0.35	0.35	0.07	0.17	0.14	0.17	0.04	0.38	0.18	0.25	0.30	0.15	0.27
K2O	0.02	0.00	0.00	0.00	0.00	0.01	0.02	0.00	0.02	0.00	0.01	0.00	0.00
ZnO	11.66	9.57	4.45	5.10	3.75	4.13	2.19	13.35	6.07	7.39	11.61	5.32	6.49
Total	101.84	104.03	99.61	100.96	99.43	102.27	101.41	106.14	101.90	103.53	103.58	100.21	102.59
Si	0.00	0.00	0.00	0.00	0.00	0.00	0.00	0.00	0.00	0.00	0.00	0.00	0.00
Ti	0.00	0.00	0.00	0.00	0.00	0.00	0.00	0.00	0.00	0.00	0.00	0.00	0.00
Al	2.01	1.99	1.99	1.96	1.98	1.97	1.99	1.98	1.99	1.95	1.98	1.89	1.99
Cr	0.00	0.01	0.01	0.00	0.00	0.01	0.00	0.01	0.00	0.01	0.01	0.06	0.01
Fe	0.46	0.60	0.78	0.88	0.88	0.69	0.56	0.57	0.56	0.64	0.61	0.55	0.51
Mn	0.00	0.00	0.00	0.00	0.00	0.00	0.00	0.00	0.00	0.00	0.01	0.00	0.00
Mg	0.27	0.19	0.14	0.06	0.07	0.25	0.40	0.17	0.33	0.25	0.16	0.41	0.35
Ca	0.00	0.00	0.00	0.00	0.00	0.00	0.00	0.00	0.00	0.00	0.00	0.00	0.00
Na	0.02	0.02	0.00	0.01	0.01	0.01	0.00	0.02	0.01	0.01	0.02	0.01	0.01
K	0.00	0.00	0.00	0.00	0.00	0.00	0.00	0.00	0.00	0.00	0.00	0.00	0.00
Zn	0.23	0.19	0.09	0.11	0.08	0.08	0.04	0.27	0.12	0.15	0.24	0.11	0.13
Total	3.00	3.01	3.01	3.02	3.01	3.01	3.00	3.01	3.01	3.02	3.02	3.03	3.01
XMg	0.37	0.24	0.15	0.07	0.07	0.27	0.42	0.23	0.37	0.28	0.21	0.43	0.40

Table 3.7. Representative chemical compositions of cordierite in the central Sør Rondane Mountains.

Sample No.	AC07121303E	AC07121701C	AC07121801H	AC07121801M
Mineral	Crd	Crd	Crd	Crd
Analysis No.	7	60	35	8
SiO2	50.15	50.16	49.99	50.27
TiO2	0.00	0.00	0.00	0.00
Al2O3	33.29	33.37	33.22	33.33
Cr2O3	0.00	0.00	0.00	0.04
FeO	7.25	6.56	7.15	5.54
MnO	0.04	0.00	0.19	0.01
MgO	9.56	9.49	8.88	10.50
CaO	0.00	0.02	0.01	0.02
Na2O	0.16	0.21	0.17	0.04
K2O	0.00	0.01	0.00	0.01
Total	100.45	99.82	99.60	99.75
Si	5.02	5.04	5.05	5.03
Ti	0.00	0.00	0.00	0.00
Al	3.93	3.95	3.95	3.93
Cr	0.00	0.00	0.00	0.00
Fe	0.61	0.55	0.60	0.46
Mn	0.00	0.00	0.02	0.00
Mg	1.43	1.42	1.34	1.57
Ca	0.00	0.00	0.00	0.00
Na	0.03	0.04	0.03	0.01
K	0.00	0.00	0.00	0.00
Total	11.03	11.01	10.99	11.01
XMg	0.70	0.72	0.69	0.77

Table 3.8. Representative chemical compositions of epidote in the central Sør Rondane Mountains.

Sample No.	AC07121901A	BC08010504A	BC08010602J	BC08010604A	B08012201A	B08012302A	B08012305D
Mineral	Ep	Ep	Ep	Ep	Ep	Ep	Ep
No.	54	184	27	37	7	93	12
SiO2	37.88	38.52	39.01	38.49	37.70	38.00	37.76
TiO2	0.13	0.08	0.12	0.06	0.10	0.00	0.11
Al2O3	23.21	23.50	24.75	24.15	23.32	21.77	23.78
Cr2O3	0.00	0.00	0.02	0.02	0.00	0.00	0.00
FeO	12.48	12.09	10.41	11.17	12.14	14.29	11.56
MnO	0.10	0.18	0.42	0.35	0.40	0.00	0.37
MgO	0.00	0.01	0.03	0.00	0.02	0.00	0.06
CaO	22.67	23.18	23.18	23.49	23.04	22.97	22.69
Na2O	0.02	0.00	0.01	0.00	0.01	0.00	0.00
K2O	0.02	0.03	0.00	0.01	0.00	0.00	0.00
Total	96.50	97.58	97.96	97.73	96.76	97.03	96.32
Si	3.12	3.13	3.13	3.11	3.10	3.13	3.10
Ti	0.01	0.00	0.01	0.00	0.01	0.00	0.01
Al	2.25	2.25	2.34	2.30	2.26	2.19	2.30
Cr	0.00	0.00	0.00	0.00	0.00	0.00	0.00
Fe3+	0.86	0.82	0.70	0.76	0.84	0.91	0.79
Mn	0.01	0.01	0.03	0.02	0.03	0.02	0.03
Mg	0.00	0.00	0.00	0.00	0.00	0.00	0.01
Ca	2.00	2.02	1.99	2.03	2.03	2.01	2.00
Na	0.00	0.00	0.00	0.00	0.00	0.00	0.00
K	0.00	0.00	0.00	0.00	0.00	0.00	0.00
Total	8.25	8.24	8.20	8.23	8.27	8.28	8.25
Ps	0.83	0.80	0.69	0.74	0.81	0.88	0.77

Table 3.9. Representative chemical composition of plagioclasel in the central Sør Rondane Mountains.

Sample No.	AC07121302B	AC07121302B	AC07121303E	AC07121702B p	AC07121702B a	AC07121702D	AC07121702D	AC07121801H	BC07122801D	BC07122801D	BC07122804A	BC07122804A	BC07122805C
Occurrence	matrix	aggregate	matrix	aggregate	matrix	matrix	aggregate	matrix	matrix	aggregate	matrix	aggregate	matrix
Analysis No.	106	1	78	4	54	21	6	37	86	8	49	9	17
SiO_2	62.83	62.82	62.58	63.60	56.09	63.36	64.73	60.46	62.86	61.22	59.03	62.02	59.51
TiO_2	0.00	0.03	0.00	0.00	0.00	0.01	0.00	0.00	0.02	0.03	0.06	0.02	0.00
Al2O3	24.98	24.17	24.31	24.06	28.33	24.21	23.16	25.34	24.46	24.32	26.51	24.66	26.47
Cr_2O_3	0.00	0.03	0.00	0.00	0.02	0.00	0.00	0.00	0.00	0.04	0.03	0.00	0.00
FeO	0.01	0.32	0.05	0.50	0.10	0.02	0.28	0.04	0.00	0.07	0.00	0.35	0.00
MnO	0.00	0.00	0.01	0.03	0.00	0.01	0.00	0.00	0.00	0.00	0.01	0.00	0.01
MgO	0.00	0.00	0.00	0.00	0.02	0.00	0.01	0.01	0.00	0.01	0.00	0.00	0.02
CaO	5.86	5.56	5.53	5.08	10.26	5.19	4.18	7.33	5.37	6.51	8.41	6.16	8.38
Na_2O	8.31	8.51	8.30	8.50	5.52	8.27	9.11	7.13	8.42	7.62	6.64	7.66	6.83
K_2O	0.05	0.07	0.08	0.13	0.08	0.17	0.11	0.02	0.27	0.20	0.07	0.11	0.15
Total	102.06	101.52	100.87	101.91	100.48	101.23	101.58	100.33	101.45	100.01	100.75	100.98	101.36
Si	2.73	2.75	2.75	2.77	2.51	2.77	2.81	2.68	2.75	2.72	2.62	2.73	2.62
Ti	0.00	0.00	0.00	0.00	0.00	0.00	0.00	0.00	0.00	0.00	0.00	0.00	0.00
Al	1.28	1.25	1.26	1.23	1.49	1.25	1.19	1.32	1.26	1.27	1.38	1.28	1.37
Cr	0.00	0.00	0.00	0.00	0.00	0.00	0.00	0.00	0.00	0.00	0.00	0.00	0.00
Fe	0.00	0.01	0.00	0.02	0.00	0.00	0.01	0.00	0.00	0.00	0.00	0.01	0.00
Mn	0.00	0.00	0.00	0.00	0.00	0.00	0.00	0.00	0.00	0.00	0.00	0.00	0.00
Mg	0.00	0.00	0.00	0.00	0.00	0.00	0.00	0.00	0.00	0.00	0.00	0.00	0.00
Ca	0.27	0.26	0.26	0.24	0.49	0.24	0.19	0.35	0.25	0.31	0.40	0.29	0.40
Na	0.70	0.72	0.71	0.72	0.48	0.70	0.77	0.61	0.71	0.66	0.57	0.65	0.58
K	0.00	0.00	0.00	0.01	0.00	0.01	0.01	0.00	0.02	0.01	0.00	0.01	0.01
Total	4.98	4.99	4.98	4.98	4.99	4.97	4.98	4.97	4.99	4.98	4.98	4.97	4.99
An	0.28	0.26	0.27	0.25	0.50	0.25	0.20	0.36	0.26	0.32	0.41	0.31	0.40

Table 3.9. Continued

Sample No.	AC07121901A	07120402A	07120402A	A07123001E	A07123001N	A07123001P	A07123001R	A0723001AC	A07123001AF	BC08010302A	BC08010302A	BC08010302B	BC08010302C
Occurrence	matrix	aggregate	matrix	matrix	matrix	matrix	matrix	matrix	matrix	matrix	aggregate	matrix	matrix
Analysis No.	41	34	44	33	157	73	38	6	71	90	95	49	11
SiO_2	61.91	58.40	62.72	57.71	49.14	57.08	56.54	60.59	57.19	61.55	68.28	57.42	66.44
TiO_2	0.01	0.00	0.02	0.00	0.00	0.00	0.00	0.03	0.01	0.00	0.00	0.00	0.05
Al2O3	24.90	26.59	23.78	27.10	32.84	28.31	27.43	23.72	26.42	24.45	20.28	27.89	21.63
Cr_2O_3	0.01	0.00	0.04	0.00	0.01	0.00	0.00	0.00	0.02	0.00	0.00	0.00	0.00
FeO	0.25	0.50	0.01	0.00	0.30	0.00	0.08	0.10	0.03	0.05	0.03	0.79	0.02
MnO	0.01	0.00	0.00	0.00	0.00	0.07	0.00	0.01	0.04	0.00	0.02	0.00	0.00
MgO	0.00	0.00	0.02	0.01	0.02	0.00	0.00	0.00	0.01	0.00	0.01	0.00	0.00
CaO	5.96	8.33	5.33	9.36	15.81	10.41	9.23	6.16	9.23	5.66	0.66	10.01	2.68
Na_2O	8.14	6.63	7.99	5.93	2.68	5.76	6.52	7.79	5.93	8.18	10.50	5.91	9.62
K_2O	0.18	0.08	0.16	0.42	0.04	0.05	0.08	0.23	0.19	0.20	0.04	0.07	0.08
Total	101.35	100.53	100.07	100.58	100.92	101.75	99.87	98.63	99.07	100.09	99.82	102.14	100.52
Si	2.71	2.60	2.77	2.57	2.23	2.52	2.54	2.73	2.59	2.73	2.98	2.53	2.90
Ti	0.00	0.00	0.00	0.00	0.00	0.00	0.00	0.00	0.00	0.00	0.00	0.00	0.00
Al	1.29	1.40	1.24	1.42	1.76	1.47	1.45	1.26	1.41	1.28	1.04	1.45	1.11
Cr	0.00	0.00	0.00	0.00	0.00	0.00	0.00	0.00	0.00	0.00	0.00	0.00	0.00
Fe	0.01	0.02	0.00	0.00	0.01	0.00	0.00	0.00	0.00	0.00	0.00	0.03	0.00
Mn	0.00	0.00	0.00	0.00	0.00	0.00	0.00	0.00	0.00	0.00	0.00	0.00	0.00
Mg	0.00	0.00	0.00	0.00	0.00	0.00	0.00	0.00	0.00	0.00	0.00	0.00	0.00
Ca	0.28	0.40	0.25	0.45	0.77	0.49	0.44	0.30	0.45	0.27	0.03	0.47	0.13
Na	0.69	0.57	0.68	0.51	0.24	0.49	0.57	0.68	0.52	0.70	0.89	0.51	0.81
K	0.01	0.00	0.01	0.02	0.00	0.00	0.00	0.01	0.01	0.01	0.00	0.00	0.00
Total	4.99	4.99	4.96	4.98	5.01	4.99	5.02	4.99	4.98	4.99	4.95	5.00	4.95
An	0.29	0.41	0.27	0.45	0.76	0.50	0.44	0.30	0.46	0.27	0.03	0.48	0.13

Table 3.9. Continued

Sample No.	BC08010302C	BC08010401B	BC08010502B	BC08010504A	85011511B	84021904B	AC08011301M	AC012001A	AC08011601A	BC08010602J	BC08010604A	B08012201A	B08012201I
Occurrence	aggregate	matrix	matrix	matrix	matrix	matrix	matrix	matrix	matrix	matrix	matrix	matrix	matrix
Analysis No.	13	67	168	160	31	69	13	28	107	43	56	4	105
SiO_2	68.14	63.71	60.80	62.43	67.68	63.77	61.86	61.76	65.63	58.75	61.53	61.37	59.37
TiO_2	0.00	0.02	0.00	0.05	0.03	0.00	0.04	0.00	0.01	0.00	0.01	0.00	0.00
Al2O3	20.12	24.30	24.45	23.68	23.31	24.32	25.12	24.39	21.66	26.48	24.10	24.86	25.07
Cr_2O_3	0.00	0.00	0.00	0.00	0.00	0.03	0.01	0.00	0.00	0.02	0.00	0.00	0.00
FeO	0.17	0.02	0.04	0.40	0.03	0.25	0.00	0.00	0.12	0.03	0.05	0.28	0.16
MnO	0.00	0.02	0.02	0.00	0.05	0.00	0.04	0.00	0.08	0.09	0.00	0.08	0.44
MgO	0.02	0.01	0.00	0.00	0.00	0.00	0.01	0.01	0.00	0.00	0.01	0.01	0.02
CaO	0.58	5.24	6.22	5.28	3.39	5.07	6.26	6.01	2.87	8.54	5.95	6.31	7.36
Na_2O	11.41	8.23	7.78	8.50	9.12	8.72	7.98	8.01	9.77	7.28	8.11	7.80	7.64
K_2O	0.31	0.18	0.22	0.10	0.12	0.11	0.21	0.27	0.23	0.06	0.21	0.10	0.05
Total	100.77	101.73	99.52	100.44	103.74	102.26	101.51	100.45	100.36	101.26	99.97	100.80	99.66
Si	2.96	2.77	2.71	2.76	2.86	2.76	2.71	2.73	2.88	2.60	2.73	2.71	2.66
Ti	0.00	0.00	0.00	0.00	0.00	0.00	0.00	0.00	0.00	0.00	0.00	0.00	0.00
Al	1.03	1.24	1.29	1.23	1.16	1.24	1.30	1.27	1.12	1.38	1.26	1.29	1.32
Cr	0.00	0.00	0.00	0.00	0.00	0.00	0.00	0.00	0.00	0.00	0.00	0.00	0.00
Fe	0.01	0.00	0.00	0.01	0.00	0.01	0.00	0.00	0.00	0.00	0.00	0.01	0.01
Mn	0.00	0.00	0.00	0.00	0.00	0.00	0.00	0.00	0.00	0.00	0.00	0.00	0.00
Mg	0.00	0.00	0.00	0.00	0.00	0.00	0.00	0.00	0.00	0.00	0.00	0.00	0.00
Ca	0.03	0.24	0.30	0.25	0.15	0.24	0.29	0.28	0.13	0.41	0.28	0.30	0.35
Na	0.96	0.69	0.67	0.73	0.75	0.73	0.68	0.69	0.83	0.62	0.70	0.67	0.66
K	0.02	0.01	0.01	0.01	0.00	0.01	0.01	0.02	0.01	0.00	0.01	0.01	0.00
Total	5.01	4.96	4.99	4.99	4.93	4.99	4.99	4.99	4.99	5.02	4.99	4.98	5.01
An	0.03	0.26	0.30	0.25	0.17	0.24	0.30	0.29	0.14	0.39	0.28	0.31	0.35

Table 3.9. Continued

Sample No.	B08012203A	B08012204	B08012302A	B08012304C	B08012304D	B08012304E	B08012305D
Occurrence	matrix	matrix	matrix	matrix	matrix	matrix	matrix
Analysis No.	28	256	88	136	23	36	18
SiO_2	64.33	58.19	64.70	59.70	54.61	56.93	60.80
TiO_2	0.01	0.01	0.00	0.00	0.00	0.02	0.00
Al2O3	22.14	26.70	22.43	24.67	28.71	27.26	24.68
Cr_2O_3	0.00	0.04	0.00	0.00	0.01	0.00	0.00
FeO	0.04	0.19	0.24	0.03	0.05	0.19	0.05
MnO	0.03	0.44	0.00	0.00	0.04	0.00	0.13
MgO	0.00	0.00	0.00	0.01	0.01	0.00	0.00
CaO	3.41	8.68	3.63	6.89	11.72	9.68	6.33
Na_2O	9.21	6.47	9.12	7.64	4.83	5.75	7.80
K_2O	0.18	0.09	0.13	0.11	0.08	0.04	0.11
Total	99.34	100.35	100.24	99.05	100.05	99.87	99.91
Si	2.85	2.59	2.84	2.68	2.46	2.56	2.71
Ti	0.00	0.00	0.00	0.00	0.00	0.00	0.00
Al	1.16	1.40	1.16	1.31	1.53	1.44	1.29
Cr	0.00	0.00	0.00	0.00	0.00	0.00	0.00
Fe	0.00	0.01	0.01	0.00	0.00	0.01	0.00
Mn	0.00	0.00	0.00	0.00	0.00	0.00	0.00
Mg	0.00	0.00	0.00	0.00	0.00	0.00	0.00
Ca	0.16	0.41	0.17	0.33	0.57	0.47	0.30
Na	0.79	0.56	0.78	0.67	0.42	0.50	0.67
K	0.01	0.00	0.01	0.01	0.00	0.00	0.01
Total	4.97	4.99	4.97	5.00	4.99	4.98	4.99
An	0.17	0.42	0.18	0.33	0.57	0.48	0.31

Table 3.10. P-T estimations with several geothermobarometers in the central Sør Rondane Mountains.

sample No	T_1 (℃)	P_1 (GPa)
A07123001E	770	0.72
A07123001I	750	0.80
A07123001R	752	0.82

sample No	T_2 (℃)	T_3 (℃)	P (GPa)
A0712301N	812	802	0.80

sampleNo	T_4 (℃)
AC07121303E	736
AC07121701C	760
AC07121801M	777

sample No	T_5 (℃)	$P_{2\text{-}Mg}$ (GPa)	$P_{2\text{-}Fe}$ (GPa)	T_6 (℃)	$P_{2\text{-}Mg}$ (GPa)	$P_{2\text{-}Fe}$ (GPa)
AC07121901A				700	0.70	
AC08012001A2				619	0.70	
BC08010604E	600	0.67	0.69	610	0.67	0.69
B08012201I	552	0.69	0.72	662	0.71	0.80
B08012204	653	0.81	0.86	712	0.82	0.91
B08012304E	590	0.52	0.53	654	0.51	0.56

sample No	T_7 (℃)	P_3 (GPa)	
A07123001P	747	0.70	prograde
BC08010302B	782	0.70	prograde
A07123001AF	769	0.92	near Peak
AC08011301M	754	0.72	near Peak
AC07121702B a	554	0.40	retrograde

Numbers shown in red letters are assumed pressure. T_1: Harley (1984), T_2: Wells (1977), T_3: Taylor (1998), T_4: Perchuk&Lavrent'eva (1983), T_5: Graham&Powell (1984), T_6: Holland&Blundy (1994), T_7: Holdaway (2000), P_1: Newton&Perkins (1982), P_2: Kohn&Spear (1990), P_3: Wu et al. (2004)

Chapter 4. Titanium behavior in quartz during metamorphic process

4.1. Introduction

Recent experimental studies have noted the temperature dependence of Ti solubility in quartz. Wark and Watson (2006) and Kawasaki and Osanai (2008) developed calibrated Ti-in-quartz thermometers that enable estimates of the temperature conditions of igneous and metamorphic rocks. In high-temperature metamorphic terranes, rutile exsolution is commonly observed in silicate minerals such as quartz, garnet, orthopyroxene, sapphirine, K-feldspar, and osumilite (e.g., Osanai et al*.,* 2001; Osanai and Yoshimura, 2002). Rutile exsolution is generally considered to occur when a Ti-rich precursor precipitates excess Ti in response to decreasing Ti solubility during cooling or decompression (e.g., Kawasaki and Motoyoshi, 2007; Zhang et al., 2003). Accordingly, the chemical composition of pre-exsolution quartz probably preserves a record of metamorphism prior to the final equilibrium conditions.

The Sør Rondane Mountains, East Antarctica, is a high-grade metamorphic terrane that contains voluminous late-stage igneous rocks (e.g., Kojima and Shiraishi, 1986). The area is subdivided into the Northeastern (NE) and Southwestern (SW) terranes, with the former containing

orthopyroxene-bearing metamorphic rocks (Osanai et al., 1992). However, the orthopyroxene-bearing gneisses are commonly surrounded by orthopyroxene-free gneisses. Moreover, in large parts of the NE Terrane, felsic and pelitic rocks are strongly retrogressed, resulting in modification to the original mineral assemblages and chemical compositions attained at the peak metamorphic conditions. This overprinting makes it difficult to recognize the primary distribution of granulite in the Sør Rondane Mountains. Rrutile exsolution textures in the retrograde rocks are found, the textures are widespread throughout the NE Terrane (Fig. 4.1). The exsolution probably indicates an early high-grade metamorphic event; consequently, it may represent a key in understanding the granulite metamorphism observed in the Sør Rondane Mountains.

In this chapter, orthopyroxene felsic gneiss (OPG) and hornblende-biotite felsic gneiss (HBG) collected from the same outcrop, where HBG occurs as a narrow 1–2 m zone at the boundary between OPG and a pegmatite intrusion were investigated. Field relation indicates that OPG was converted to HBG by the effects of pegmatite intrusion. Rutile exsolution in quartz is found only in HBG. A comparison of Ti behavior between OPG and HBG,

combined with data regarding petrogenetic relationships, enables us to consider those factors that controlled the occurrence of rutile exsolution. Measurement of Ti concentrations in quartz was performed using an electron probe micro-analyzer (EPMA) and Ti-in-quartz thermometers were applied to exsolution-free OPG, exsolution-bearing HBG and several samples collected from the broad area of the central Sør Rondane Mountains. Based on the results, the implications of rutile exsolution for metamorphism in this region are discussed.

4.2. Field relationships

Samples of OPG (sample 07121003A) and HBG (sample 07121003B) were collected from the Koyubi Ridge in the western part of the Brattnipene area in the Sør Rondane Mountains. At this outcrop, the host rock, brownish OPG, is intruded by K-feldspar-plagioclase-quartz-mica pegmatite (Fig. 4.2a). These two rock types are not in direct contact, as grayish HBG occurs along the OPG–pegmatite boundary (Fig. 4.2b). A foliation, oriented oblique to the lithological boundary, is continuous from OPG to HBG (Fig. 4.2c). Based on these observations, it can be interpreted that HBG is the hydrated (bleached)

equivalent of OPG.

Shiraishi and Kagami (1992) reported a similar relationship at a neighboring outcrop in the Brattnipene area. The authors reported Sm-Nd and Rb-Sr ratios of orthopyroxene-bearing enderbitic gneisses and bleached hornblende-biotite-bearing felsic gneisses. Sm-Nd and Rb-Sr isochrones for whole-rock samples of the two lithologies yielded ages of 978 ± 52 Ma and 961 ± 101 Ma, respectively. Shiraishi et al. (2008) reported zircon U-Pb ages from the enderbitic gneisses: 951 ± 17 Ma from oscillatory zoned prismatic cores and 602 ± 15 Ma from unzoned rims, interpreted as the timing of magmatism of the protolith and granulite facies metamorphism, respectively.

4.3. Petrography, whole-rock chemistry, and mineral chemistry

4.3.1 Petrography and mineral chemistry

The mineral assemblages within the analyzed samples are listed in Table 4.1. Mineral compositions were analyzed using an EPMA (JEOL JXA-8200) with a 5 ch wavelength-dispersive X-ray analytical system (WDS), as installed at the National Institute of Polar Research, Japan. Representative mineral compositions are listed in Table 4.2. The analyses were performed at 15

kV accelerating voltage, 12 nA probe current, and 2 μm probe diameter. Mineral abbreviations are after Kretz (1983), and amphibole nomenclature is after Leake et al. (1997).

4.3.1-1 Orthopyroxene felsic gneiss

OPG (sample 07121003A) is composed mainly of quartz, plagioclase, orthopyroxene, clinopyroxene, hornblende, biotite, ilmenite, and magnetite, with accessory apatite and zircon. Orthopyroxene (X_{Mg} = 0.41) makes up a large portion of the mafic minerals in OPG (Fig. 4.3a). Orthopyroxene grains are up to 1 mm in diameter. Clinopyroxene (X_{Mg} = 0.55) is 300–500 μm in size, and is present in the matrix. Hornblende (X_{Mg} = 0.37, TiO_2 = 2.1 wt%) is brownish, classified as ferro-pargasite, and 0.5–1 mm in size. Biotite (XMg = 0.41, TiO_2 = 4.2 wt%) is rare and relatively fine grained (< 300 μm). Plagioclase (1–3 mm) shows antiperthitic texture (Fig. 4.3b). Host plagioclase is of anorthite–albite solid solution with a minor orthoclase component ($An_{30}Ab_{68}Or_2$), and K-feldspar blebs have a composition of $Or_{95}Ab_5An_{<1}$. Quartz (1–3 mm) contains sparse mineral inclusions (Fig. 4.3d). Apatite in this sample includes monazite needles with a shape-preferred orientation (Fig. 4.3b).

4.3.1-2 Hornblende-biotite felsic gneiss

HBG (sample 07121003B) is composed mainly of quartz, plagioclase, hornblende, biotite, ilmenite, and magnetite, with accessory apatite, allanite, and zircon. Hornblende can be divided into two types based on mode of occurrence and composition. Type 1 consists of relatively large grains (up to 2 mm) with X_{Mg} = 0.30 and TiO_2 concentrations varying from 2.1 wt% in the core to 0.8 wt% in the rim (Fig. 4.4a). The mineral color changes from brownish in the core to greenish in the rim. Type 2 consists of a greenish and fine-grained (up to 40μm) aggregate with quartz, with X_{Mg} = 0.32 and TiO_2 < 0.3 wt% (Fig. 4.4b). Biotite (X_{Mg} = 0.34, TiO_2 = 2.6 wt%) shows a radial shape, is 1–2 mm in size, and is commonly in contact with hornblende. The TiO_2 content of biotite in HBG is lower than that in OPG. Plagioclase (1–3 mm) is antiperthite (Fig. 4.4c). The host plagioclase and K-feldspar blebs have compositions of $An_{28}Ab_{71}Or_1$ and $Or_{93}Ab_7An_{<1}$, respectively. The proportion of blebs in HBG appears to be less than that in OPG. Quartz (1–3 mm) contains rutile needles with shape-preferred orientations in three directions (Fig. 4.4d). The needles, which are less than 1 μm thick and occur throughout the host grains, are interpreted to be of exsolution

origin.

4.3.2. Whole-rock chemistry

Bulk chemical analyses were carried out using a RIGAKU RIX3000 X-ray fluorescence spectrometer installed at the National Institute of Polar Research. The procedures followed in sample preparation and analysis are given in Seno et al. (2002), and the results are listed in Table. 4.1. For HBG, I also present values normalized to Al, which is generally thought to be relatively immobile compared with other elements. As stated above, field relationships indicate that HBG was formed from OPG during intrusion of the pegmatite. The modal abundance of hydrous minerals (including hornblende, biotite, and epidote) in HBG is higher than that in OPG, thereby indicating a supply of fluid from the pegmatite. However, the bulk composition of OPG and the Al-normalized bulk composition of HBG are similar, except for Si, K, and Fe, suggesting that only limited chemical modification resulted from fluid filtration from the pegmatite.

4.4. Measurements of Ti concentrations in quartz

Recent experimental studies have revealed the temperature dependence of the saturated concentration of Ti in quartz (Kawasaki and Osanai, 2008; Wark and Watson, 2006). Wark and Watson (2006) carried out synthetic experiments at temperatures of 600–1000°C at 1.0 GPa, and Kawasaki and Osanai (2008) calibrated Ti solubility using synthesized quartz at 1300 °C in atmospheric pressure, combined with empirical data for natural quartz. Wark et al. (2007) succeeded in applying this thermometer to natural rhyolite, thereby indicating its applicability at least to felsic rocks such as OPG and HBG. In addition, Kawasaki and Osanai (2008) reported a linear relation between temperature and the logarithm of TiO_2 content in quartz, for several rock types including quartzo-feldspathic rock, Mg-Al rock, and eclogite derived from a mixed pelite–basalt protolith. This finding of a similar relation for different rock types may indicate that the effect of bulk rock chemistry is of little importance, suggesting in turn that Ti-in-quartz thermometers are potentially applicable to a wide range of rock types. According to Wark and Watson (2006), the saturated concentration of Ti in quartz is 526 ppm (TiO_2 = 0.088 wt%) at 1000 °C, and 140 ppm (TiO_2 = 0.023 wt%) at 800 °C. To quantify such low concentrations of Ti

using EPMA requires the selection of an appropriate dispersive crystal, measurement time, and standard for Ti.

4.4.1 Optimum analytical conditions in analyzing homogeneous domains

Measurements were performed using a JEOL JXA-8200 electron probe micro-analyzer installed at the National Institute of Polar Research, at conditions of 15 kV accelerating voltage, 150 nA probe current, and 2 μm probe diameter.

4.4.1-1. Dispersive crystal and acquisition time

Quartz in OPG was fully scanned by WDS with normal PET and PETH crystals at acquisition times of 10–50 seconds (Fig. 4.5). Compared with normal PET, higher counts of Ti-Kα are obtained with PETH; however, a linear baseline cannot be obtained. Because a linear background is essential to obtain precise peak counts, I used a normal PET crystal for Ti analyses. Regarding acquisition time, 50-second measurements at each step yield clearer peaks than those obtained using 10-second measurements. For the unknown samples, acquisition time was set to 150 seconds for both peak and background, which yielded a detection limit of less than 10 ppm.

4.4.1-2 Standard for Ti

Chromite (TiO_2 = 0.120 wt%), spessartine (TiO_2 = 0.108 wt%), and rutile were considered for use as a standard for Ti, and I assessed the disparity between the reference value and the measured value of standard spessartine and chromite (Fig. 4.6). Calculated using a rutile standard, Ti content in spessartine was estimated to be 3.3% less than that in the reference value, whereas the content in chromite was 2.2% higher than that in the reference. Calculations using a spessartine standard yielded over-estimates for both spessartine (+0.6%) and chromite (+6.3%), whereas calculations using a chromite standard yielded under-estimates (–6.7% for spessartine and –1.3% for chromite). Given that the Ti-in-quartz thermometer provides the minimum temperature, I selected chromite as the standard for Ti measurements, to constrain the minimum concentration.

4.4.2 Analytical conditions and methods for the reintegration of Ti concentration in pre-exsolution quartz

I examined a procedure to reconstruct the Ti concentration in

pre-exsolution quartz. Several methods have been proposed in this regard: estimation based on chemical composition data and the area ratio of the host phase to the exsolved phase (e.g., Hokada, 2001; Raase, 1998), and estimation of a large-area-averaged chemical composition using a defocused beam (e.g., Bohlen and Essene, 1977; Harley, 1986). In the present case, exsolved rutile is less than 1 μm wide, making it difficult to calculate the area ratio. In addition, the variable length of the needles means that it is not always true that the area ratio of the rutile visible in the analyzed area is representative of the area ratio in the entire host grain. These limitations make it difficult to apply the former method for the reintegration. The large-area-averaged approach involves systematic matrix-effect errors of up to 10% (Bohlen and Essene, 1977; Raase, 1998). Taking these errors into account, I adopted the latter method due to the difficulty in applying the former method to such fine exsolutions. To minimize the mixed-matrix effect, measurements were performed with an accelerating voltage of 25 kV to enable deeper penetration of the incident electrons into the sample. The analytical conditions were as follows: 25 kV accelerating voltage, 150 nA electron current, and 50 and 100 μm probe diameter.

4.4.3 Results

The Ti concentrations obtained for grains in OPG are largely independent of probe diameter (0.018–0.020 wt% on average; Fig. 4.7). The exsolution-free area of a quartz grain in HBG yields TiO_2 = 0.007 wt%, suggesting the post-exsolution Ti content. The Ti concentrations obtained for HBG with settings of 100 μm and 25 kV are 0.018 wt% on average, with a similar range in data as that obtained for OPG. The results obtained with 50 μm and 25 kV show a wide scatter (Fig. 4.7), indicating that a probe diameter of 50 μm is insufficient considering the 20–30 μm intervals between needles, and indicating that these results would not represent the composition throughout the entire grain.

4.5. Discussion

4.5.1 Metamorphic reactions and pressure–temperature conditions

Based on mineral textures and chemistry, the mineral assemblages of OPG and HBG are interpreted as orthopyroxene + clinopyroxene + hornblende + biotite + quartz + plagioclase, and hornblende + biotite + epidote + quartz + plagioclase, respectively. The OPG sample probably records near-peak metamorphic conditions, as there is no clear evidence of retrogression.

Orthopyroxene–clinopyroxene thermometers (Taylor, 1998; Wells, 1977) yield temperature conditions of 820–840 °C for OPG and HBG (Table 4.3), consistent with the estimations described in previous chapter.

Type 1 hornblende in HBG has a near-constant X_{Mg} value from core (0.29) to rim (0.30), whereas Al_2O_3 and TiO_2 contents show significant core–rim variation (Al_2O_3, 11.2–12.34 wt%; TiO_2, 2.1–0.8 wt%), possibly related to cooling. Ti concentrations within the cores of type 1 hornblende in HBG are similar to those in OPG. These observations suggest that the rims of Ti-rich type 1 hornblende (= hornblende in OPG) were replaced by Ti-poor hornblende via the following reaction:

Hbl (Ti-rich) + Kfs + H_2O = type 1-Hbl rim (Ti-poor) + Bt + Qtz (1)

In this reaction, the Ti in hornblende from OPG is possibly distributed in biotite. Plagioclase in HBG contains a lower proportion of K-feldspar blebs than does plagioclase in OPG, indicating consumption of the orthoclase component in plagioclase via the above reaction.

Type 2 hornblende (X_{Mg} = 0.32, TiO_2 = 0.3 wt%) has a much lower Ti

content than does the rim of type 1 hornblende (X_{Mg} = 0.30, TiO_2 = 0.8 wt%), although X_{Mg} values are similar between the two types. In addition, the mode of occurrence of type 2 hornblende, which occurs as aggregates with quartz (Fig. 4.4b), indicates an origin via the break-down of orthopyroxene, as follows:

$$Opx + Pl + H_2O = \text{type 2-Hbl} + Qtz \quad (2)$$

The low Ti concentration in type 2 hornblende is consistent with an origin after orthopyroxene, which generally contains little Ti. I applied a hornblende–plagioclase thermometer (Holland and Blundy, 1994) to the rims of type 1 and type 2 hornblende, yielding equilibrium temperatures of 700–720 °C and 670–680 °C, respectively (Table 4.3). The rims are therefore interpreted to represent the products of intense hydration associated with intrusion of the pegmatite, and these estimated temperatures constrain the minimum temperature of the hydration event. These temperature estimates are about 100 °C higher than the previously estimated temperature of regional retrogression (580–530 °C; e.g., Asami et al., 1992).

Clinopyroxene is present in OPG but absent in HBG, which contains

epidote, suggesting the following reaction:

$$Cpx + Pl + H_2O + O_2 = \text{type 1-Hbl rim} + Ep + Qtz \quad (3)$$

The content of ferric iron in the rims of type 1 hornblende is higher than that in the cores, and epidote contains significant amounts of ferric iron. These observations indicate that oxygen entered the system in association with fluid infiltration. Reaction (3) might lie on the lower-pressure side of reaction curve (a) in Fig. 4.8, as proposed by Ellis and Thompson (1986), due to the presence of iron in epidote. Consequently, it is inferred that HBG preserves hydration conditions of around 650–700 °C and 0.6-0.8 GPa.

4.5.2 Temperature estimates based on Ti in quartz

Rutile exsolutions are distributed throughout the entire areas of quartz grains. If intracrystalline diffusion is effective, TiO_2 located near the grain boundary may be diffused out of the grain to form an exsolution-free rim; however, such a rim is not observed in the quartz grains from HBG, thereby indicating insignificant Ti diffusion. In addition, the bulk rock chemistry shows no

significant variation in Ti concentration between OPG and HBG. Consequently, I interpret that quartz in both OPG and HBG retains its pre-exsolution Ti concentrations. Ti concentrations in homogeneous quartz in OPG are similar to reconstructed concentrations calculated for quartz in HBG that contains rutile exsolutions. This finding indicates that quartz in OPG and pre-exsolution quartz in HBG had equivalent Ti concentrations.

The Ti concentration can be converted to temperature using a Ti-in-quartz thermometer (Kawasaki and Osanai, 2008; Wark and Watson, 2006). Using the thermometer of Kawasaki and Osanai (2008), I obtain a temperature of 550 °C for the pre-hydration quartz and 440 °C for the post-hydration quartz (Table 4.4). This thermometer requires the analysis of Ti-saturated rutile; however, rutile is absent in both OPG and HBG, suggesting that these estimates represent minimum temperatures. The thermometer proposed by Wark and Watson (2006) is based on the degree of Ti saturation (a_{TiO2}). Wark et al. (2007) reported that felsic rocks have an a_{TiO2} value of 0.6–1.0 in the presence of a Ti-rich phase such as ilmenite or titanite. In the present study, ilmenite is present instead of rutile in both OPG and HBG; therefore, values of 0.6–1.0 were applied.

Using the method of Wark and Watson (2006), I obtained temperatures of 830 °C (a_{TiO2} = 0.6) to 760 °C (a_{TiO2} = 1.0) for homogeneous quartz in OPG, and 820 °C (a_{TiO2} = 0.6) to 750 °C (a_{TiO2} = 1.0) for the reconstructed pre-exsolution quartz composition in HBG, which is interpreted as the pre-hydration temperature. These values are consistent with estimates obtained using orthopyroxene–clinopyroxene thermometers (820–840 °C) for OPG. An exsolution-free portion of a quartz grain in HBG yields a temperature of 690 °C (a_{TiO2} = 0.6) to 640 °C (a_{TiO2} = 1.0), which is interpreted as the temperature during the hydration event, consistent with the temperature obtained using the hornblende–plagioclase thermometer (670–720 °C) for HBG (Table 4.4 and Fig. 4.8).

The retrogression event had a marked effect on the chemical composition of hornblende and plagioclase; however, the reconstructed pre-exsolution quartz composition in HBG is probably a near-peak temperature. This indicates that the Ti-in-quartz thermometer has the advantage of being able to estimate the peak metamorphic temperature from intensely retrogressed samples.

4.5.3. Implications for rutile exsolution in HBG

The mechanism of exsolution is generally controlled by the degree of super-saturation, which in turn is related mainly to cooling. In the case of the studied samples, the rutile-exsolution-free quartz in OPG and the rutile-exsolution-bearing quartz in HBG are thought to have experienced the same pressure-temperature-time path. Moreover, Ti concentrations are similar in quartz from both OPG and HBG. The main difference between OPG and HBG is that the former shows little evidence of hydration, whereas the latter experienced intense hydration during cooling. These observations suggest that intense hydration may play a role in triggering the nucleation of rutile lamellae, and thereby the occurrence of rutile exsolution. Although the mechanism of nucleation of the lamellae, driven by hydration, is beyond the scope of this paper, I note two ways in which hydration might influence nucleation: hydration results in an increase in the degree of super-saturation, or a retrograde reaction within HBG involved quartz. I found a wide distribution of rutile exsolution in quartz across a large part of the NE terrane of the Sør Rondane Mountains (Fig. 4.1). If retrograde hydration is related to the occurrence of exsolution, the widespread distribution of exsolved rutile may indicate the extent of large-scale high-grade

(granulite facies?) metamorphism and subsequent hydration.

Given that rutile exsolution has been reported in several minerals from ultra-high pressure and/or ultra-high temperature metamorphic terranes, these textures could be indicative of such extreme conditions (e.g., Osanai et al., 2001; Zhang et al., 2003). However, in the present study, rutile exsolution occurred in quartz during a temperature drop from <850 °C to 650–700 °C. This finding suggests that ultra-high temperature is not essential for the development of rutile exsolution in quartz.

4.5.4. Application of the Ti-in-quartz thermometer for the metamorphic rocks in the central Sør Rondane Mountains and its implication for the metamorphic process.

The method with Ti-in-quartz thermometer tested in the previous section was applied for the metamorphic rocks for the representative lithologies in the central Sør Rondane Mountains (Table 4.5, Fig 4.9). Based on these estimations, temperature conditions of ±800 °C are recognized regionally in the NE terrane. These temperature estimations with Ti-in-quartz thermometer are consistent with the estimation for the rocks which escape retrograde hydration and preserve

peak mineral assemblage and composition. This widespread distribution of the granulite-facies condition estimated using Ti-in-quartz thermometer suggests that the granulite-facies metamorphism was certainly pervasive event in the NE terrane. However the rocks, which do not record the granulite-facies condition, also occur locally in the NE terrane. Although I have not have enough data for field relationship between the granulite-facies rocks and lower-grade rocks in the NE terrane, geochronological studies should provide a clue for the geological relation of the both lithologies (see next chapter). Most of the metamorphic conditions of the rocks in the SW terrane with Ti-in-quartz thermometer were estimated as <600 °C except for 720 °C of the garnet-biotite gneiss (BC08010604A) from the northern Walnumfjella. These conditions are consistent with the petrographical characteristics and thermometric result with matrix mineral pairs. This indicates that metamorphism of which condition is <600 °C should be regional event in the SW terrane. Such contrast of metamorphic conditions between the NE and the SW terranes implies that the two terranes had experienced different tectonic history.

In both terranes, rocks which do not show typical metamorphic conditions in each terrane also occur locally. Although I have not have enough

data for field relationship between the “proper” rocks and other rocks in each terrane, geochronological studies should provide a clue for the geological relation of the both lithologies (see next chapter).

4.6 Summary

1. Rutile exsolution in quartz was found in retrograde hornblende-biotite gneiss derived (bleached) from orthopyroxene felsic gneiss.

2. The compositions of orthopyroxene and clinopyroxene in OPG indicate a temperature of 840 °C, interpreted as the near-peak temperature. The compositions of hornblende and plagioclase in HBG suggest temperatures of 670–700 °C, interpreted as the temperature of the hydration event.

3. Ti concentrations in quartz were 110 ppm (equivalent to 760–820 °C) for homogeneous quartz in OPG and 35 ppm (650–700 °C) for an exsolution-free area in quartz within HBG. The pre-exsolution Ti concentration in quartz within HBG is 103 ppm, similar to the value in homogeneous quartz within OPG.

4. Although the main constituent minerals in HBG record the conditions of the hydration event, the reconstructed Ti content in pre-exsolution quartz

within HBG records pre-hydration conditions. Thus, the Ti-in-quartz thermometer has the potential to be a powerful tool in reconstructing the history of metamorphic rocks modified by retrogression.

5. On the basis of the estimations with Ti-in-Quartz thermometer, granulite-facies metamorphism should be pervasive event in the NE terrane. On the other hand, <600 °C of the metamorphic condition is typically recognized in the SW terrane. This contrast of the metamorphic condition between the two tarranes implies that they had experienced different tectonic history.

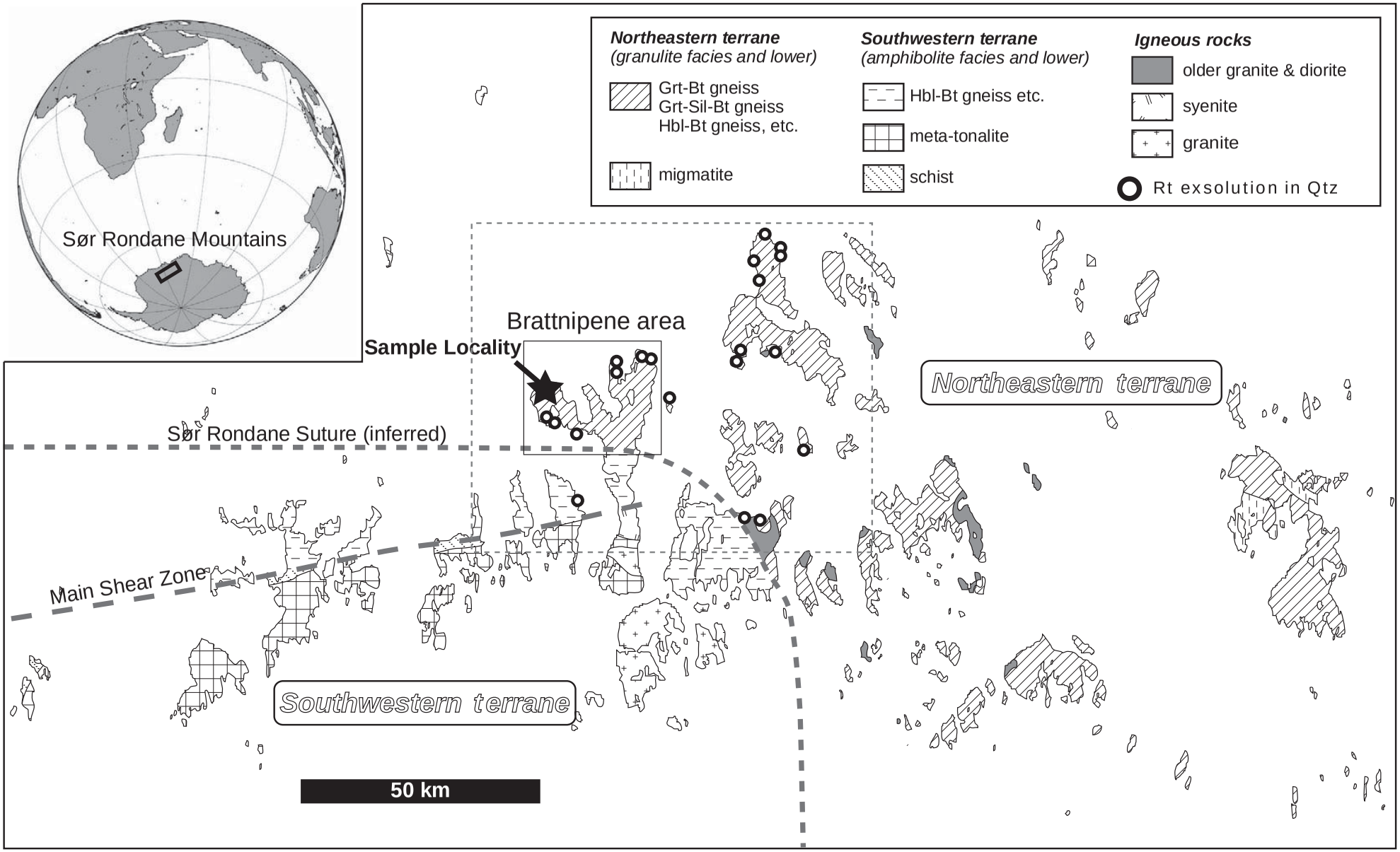

Fig.4.1. Geological map of the Sør Rondane Mountains (modified after Shiraishi et al., 1997). The sample locality is marked with a star. The location of the Sør Rondane Suture follows that proposed by Osanai et al. (1992). The dashed rectangle shows the area investigated in the present study.

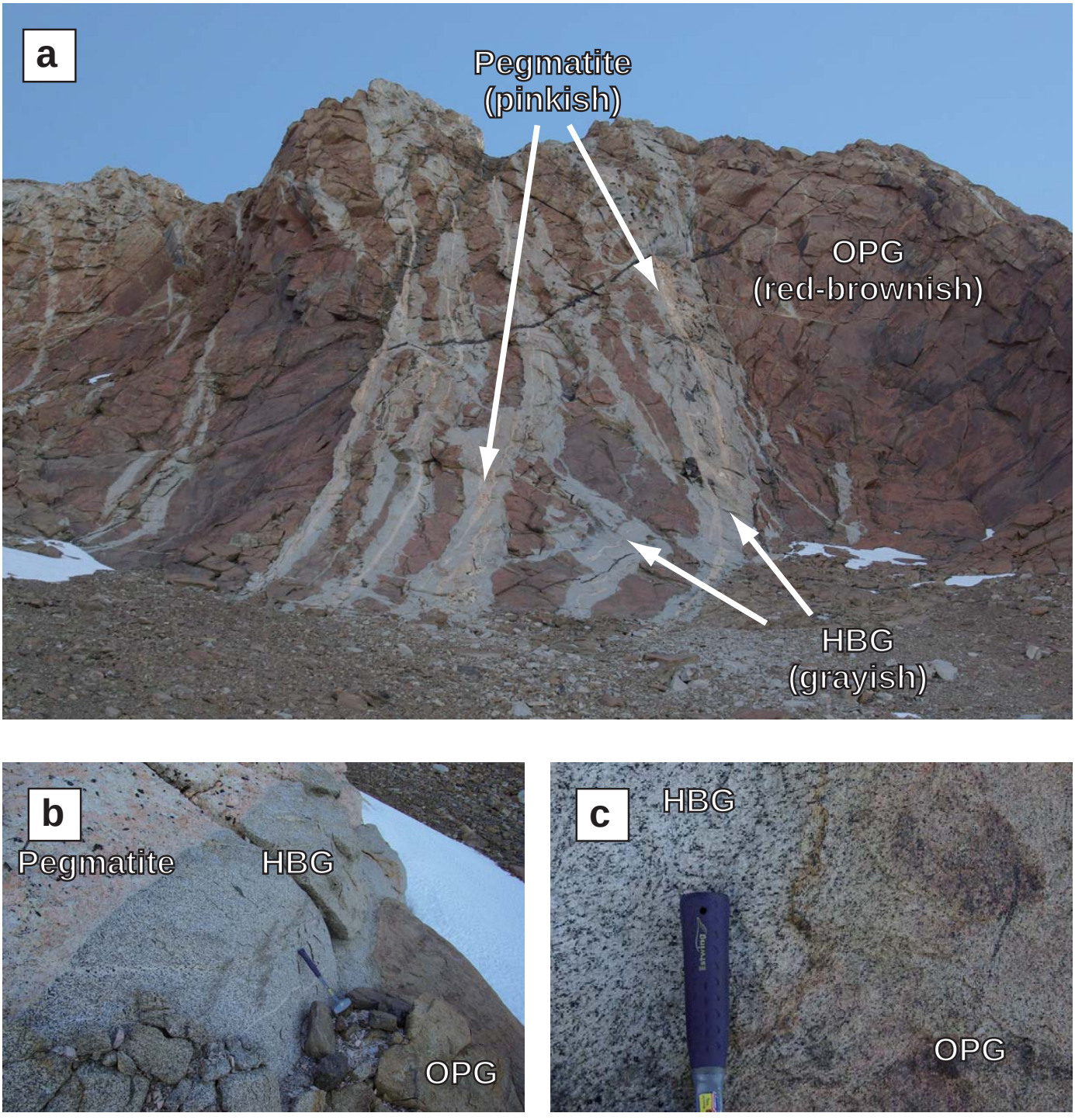

Fig. 4.2. Photographs of the sampled outcrop. (a) Large-scale field relationships among the studied rocks. Hornblende-Biotite felsic gneiss (HBG; grayish color) occurs within a bleached zone (about 1–2 m wide) in association with pegmatite veins (pinkish color), entirely within orthopyroxene felsic gneiss (OPG; red-brownish color). OPG is never in direct contact with pegmatite. (b) Photograph of the contacts between the three lithologies. (c) Close-up photograph of OPG and HBG. A foliation is continuous between OPG and HBG.

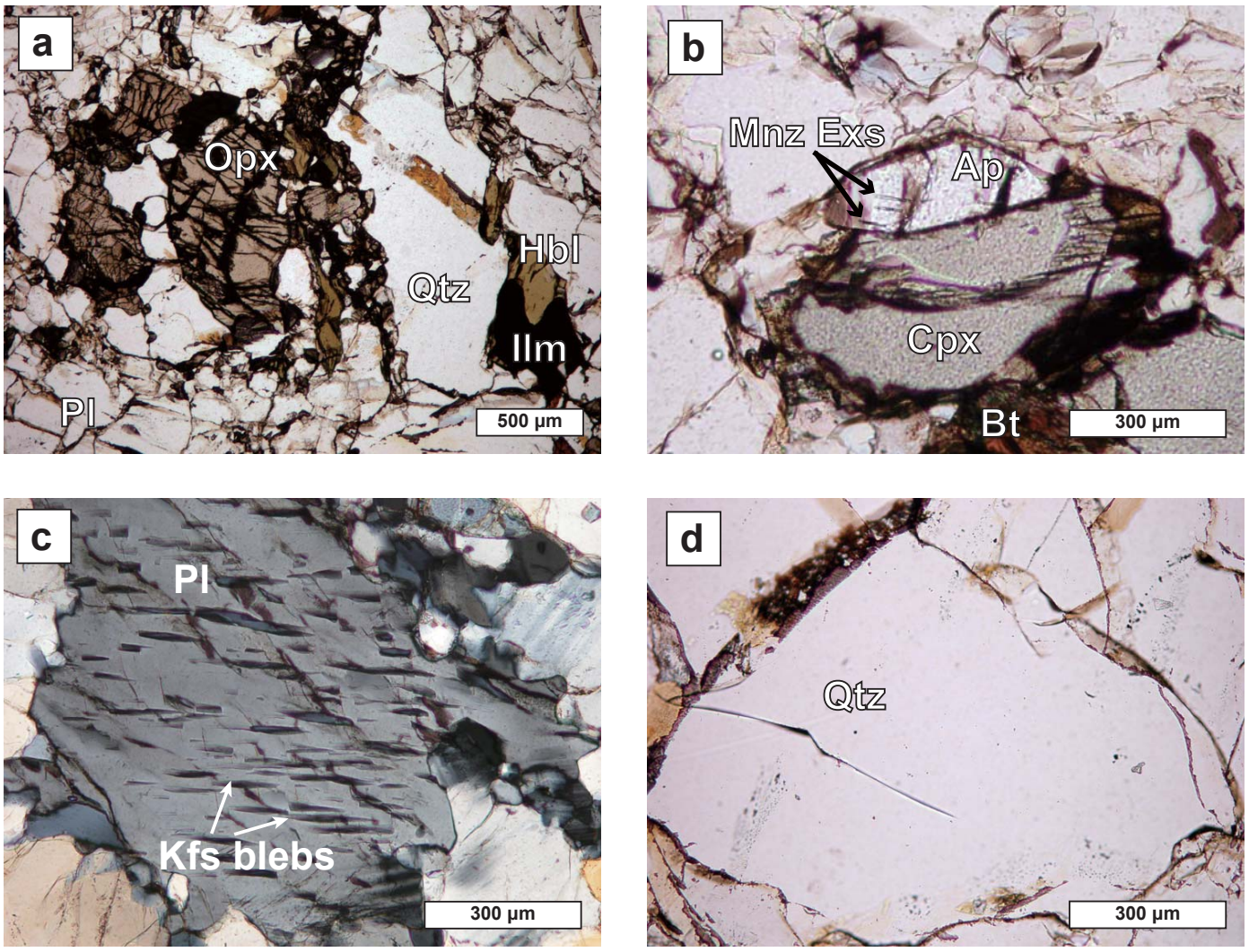

Fig. 4.3. Photomicrographs of orthopyroxene felsic gneiss (OPG). (a) Mineral relationships in OPG. Orthopyroxene is the main mafic mineral. (b) Occurrence of clinopyroxene and apatite. Clinopyroxene is present in the matrix. Apatite includes monazite needles. (c) Mode of occurrence of plagioclase, showing antiperthitic texture. (d) Quartz in OPG containing scarce mineral inclusions.

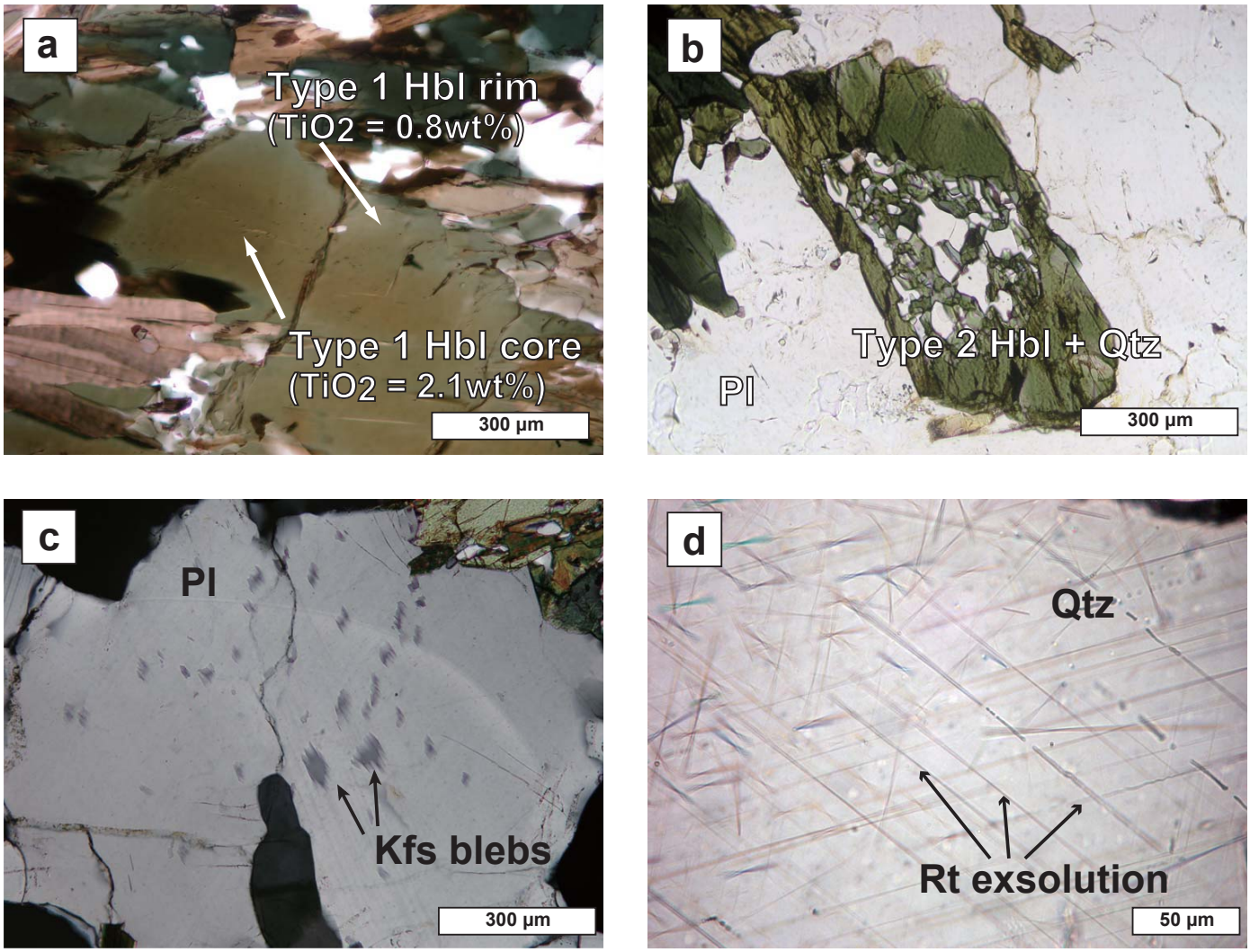

Fig. 4.4. Photomicrographs of hornblende-biotite felsic gneiss (HBG). (a) Type 1 hornblende shows compositional zoning from a brownish core to a greenish rim. (b) Mode of occurrence of type 2 hornblende, forming an aggregate with quartz. (c) Antiperthitic plagioclase in HBG. The proportion of K-feldspar blebs is less than that in OPG. (d) Rutile exsolution texture in quartz. Rutile needles have a shape-preferred orientation.

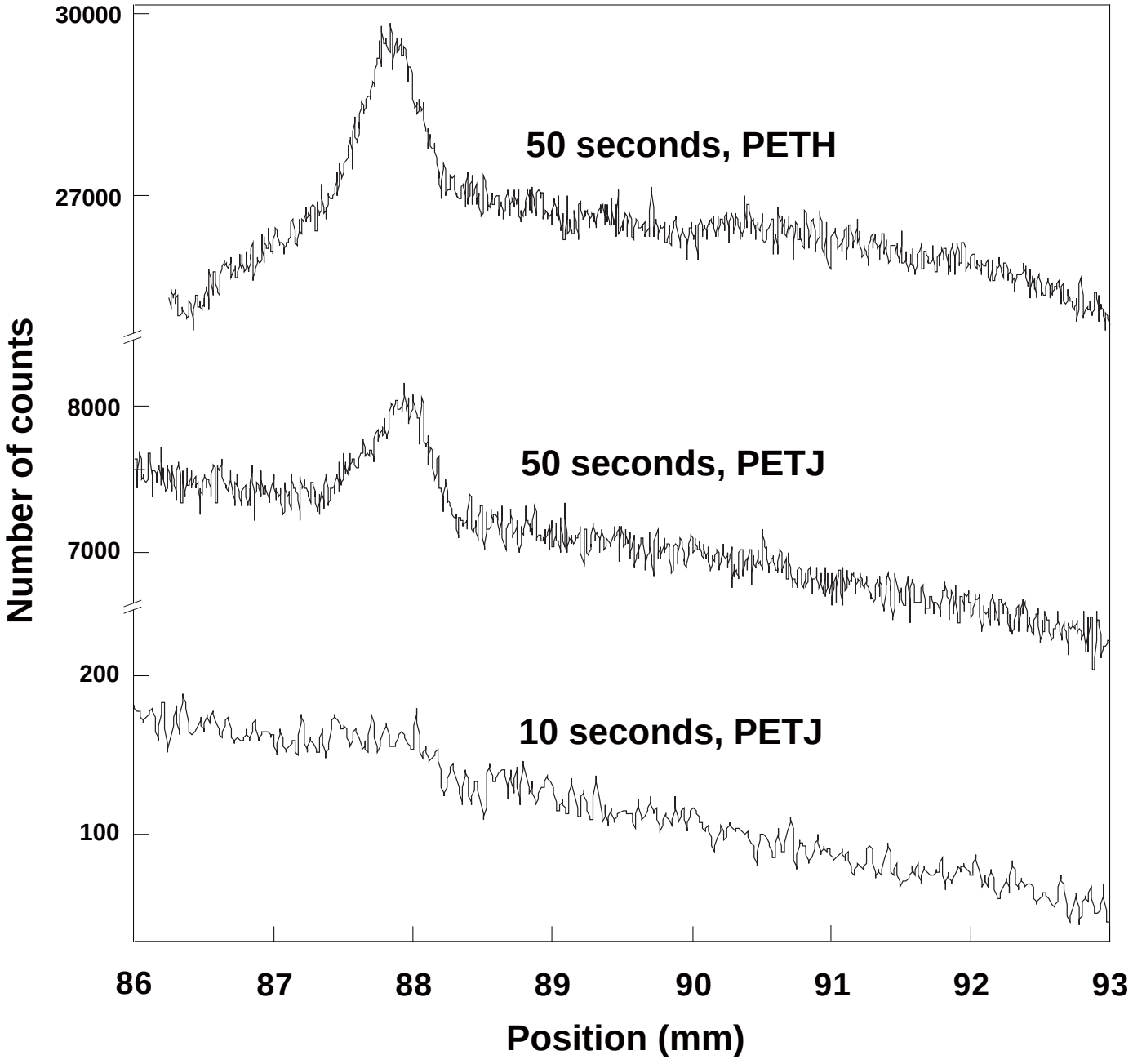

Fig. 4.5. X-ray spectra of quartz in OPG, as obtained by electron probe micro-analyzer (EPMA) with wavelength-dispersive X-ray analytical system (WDS) mode. PETH gives higher counts of Ti-Kα (top) than does normal PET; however, a linear baseline cannot be obtained using this approach. With normal PET using a 50-second measurement at each step, a linear baseline and sufficient counts are obtained (middle); however, there is no clear Ti-Kα peak for 10-second measurements (bottom).

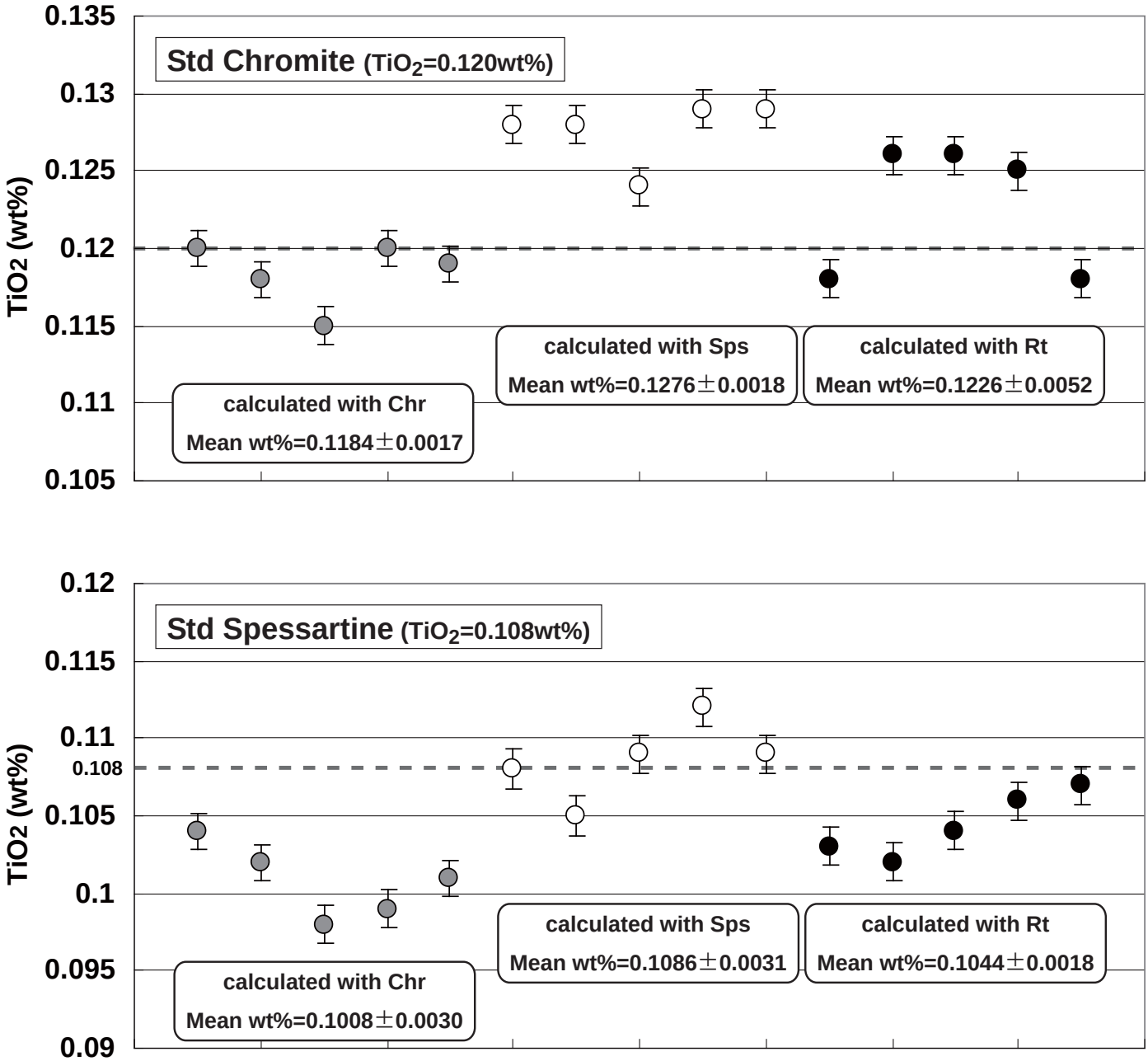

Fig. 4.6. Difference in the measured concentration of Ti in quartz when calibrated using three different standard materials. Dashed lines represent the reference values for the standards. Top: calibrated concentration of standard chromite. Bottom: calibrated concentration of standard spessartine.

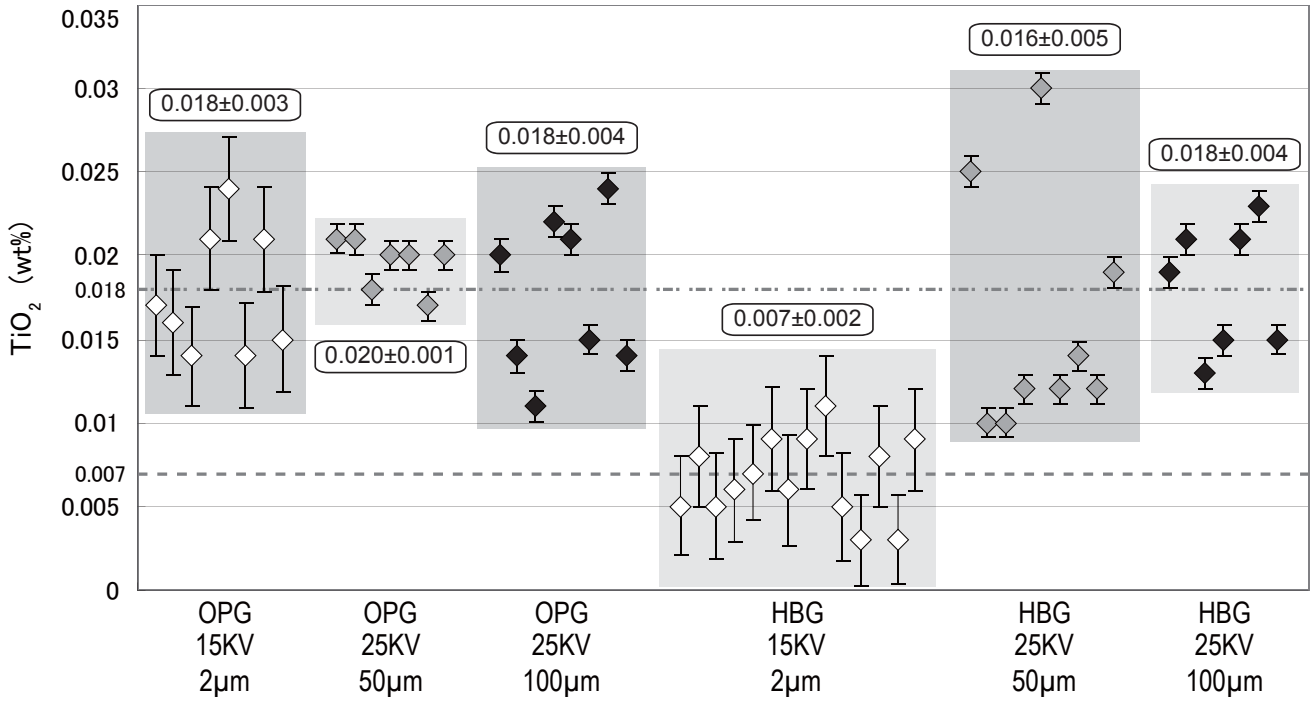

Fig. 4.7. Ti concentration measured using various accelerating voltages and beam diameters. Shaded boxes indicate the range of results for each setting. The values above each box are the weighted mean average of TiO2 wt%. Chain line: average value obtained for OPG (0.018 wt%); dashed line: average value obtained for HBG with a beam diameter of 2 μm and accelerating voltage of 15 kV (0.007 wt%).

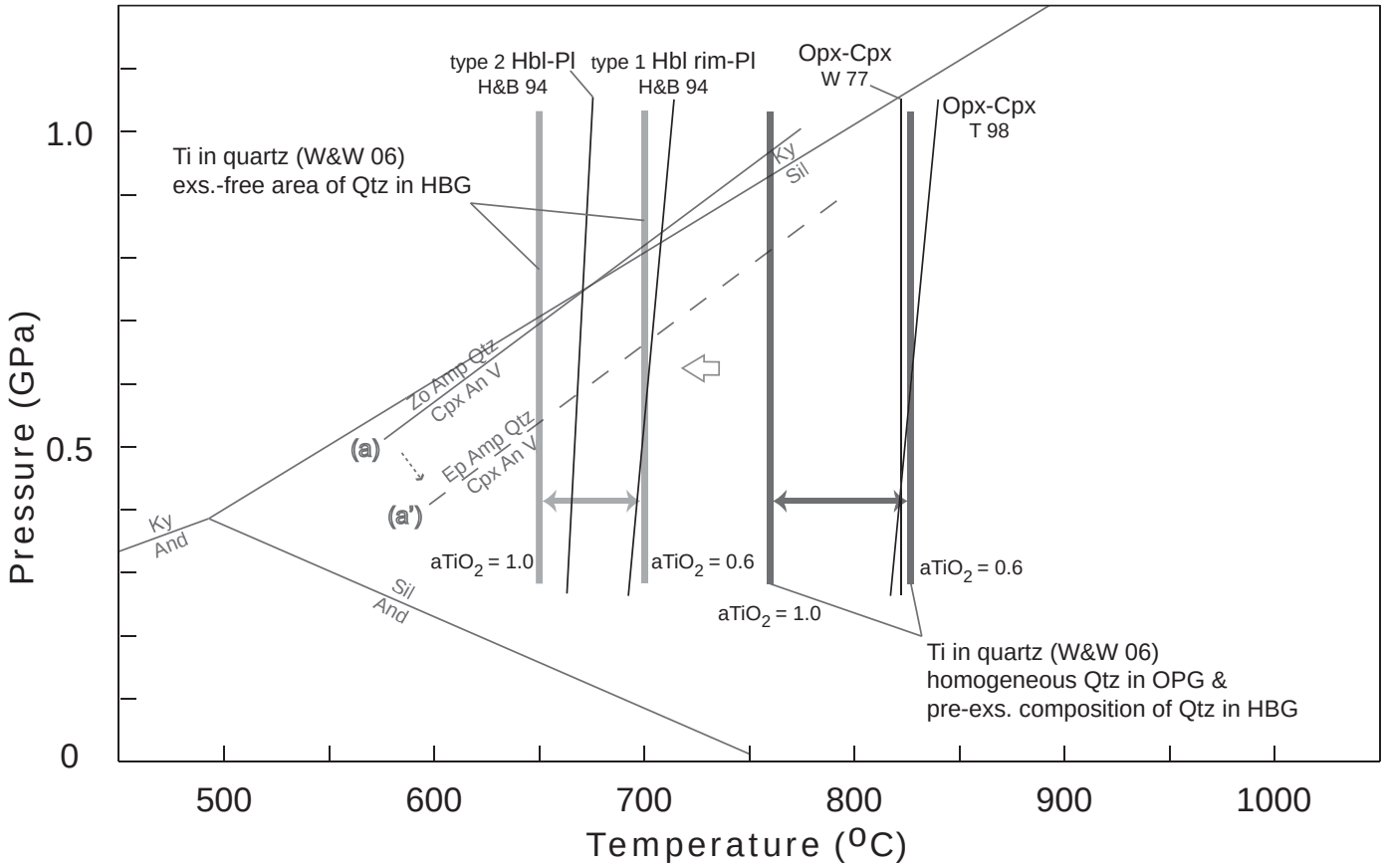

Fig. 4.8. Pressure–temperature conditions estimated for OPG and HBG. The dark and light grey thick lines indicate the temperature ranges estimated using a Ti-in-quartz thermometer of OPG and HBG, respectively (Wark and Watson, 2006). Reaction curve (a) is after Ellis and Thompson (1986). Temperature calibrations are as follows: H&B 94, Holland and Blundy (1994); T 98, Taylor (1998); W 77, Wells (1997).

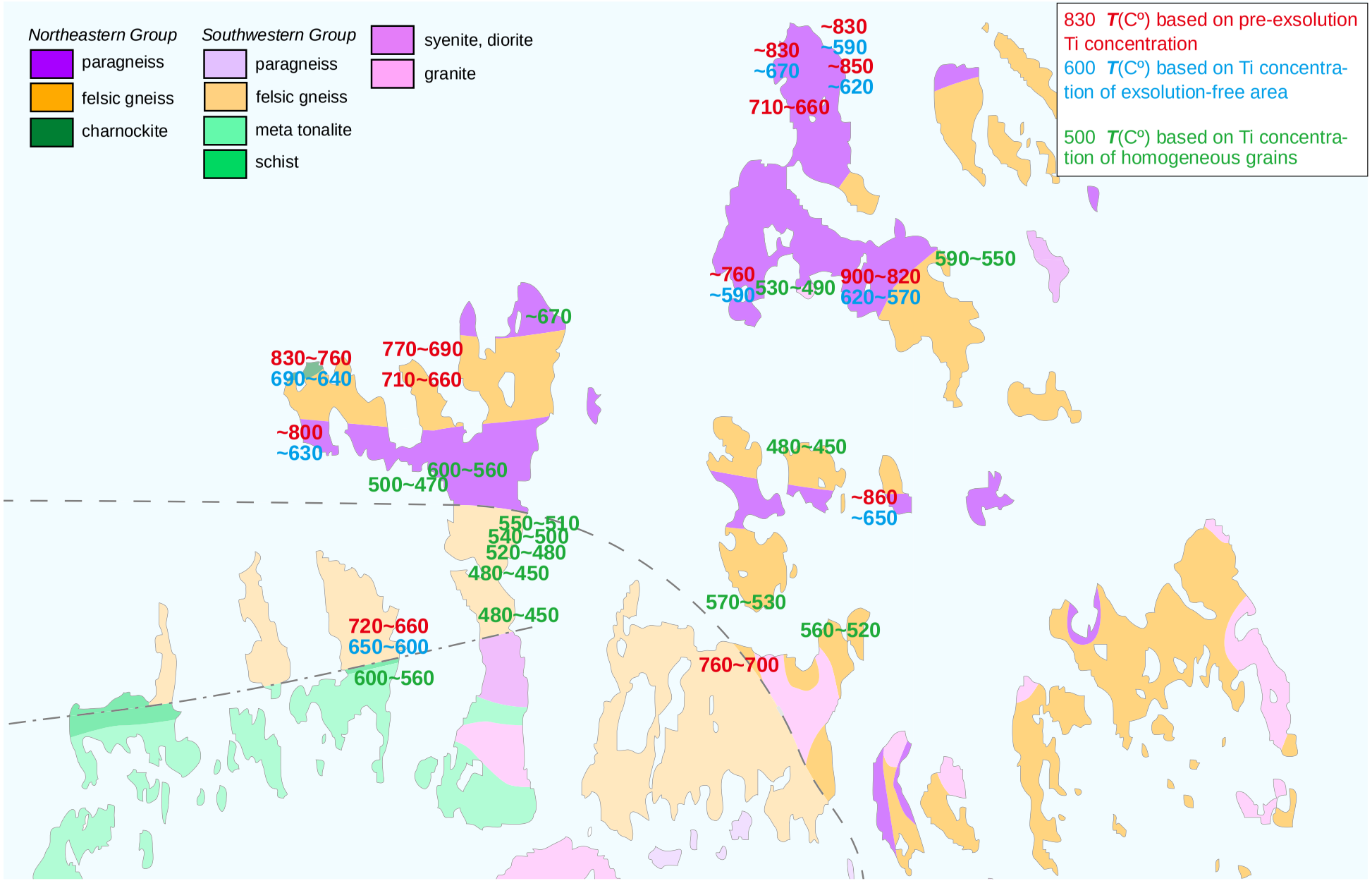

Fig. 4.9. Metamorphic temperatures estimated with Ti-in-Qtz thermometer (Wark&Watson, 2006) in the central Sør Rondane Mountains.

Table 4.1. Mineral assemblages and bulk chemistry for felsic gneisses from the Brattnipene area, Sør Rondane Mountains.

	OPG	HBG	HBG*
Qtz	○	○	
Pl	○	○	
Opx	○		
Cpx	×		
Hbl	△	○	
Bt	×	○	
Ep		△	
Ilm	–	–	
Mag	–	–	
Zrn	–	–	
Aln		–	
Ap	–	–	
SiO_2	73.00	70.63	65.84
TiO_2	0.33	0.39	0.36
Al_2O_3	13.74	14.74	13.74
$Fe_2O_3^{\dagger}$	3.64	4.46	4.16
MnO	0.07	0.08	0.07
MgO	0.74	0.98	0.91
CaO	3.52	3.92	3.65
Na_2O	3.98	4.43	4.13
K_2O	1.27	1.01	0.94
P_2O_5	0.08	0.09	0.08
LOI	0.05	0.24	0.22
Total	100.41	100.98	

○: common, △: moderately common, ×: rare, –: accessory

Mineral abbreviations are after Kretz (1983).

$Fe_2O_3^{\dagger}$, total Fe as Fe_2O_3. HBG* is Al-normalized value.

Table.4.2 Representative mineral compositions for felsic gneisses from the Brattnipene area, Sør Rondane Mountains.

Rock type	OPG	OPG	OPG	HBG	HBG	HBG	OPG	HBG	HBG	OPG	HBG	OPG	HBG
Minerals	Opx	Cpx	Hbl	Hbl 1-core	Hbl 1-rim	Hbl 2	Bt	Bt	Ep	Pl	Pl	Kfs bleb	Kfs bleb
SiO_2	50.35	51.16	40.80	39.95	40.92	41.64	36.20	35.21	38.18	61.19	61.46	63.98	63.70
TiO_2	0.09	0.17	2.13	2.09	0.76	0.33	4.21	2.58	0.08	0.02	0.01	0.04	0.03
Al_2O_3	0.79	1.64	11.43	11.22	12.36	11.60	14.49	15.22	23.69	24.24	24.04	18.25	18.41
Cr_2O_3	0.02	0.01	0.01	0.00	0.03	0.01	0.02	0.01	0.02	0.01	0.01	0.01	0.01
FeO^{total}	34.65	14.55	21.56	24.13	24.07	23.39	23.31	25.73	11.21	0.10	0.07	0.03	0.04
MnO	1.30	0.57	0.30	0.49	0.59	0.61	0.14	0.33	0.19	0.02	0.02	0.02	0.02
MgO	13.37	10.01	7.13	5.41	5.66	6.24	8.96	7.44	0.02	0.00	0.00	0.00	0.00
CaO	0.74	21.01	11.08	11.11	11.18	11.61	0.02	0.03	23.31	6.17	5.85	0.04	0.02
Na_2O	0.02	0.50	1.39	1.45	1.30	1.04	0.02	0.04	0.00	7.88	8.21	0.52	0.72
K_2O	0.01	0.01	1.90	1.85	1.60	1.26	9.62	9.45	0.02	0.39	0.23	15.75	15.25
Total	101.33	99.63	97.73	97.70	98.46	97.72	97.01	96.05	96.71	100.01	99.90	98.64	98.20
Si	1.97	1.97	6.33	6.26	6.28	6.39	5.55	5.52	3.03	2.72	2.73	2.99	2.99
Ti	0.00	0.00	0.25	0.24	0.08	0.04	0.49	0.30	0.00	0.00	0.00	0.00	0.00
Al	0.04	0.07	2.09	2.07	2.24	2.10	2.62	2.81	2.21	1.27	1.26	1.01	1.02
Cr	0.00	0.00	0.00	0.00	0.00	0.00	0.00	0.00	0.00	0.00	0.00	0.00	0.00
Fe^{3+} *				0.26	0.49	0.58			0.74				
Fe^{2+}	1.14	0.47	2.80	2.90	2.60	2.42	2.99	3.38	0.00	0.00	0.00	0.00	0.00
Mn	0.04	0.02	0.04	0.07	0.08	0.08	0.02	0.04	0.01	0.00	0.00	0.00	0.00
Mg	0.78	0.57	1.65	1.26	1.30	1.43	2.05	1.74	0.00	0.00	0.00	0.00	0.00
Ca	0.03	0.87	1.84	1.86	1.84	1.91	0.00	0.00	1.98	0.29	0.28	0.00	0.00
Na	0.00	0.04	0.42	0.44	0.39	0.31	0.01	0.01	0.00	0.68	0.71	0.05	0.07
K	0.00	0.00	0.38	0.37	0.31	0.25	1.88	1.89	0.00	0.02	0.01	0.94	0.91
Cation Total	4.01	4.01	15.78	15.73	15.61	15.51	15.60	15.71	7.99	4.99	5.00	4.99	4.99
O total	6	6	23	23	23	23	22	22	12.5	8	8	8	8
X_{Mg}	0.41	0.55	0.37	0.30	0.33	0.37	0.41	0.34					
An										0.30	0.28		

* Fe^{3+} is calculated value. X_{Mg}=Mg/(Mg+Fe), *An* =Ca/(Ca+Na+K)×100, *Or* =K/(Ca+Na+K)×100.

Table 4.3 Estimated P-T conditions for felsic gneisses from the Brattnipene area, Sør Rondane Mountains.

Rock type	Pair	K	$T_{1\ (°C)}$	$T_{2\ (°C)}$ -5Kbar	$T_{2\ (°C)}$ -10Kbar
OPG	Opx-Cpx	0.15	824	829	843

		Xab	$T_{3\ (°C)}$ -5Kbar	$T_{3\ (°C)}$ -10Kbar
HBG	Hbl 1 rim-Pl	0.28	703	715
	Hbl 2 -Pl		668	677

T_1: Wells (1977). T_2:Taylor (1998). T_3: Holland & Blundy (1994)

Table 4.4. Measured Ti contents in quartz and *T* estimation with Ti-in-quartz thermometers.

Rock type	Analytical condition	Ti content (ppm)	T_1 (°C)		T_2 (°C)
			a_{TiO2} = 0.6	a_{TiO2} = 1.0	
OPG	2 μm, 15 keV	107	822	756	545
	100 μm, 25 keV	111	827	760	552
HBG	2 μm, 15 keV	35	686	635	439
	100 μm, 25 keV	103	817	751	543

T_1: Wark & Watson (2006). T_2: Kawasaki & Osanai (2008)

Table.4.5 Measured Ti contents in quartz and *T* estimation with Ti-in-quartz thermometers.

Area	sample No.	Rt Exs.	Ti phase	Analytical condition	Ti content (ppm)	$T_{Ti\text{-}in\text{-}Qtz}$ (°C) a_{TiO2} = 0.6	a_{TiO2} = 1.0	T range (°C)
Brattnipene	07120402A	-	Rt	F	49		668	~670
	07121003A	-	Ilm	F	107	822	756	820~760
				D	111	827	760	830~760
	07121003B	○	Ilm	F	35	686	635	690~640
				D	103	817	751	820~750
	AC07123001F	-	Ilm	F	72	770	709	770~710
	AC07123001R	-	Ilm	F	59	745	688	750~690
	AC07123001AF	-	Ilm	F	43	709	655	710~660
	BC08010302A	○	Rt	F	49		668	~670
				D	147		796	~800
	BC08010302C	○	Rt	F	32		627	~630
				D	88		732	~730
	BC08010502B	-	Ttn	F	15	604	561	600~560
	BC08010504A	-	Ttn	F	4	501	467	500~470
Menipa	AC08011301M	○	Rt	F	41		650	~650
				D	228		857	~860
	AC08011601A	-	-	F	10	570	530	570~530
	AC08012001A	○	Ttn	F	-	-	-	
				D	3	481	449	480~450
Austkampane	AC07121302B	○	Rt	F	29		618	~620
				D	223		854	~850
	AC07121701C	○	Rt	F	48		666	~670
				D	188		829	~830
	AC07121702B	-	-	F	45	714	660	710~660
	AC07121801M	○	Rt	F	22		593	~590
				D	186		828	~830
	BC07122801C	○	Rt	F	22		593	~590
				D	115		764	~760
	BC07122805C	-	Ttn	F	6	530	494	530~490
	BC07122903A	○	Ilm	F	17	615	571	620~570
				D	177	896	821	900~820
	AC07121901A	-	-	F	13	592	550	590~550
Walnumfjelle	BC08010602J	-	-	F	15	604	561	600~560
	BC08010604E	○	Ilm	F	24	648	601	650~600
				D	46	716	662	720~660
Lunckeryggen	BC08012201I	-	-	F	8	552	514	550~510
	BC08012203A	-	Ilm	F	7	541	504	540~500
	BC08012204	-	Ilm	F	5	516	481	520~480
	BC08012302A	-	Ttn	F	3	481	449	480~450
	BC08012304E	-	-	F	3	481	449	480~450

$T_{Ti\text{-}in\text{-}Qtz}$: based on Wark & Watson (2006). D: with 100 μm of probe diameter and 25 kV of accerelating voltage, F: with 2 μm and 15 kV.

Chapter 5. Geochronology

5.1. Introduction

In the early stage of geochronological works in the Sør Rondane Mountains, Rb-Sr and K-Ar dating were performed in the whole mountains, and gave ages from 500 to 420 Ma, attributed to intense thermal event associated with plutonic activity (e.g. Picciotto et al., 1964, Takahashi et al., 1990). Shiraishi and Kagami (1992) reported ca. 1000 Ma from orthogneiss with Sm-Nd and Rb-Sr whole-rock isochron methods, and considered the timing of granulite-facies metamorphism in the NE terrane. They also obtained internal mineral isochrons from orthogneisses and paragneisses yielded 556 Ma and 624 Ma ages for Rb-Sr and Sm-Nd systems, respectively. These ages were interpreted as the timing of thermal events associated with granitic intrusions (Shiraishi & Kagami, 1992).

Asami et al. (1996, 1997, 2005) reported U-Pb monazite and zircon EPMA ages in granulites from the Sør Rondane Mountains. Monazite from granulite-grade metamorphic assemblages yielded chemical Th-U-total Pb isochron method (CHIME) ages that mostly range from 550 to 510 Ma, interpreted as the granulite-facies metamorphism. The authors explained ca.

1000 Ma as ages of the formation of protoliths, either of igneous or high-grade metamorphic lithologies.

Recently Shiraishi et al. (2008) reported sub-grain U-Pb ages of zircon with Sensitive High Resolution Ion Micro Probe (SHRIMP-II) in widespread area of the Sør Rondane Mountains. According to them, granulite-facies metamorphism in the NE terrane would be at ca. 650-600 Ma and amphibolite-facies metamorphism in thee SW terrane at ca. 570-550 Ma.

However metamorphic rocks in the Sør Rondane Mountains have experienced complex thermal history as described previous chapters, correspondence of metamorphic events to their timing should require precise petrological investigation. In this chapter, U-Pb zircon SHRIMP dating and U-Th-Pb monazite EPMA dating are performed. Analyzed samples were selected based on the combination of petrography and metamorphic condition estimated with Ti-in-quartz thermometer (Wark & Watson, 2006) which can estimate initial metamorphic condition from even intensely retrogressed rocks (see Chapter. 4). These results allow us to correlate metamorphic events with the ages precisely.

5.2. Sensitive High Resolution Ion Micro Probe (SHRIMP II) zircon U-Pb dating

Samples and analytical procedures

The present study compiles SHRIMP U-Pb zircon analyses for 14 samples obtained with the Sensitive High Resolution Ion Micro Probe (SHRIMP II) facilities at the National Institute of Polar Research, Japan. Data reduction and processing was performed using the Excel add-in program SQUID (v.1.12a; Ludwig, 2001) and plots were generated using ISOPLOT (v.3.50; Ludwig 2003). For zircon analysis, abundance of U was calibrated against standard SL13 (238ppm), and U-Pb measurements were calibrated against ^{204}Pb-corrected (Pb/U)/(UO/U)^2 values for standard FC1 (1099 Ma, Paces & Miller 1993). For each standard dataset, scatter on (Pb/U)/(UO/U)^2 ratios and external spot-to-spot errors are quoted with data from each sample in Tables 5.2-5.15.

All measurements on zircon were corrected for common Pb content using measured ^{204}Pb and a Stacey and Kramers (1975) model for ages approximating those of standard and unknown zircon ages (see Ludwig 2001 for details). Wherever possible, pooled ages were calculated from single analytical sessions using the Concordia Age function of SQUID, which has the advantage

of providing a test of concordance between pooled $^{206}Pb/^{238}U$ and $^{207}Pb/^{206}Pb$ ages. Mean $^{206}Pb/^{238}U$ ages for pooled data are also provided in the Tera-Wasserberg plots. Errors on individual spot ratios and ages are quoted at 1 sigma, whereas pooled ages and concordia intercept ages are quoted at 95% confidence levels. Concordia ages are always calculated separately from single sessions with a standard calibration. Where pooled ages were obtained using data from multiple sessions, mean $^{206}Pb/^{238}U$ ages were calculated incorporating errors from standard reproducibility in each session.

Samples selected for analyses are listed in Table 5.1. Localities are shown in Fig. 5.1 and mode of occurrences of analyzed samples are shown in Fig. 5.2. Zircon grains were separated from each sample, mounted in epoxy, polished and coated in high-purity gold using an evaporative coater. Sub-grain ion beam analysis of zircon with complex internal zoning requires careful attention to spot positioning, so backscattered electron and cathodoluminescence imaging was performed with a Scanning Electron Microscope before and after analysis, to identify spot positions overlapping multiple growth zones, grain edges, cracks or damaged zircon. Representative analyzed grains and spots are shown in Fig. 5.3. Data from analyses or sessions

with analytical problems (such as ion beam instability) are not included in the tables. On Tera-Wasserburg plots, data from spots on cracked or damaged zircon or with strongly discordant isotopic ratios are marked with error crosses (1 sigma) and are excluded from interpretation.

5.2.1. Brattnipene area

BC08010302C

This pelitic gneiss is collected at the southern part of Brattnipene. This sample is mainly composed of garnet, sillimanite, biotite, plagioclase, K-feldspar and quartz with minor zircon, monazite, apatite, magnetite and ilmenite. Quartz in this sample shows rutile exsolution texture, and the averaged Ti concentrations of the pre-/post- exsolution are estimated as 88 and 15 ppm, respectively. On the basis of these Ti concentrations, the temperature conditions of the pre-/post-exsolutions are calibrated using Ti-in-quartz thermometer (Wark & Watson 2006) as 800-730 °C and 600-560 °C, respectively (see the Chapter 4 for details).

Zircon grains have typical “soccer ball”-like morphology and internal structures (Fig. 5.3). The majority are rounded sector-zoned portion, with prismatic and oscillatory-zoned cores. These oscillatory-zoned cores are truncated by the

sector-zoned portion. In the sector-zoned portion, the difference of the CL brightness mainly associated with U concentration is recognized. However the correlation between the ages and the CL brightness is not clear.

From this sample, total of 31 analyses from 25 grains (Table 5.2) were obtained.

The oscillatory-zoned cores have U contents between 200 and 800 ppm and Th/U ratios between 0.2 and 0.75. Ages from 5 cores define a concordia age of 1056±12 Ma (MSWD=2.4, probability of concordance = 0.12). The age is of detrital zircon from an igneous source, probably of local derivation (see discussion). Just 1 grain (analyses 41) indicates ca. 900 Ma. This core preserves clear oscillatory zoning and show a concordance. This implies the possibility of the sedimentation after ca. 900 Ma.

The sector-zoned portions are characterized by high U (180-1820ppm) and relatively low Th/U (0.03-0.53). Most analyses indicate concordant ages, and these ages are interpreted as metamorphic origin. However their $^{206}Pb/^{238}U$ ages are scattered from 660 Ma to 580 Ma (Fig.5.4). The relative probability $^{206}Pb/^{238}U$ age distribution curve indicate the intense 620-630 Ma age peak and relatively small 580-590 Ma peak. Zircon textures or compositions in each age

group cannot be distinguished, it is therefore uncertain whether each age group represents a discrete metamorphic event in this sample alone.

07121003A

This felsic orthogneiss is collected at the northern part of the area. This sample is mainly composed of orthopyroxene, clinopyroxene, hornblende, biotite, plagioclase, k-feldspar and quartz with minor magnetite, ilmenite, apatite and zircon. The averaged Ti concentrations in quartz are 107 ppm, indicating the temperature conditions using Ti-in-quartz thermometer (Wark & Watson 2006) are 820-760 °C.

Zircon grains preserve euhedral oscillatory-zoned cores truncated and partially replaced by unzoned high-CL domains (Fig. 5.3).

From this sample, total of 21 analyses from 14 grains (Table 5.3) were obtained.

The structureless high-CL domains have U content between 60-180 ppm and Th/U ratio between 0.22 and 0.25. The $^{206}Pb/^{238}U$ ages are scattered around 650-600 Ma and their weighted mean averaged $^{206}Pb/^{238}U$ age defines 627±15 Ma (MSWD=4.1) (Fig. 5.4). This age is interpreted as the timing of the

metamorphism on this sample.

The oscillatory zoned cores have U contents ranging 110-850 ppm and Th/U ratio between 0.18 and 0.34. Most of the core ages are discordant and their $^{206}Pb/^{238}U$ ages are scattered between 670 and 990 Ma. However the error-weighted regression (n=15, MSWD=2.2) gave an upper concordia intercept at 990±55 Ma when the lower intercept is anchored at 627±15 Ma. This age is interpreted as the magmatic zircon growth in the igneous protolith.

BC08010502B

This deformed granitic orthogneiss is collected at the southern part of the area. This sample is mainly composed of garnet, biotite, plagioclase, microcline and quartz with minor zircon, apatite, magnetite, ilmenite and titanite. The averaged Ti concentrations in quartz are 15 ppm, indicating the temperature conditions using Ti-in-quartz thermometer (Wark & Watson 2006) are 560-600 °C.

Zircon grains preserve euhedral oscillatory-zoned cores truncated and partially replaced by unzoned low-CL domains (Fig. 5.3).

From this sample, total of 23 analyses from 20 grains (Table 5.4) were obtained.

The oscillatory zoned cores have U contents ranging 74-2800 ppm and Th/U ratio between 0.07and 0.62. The core ages cluster around 800 Ma, especially concentrate at ca. 780Ma. 8 data from 8 grains define a concordia age of 784±2 Ma (MSWD=0.72, probability of concordance = 0.40) (Fig.5.4). This age is interpreted as the magmatic zircon growth in the igneous protolith.

The structureless low-CL domains have U content between 260-3620 ppm and Th/U ratio between 0.07 and 0.50. With the exception of analysis 32.2 indicating 640 Ma, the majority of ages cluster around 700 Ma and they define a concordia age of 692±6 Ma (MSWD=0.85, probability of concordance = 0.36, 6 data from 6 grain). This age is interpreted as the timing of the metamorphism on this sample.

07121003D (pegmatite)

This undeformed pegmatite is collected at the Koyubi Ridge. This pegmatite intrudes the orthopyroxene-bearing felsic gneiss (sample 07121003A) which is converted into hornblende-biotite bearing felsic gneiss (sample 07121003B, see chapter 4). This sample is mainly composed of quartz, plagioclase, K-feldspar and biotite with minor zircon, apatite and monazite.

Zircon grains have euhedral and prismatic shape. Most of them are partly metamictized. CL emission is extremely low, and zonation is unclear (Fig. 5.3).

From this sample, total of 12 analyses from 7 grains (Table 5.5) were obtained.

The grains have very high-U content (4290-20150 ppm) and very low Th/U ratio (<0.06). Most of the ages are discordant due to the matrix effect caused by high-U content. However $^{207}Pb/^{206}Pb$ ages cluster around 550 Ma and define weighted mean averaged $^{207}Pb/^{206}Pb$ age of 546±4 Ma (MSWD=1.3) (Fig.5.4). This age is interpreted as the timing of the intrusion of this pegmatite.

BC07121703A (pegmatite)

This undeformed pegmatite is collected Hitosashiyubi Ridge. This pegmatite is mainly composed of quartz, plagioclase, K-feldspar and biotite with minor zircon, apatite.

Zircon grains have slightly rounded euhedral shape. Grains have vague sector zoning and CL emission is commonly low (Fig. 5.3).

From this sample, total of 12 analyses from 12 grains (Table 5.6) were obtained.

The grains have very high-U content (560-1130 ppm) and Th/U ratio between

0.1 and 0.2. The ages define a concordia of 546±5 Ma (MSWD=0.67, probability of concordance = 0.79) (Fig.5.4). This age is interpreted as the timing of the intrusion of this pegmatite. And this age is highly consistent with the age of sample 07121003D which is the pegmatite occurring at the other ridge in Brattnipene area.

5.2.2. Austkampane

AC07121901A

This felsic gneiss is collected at the southeastern part of Austkampane. This sample is mainly composed of hornblende, biotite, plagioclase, K-feldspar and quartz with minor zircon, apatite and titanite. The averaged Ti concentrations in quartz are 13 ppm indicating the temperature conditions using Ti-in-quartz thermometer (Wark & Watson 2006) are 550-590 °C.

Zircon grains have oscillatory zoned cores with unzoned low CL rim (Fig. 5.3).

From this sample, total of 76 analyses from 62 grains (Table 5.7) were obtained.

The cores well-preserving the original oscillatory zoning have U contents between 290 and 1540 ppm and Th/U ratios between 0.03 and 0.75. 11 analyses

from 11 grains define a concordia of 887±2 Ma (MSWD=1.4, probability of concordance = 0.24) (Fig.5.4). This age is interpreted as a timing of magmatic zircon growth in the igneous protolith.

The grains indicate 800-850Ma are discordant and their internal textures are vague compared with the concordant grains. This suggests incomplete recrystallization or partial Pb resetting during the later stage events. The unzoned rims have U contents between 120 and 3160 ppm and Th/U ratios between 0.03 and 0.89. Most results are scattered between 650 and 550 Ma. The relative probability $^{206}Pb/^{238}U$ age distribution curve indicates the peak at 600 Ma and 550-570 Ma. Zircon textures or compositions in each age group cannot be distinguished. These ages are interpreted as the timing of metamorphism, however whether such event is discrete or continuous is not unclear. Just 3 analyses indicate ca. 700 Ma concordant ages. Although the number of analyses is sufficient, it might suggest the possibility of metamorphism at this period.

BC07122805C

This felsic gneiss is collected at the southwestern part of Austkampane. This sample is mainly composed of garnet, biotite, plagioclase, K-feldspar and quartz

with minor zircon, apatite and monazite. The averaged Ti concentrations in quartz are 6 ppm indicating the temperature conditions using Ti-in-quartz thermometer (Wark & Watson 2006) are ca. 500 °C.

Zircon grains have oscillatory zoning and euhedral and prismatic shape. Few grains have unzoned low-CL rim (Fig. 5.3).

From this sample, total of 26 analyses from 20 grains (Table 5.8) were obtained.

The analyzed grains have U contents between 52 and 550 ppm and their Th/U ratios concentrate around 0.25. The ages concentrate at ca. 640Ma and the age difference between oscillatory zoned domain and structureless low-CL domain is not recognized. The ages define a concordia of 634±5 Ma (MSWD=1.3, probability of concordance = 0.24, 16 grains) (Fig.5.4). This age is interpreted as a timing of magmatic zircon growth in the igneous protolith.

AC07121501U (granite)

This undeformed granite is collected at the northern part of the Austkampane. This granite is including large ultra mafic body (200 m200m). This rock is mainly composed of quartz, plagioclase and K-feldspar with minor biotite, zircon, apatite

and monazite.

Zircon grains have euhedral shape and show oscillatory zoning which can be observed with BSE. CL emission is commonly low (Fig. 5.3).

From this sample, total of 15 analyses from 15 grains (Table 5.9) were obtained.

The grains have very high-U and Th contents (U: 4660-16390 ppm, Th: 1690-8060 ppm) except grains have relatively high CL (U: 240-760 ppm, Th: 240-340 ppm). Most of the ages are discordant due to the matrix effect caused by high-U content. $^{207}Pb/^{206}Pb$ ages cluster around 500 Ma and define weighted mean averaged $^{207}Pb/^{206}Pb$ age of 502±4 Ma (MSWD=1.3) (Fig.5.4). This age is interpreted as the timing of crystallization of zircons in this granite. Two grains (analyses 15 and 17) which have concordant ages of ca. 1000Ma and ca. 850 Ma are explained as inherited grains in ca. 500 Ma magmatism.

AC07121601A (granite)

This undeformed massive granite is collected Nordhaugen. This granite is mainly composed of quartz, plagioclase, K-feldspar and biotite with minor zircon, apatite and monazite.

Zircon grains have euhedral and prismatic shape. Except a few grains which have clear oscillatory zoning, most grains are structureless and their CL emission is extremely low (Fig. 5.3).

From this sample, total of 19 analyses from 19 grains (Table 5.10) were obtained.

Except a few grains, the grains have very high-U content (2390-9520 ppm) and Th content between 709 and 5405 ppm. Most of the ages are discordant due to the matrix effect caused by high-U content. $^{207}Pb/^{206}Pb$ ages from 13 grains define weighted mean averaged $^{207}Pb/^{206}Pb$ age of 512±4 Ma (MSWD=1.54) (Fig.5.4). This age is interpreted as the timing of the crystallization of zircon in this granite. Just one grain (analysis 12) indicates ca. 1000Ma which is interpreted as an inherited zircon.

5.2.3. Menipa

AC08011301M

This quartzo-feldspathic gneiss is collected from at the southeastern part of Menipa. This sample is mainly composed of garnet, biotite, plagioclase, K-feldspar and quartz with minor zircon, apatite, rutile, magnetite and ilmenite.

Quartz in this sample has rutile exsolution texture, and the averaged Ti concentrations of the pre-/post- exsolution are estimated as 228 and 41 ppm, respectively. On the basis of these Ti concentrations, the temperature conditions of the pre-/post- exsolutions are calibrated using Ti-in-quartz thermometer (Wark & Watson 2006) as 860 °C and 650 °C, respectively.

Zircon grains have rounded or elongated shape. Commonly oscillatory-zoned cores are recognized with low-CL and vague internal texture rim (Fig. 5.3). At the boundary between the oscillatory-zoned core and low CL domains, high-CL ring is commonly found.

From this sample, total of 24 analyses from 18 grains (Table 5.11) were obtained.

The oscillatory-zoned cores have U contents between 130 and 1330 ppm and Th/U ratios between 0.06 and 0.67. The ages are highly scattered, and they does not define any concordant or intercept ages (Fig.5.4). However most of the ages obtained from the core are older than 1000Ma. Just 2 analyses (analyses 29.2 and 31.2) show the near concordant ages at ca. 780 Ma.

The combination of the zircon texture, composition and age distribution indicates the origin as detrital zircon with several igneous sources. The youngest

concordant age, ca 780 Ma, might imply the magmatism at this period and subsequent sedimentation.

The structureless rims have U content between 280 and 650 ppm and relatively low Th/U ratio (0.05-0.47). The ages from the rim are also highly scattered, and they does not define any concordant or intercept ages. The $^{206}Pb/^{238}U$ ages from the structureless rim range between 670-580 Ma. This might be interpreted as the timing of metamorphism.

AC08012001A

This felsic orthogneiss is collected at the northern part of Menipa. This sample is mainly composed of hornblende, biotite, plagioclase and quartz with minor zircon, apatite, magnetite, ilmenite, titanite and allanite. The averaged Ti concentrations in quartz are below detection limit (< 5 ppm) indicating the temperature conditions using Ti-in-quartz thermometer (Wark & Watson 2006) are < 500 °C.

Zircon grains preserve oscillatory-zoned cores however intensely replaced by unzoned low-CL domains (Fig. 5.3).

From this sample, total of 26 analyses from 22 grains (Table 5.12) were

obtained.

The structureless low-CL domains have U content between 320-2350 ppm and Th/U ratio between 0.05 and 0.4. Ages from 16 data from 14 grains define a concordia age of 564±3 Ma (MSWD=0.05, probability of concordance = 0.82) (Fig.5.4). This age is interpreted as the timing of the metamorphism on this sample.

The oscillatory zoned cores have low U and Th contents (U: 37-62 ppm, Th: 11-22 ppm). The core ages are highly ranging 730 to 890 Ma. Because of the scattering of the age and the fewness of the data, it is difficult to discuss the significance of these data.

5.2.4. Lunckeryggen

B08012201I

This intermediate orthogneiss is collected at lunckeryggen. This sample is mainly composed of garnet, hornblende, biotite, plagioclase, microcline and quartz with minor zircon, apatite, magnetite and ilmenite. The averaged Ti concentrations in quartz are 22 ppm, indicating the temperature conditions using Ti-in-quartz thermometer (Wark & Watson 2006) are 590-640 °C.

Zircon grains commonly show oscillatory-zoning partially replaced by high-CL domains at the rim portion (Fig. 5.3).

From this sample, total of 14 analyses from 13 grains (Table 5.13) were obtained.

The oscillatory zoned cores have U contents ranging 360-3290 ppm and Th/U ratio between 0.23and 0.77. The ages define a concordia age of 986±4 Ma (MSWD=1.3, probability of concordance = 0.45) (Fig.5.4). This age is interpreted as the magmatic zircon growth in the igneous protolith.

Partial replacement with the high-CL domains would be due to the late metamorphism or related event, however they are too thin to analyze with SHRIMP.

B08012304E

This intermediate orthogneiss is collected at Lunckerrygen. This sample is mainly composed of garnet, hornblende, biotite, plagioclase and quartz with minor zircon, apatite. The averaged Ti concentrations in quartz are estimated as < 10 ppm . On the basis of these Ti concentrations, the temperature conditions calibrated using Ti-in-quartz thermometer (Wark & Watson 2006) are < 500 °C.

Zircon grains have prismatic and oscillatory-zoned cores truncated and replaced by low-CL domains at the rim portion (Fig. 5.3). The low-CL domain is structureless.

From this sample, total of 23 analyses from 14 grains (Table 5.14) were obtained.

The structureless low-CL domains have high-U content (2780-7240 ppm) and very low Th/U ratio (0.01-0.04). Most of the ages from this domain are discordant due to the matrix effect caused by high-U content. However $^{207}Pb/^{206}Pb$ ages cluster around 550 Ma and 9 data from 9 grains define weighted mean averaged $^{207}Pb/^{206}Pb$ age of 546±6 Ma (MSWD=0.49) (Fig.5.4). This age is interpreted as the timing of the metamorphism on this sample.

The oscillatory zoned cores have U contents between 490 and 4750 ppm, and Th/U ratios between 0.12 and 0.31. Most of the core ages are discordant however the error-weighted regression (n=12, MSWD=0.71) gave an upper concordia intercept at 1000±16 Ma when the lower intercept was anchored at 546±6 Ma. Such good regression indicates that these igneous cores are derived from the single magmatic source; the protolith of this rock is magmatic origin.

5.2.5. Walnumfjella

BC08010604A

This intermediate orthogneiss is collected at the northeastern part of Walnumfjella. This sample is mainly composed of garnet, hornblende, biotite, epidote, plagioclase and quartz with minor zircon, apatite, magnetite and ilmenite. Quartz in this sample contains small amount of exsolved rutile, and the averaged Ti concentrations of the pre-/post- exsolution are estimated as 46 and 24 ppm, respectively. On the basis of these Ti concentrations, the temperature conditions of the pre-/post- exsolutions are calibrated using Ti-in-quartz thermometer (Wark & Watson 2006) as 720-660 °C and 650-600 °C, respectively.

Zircon grains have prismatic and oscillatory-zoned cores replaced by low-CL domains at the rim portion (Fig. 5.3). The low-CL domain is structureless. At the boundary between the oscillatory-zoned core and low CL domain, high-CL ring is commonly recognized.

From this sample, total of 46 analyses from 39 grains (Table 5.15) were obtained.

The structureless low-CL domains have U content between 490 and 2250

ppm and relatively low Th/U ratio (0.02-0.33). Most of them are concentrated at ca. 600 Ma, and they define a concordia age of 605±4 Ma (MSWD=0.85, probability of concordance = 0.7, 7 analyses from 7grains) (Fig.5.4). This age is interpreted as of timing of metamorphism. Several concordant ages are also found around 780 Ma (analyses 13 and 13.2). These older metamorphic ages imply at least two possibilities: the metamorphism on this rock prior to the 605 Ma metamorphism or the detrital grains derived from 780 Ma metamorphic body.

The oscillatory zoned cores have U contents between 280 and 2520 ppm, and Th/U ratios between 0.34 and 0.67. Most of the core ages are discordant and their $^{206}Pb/^{238}U$ ages are scattered between 860 and 1030 Ma. However the error-weighted regression (n=31, MSWD=1.3) gave an upper concordia intercept at 1015±12 Ma when the lower intercept is anchored at 605±4 Ma. Several cores (analyses 8, 41, 47 and 52) show concordant ages at ca. 780 Ma which is also found in the low-CL portion. Although the number of analyses is not sufficient, it might suggest some geological event at this period.

5.3. Electron Probe Micro Analyzer (EPMA) monazite Th-U-Pb dating

Samples and analytical procedures

U-Th-Pb ages for monazite are determined using an Electron Probe Micro Analyzer (EPMA) at the National Institute of Polar Science, Tokyo. The procedures followed in analyses and data assessment are given in Hokada & Motoyoshi (2006). Samples selected for analyses are listed in Table 5.1. Localities are shown in Fig. 5.1. Data of which measured PbO is lower than 0.1 wt% are not included in the interpretation because of large age error.

AC07121701C

This pelitic gneiss is collected at the northwestern part of Austkampane. This rock is mainly composed of garnet, cordierite, biotite, plagioclase and quartz with minor apatite, magnetite, rutile, zircon and monazite. No obvious signatures indicating retrogression can be observed.

Monazite occurs in matrix. Most grains show euhedral shape and faint internal structure (Fig. 5.5).

From this sample, total of 52 analyses from 8 grains (Table 5.16) were obtained.

There is no clear relationship between the ages and the analytical spot within the grain. The ages cluster around 650 Ma and the data define weighted mean averaged age of 642.7±9.8 Ma (MSWD=0.4) (Fig.5.6). This age is interpreted as the timing of the peak metamorphism on this sample.

AC07121801M

This pelitic gneiss is collected at the northeastern part of Austkampane. This rock is mainly composed of garnet, cordierite, low-Ca amphibole, plagioclase and quartz with minor rutile, zircon and monazite. No obvious signatures indicating retrogression can be observed.

Monazite grains occur mainly as inclusion in cordierite. Commonly the grains preserve internal structure due to the difference of chemical composition (Fig. 5.5).

From this sample, total of 140 analyses from 10 grains (Table 5.17) were obtained.

There is no clear relationship between the calculated ages and the analytical spot within the grain. The ages cluster around 600 Ma and the data define weighted mean averaged age of 607.7±4.9 Ma (MSWD=0.5) (Fig.5.6). This age

is interpreted as the timing of the peak metamorphism on this sample.

07120402A

This pelitic gneiss is collected at the northeastern part of Brattnipene. This rock is mainly composed of garnet, biotite, sillimanite, plagioclase, k-feldspar and quartz with minor rutile, apatite, zircon and monazite.

Textual signature of the retrogression can be observed as the replacement of the rim of garnet by fine-grained aggregate of biotite and plagioclase.

Monazite occurs in matrix and as inclusions in garnet. The grains show complex internal structure (Fig. 5.5). From this sample, total of 65 analyses from 10 grains (Table 5.18) were obtained.

The ages are distributed in the range between 500 Ma and 700 Ma. The ages obtained from the rim portion seem to be slightly younger than that from the core (Fig. 5.5). The relative probability age distribution curve indicates intense peak at 600-620 Ma and small peak at 550-570 Ma (Fig. 5.6).

5.4. Discussion - Interpretation of the ages and their implication for geology of the central Sør Rondane Mountains.

Population of zircon SHIMP age and monazite EPMA age identified in all

17 samples, and the magmatic or metamorphic origin of zircon as determined from mainly grain textures and compositions, are summarized in Fig. 5.7 and Fig. 5.8. Data reported by Shiraishi et al. (2008) also shown in Fig. 5.7and Fig. 5.8.

In both the NE and the SW terranes, magmatic zircons from metamorphic rocks are commonly older than 700 Ma, and cluster at ca. 800 Ma and ca. 1000 Ma. It is consistent with Shiraishi et al. (2008). Most of the domains giving ca. 800 Ma and ca. 1000 Ma provide a detrital age signature for the terrane, with magmatic activity at ca. 1000 Ma and ca. 800 Ma (Fig. 5.7). This detrital signature possibly indicates that sediments are derived from local syn-sedimentary volcanism or basement lithologies. Large amount of the Sør Rondane Mountains was formed as juvenile crust during ca. 1600-900 Ma based on Nd model ages (Shiraishi et al., 2008). Absence of detrital zircon with age older than ca.1100 Ma in this study is consistent with the results of Shiraishi et al. (2008).

In Brattnipene area, ca. 550 Ma ages are also obtained from pegmatites. These pegmatites are highly associated with the activity of normal fault, indicating extensional tectonics. In Austkampane area, granites with ca. 500 Ma occur locally. Intrusions with ca. 500 Ma have been reported from A-type granitic

bodies including syenite (Takigami & Funaki, 1991; Tainosho et al., 1992).

Metamorphic ages from gneisses of which temperature is higher than 700 °C using Ti-in-quartz thermometer (Wark & Watson, 2006) concentrate between 640 and 600 Ma. The samples 07041202A, AC07121901A and BC08010502B also yield ca. 600 Ma although Ti contents in quartz give lower than 700 °C. Such age population indicates that main metamorphic event, associated with granulite-facies metamorphism, occurred at 640-600 Ma. Ages younger than 600 Ma are characteristically obtained from the samples highly affected by retrograde hydration (07120402A, BC08010302C), indicating subsequent retrograde hydration occurred at 570-550 Ma. These ages are close to the timing of pegmatite intrusion in Brattnipene area. It is likely that hydration on the metamorphic rocks in the NE terrane is related to the extension and subsequent magmatism. In Austkampane area, ca. 500 Ma granites are recognized. Locally gneiss which records neither ca. 600 Ma nor temperature higher than 700 °C is distributed in the NE terrane (sample AC08012001A). Lack of ca. 600 Ma domains in zircon can be explained by at least two possibilities; (1) the rocks have not experienced ca. 600 Ma or (2) the domains formed by ca. 600 Ma event were completely modified during later retrograde metamorphism at

570-550 Ma. The grains from AC08012001A preserved oscillatory-zoned igneous cores, and such cores yield ages older than 700 Ma. It is unlikely to overprint just only metamorphic domain completely, therefore possibility (1) would be reasonable. Such low-grade gneiss with no ca. 600 Ma signature in the NE terrane has been also reported from Isachsenfjella (sample 90102801A) (Shiraishi et al., 2008).

In the SW terrane, metamorphic domains of zircon with ca. 550 Ma are common, otherwise grains have no clear metamorphic growth. Shiraishi et al. (2008) reported 570-520 Ma of U-Pb titanite SHRIMP ages from the samples of which zircon are without clear metamorphic growth. This age concentration indicates that ca. 550 Ma should be the timing of metamorphism of the SW terrane. Most important point is lack ca. 640-600 Ma event in most of the SW terrane. The grains yielding ca. 550 Ma also preserve the clear igneous domain. As described above, these rocks certainly have not experienced ca. 600 Ma event. Gneisses in the SW terrane show different petrological signatures from the gneisses in the NE terrane (see Chapter 3 and 4 in details). These petrological and geochronological differences between the NE and the SW terranes imply that there are at least two geological units in the Sør Rondane

Mountains, and the two units probably have shared a common history after ca. 550 Ma.

However, Gneiss from Walnumfjella (BC08010604A) record ca. 600 Ma metamorphism. Additionally signature of high-grade condition (> 700 °C) is recognized from adjacent sample (BC08010604E) with Ti-in-quartz thermometer (Wark & Watson, 2006). These indicate affinity with the gneisses of the NE terrane.

Roughly speaking, the NE terrane comprises high-grade (> 700 °C) rocks metamorphosed at ca. 640-600 Ma, whereas the SW terrane comprises relatively low-grade (< 700 °C) rocks metamorphosed at ca. 550 Ma. However, rocks which do not show “proper” characteristics of occurring terrane also distributed in both terranes (Fig. 5.7, 5.8). To explain such comprehensive distribution of the metamorphic grade and metamorphic ages in the central Sør Rondane Mountains, it is unreasonable to infer a high-angle tectonic boundary between the two terranes.

5.5. Summary of the geochronology in the central Sør Rondane Mountains

1. ca. 640-600 Ma obtained from the metamorphic zircon and monazite is interpreted as the timing of high-grade (> 700 °C) metamorphism in the NE

terrane. 570-550 Ma, which is characteristically recognized in intensely retrogressed rocks, should be the timing of hydration in the NE terrane.

2. Most of rocks in the SW terrane lack ca. 640-600 Ma age, but ca. 550 Ma ages are widely recognized. The age of ca. 550 Ma is interpreted as the timing of main metamorphism (< 700 °C) in the SW terrane.

3. In both the NE and SW terranes, the rocks which do not show typical metamorphic condition and ages are distributed locally. It is difficult to explain such comprehensive distribution by a high-angle tectonic boundary between the two terranes.

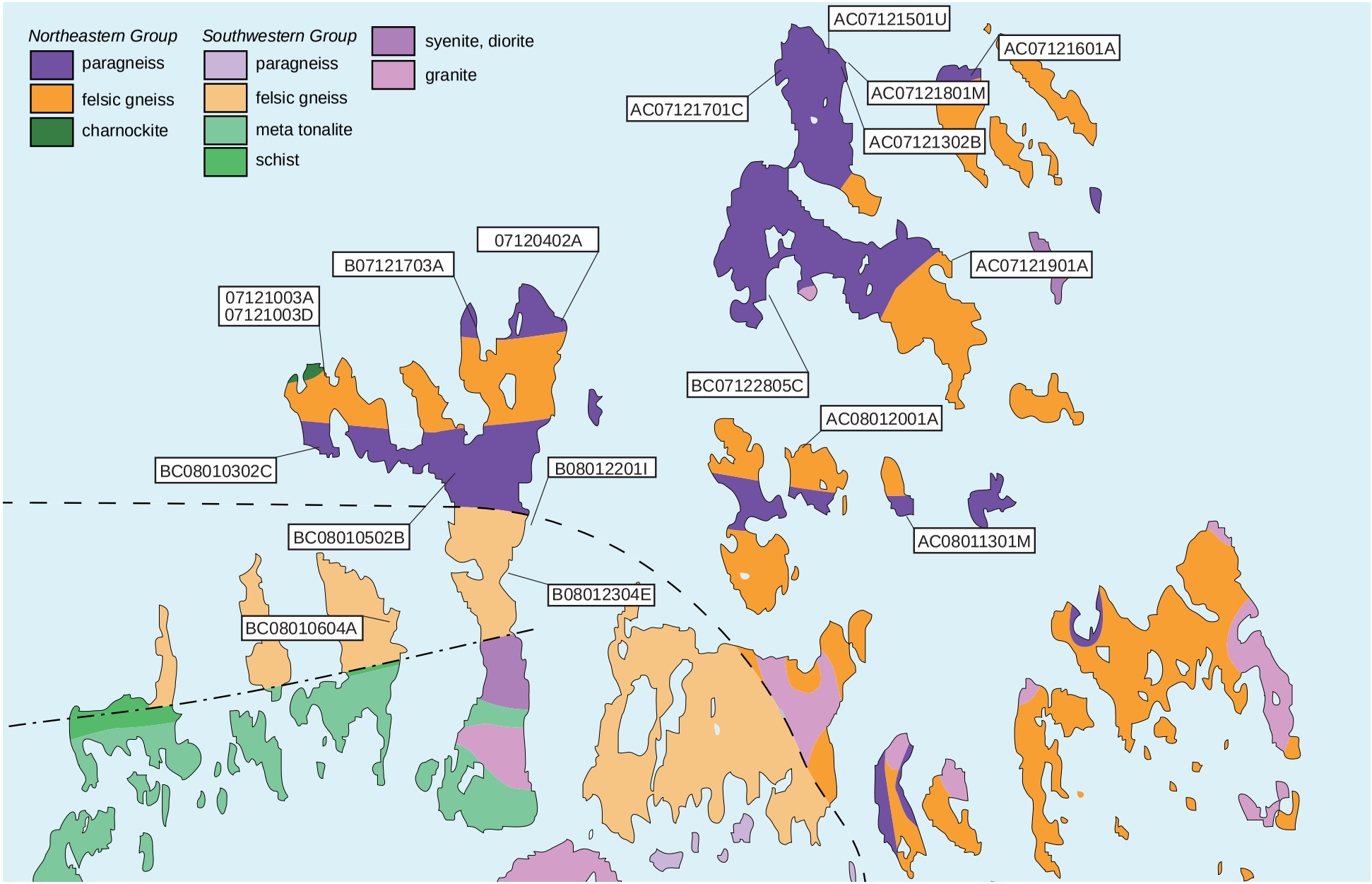

Fig. 5.1. SHRIMP and EPMA age analyzed samples and their locality in the central Sør Rondane Mountains.

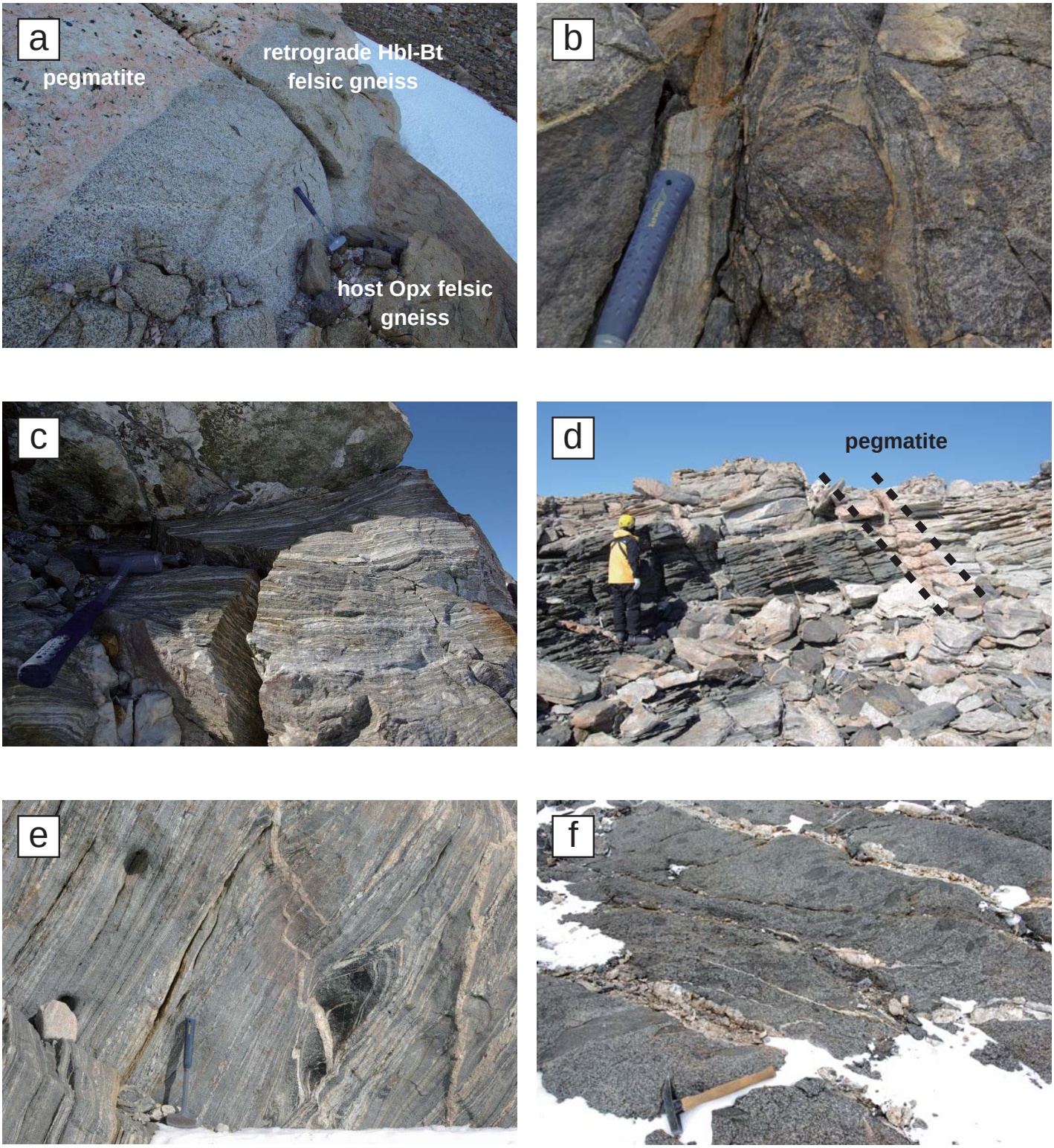

Fig. 5.2. Field occurrence of the SHRIMP analyzed samples. (a) Opx felsic gneiss (07121003A) intruded by pegmatite (07121003D) in Brattnipene area. Opx felsic gneiss is converted to hbl-Bt felsic gneiss by the effect off pegmatite intrusion. (b) Mode of occurrence of Grt-Sil-Bt gneiss (BC08010302C) in the southern part of Brattnipene area. (c) Mode of occurrence of Grt-bt gneiss (BC08010502B). This rock overlies marble in the southern part of Brattnipene area. (d) Pegmatite (BC07121703A) intruding host gneisses in Brattnipene area. (e) Mode of occurrence of Hbl-Bt gneiss (AC07121901A) in Austkampane area. (f) Mode of occurrence of dioritic Grt-Bt gneiss (BC08122805C) in the southern part of Austkampane area. Dark-colored and rounded inclusions are observed.

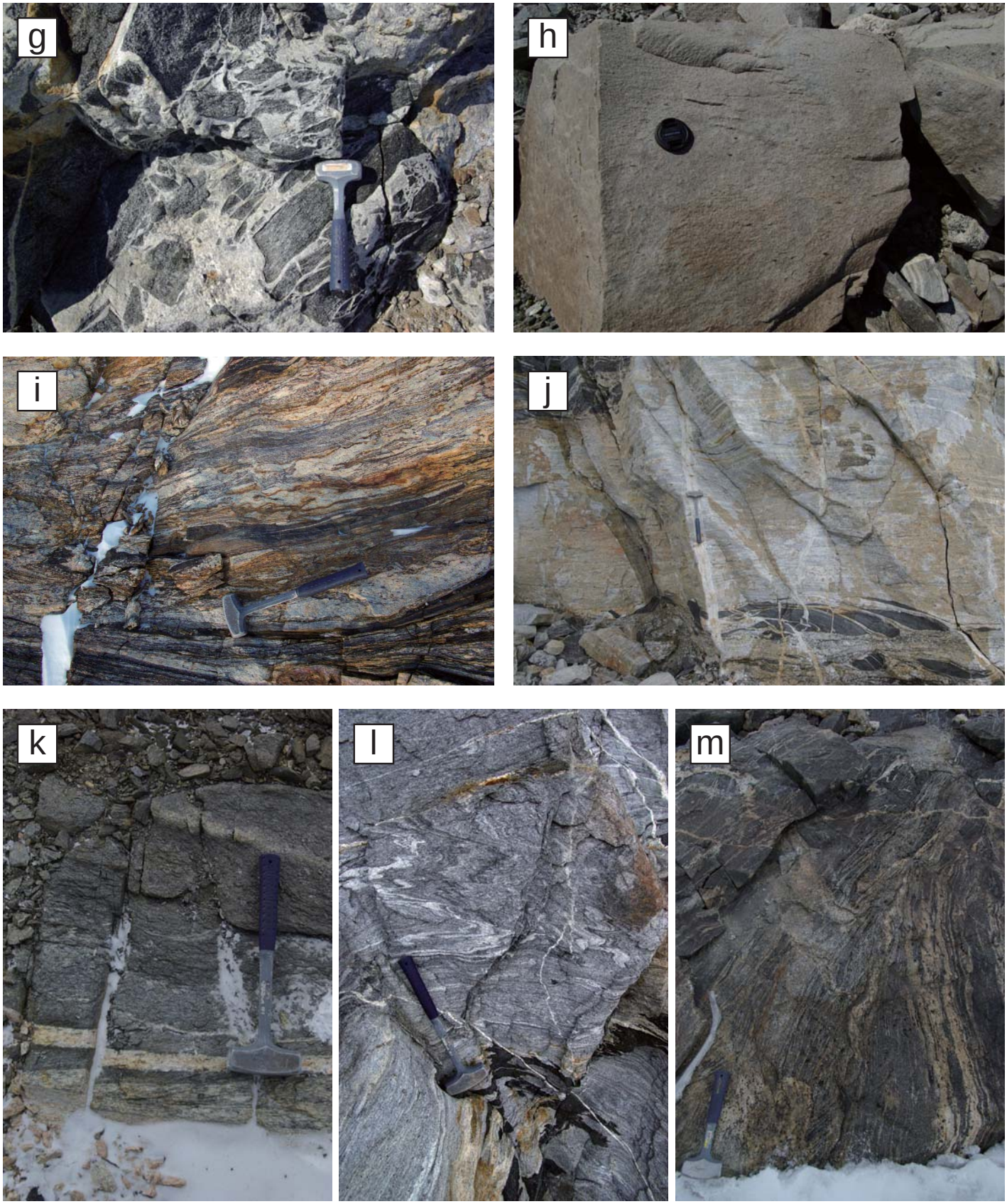

Fig. 5.2, continued. Field occurrence of the SHRIMP analyzed samples. (g) Granite (AC07121501U) including dark-colored xenoliths of host metamorphic rocks in Austkampane area. (h) Mode of occurrence of granite (AC07121601A) in Norhaugen area. (i) Mode of occurrence of Grt-Bt gneiss (AC08011301M) in Menipa area. (j) Mode of occurrence of Hbl-Bt gneiss (AC08012001A2) in the northern part of Menipa area. This rock is apparently overlain by paragneisses including Grt-Bt gneiss and marble. (k) Mode of occurrence of Grt-Hbl-Bt gneiss (B08012201I) in Lunckeryggen area. (l) Mode of occurrence of Grt-Hbl-Bt gneiss (B08012304E) in Lunckeryggen area. (m) Mode of occurrence of Grt-Bt gneiss (BC08010604A) in the northern part of Walnumfjella.

Fig. 5.2, continued. Field occurrence of the EPMA analyzed samples. (n) Mode of occurrence of Grt-Crd-Bt gneiss (AC07121701C) in Austkampane area. (o) Mode of occurrence of Grt-Crd-Oam gneiss (AC07121801M) in Austkampane area. (p) Mode of occurrence of Grt-Sil-Bt gneiss (07120402A) in Brattnipene area.

Brattnipene

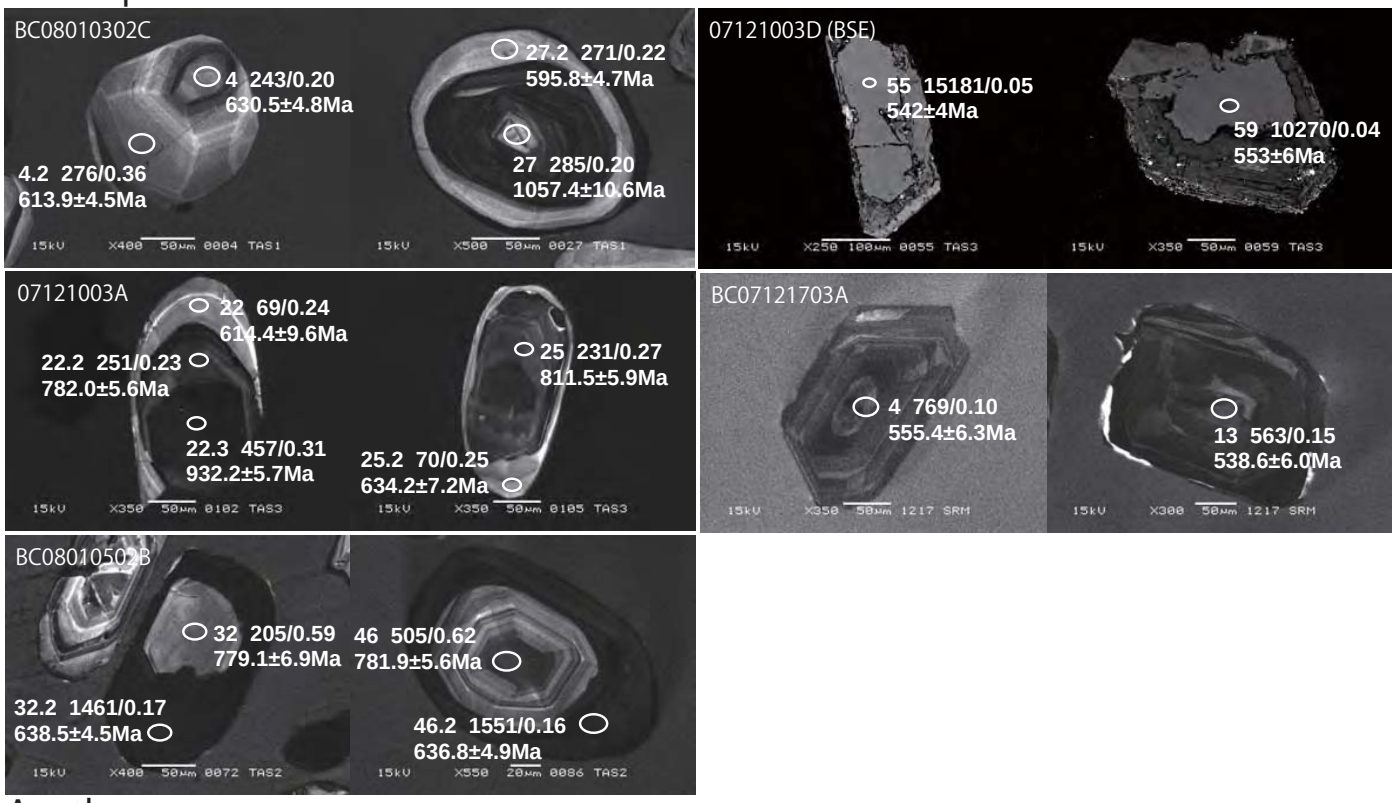

Austkampane

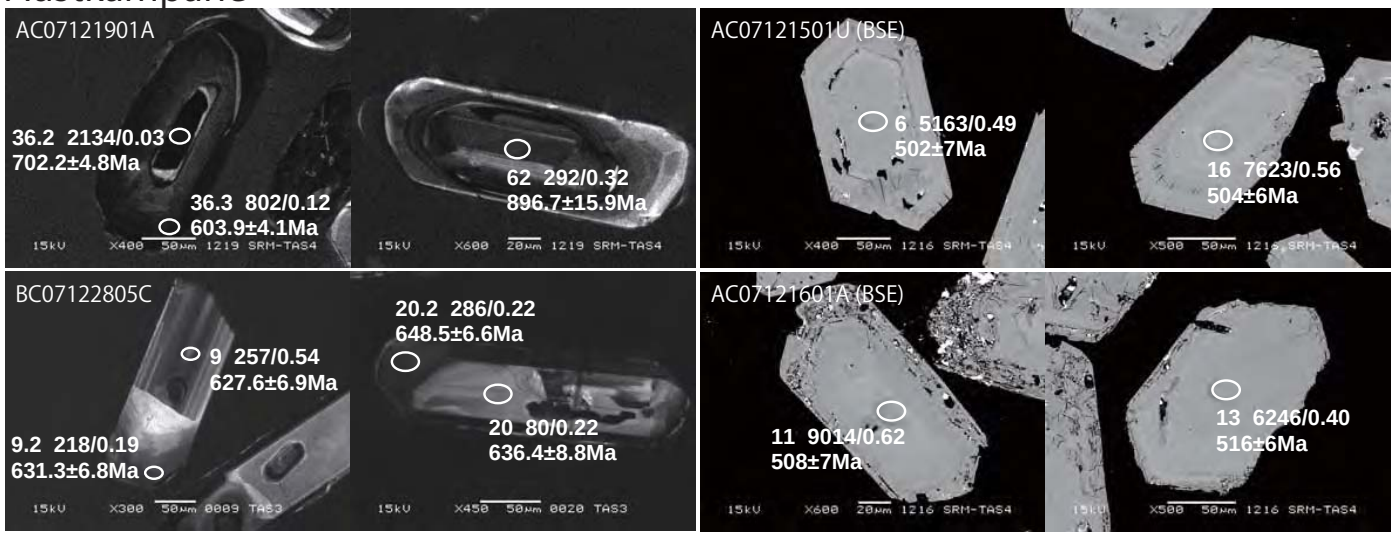

Fig. 5.3. CL/BSE images of representative analyzed Zrn grains. All images are of CL unless otherwise marked (BSE). Each SHRIMP analysis spot is labelled with grain analysis number, U content (ppm)/ Th/U ratio and ^{204}Pb-corrected $^{206}Pb/^{238}U$ age with 1σ error.

Menipa

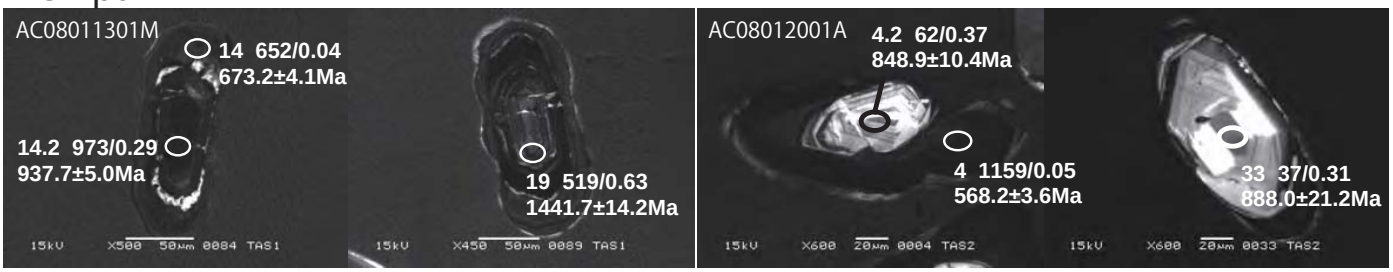

Lunckeryggen/Walnumfjella

Fig. 5.3, continued. CL/BSE images of representative analyzed Zrn grains. All images are of CL unless otherwise marked (BSE). Each SHRIMP analysis spot is labelled with grain analysis number, U content (ppm)/ Th/U ratio and ^{204}Pb-corrected $^{206}Pb/^{238}U$ age with 1σ error.

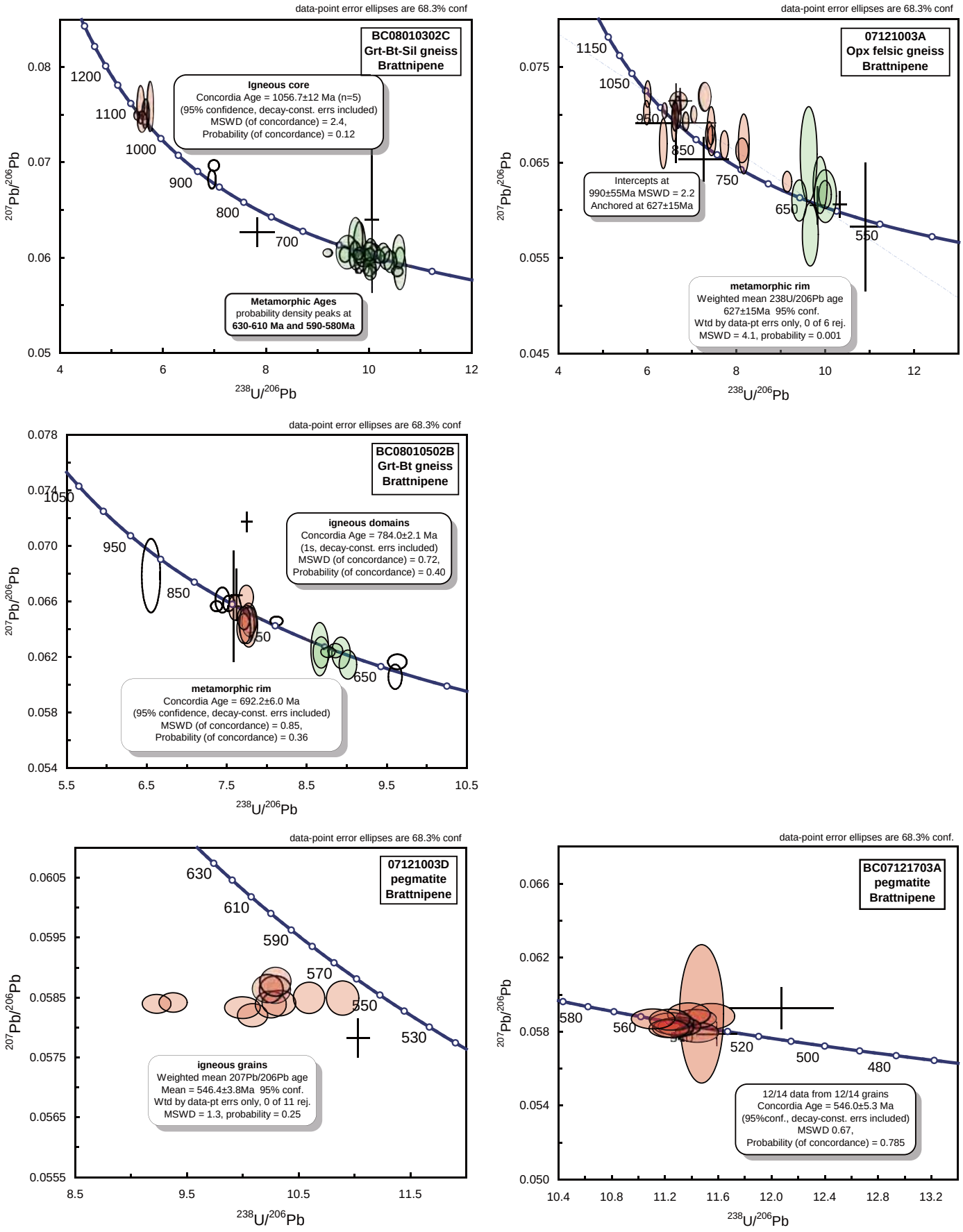

Fig. 5.4. Terra-Wasserburg concordia diagrams of U-Pb SHRIMP data from Brattnipene area.

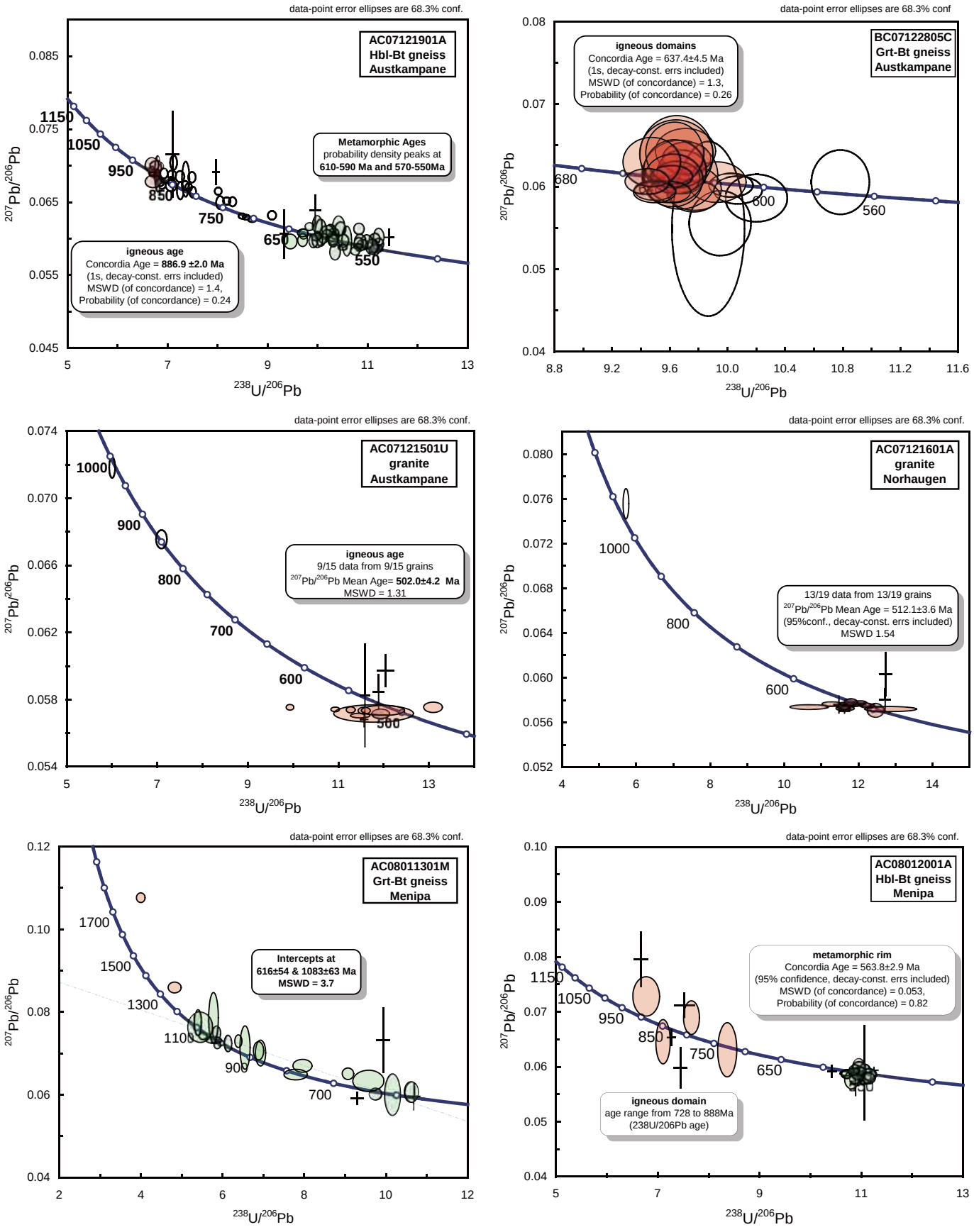

Fig. 5.4, continued. Terra-Wasserburg concordia diagrams of U-Pb SHRIMP data from Austkampane area and Menipa area.

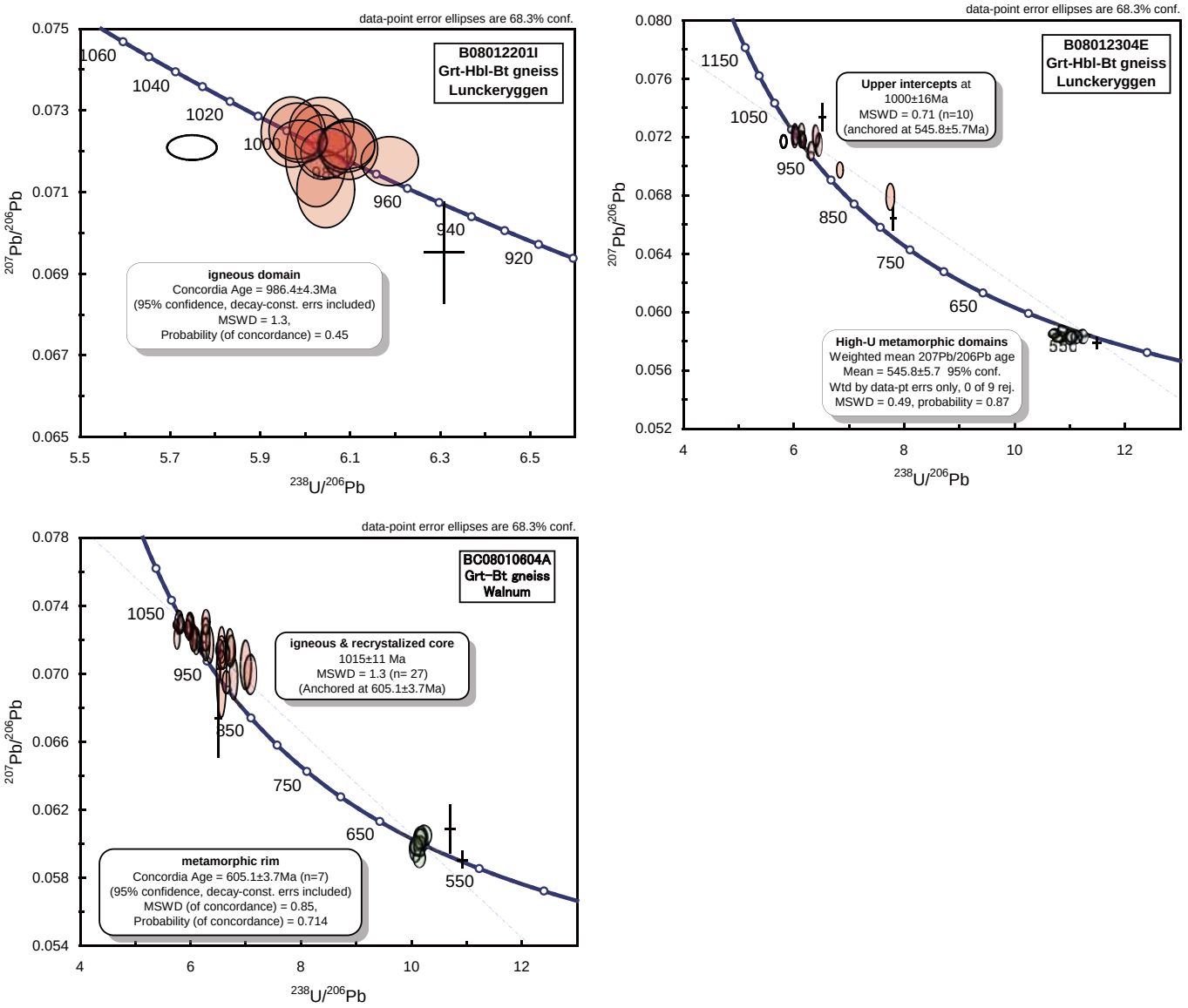

Fig. 5.4, continued. Terra-Wasserburg concordia diagrams of U-Pb SHRIMP data from Lunckeryggen area and Walnumfjella area.

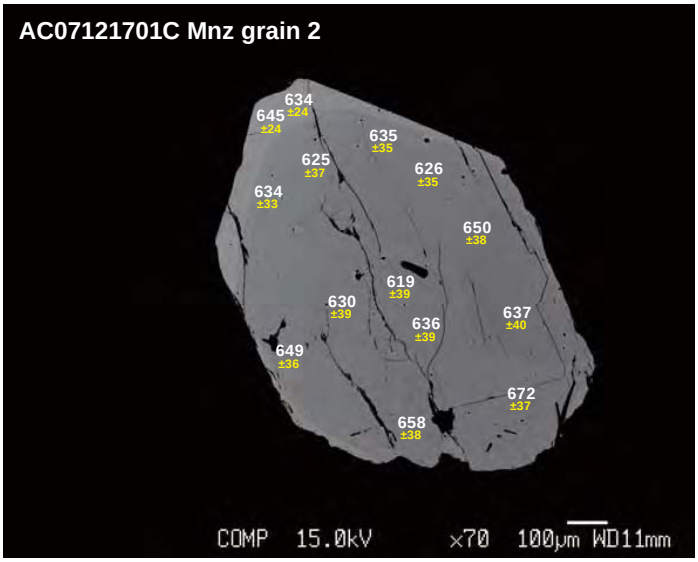

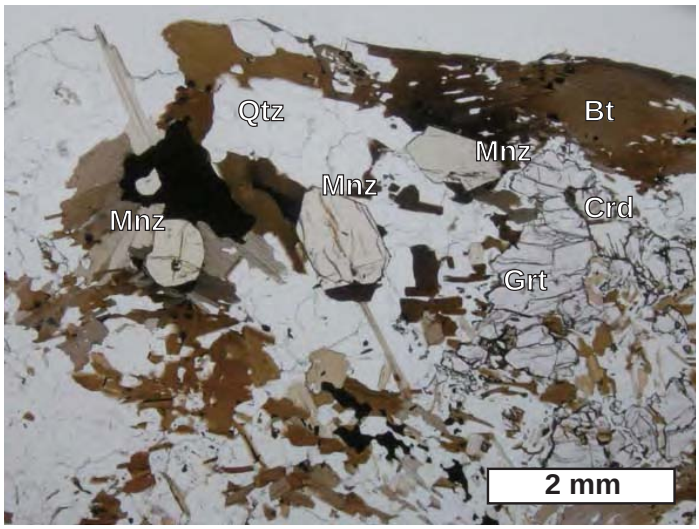

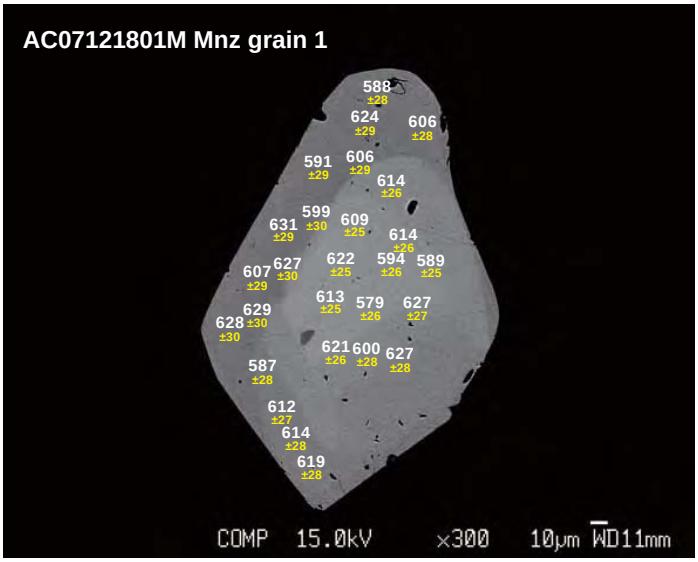

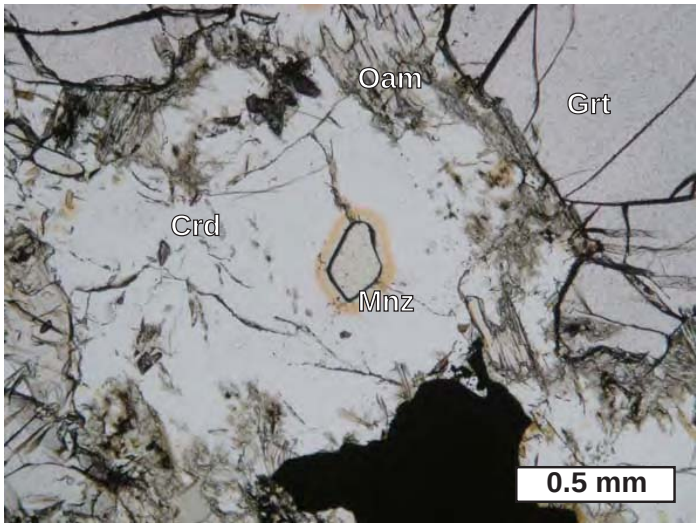

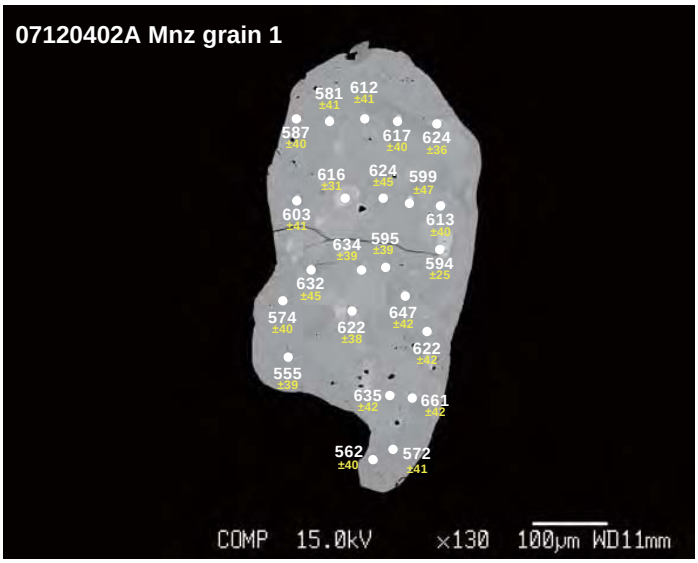

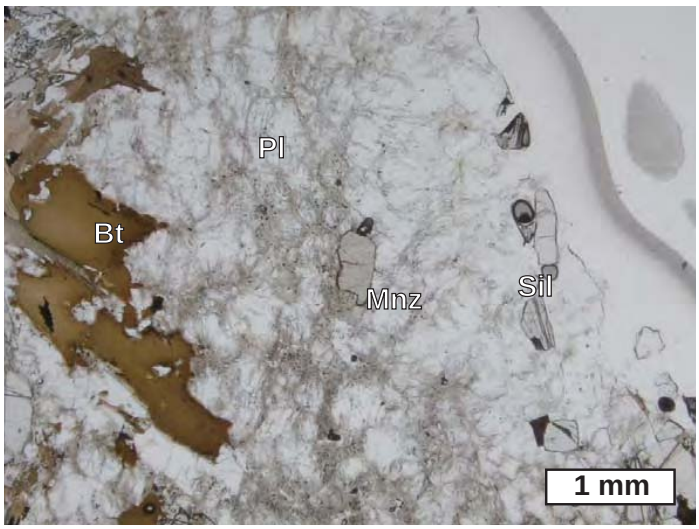

Fig. 5.5. BSE images and photomicrgraphs of representative analyzed Mnz grains. Each EPMA analysis spot is labelled with U-Th-Pb apparent age with 1σ error (Ma).

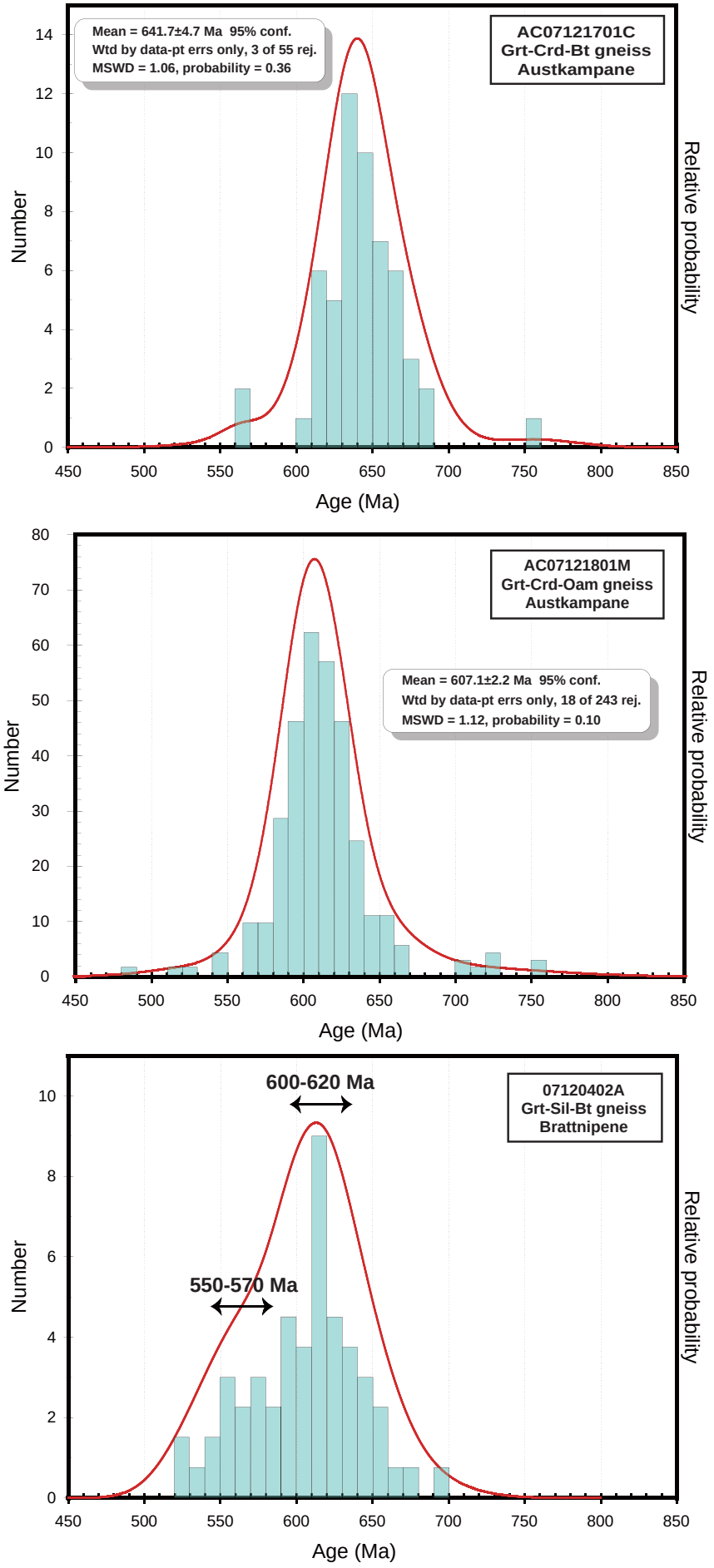

Fig. 5.6. Histograms of U-Th-Pb EPMA ages of Mnz from Austkampane area and Brattnipene area.

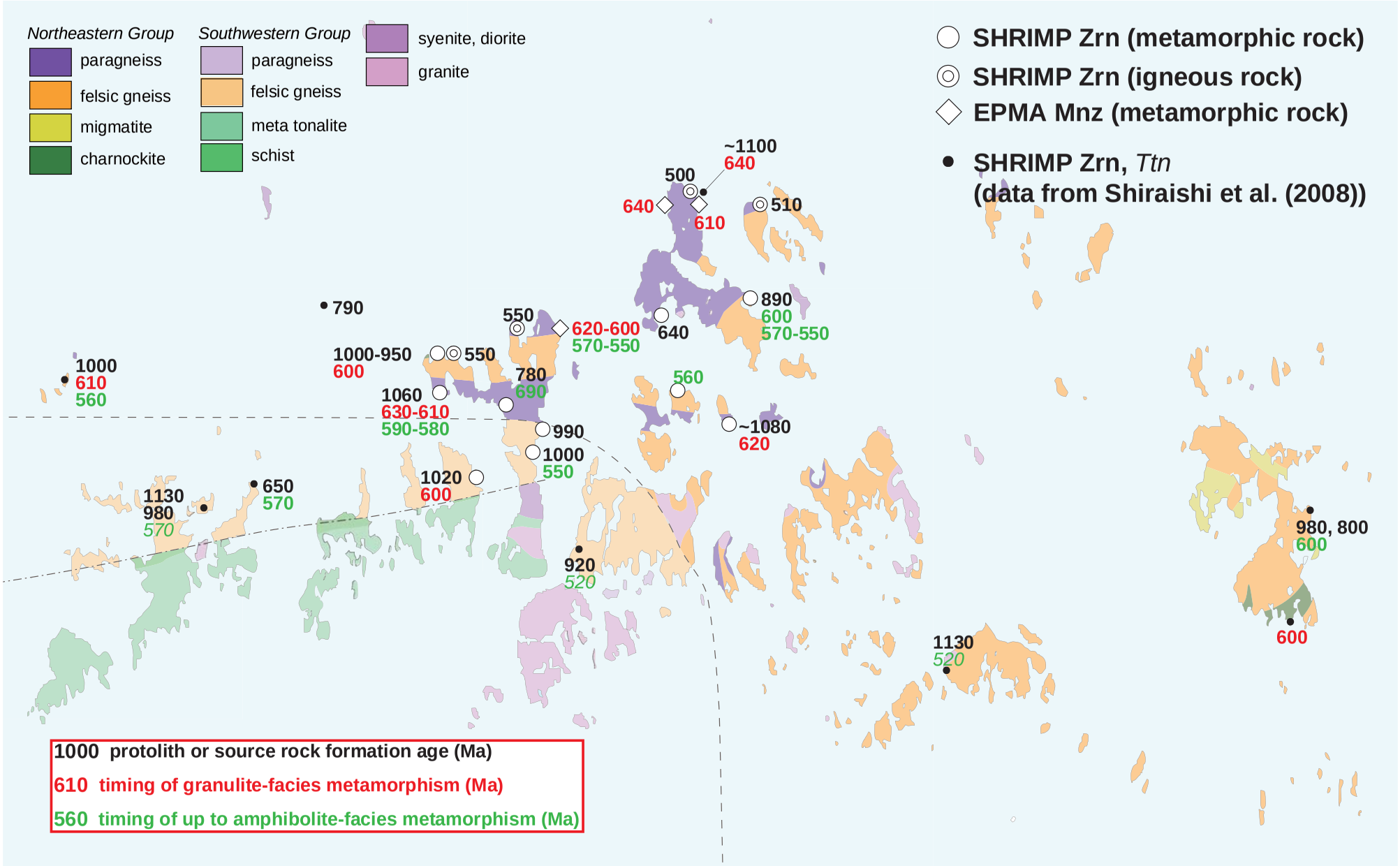

Fig. 5.7. SHRIMP and EPMA ages in the central Sør Rondane Mountains.

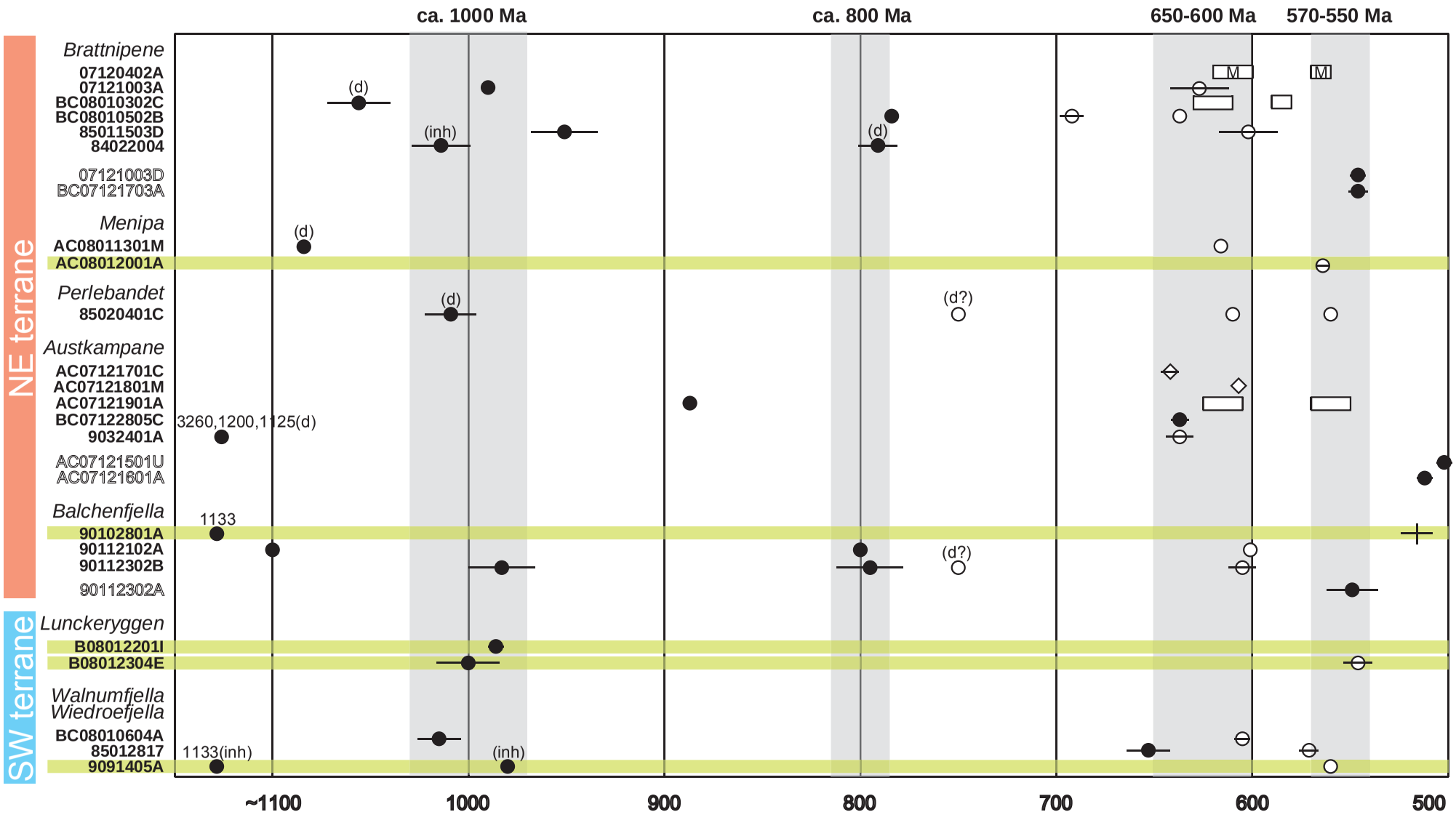

Fig. 5.8. Summary of U-Pb ages from the Sør Rondane Mountains. Closed circles: igneous zircon, open circles: metamorphic zircon, cross: titanite, diamond: monazite, inh: inherited grains, d: detrital grains. Bars indicate 1σ error (Ma). Open rectangles indicate age range of date which do not define either concordia or intercept age.Samples with outline charactors are intrusive rocks. Samples which are marked with light-green line record no 650-600 Ma events.

Table. 5.1 Mineral assemblage of the age-analyzed samples in the central Sør Rondane Mountains

Sample No./Abb	Qtz	Pl	Kfs	Bt	Grt	Amp	Opx	Cpx	Sil	Opq	Ap	Mnz	Zrn	Rock type	Method
Brattnipene															
07120402A	+	+	+	+ R	+				+	−		−	−	pelitic	EMP
07121003A	+	+		+		+	+	+		−	−		−	felsic	SHRIMP
07121003D	+	+	+	+						−			−	pegmatite	SHRIMP
BC010302C	+	+	+	+ R	+				+	−		−	−	pelitic	SHRIMP
BC010502B	+	+	+	+	+					−			−	felsic	SHRIMP
BC07121703A	+	+	+	+						−			−	pegmatite	SHRIMP
Austkampane															
AC07121701C	+	+	+	+	+				I	−		−	−	pelitic	EMP
AC07121801M	+	+		+	+	R?			I	−		−	−	pelitic	EMP
AC07121901A	+	+		+						−			−	felsic	SHRIMP
AC07121501U	+	+	+	+						−		−	−	granite	SHRIMP
AC07121601A	+	+		+						−			−	granite	SHRIMP
BC07122805C	+	+	+	+	+					−			−	felsic	SHRIMP
Menipa															
AC08011301M	+	+	+	+	+					−			−	psammitic	SHRIMP
AC08012001A2	+	+		+		+				−			−	felsic	SHRIMP
Lunckeryggen															
B08012201I	+	+		+	+	+				−			−	felsic	SHRIMP
B08012304E	+	+		+	+	+				−			−	felsic	SHRIMP
Walnumfjella															
BC010604A	+	+		+	+	+				−			−	intermediate	SHRIMP

+: present, −: minor, I: inclusion, R: retrograde phase Mineral abbreviations are after Kretz (1983)

Table. 5.2 SHRIMP U-Pb data for zircons from the sample BC08010302C

Spot	ppm U	ppm Th	$^{232}Th/^{238}U$	$\%\ ^{206}Pb_c$	ppm $^{206}Pb^*$	Total $^{238}U/^{206}Pb$	±%	Total $^{207}Pb/^{206}Pb$	±%	(1) $^{238}U/^{206}Pb^*$	±%	(1) $^{207}Pb^*/^{206}Pb^*$	±%	(1) $^{206}Pb/^{238}U$ Age	1sigma err	(1) $^{207}Pb/^{206}Pb$ Age	1sigma err	% Dis-cor-dant	classification
010302C-01	694	137	0.20	0.01	85.3	6.988	0.97	0.06972	0.52	6.989	0.97	0.06968	0.54	862.1	7.8	919	11	7	core
010302C-02	862	335	0.40	0.03	134	5.511	0.67	0.07518	0.41	5.512	0.67	0.07497	0.44	1074.7	6.7	1068	9	-1	igneous
010302C-03	500	125	0.26	0.09	74.6	5.764	0.72	0.0767	2.2	5.769	0.72	0.0759	2.3	1030.5	6.9	1092	46	6	igneous
010302C-04	243	47	0.20	0.19	21.5	9.719	0.79	0.06181	1.1	9.738	0.8	0.06024	1.6	630.2	4.8	612	35	-3	core
010302C-04.2	276	97	0.36	--	23.7	10.009	0.77	0.05903	1.1	10.008	0.77	0.0591	1.1	613.9	4.5	571	23	-7	rim
010302C-08	849	56	0.07	0.04	72.9	10.007	0.68	0.06068	0.6	10.01	0.68	0.06038	0.67	613.8	4.0	617	15	1	core
010302C-08.2	382	37	0.10	--	31.5	10.415	0.75	0.05908	0.96	10.408	0.75	0.05961	1.2	591.4	4.2	589	27	0	rim
010302C-10	327	165	0.52	--	28.1	10.017	0.97	0.06001	1.1	10.011	0.97	0.0605	1.2	613.8	5.7	621	26	1	core
010302C-11	876	238	0.28	--	73.8	10.192	0.68	0.06011	0.59	10.191	0.68	0.06016	0.7	603.4	3.9	609	15	1	rim
010302C-13	295	153	0.53	1.34	26.2	9.688	0.76	0.0721	1.5	9.82	0.78	0.0611	2.9	625.1	4.6	642	62	3	core
010302C-13.2	1613	61	0.04	0.10	132	10.53	0.66	0.05944	0.47	10.54	0.66	0.05863	0.59	584.3	3.7	553	13	-5	rim
010302C-16.2	459	191	0.43	0.32	39.4	9.999	0.75	0.06335	0.84	10.032	0.76	0.06069	1.4	612.6	4.4	628	31	3	rim
010302C-18.2	365	167	0.47	0.31	29.7	10.558	0.75	0.06145	1.6	10.591	0.77	0.0589	2.5	581.6	4.3	563	54	-3	rim
010302C-21.2	286	88	0.32	--	23.9	10.274	0.78	0.06031	1.1	10.271	0.78	0.06053	1.1	598.9	4.5	623	24	4	rim
010302C-23	500	126	0.26	1.04	41.1	10.46	0.72	0.06916	0.77	10.57	0.73	0.0607	1.9	582.7	4.1	628	41	8	core
010302C-27	285	55	0.20	0.05	43.6	5.608	1.1	0.07474	0.94	5.61	1.1	0.07433	1	1057.4	10.6	1050	20	-1	igneous
010302C-27.2	271	59	0.22	0.02	22.6	10.325	0.83	0.06012	1.3	10.327	0.83	0.05996	1.3	595.8	4.7	602	28	1	rim
010302C-30.2	522	75	0.15	0.15	45.4	9.875	0.98	0.06127	0.75	9.891	0.98	0.06001	0.98	620.9	5.8	604	21	-3	rim
010302C-32	1638	99	0.06	0.02	153	9.203	0.67	0.06071	0.42	9.205	0.67	0.06053	0.46	664.8	4.2	623	10	-6	core
010302C-32.2	432	160	0.38	--	37.1	10.022	0.73	0.05847	0.86	10.022	0.73	0.05847	0.86	613.1	4.3	547	19	-11	rim
010302C-34	1070	99	0.10	0.23	94.6	9.722	0.9	0.064	1.9	9.744	0.91	0.0621	2.3	629.8	5.4	678	48	8	core
010302C-40	195	141	0.75	0.45	30.2	5.562	0.85	0.07992	0.98	5.587	0.86	0.0761	1.7	1061.4	8.4	1098	34	3	igneous
010302C-41	445	76	0.18	0.22	55.2	6.936	0.71	0.07002	0.66	6.951	0.72	0.06821	0.93	866.4	5.8	875	19	1	core
010302C-42	175	67	0.40	0.03	14.9	10.1	0.85	0.06028	1.3	10.103	0.85	0.06003	1.6	608.4	4.9	605	34	-1	rim

Error in Standard calibration was 0.22%(not included in above errors but required when comparing data from different mounts).

Errors are 1-sigma; Pb_c and Pb^* indicate the common and radiogenic portions, respectively.

(1) Common Pb corrected using measured ^{204}Pb.

Table. 5.3 SHRIMP U-Pb data for zircons from the sample 07121003A

Spot	ppm U	ppm Th	$^{232}Th/^{238}U$	% $^{206}Pb_c$	ppm $^{206}Pb^*$	Total $^{238}U/^{206}Pb$	±%	Total $^{207}Pb/^{206}Pb$	±%	(1) $^{238}U/^{206}Pb^*$	±%	(1) $^{207}Pb^*/^{206}Pb^*$	±%	(1) $^{206}Pb/^{238}U$ Age	1sigma err	(1) $^{207}Pb/^{206}Pb$ Age	1sigma err	% Dis-cor-dant	classification
121003A-10	470	155	0.34	0.01	57.2	7.064	0.66	0.07013	0.76	7.065	0.66	0.07005	0.84	853.4	5.3	930	17	9	igneous
121003A-10.2	848	177	0.22	0.05	110	6.637	0.6	0.0693	1.5	6.64	0.6	0.0689	1.5	904.4	5.1	895	31	-1	igneous
121003A-12	191	34	0.18	0.10	22	7.463	0.87	0.06816	1.2	7.471	0.87	0.0673	1.5	809.8	6.6	849	31	5	igneous
121003A-15	343	82	0.25	--	32.2	9.157	0.76	0.06285	1.1	9.154	0.76	0.0631	1.1	668.4	4.8	712	24	6	igneous
121003A-15.2	109	24	0.23	0.06	9.46	9.88	1	0.0632	2	9.89	1	0.0628	3.1	620.9	6.2	700	66	13	rim
121003A-17	182	36	0.21	--	15.7	9.994	0.92	0.06157	1.5	9.992	0.92	0.06176	1.5	614.9	5.4	666	33	8	rim
121003A-18	192	38	0.20	--	22.6	7.317	1.2	0.07181	1.4	7.317	1.2	0.07188	1.4	825.8	9.6	982	28	19	igneous
121003A-18.2	114	21	0.19	--	11.9	8.208	0.97	0.065	1.7	8.188	0.99	0.067	3.1	742.8	7.0	838	64	13	igneous
121003A-20	249	58	0.24	0.00	31.9	6.716	0.74	0.0703	1.5	6.716	0.74	0.0702	1.5	894.8	6.2	935	32	4	igneous
121003A-20.2	182	38	0.22	0.03	24.5	6.392	0.89	0.0673	2.3	6.394	0.89	0.067	2.6	936.7	7.8	839	53	-10	rim
121003A-22	69	16	0.24	0.16	5.93	9.99	1.6	0.0629	2.4	10	1.6	0.0616	2.9	614.4	9.6	660	62	7	rim
121003A-22.2	251	55	0.23	--	27.8	7.762	0.76	0.06603	1.2	7.754	0.77	0.06691	1.5	782.0	5.6	835	31	7	igneous
121003A-22.3	457	136	0.31	0.02	61.2	6.426	0.66	0.07065	0.74	6.427	0.66	0.07045	0.76	932.2	5.7	941	16	1	igneous
121003A-25	231	60	0.27	0.15	26.7	7.443	0.77	0.0701	1.6	7.454	0.77	0.0689	1.9	811.5	5.9	896	39	10	igneous
121003A-25.2	70	17	0.25	0.27	6.21	9.65	1.2	0.0598	2.5	9.67	1.2	0.0576	3.8	634.2	7.2	516	82	-19	rim
121003A-30	172	36	0.22	0.00	20.4	7.26	3.8	0.0653	1.7	7.26	3.8	0.0653	1.7	832.0	29.5	785	36	-6	igneous
121003A-33	61	13	0.22	--	5.4	9.68	1.3	0.0616	2.6	9.63	1.3	0.066	4.9	636.9	7.9	805	103	26	rim
121003A-35	293	86	0.30	0.11	34	7.409	0.72	0.06885	1.1	7.417	0.72	0.06792	1.3	815.3	5.5	866	28	6	igneous
121003A-36	273	60	0.22	0.13	28.9	8.139	1.1	0.06741	1	8.149	1.1	0.06634	1.3	746.1	7.9	817	26	10	igneous
121003A-38	425	104	0.25	0.07	54.8	6.654	0.7	0.07043	1.4	6.658	0.7	0.0699	1.4	902.0	5.9	924	29	2	igneous
121003A-40	222	38	0.18	0.06	31.6	6.023	0.76	0.07073	1	6.026	0.77	0.07025	1.2	989.7	7.0	936	24	-5	igneous

Errors are 1-sigma; Pb_c and Pb^* indicate the common and radiogenic portions, respectively.

Error in Standard calibration was 0.19%(not included in above errors but required when comparing data from different mounts).

(1) Common Pb corrected using measured ^{204}Pb.

Table. 5.4 SHRIMP U-Pb data for zircons from the sample BC08010502B

Spot	ppm U	ppm Th	$^{232}Th/^{238}U$	% $^{206}Pb_c$	ppm $^{206}Pb^*$	Total $^{238}U/^{206}Pb$	±%	Total $^{207}Pb/^{206}Pb$	±%	(1) $^{238}U/^{206}Pb^*$	±%	(1) $^{207}Pb^*/^{206}Pb^*$	±%	(1) $^{206}Pb/^{238}U$ Age	1sigma err	(1) $^{207}Pb/^{206}Pb$ Age	1sigma err	% Dis-cor-dant	classification
010502B-13	74	25	0.35	0.29	9.73	6.535	1.2	0.0703	1.9	6.554	1.2	0.0679	2.6	915.4	9.9	865	54	-6	igneous
010502B-14	264	81	0.32	0.32	26.2	8.636	0.84	0.06523	1.2	8.664	0.85	0.0626	2	704.2	5.7	694	43	-1	recrystalized core
010502B-15	2585	178	0.07	0.02	295	7.525	0.64	0.06599	0.56	7.526	0.64	0.06587	0.57	804.3	4.8	802	12	0	recrystalized core
010502B-15.2	459	212	0.48	0.18	51.2	7.713	0.73	0.06553	0.87	7.727	0.73	0.06408	1.1	784.6	5.4	744	23	-5	igneous
010502B-17	1771	151	0.09	--	172	8.859	0.67	0.06237	0.52	8.858	0.67	0.06248	0.54	689.5	4.4	691	12	0	rim
010502B-17.2	3619	330	0.09	--	383	8.122	0.63	0.06458	0.34	8.122	0.63	0.06459	0.34	748.5	4.4	761	7	2	rim
010502B-19	442	160	0.37	--	50.9	7.446	0.79	0.06602	0.91	7.445	0.79	0.06611	0.91	812.4	6.0	810	19	0	igneous
010502B-24	986	265	0.28	0.15	111	7.603	0.68	0.06685	0.74	7.614	0.68	0.06559	0.93	795.5	5.1	793	19	0	recrystalized core
010502B-32	205	117	0.59	0.19	22.6	7.769	0.94	0.06589	1.3	7.784	0.94	0.0643	1.6	779.1	6.9	752	34	-3	igneous
010502B-32.2	1461	244	0.17	--	131	9.605	0.72	0.06056	1.2	9.604	0.72	0.06058	1.2	638.5	4.4	624	26	-2	rim
010502B-37	561	193	0.36	0.03	62.4	7.725	0.71	0.06507	0.78	7.727	0.71	0.06482	0.82	784.5	5.2	769	17	-2	igneous
010502B-39	2410	172	0.07	0.01	236	8.766	0.65	0.06248	0.42	8.767	0.65	0.0624	0.42	696.3	4.3	688	9	-1	rim
010502B-40	2801	690	0.25	0.03	326	7.371	0.63	0.06588	0.35	7.373	0.63	0.06567	0.37	819.9	4.9	796	8	-3	recrystalized core
010502B-42	383	115	0.31	0.11	37.9	8.676	0.76	0.06329	1	8.686	0.76	0.06236	1.2	702.4	5.1	686	25	-2	igneous
010502B-43	245	88	0.37	0.06	27.1	7.756	0.84	0.06487	1.2	7.761	0.84	0.06438	1.4	781.3	6.2	754	30	-3	igneous
010502B-46	505	301	0.62	--	55.9	7.755	0.76	0.0663	0.84	7.754	0.76	0.06635	0.84	781.9	5.6	817	18	5	igneous
010502B-46.2	1551	237	0.16	--	138	9.633	0.8	0.06157	0.57	9.632	0.8	0.06166	0.58	636.8	4.9	662	12	4	rim
010502B-48	321	182	0.59	0.02	35.4	7.79	0.8	0.06479	1.1	7.792	0.8	0.0646	1.1	778.4	5.9	761	23	-2	igneous

Errors are 1-sigma; Pb_c and Pb^* indicate the common and radiogenic portions, respectively.
Error in Standard calibration was 0.14%(not included in above errors but required when comparing data from different mounts).
(1) Common Pb corrected using measured ^{204}Pb.

Table. 5.5 SHRIMP U-Pb data for zircons from the sample 07121003D

Spot	ppm U	ppm Th	$^{232}Th/^{238}U$	% $^{206}Pb_c$	ppm $^{206}Pb^*$	Total $^{238}U/^{206}Pb$	±%	Total $^{207}Pb/^{206}Pb$	±%	(1) $^{238}U/^{206}Pb^*$	±%	(1) $^{207}Pb^*/^{206}Pb^*$	±%	(1) $^{206}Pb/^{238}U$ Age	1sigma err	(1) $^{207}Pb/^{206}Pb$ Age	1sigma err	% Dis-cor-dant	classification
121003D-50	19706	1017	0.05	0.00	1800	9.392	0.87	0.05844	0.18	9.392	0.87	0.05842	0.18	652.2	5.4	545	4	-16	igneous
121003D-50.2	20154	886	0.05	--	1870	9.246	0.92	0.05839	0.18	9.246	0.92	0.0584	0.18	662.0	5.8	545	4	-18	igneous
121003D-52	10064	430	0.04	0.01	845	10.227	0.87	0.05876	0.25	10.228	0.87	0.05865	0.26	601.3	5.0	554	6	-8	igneous
121003D-53	4293	90	0.02	0.17	335	11.015	0.89	0.0592	0.4	11.034	0.89	0.05783	0.54	559.3	4.7	523	12	-6	igneous
121003D-53.2	7583	190	0.03	0.01	598	10.895	0.88	0.05855	0.3	10.896	0.88	0.05849	0.32	566.0	4.8	548	7	-3	igneous
121003D-55	15181	668	0.05	--	1300	10.01	1	0.0583	0.2	10.01	1	0.05833	0.2	614.0	6.1	542	4	-12	igneous
121003D-56	11637	513	0.05	0.00	968	10.329	0.96	0.05844	0.24	10.33	0.96	0.05841	0.24	595.7	5.5	545	5	-8	igneous
121003D-57	9238	376	0.04	0.01	771	10.3	0.88	0.05884	0.26	10.301	0.88	0.05877	0.27	597.3	5.0	558	6	-6	igneous
121003D-57.2	8266	322	0.04	--	670	10.6	0.87	0.05847	0.29	10.599	0.87	0.05849	0.29	581.2	4.8	548	6	-6	igneous
121003D-59	10270	420	0.04	0.00	857	10.296	0.87	0.05864	0.25	10.296	0.87	0.05863	0.26	597.5	5.0	553	6	-7	igneous
121003D-60	14471	795	0.06	--	1230	10.097	0.87	0.0582	0.22	10.097	0.87	0.05821	0.22	608.8	5.1	538	5	-12	igneous
121003D-60.2	10712	499	0.05	0.00	897	10.259	0.88	0.0584	0.25	10.259	0.88	0.05839	0.25	599.6	5.0	544	6	-9	igneous

Errors are 1-sigma; Pb_c and Pb^* indicate the common and radiogenic portions, respectively.

Error in Standard calibration was 0.24%(not included in above errors but required when comparing data from different mounts).

(1) Common Pb corrected using measured ^{204}Pb.

Table. 5.6 SHRIMP U-Pb data for zircons from the sample BC07121703A

Spot	ppm U	ppm Th	$^{232}Th/^{238}U$	% $^{206}Pb_c$	ppm $^{206}Pb^*$	Total $^{238}U/^{206}Pb$	±%	Total $^{207}Pb/^{206}Pb$	±%	(1) $^{238}U/^{206}Pb^*$	±%	(1) $^{207}Pb^*/^{206}Pb^*$	±%	(1) $^{206}Pb/^{238}U$ Age	1sigma err	(1) $^{207}Pb/^{206}Pb$ Age	1sigma err	% Dis-cor-dant	classification
121703A-01	555	77	0.14	--	41.2	11.56	1.2	0.05833	0.83	11.55	1.2	0.05885	0.96	535.3	6.3	562	21	5	igneous
121703A-02	913	167	0.19	0.02	69.9	11.23	1.1	0.05832	0.65	11.23	1.1	0.05818	0.68	549.7	5.8	537	15	-2	igneous
121703A-03	704	88	0.13	--	53.8	11.24	1.1	0.05841	0.73	11.24	1.1	0.05867	0.78	549.5	5.8	555	17	1	igneous
121703A-04	769	75	0.10	--	59.4	11.12	1.2	0.05858	0.71	11.11	1.2	0.05871	0.75	555.4	6.3	556	16	0	igneous
121703A-05	996	191	0.20	0.04	74.8	11.44	1.2	0.05833	0.72	11.44	1.2	0.05798	0.74	540.2	6.0	529	16	-2	igneous
121703A-07	841	118	0.15	0.01	64.1	11.26	1.1	0.05826	0.7	11.26	1.1	0.05821	0.71	548.4	5.8	538	15	-2	igneous
121703A-08	891	169	0.20	0.03	67	11.43	1.1	0.05897	0.67	11.43	1.1	0.05873	0.7	540.5	5.7	557	15	3	igneous
121703A-10	1128	223	0.20	0.04	86	11.27	1.1	0.05864	0.59	11.27	1.1	0.05831	0.62	548.0	5.7	541	14	-1	igneous
121703A-11	1091	93	0.09	--	83.3	11.26	1.2	0.05838	0.61	11.25	1.2	0.05856	0.64	548.7	6.2	551	14	0	igneous
121703A-12	591	97	0.17	0.02	44.7	11.38	1.1	0.0591	0.82	11.38	1.1	0.05897	0.85	543.0	5.8	566	18	4	igneous
121703A-13	563	83	0.15	--	42.2	11.48	1.1	0.05875	0.81	11.48	1.2	0.059	5.2	538.6	6.0	566	113	5	igneous
121703A-14	868	113	0.14	0.04	66	11.3	1.1	0.05863	0.67	11.31	1.1	0.0583	0.7	546.2	6.0	541	15	-1	igneous

Errors are 1-sigma; Pb_c and Pb^* indicate the common and radiogenic portions, respectively.

Error in Standard calibration was 0.53%(not included in above errors but required when comparing data from different mounts).

(1) Common Pb corrected using measured ^{204}Pb.

Table. 5.7 SHRIMP U-Pb data for zircons from the sample AC07121901A

Spot	ppm U	ppm Th	$^{232}Th/^{238}U$	$\%\ ^{206}Pb_c$	ppm $^{206}Pb^*$	Total $^{238}U/^{206}Pb$	±%	Total $^{207}Pb/^{206}Pb$	±%	(1) $^{238}U/^{206}Pb^*$	±%	(1) $^{207}Pb^*/^{206}Pb^*$	±%	(1) $^{206}Pb/^{238}U$ Age	1sigma err	(1) $^{207}Pb/^{206}Pb$ Age	1sigma err	% Dis-cor-dant	classification
121901A-01	1023	26	0.03	0.59	125	7.029	0.77	0.0727	0.45	7.071	0.78	0.06781	0.74	852.7	6.2	863	15	1	recrystalized
121901A-02	338	56	0.17	--	39.4	7.361	0.79	0.06794	0.84	7.359	0.82	0.0681	2.9	821.4	6.3	873	60	6	recrystalized
121901A-03.2	523	152	0.30	0.04	61.2	7.348	0.73	0.06766	0.66	7.351	0.73	0.0673	0.75	822.2	5.7	847	16	3	recrystalized
121901A-03.3	1541	140	0.09	0.09	195	6.79	0.7	0.06931	0.37	6.796	0.7	0.06858	0.42	884.9	5.8	886	9	0	igneous
121901A-06	1920	86	0.05	0.07	193	8.567	0.69	0.06348	0.39	8.572	0.69	0.06292	0.45	711.3	4.6	706	10	-1	recrystalized
121901A-06.2	1549	75	0.05	0.02	157	8.487	0.69	0.06329	0.44	8.489	0.69	0.06309	0.47	717.9	4.7	711	10	-1	recrystalized
121901A-08	538	119	0.23	0.08	55.8	8.29	0.73	0.06573	0.69	8.297	0.73	0.06506	0.79	733.6	5.1	776	17	6	recrystalized
121901A-09	456	11	0.02	0.42	39.4	9.942	0.77	0.06523	0.87	9.983	0.78	0.0618	1.6	615.4	4.6	667	34	8	rim
121901A-11	410	14	0.04	--	35.6	9.906	0.76	0.05921	0.93	9.901	0.76	0.05958	1.3	620.2	4.5	588	28	-5	rim
121901A-12	490	83	0.17	--	37.5	11.216	0.75	0.05838	0.92	11.206	0.76	0.05911	1.1	551.0	4.0	571	25	4	rim
121901A-12.2	496	85	0.18	0.05	38.4	11.086	0.76	0.05929	1.2	11.091	0.76	0.05889	1.3	556.5	4.0	563	28	1	rim
121901A-14	438	75	0.18	0.00	33.8	11.122	0.76	0.05831	0.95	11.122	0.76	0.0583	0.95	555.0	4.0	541	21	-2	rim
121901A-17	460	56	0.13	0.21	40.9	9.669	0.77	0.06136	0.87	9.689	0.78	0.05966	1.2	633.2	4.7	591	26	-7	rim
121901A-18	620	48	0.08	0.02	65.1	8.18	0.74	0.06529	0.65	8.181	0.74	0.06514	0.66	743.4	5.2	779	14	5	recrystalized
121901A-18.2	525	78	0.15	--	67.1	6.718	0.74	0.06866	0.61	6.717	0.74	0.06881	0.62	894.7	6.2	893	13	0	igneous
121901A-26	344	44	0.13	0.00	27.3	10.812	0.78	0.06124	1.1	10.812	0.78	0.06122	1.1	570.2	4.3	647	23	13	rim
121901A-27	546	38	0.07	--	42.1	11.134	0.75	0.05914	0.86	11.125	0.75	0.05984	1	554.9	4.0	598	22	8	rim
121901A-34	451	37	0.08	--	37.5	10.315	0.75	0.06048	0.91	10.314	0.75	0.06057	0.95	596.5	4.3	624	20	5	rim
121901A-35	647	65	0.10	--	56.6	9.824	0.73	0.06105	0.72	9.818	0.73	0.06154	0.77	625.2	4.3	658	17	5	rim
121901A-36.2	2134	53	0.03	0.00	211	8.689	0.72	0.06256	0.37	8.689	0.72	0.06256	0.37	702.2	4.8	693	8	-1	recrystalized
121901A-36.3	802	94	0.12	--	67.6	10.186	0.71	0.06031	0.76	10.183	0.72	0.0605	0.81	603.9	4.1	622	18	3	rim
121901A-38	123	33	0.28	--	10.2	10.422	0.94	0.0605	1.7	10.408	0.95	0.0616	1.8	591.4	5.3	660	39	12	rim
121901A-42	320	56	0.18	0.02	29.1	9.44	1.1	0.05964	1.4	9.44	1.1	0.0595	1.4	648.9	7.0	585	30	-10	rim
121901A-43	479	139	0.30	0.03	40.8	10.103	0.75	0.06017	0.86	10.107	0.75	0.05989	0.9	608.2	4.3	600	20	-1	rim
121901A-43.2	308	125	0.42	--	25.3	10.452	0.79	0.06064	1.1	10.444	0.79	0.06127	1.2	589.4	4.4	649	26	10	rim
121901A-43.3	582	138	0.25	--	49	10.191	0.88	0.06096	0.81	10.19	0.88	0.06104	0.82	603.5	5.1	640	18	6	rim
121901A-47	710	79	0.11	0.04	54.7	11.162	0.85	0.05885	0.74	11.166	0.85	0.05856	0.8	552.9	4.5	551	17	0	rim
121901A-48	307	87	0.29	--	26.2	10.062	0.92	0.06039	1.1	10.058	0.94	0.0607	2.5	611.0	5.5	628	54	3	rim
121901A-49	446	122	0.28	0.10	55.4	6.919	0.87	0.06972	0.69	6.926	0.88	0.06892	0.79	869.4	7.1	896	16	3	recrystalized
121901A-50	718	54	0.08	0.00	90.1	6.847	0.84	0.06764	0.56	6.847	0.84	0.06763	0.56	878.8	6.9	857	12	-2	igneous
121901A-51	234	49	0.22	0.04	24.9	8.045	0.82	0.06523	1.1	8.048	0.82	0.06493	1.1	755.0	5.8	772	23	2	recrystalized
121901A-52	744	226	0.31	0.14	86.2	7.408	0.72	0.06822	0.56	7.419	0.72	0.06704	0.68	815.2	5.5	839	14	3	recrystalized
121901A-52.2	219	68	0.32	0.01	17.1	10.969	0.84	0.05952	1.3	10.97	0.84	0.05944	1.3	562.4	4.5	583	29	4	rim
121901A-53	309	14	0.05	0.03	26	10.244	0.79	0.06131	1	10.246	0.79	0.0611	1.1	600.3	4.5	643	23	7	rim
121901A-53.2	439	143	0.34	0.04	34.6	10.88	0.76	0.05934	0.94	10.885	0.76	0.059	1	566.6	4.1	567	22	0	rim

Table. 5.7 Continued.

Spot	ppm U	ppm Th	$^{232}Th/^{238}U$	% $^{206}Pb_c$	ppm $^{206}Pb^*$	Total $^{238}U/^{206}Pb$	±%	Total $^{207}Pb/^{206}Pb$	±%	(1) $^{238}U/^{206}Pb^*$	±%	(1) $^{207}Pb^*/^{206}Pb^*$	±%	(1) $^{206}Pb/^{238}U$ Age	1sigma err	(1) $^{207}Pb/^{206}Pb$ Age	1sigma err	% Dis-cor-dant	classification
121901A-54	404	61	0.16	--	52	6.68	1.6	0.06987	0.7	6.68	1.6	0.07	1.2	899.7	13.7	928	24	3	igneous
121901A-55	546	61	0.12	--	51.6	9.089	0.75	0.06285	0.72	9.086	0.75	0.06319	0.77	673.1	4.8	715	16	6	recrystalized
121901A-56	739	147	0.21	0.13	79.4	7.999	0.71	0.06759	0.54	8.009	0.71	0.0665	0.63	758.4	5.1	822	13	8	recrystalized
121901A-57	560	409	0.75	--	71.1	6.769	0.74	0.06861	0.9	6.769	0.74	0.06865	0.91	888.3	6.1	888	19	0	igneous
121901A-58	766	204	0.28	--	66.1	9.961	0.73	0.06002	0.65	9.96	0.73	0.0601	0.68	616.8	4.3	607	15	-2	rim
121901A-59	289	56	0.20	0.07	34.3	7.24	0.98	0.06904	0.83	7.245	0.98	0.0685	0.92	833.5	7.7	884	19	6	recrystalized
121901A-60	348	81	0.24	--	44	6.78	1.6	0.06956	0.76	6.78	1.6	0.06986	0.78	887.2	13.4	924	16	4	igneous
121901A-61	376	75	0.21	0.12	31.4	10.288	0.75	0.06085	0.9	10.301	0.76	0.05983	1.1	597.3	4.3	597	24	0	rim
121901A-62	292	92	0.32	0.02	37.5	6.7	1.9	0.06791	1	6.7	1.9	0.06777	1	896.7	15.9	862	21	-4	igneous
121901A-63	299	96	0.33	0.01	38.5	6.676	0.78	0.06915	0.83	6.677	0.78	0.06908	0.84	899.7	6.5	901	17	0	igneous
121901A-64	254	81	0.33	0.06	19.5	11.199	0.8	0.06059	1.5	11.206	0.8	0.06012	1.6	551.0	4.2	608	35	10	rim
121901A-65	310	103	0.34	1.25	39.7	6.711	0.76	0.0792	1.3	6.796	0.79	0.0688	2.9	885.0	6.5	893	61	1	igneous
121901A-66	1351	155	0.12	--	111	10.488	0.7	0.05868	0.54	10.488	0.7	0.0587	0.54	587.1	3.9	556	12	-5	rim
121901A-66.2	170	140	0.85	0.04	13.5	10.832	0.88	0.0597	1.5	10.836	0.88	0.05933	1.6	569.0	4.8	579	36	2	rim
121901A-67	397	122	0.32	0.31	47.1	7.229	0.76	0.06913	0.69	7.251	0.76	0.06657	1.5	832.8	6.0	824	30	-1	recrystalized
121901A-68	304	49	0.16	0.04	37	7.065	1.2	0.06764	0.84	7.068	1.2	0.06727	0.94	853.0	9.9	846	20	-1	recrystalized
121901A-68.2	639	39	0.06	0.04	80.8	6.793	0.72	0.06889	0.56	6.796	0.72	0.06855	0.59	885.0	5.9	885	12	0	igneous
121901A-69	286	33	0.12	--	23.4	10.507	0.8	0.05897	1.1	10.5	0.8	0.05959	1.2	586.5	4.5	589	26	0	rim
121901A-70	817	65	0.08	--	66.4	10.571	0.71	0.05941	0.67	10.57	0.74	0.0595	2.8	582.8	4.1	587	61	1	rim
121901A-70.2	93	44	0.49	--	8.05	9.97	1.1	0.062	2.8	9.95	1.1	0.0639	3.2	617.3	6.3	739	67	20	rim
121901A-71	1860	212	0.12	--	148	10.8	0.69	0.05878	0.45	10.8	0.69	0.05884	0.46	570.9	3.8	561	10	-2	rim
121901A-72	591	14	0.02	0.04	73.8	6.885	0.85	0.06764	0.59	6.887	0.85	0.06734	0.62	874.0	6.9	848	13	-3	recrystalized
121901A-74	484	122	0.26	0.37	55.7	7.472	0.73	0.06944	0.62	7.5	0.73	0.06639	0.91	806.9	5.5	819	19	1	recrystalized
121901A-76	176	48	0.28	0.07	15.1	9.976	0.86	0.06026	1.4	9.982	0.86	0.05973	1.5	615.4	5.0	594	33	-4	rim
121901A-77	1188	36	0.03	0.03	150	6.814	0.89	0.0681	0.41	6.816	0.89	0.06783	0.44	882.5	7.3	863	9	-2	igneous
121901A-78	352	68	0.20	--	31.2	9.706	0.76	0.0604	0.92	9.704	0.76	0.06052	0.94	632.2	4.6	622	20	-2	rim
121901A-79	561	136	0.25	--	44.8	10.744	0.73	0.05813	0.8	10.742	0.73	0.05822	0.84	573.8	4.0	538	18	-6	rim
121901A-80	1082	87	0.08	0.14	90.4	10.29	0.7	0.06104	0.5	10.304	0.7	0.0599	0.61	597.1	4.0	600	13	0	rim
121901A-81	364	22	0.06	--	30.4	10.301	0.77	0.05904	1	10.293	0.77	0.05962	1.2	597.7	4.4	590	26	-1	rim
121901A-82	300	99	0.34	--	36.1	7.122	0.79	0.06979	0.82	7.117	0.79	0.07041	1.1	847.5	6.3	940	23	11	recrystalized
121901A-83	724	162	0.23	--	64.2	9.689	0.88	0.06046	0.67	9.686	0.88	0.06068	0.7	633.4	5.3	628	15	-1	rim
121901A-84	179	153	0.89	--	13.9	11.067	0.86	0.05858	1.4	11.065	0.86	0.05875	1.5	557.8	4.6	558	32	0	rim
121901A-85	215	43	0.21	0.15	17.9	10.321	0.83	0.0593	1.2	10.337	0.83	0.05805	1.6	595.3	4.7	532	34	-11	rim

Error in Standard calibration was 0.16%(not included in above errors but required when comparing data from different mounts).

Errors are 1-sigma; Pb_c and Pb^* indicate the common and radiogenic portions, respectively.

(1) Common Pb corrected using measured ^{204}Pb.

Table. 5.8 SHRIMP U-Pb data for zircons from the sample BC07122805C

Spot	ppm U	ppm Th	$^{232}Th/^{238}U$	% $^{206}Pb_c$	ppm $^{206}Pb^*$	Total $^{238}U/^{206}Pb$	±%	Total $^{207}Pb/^{206}Pb$	±%	(1) $^{238}U/^{206}Pb^*$	±%	(1) $^{207}Pb^*/^{206}Pb^*$	±%	(1) $^{206}Pb/^{238}U$ Age	1sigma err	(1) $^{207}Pb/^{206}Pb$ Age	1sigma err	% Dis-cor-dant	classification
122805C-01	206	69	0.34	0.12	17.6	10.06	1.1	0.06058	1.6	10.07	1.1	0.0596	1.9	610.3	6.5	588	40	-4	igneous
122805C-02	122	41	0.35	0.19	10.5	9.91	1.3	0.0621	2.1	9.93	1.3	0.0606	2.7	618.6	7.9	624	58	1	igneous
122805C-03	112	36	0.34	--	9.85	9.73	1.4	0.0626	2.3	9.71	1.4	0.0643	2.8	631.7	8.4	752	59	19	igneous
122805C-04	124	26	0.22	0.01	10.9	9.77	1.3	0.0598	2.2	9.77	1.3	0.0597	3	628.1	7.7	593	66	-6	igneous
122805C-05	457	131	0.30	0.06	40.9	9.61	0.99	0.06172	1.1	9.616	0.99	0.06125	1.4	637.8	6.0	648	30	2	igneous
122805C-06.2	170	29	0.18	--	15	9.7	1.2	0.0604	2.7	9.69	1.2	0.0618	2.8	633.2	7.1	666	61	5	igneous
122805C-08	169	44	0.27	0.15	13.5	10.77	1.2	0.0617	2	10.78	1.2	0.0605	4.2	571.7	6.7	623	92	9	igneous
122805C-09	257	135	0.54	0.19	22.6	9.76	1.1	0.0605	1.5	9.78	1.1	0.0589	2	627.6	6.9	564	43	-10	igneous
122805C-09.2	218	40	0.19	--	19.2	9.74	1.1	0.0618	1.6	9.72	1.1	0.0634	2.1	631.3	6.8	723	44	15	igneous
122805C-10	47	15	0.33	--	4.13	9.69	1.8	0.06	4.4	9.67	1.8	0.0615	4.5	634.1	10.7	656	96	3	igneous
122805C-12	414	115	0.29	0.09	35.5	10.01	1	0.06091	1.2	10.02	1	0.06016	1.6	613.1	5.9	609	34	-1	igneous
122805C-13	439	95	0.22	0.14	39.7	9.486	10	0.06047	1.2	9.499	1	0.05935	1.4	645.3	6.1	580	31	-10	igneous
122805C-13.2	122	37	0.31	0.39	10.3	10.16	1.4	0.0618	2.2	10.2	1.4	0.0586	3.2	602.9	8.0	552	71	-8	igneous
122805C-15	248	44	0.18	0.24	22.2	9.63	1.1	0.06306	1.5	9.65	1.1	0.0611	2.1	635.7	6.7	642	46	1	igneous
122805C-20	80	17	0.22	--	7.09	9.65	1.5	0.0607	4	9.64	1.5	0.0619	4.1	636.4	8.8	670	87	5	igneous
122805C-20.2	286	61	0.22	--	26	9.46	1.1	0.05994	1.5	9.45	1.1	0.0606	1.7	648.5	6.6	627	36	-3	igneous
122805C-22	52	12	0.23	--	4.63	9.71	1.7	0.0591	3.4	9.65	1.7	0.0639	4.9	635.4	10.4	738	103	16	igneous
122805C-24	550	163	0.31	0.16	49.8	9.485	0.97	0.06088	1	9.5	0.98	0.05959	1.3	645.2	6.0	589	29	-9	igneous
122805C-25	429	100	0.24	0.09	38.5	9.591	1	0.06008	1.2	9.599	1	0.05938	1.4	638.8	6.1	581	31	-9	igneous
122805C-26	98	20	0.21	0.31	8.79	9.6	1.4	0.0633	2.4	9.63	1.4	0.0608	3.5	637.0	8.4	631	75	-1	igneous
122805C-26.2	383	92	0.25	0.17	35.1	9.38	1.1	0.06164	1.3	9.39	1.1	0.0603	1.7	652.2	6.7	613	37	-6	igneous

Errors are 1-sigma; Pb_c and Pb^* indicate the common and radiogenic portions, respectively.

Error in Standard calibration was 0.24%(not included in above errors but required when comparing data from different mounts).

(1) Common Pb corrected using measured ^{204}Pb.

Table. 5.9 SHRIMP U-Pb data for zircons from the sample AC07121501U

Spot	ppm U	ppm Th	$^{232}Th/^{238}U$	% $^{206}Pb_c$	ppm $^{206}Pb^*$	Total $^{238}U/^{206}Pb$	±%	Total $^{207}Pb/^{206}Pb$	±%	(1) $^{238}U/^{206}Pb^*$	±%	(1) $^{207}Pb^*/^{206}Pb^*$	±%	(1) $^{206}Pb/^{238}U$ Age	1sigma err	(1) $^{207}Pb/^{206}Pb$ Age	1sigma err	% Dis-cor-dant	classification
121501U-04	5492	2484	0.47	0.13	395	11.95	3.3	0.05833	0.3	11.97	3.3	0.0573	0.43	517.3	16.2	503	9	-3	igneous
121501U-05	12222	7244	0.61	0.00	962	10.915	0.67	0.05738	0.19	10.915	0.67	0.05736	0.19	565.1	3.6	505	4	-11	igneous
121501U-06	5163	2467	0.49	--	384	11.56	0.93	0.05723	0.3	11.56	0.93	0.05728	0.31	535.0	4.8	502	7	-6	igneous
121501U-09	16390	8061	0.51	0.00	1230	11.47	1.6	0.057	0.2	11.47	1.6	0.05699	0.21	539.0	8.1	491	5	-9	igneous
121501U-10	6563	1690	0.27	--	431	13.08	1.3	0.05742	0.45	13.08	1.3	0.05748	0.45	475.0	5.9	510	10	7	igneous
121501U-11	5550	2303	0.43	0.01	405	11.76	6.1	0.05715	0.74	11.76	6.1	0.05711	0.74	526.0	30.9	496	16	-6	igneous
121501U-15	755	335	0.46	0.29	108	5.986	0.89	0.07424	0.53	6.003	0.89	0.07183	0.7	993.2	8.2	981	14	-1	igneous
121501U-16	7623	4108	0.56	0.00	582	11.259	0.7	0.05734	0.25	11.259	0.7	0.05733	0.25	548.5	3.7	504	6	-8	igneous
121501U-17	589	182	0.32	0.02	71.3	7.092	1.4	0.06773	0.65	7.093	1.4	0.06755	0.66	850.2	11.1	855	14	1	igneous
121501U-18	5817	2672	0.47	0.00	419	11.92	1.4	0.05709	0.41	11.92	1.4	0.05708	0.41	519.2	7.0	495	9	-5	igneous
121501U-20	11682	7026	0.62	--	1010	9.92	0.75	0.05747	0.24	9.92	0.75	0.05749	0.24	619.2	4.4	510	5	-18	igneous

Errors are 1-sigma; Pb_c and Pb^* indicate the common and radiogenic portions, respectively.

Error in Standard calibration was 0.16%(not included in above errors but required when comparing data from different mounts).

(1) Common Pb corrected using measured ^{204}Pb.

Table. 5.10 SHRIMP U-Pb data for zircons from the sample AC07121601A

Spot	ppm U	ppm Th	$^{232}Th/^{238}U$	% $^{206}Pb_c$	ppm $^{206}Pb^*$	Total $^{238}U/^{206}Pb$	±%	Total $^{207}Pb/^{206}Pb$	±%	(1) $^{238}U/^{206}Pb^*$	±%	(1) $^{207}Pb^*/^{206}Pb^*$	±%	(1) $^{206}Pb/^{238}U$ Age	1sigma err	(1) $^{207}Pb/^{206}Pb$ Age	1sigma err	% Dis-cor-dant	classification
121601A-01	4727	1668	0.36	0.00	334	12.14	1.1	0.05761	0.29	12.15	1.1	0.05759	0.3	510.1	5.3	514	7	1	igneous
121601A-02	5597	1948	0.36	--	394	12.2	1.2	0.05749	0.28	12.2	1.2	0.05753	0.29	508.0	6.1	512	6	1	igneous
121601A-03	6004	2506	0.43	--	458	11.26	1.9	0.05765	0.26	11.26	1.9	0.05768	0.32	548.5	10.0	518	7	-6	igneous
121601A-05	8088	2965	0.38	--	598	11.62	1.1	0.05723	0.23	11.62	1.1	0.05726	0.24	532.1	5.5	501	5	-6	igneous
121601A-07	5882	2680	0.47	0.23	436	11.59	1.1	0.05931	0.26	11.61	1.1	0.05747	0.34	532.5	5.5	510	8	-4	igneous
121601A-09	5691	2444	0.44	0.28	394	12.4	1.5	0.05941	0.46	12.44	1.5	0.05713	0.88	498.6	7.1	497	19	0	igneous
121601A-11	9014	5405	0.62	--	727	10.66	4	0.05737	0.3	10.66	4	0.05742	0.3	578.1	21.9	508	7	-12	igneous
121601A-12	317	333	1.09	1.19	48	5.679	1.1	0.08559	0.73	5.748	1.1	0.0756	1.5	1034.0	10.9	1083	29	5	igneous
121601A-13	6246	2423	0.40	--	453	11.85	1.7	0.05764	0.26	11.85	1.7	0.05764	0.26	522.1	8.5	516	6	-1	igneous
121601A-14	7703	3445	0.46	0.00	551	12.01	1.2	0.0578	0.24	12.01	1.2	0.0578	0.24	515.4	6.0	522	5	1	igneous
121601A-15	9519	4044	0.44	0.00	703	11.63	1.1	0.05774	0.22	11.63	1.1	0.05771	0.22	531.9	5.8	519	5	-2	igneous
121601A-16	6070	2160	0.37	--	449	11.62	1.8	0.05726	0.28	11.62	1.8	0.05729	0.29	532.1	9.0	503	6	-6	igneous
121601A-17	5935	2260	0.39	0.22	434	11.74	1.2	0.05964	0.28	11.77	1.2	0.05786	0.43	525.7	5.9	524	10	0	igneous
121601A-19	5163	1743	0.35	--	345	12.84	4.5	0.05723	0.31	12.84	4.5	0.05724	0.31	483.4	20.7	501	7	4	igneous

Errors are 1-sigma; Pb_c and Pb^* indicate the common and radiogenic portions, respectively.

Error in Standard calibration was 0.53%(not included in above errors but required when comparing data from different mounts).

(1) Common Pb corrected using measured ^{204}Pb.

Table. 5.11 SHRIMP U-Pb data for zircons from the sample AC08011301M

Spot	ppm U	ppm Th	$^{232}Th/^{238}U$	% $^{206}Pb_c$	ppm $^{206}Pb^*$	Total $^{238}U/^{206}Pb$	±%	Total $^{207}Pb/^{206}Pb$	±%	(1) $^{238}U/^{206}Pb^*$	±%	(1) $^{207}Pb^*/^{206}Pb^*$	±%	(1) $^{206}Pb/^{238}U$ Age	1sigma err	(1) $^{207}Pb/^{206}Pb$ Age	1sigma err	% Dis-cor-dant	classification
011301M-06	385	115	0.31	--	68.4	4.827	1.3	0.08551	0.62	4.825	1.3	0.08583	0.63	1214.1	14.7	1334	12	10	inherited
011301M-06.2	1333	121	0.09	0.11	198	5.773	1.4	0.07402	0.39	5.779	1.4	0.07306	0.46	1028.8	13.1	1016	9	-1	recrystalized core
011301M-08	131	53	0.41	0.23	20.8	5.44	2.3	0.0781	1.6	5.45	2.3	0.0762	2	1085.6	23.0	1099	40	1	igneous
011301M-10	496	301	0.63	6.06	69.2	6.153	0.64	0.12157	0.52	6.55	0.78	0.0712	3	916.0	6.6	964	62	5	recrystalized core
011301M-12	972	92	0.10	--	142	5.867	0.58	0.07175	0.46	5.867	0.58	0.07185	0.47	1014.6	5.5	982	10	-3	recrystalized core
011301M-12.2	444	51	0.12	--	39.1	9.76	0.68	0.05982	0.95	9.758	0.68	0.05997	0.97	628.9	4.1	602	21	-4	recrystalized rim
011301M-14	652	27	0.04	--	61.7	9.081	0.63	0.06444	0.8	9.077	0.63	0.06487	0.87	673.8	4.1	770	18	14	recrystalized rim
011301M-14.2	973	276	0.29	0.11	131	6.38	0.57	0.07375	0.81	6.387	0.57	0.07281	0.88	937.7	5.0	1009	18	8	recrystalized core
011301M-16	181	85	0.49	0.10	26.9	5.772	0.83	0.0793	3	5.778	0.84	0.0785	3.2	1029.0	7.9	1159	63	13	igneous
011301M-17	476	120	0.26	0.06	66.7	6.129	0.65	0.07277	1.1	6.133	0.65	0.07225	1.1	973.7	5.9	993	23	2	igneous
011301M-18	445	271	0.63	0.06	70.8	5.395	0.66	0.0778	1.6	5.399	0.66	0.0773	1.6	1095.5	6.7	1130	33	3	igneous
011301M-19	519	339	0.67	--	112	3.99	1.1	0.10752	0.44	3.99	1.1	0.10759	0.45	1441.7	14.2	1759	8	22	inherited
011301M-21	1193	211	0.18	0.01	186	5.523	0.7	0.07408	0.42	5.524	0.7	0.074	0.43	1072.6	6.9	1041	9	-3	recrystalized core
011301M-22	282	53	0.19	0.79	24	10.087	0.75	0.0663	2.3	10.167	0.77	0.0598	3.5	604.8	4.5	597	75	-1	recrystalized rim
011301M-23	321	145	0.47	--	29.6	9.298	0.75	0.059	1.1	9.297	0.75	0.05908	1.1	658.5	4.7	570	25	-13	recrystalized rim
011301M-26	300	81	0.28	0.01	44	5.855	0.7	0.07473	0.9	5.855	0.7	0.07468	1	1016.5	6.6	1060	20	4	igneous
011301M-27	592	29	0.05	0.42	53.3	9.53	1.6	0.06657	0.97	9.57	1.6	0.0632	1.7	640.4	9.9	713	35	11	recrystalized rim
011301M-31	348	44	0.13	0.02	43.1	6.933	0.72	0.0701	1.8	6.934	0.72	0.0699	1.8	868.5	5.9	926	38	7	igneous
011301M-31.2	460	78	0.17	0.01	49.7	7.961	1.2	0.06686	0.96	7.962	1.2	0.06679	0.96	762.7	8.7	831	20	9	igneous
011301M-32	257	80	0.32	0.12	32.1	6.872	0.73	0.07148	1	6.881	0.73	0.07047	1.3	874.7	6.0	942	27	8	igneous

Error in Standard calibration was 0.14%(not included in above errors but required when comparing data from different mounts).

Errors are 1-sigma; Pb_c and Pb^* indicate the common and radiogenic portions, respectively.

(1) Common Pb corrected using measured ^{204}Pb.

Table. 5.12 SHRIMP U-Pb data for zircons from the sample AC08012001A

Spot	ppm U	ppm Th	$^{232}Th/^{238}U$	% $^{206}Pb_c$	ppm $^{206}Pb^*$	Total $^{238}U/^{206}Pb$	±%	Total $^{207}Pb/^{206}Pb$	±%	(1) $^{238}U/^{206}Pb^*$	±%	(1) $^{207}Pb^*/^{206}Pb^*$	±%	(1) $^{206}Pb/^{238}U$ Age	1sigma err	(1) $^{207}Pb/^{206}Pb$ Age	1sigma err	% Dis-cor-dant	classification
012001A-01	1128	54	0.05	0.19	88.5	10.949	0.66	0.06065	0.64	10.97	0.66	0.05908	0.88	562.4	3.5	570	19	1	recrystalized
012001A-04	1156	54	0.05	--	91.5	10.855	0.67	0.05895	0.69	10.854	0.67	0.05903	0.69	568.2	3.6	568	15	0	rim
012001A-04.2	62	22	0.37	0.48	7.52	7.07	1.3	0.0686	2.3	7.105	1.3	0.0646	4.1	848.9	10.4	762	87	-10	igneous
012001A-06	697	43	0.06	0.04	54.7	10.958	0.71	0.06022	0.88	10.962	0.71	0.0599	0.96	562.8	3.8	600	21	7	recrystalized
012001A-13	2346	186	0.08	0.01	188	10.695	0.64	0.05891	0.49	10.696	0.64	0.05882	0.51	576.2	3.5	560	11	-3	recrystalized
012001A-15	72	20	0.29	--	8.18	7.55	2.5	0.0683	2.2	7.53	2.5	0.0712	3	804.3	19.2	963	62	20	igneous
012001A-20	1030	46	0.05	0.00	80.7	10.971	0.68	0.05909	0.75	10.971	0.68	0.05908	0.76	562.3	3.7	570	16	1	recrystalized
012001A-23	109	42	0.40	0.23	12.9	7.252	1	0.0672	1.7	7.268	1.1	0.0653	2.2	831.0	8.2	785	46	-6	igneous
012001A-24	27	6	0.24	--	3.43	6.73	1.8	0.0722	3.3	6.67	1.9	0.0795	6.1	900.6	15.8	1186	121	32	igneous
012001A-27.2	984	44	0.05	--	78.8	10.725	0.68	0.0584	0.76	10.722	0.68	0.05868	0.85	574.8	3.8	555	19	-3	rim
012001A-29	618	70	0.12	0.07	47.6	11.146	0.72	0.05849	0.93	11.154	0.72	0.05796	1.1	553.5	3.8	528	23	-5	rim
012001A-30	37	11	0.32	0.81	4.31	7.38	1.5	0.0666	3.6	7.44	1.6	0.0598	6.2	812.6	12.1	597	133	-27	igneous
012001A-31	55	15	0.27	0.22	6.21	7.65	1.4	0.0708	2.5	7.67	1.4	0.069	2.9	790.4	10.1	898	61	14	igneous
012001A-32	424	31	0.07	0.19	33.4	10.922	0.76	0.06124	1.1	10.943	0.77	0.0597	1.9	563.7	4.2	592	41	5	rim
012001A-33	37	11	0.31	--	4.7	6.79	2.5	0.0704	2.9	6.77	2.5	0.0728	3.2	888.0	21.1	1009	66	14	igneous
012001A-34	457	133	0.30	0.12	35.5	11.058	0.76	0.05963	1.5	11.071	0.77	0.0586	2	557.4	4.1	553	44	-1	rim
012001A-38	1551	130	0.09	0.00	123	10.86	0.66	0.0595	0.82	10.86	0.66	0.05947	0.83	567.8	3.6	584	18	3	rim
012001A-40	673	258	0.40	0.12	53.2	10.87	0.72	0.05891	0.93	10.883	0.73	0.05795	1.2	566.7	3.9	528	26	-7	recrystalized
012001A-40.2	580	199	0.35	0.03	44.7	11.164	0.77	0.05886	1.1	11.168	0.77	0.05859	1.1	552.8	4.1	552	25	0	rim
012001A-46	58	15	0.27	0.40	5.93	8.33	1.5	0.0665	4.3	8.36	1.5	0.0631	5.2	728.0	10.3	713	110	-2	igneous

Errors are 1-sigma; Pb_c and Pb^* indicate the common and radiogenic portions, respectively.

Error in Standard calibration was 0.14%(not included in above errors but required when comparing data from different mounts).

(1) Common Pb corrected using measured ^{204}Pb.

Table. 5.13 SHRIMP U-Pb data for zircons from the sample B08012201I

Spot	ppm U	ppm Th	$^{232}Th/^{238}U$	% $^{206}Pb_c$	ppm $^{206}Pb^*$	Total $^{238}U/^{206}Pb$	±%	Total $^{207}Pb/^{206}Pb$	±%	(1) $^{238}U/^{206}Pb^*$	±%	(1) $^{207}Pb^*/^{206}Pb^*$	±%	(1) $^{206}Pb/^{238}U$ Age	1sigma err	(1) $^{207}Pb/^{206}Pb$ Age	1sigma err	% Dis-cor-dant	classification
012201I-10	360	133	0.38	--	51.8	5.974	0.73	0.07232	0.78	5.973	0.73	0.07247	0.78	997.9	6.8	999	16	0	igneous
012201I-11	592	199	0.35	0.08	83.4	6.095	0.68	0.07275	0.59	6.1	0.68	0.07206	0.68	978.6	6.2	988	14	1	igneous
012201I-13	1268	503	0.41	0.09	180	6.049	0.66	0.07272	0.43	6.054	0.66	0.07197	0.55	985.5	6.1	985	11	0	igneous
012201I-14	661	187	0.29	0.11	94.1	6.037	0.69	0.07303	0.6	6.043	0.69	0.07211	0.72	987.1	6.3	989	15	0	igneous
012201I-16	726	219	0.31	0.04	104	5.983	0.68	0.07285	0.58	5.985	0.68	0.0725	0.62	996.0	6.3	1000	13	0	igneous
012201I-17	1001	355	0.37	0.02	142	6.039	0.78	0.07281	0.64	6.04	0.78	0.0726	0.66	987.6	7.1	1003	13	2	igneous
012201I-18	1158	538	0.48	--	166	5.992	0.65	0.07209	0.46	5.991	0.65	0.07225	0.47	995.1	6.0	993	10	0	igneous
012201I-19	1007	383	0.39	0.05	142	6.092	0.66	0.07257	0.5	6.095	0.66	0.07216	0.53	979.3	6.0	990	11	1	igneous
012201I-19.2	3294	2471	0.77	0.00	492	5.748	0.63	0.0721	0.28	5.749	0.63	0.07209	0.28	1033.9	6.1	989	6	-4	igneous
012201I-21	388	87	0.23	0.04	55.3	6.025	0.74	0.07221	1.1	6.027	0.74	0.07189	1.1	989.6	6.8	983	23	-1	igneous
012201I-22	636	202	0.33	0.24	90.6	6.034	0.7	0.07311	0.63	6.049	0.7	0.07107	0.87	986.3	6.4	959	18	-3	igneous
012201I-23	822	406	0.51	--	116	6.095	0.68	0.07201	0.57	6.094	0.68	0.07212	0.58	979.5	6.2	989	12	1	igneous
012201I-25	919	356	0.40	--	127	6.19	0.67	0.07173	0.55	6.19	0.67	0.07176	0.55	965.4	6.0	979	11	1	igneous

Errors are 1-sigma; Pb_c and Pb^* indicate the common and radiogenic portions, respectively.

Error in Standard calibration was 0.14%(not included in above errors but required when comparing data from different mounts).

(1) Common Pb corrected using measured ^{204}Pb.

Table. 5.14 SHRIMP U-Pb data for zircons from the sample B08012304E

Spot	ppm U	ppm Th	$^{232}Th/^{238}U$	% $^{206}Pb_c$	ppm $^{206}Pb^*$	Total $^{238}U/^{206}Pb$	±%	Total $^{207}Pb/^{206}Pb$	±%	(1) $^{238}U/^{206}Pb^*$	±%	(1) $^{207}Pb^*/^{206}Pb^*$	±%	(1) $^{206}Pb/^{238}U$ Age	1sigma err	(1) $^{207}Pb/^{206}Pb$ Age	1sigma err	% Dis-cor-dant	classification
012304-E-09	1103	332	0.31	0.00	153	6.204	0.57	0.07179	0.47	6.204	0.57	0.07175	0.48	963.4	5.1	979	10	2	igneous
012304-E-09.2	3809	153	0.04	0.17	295	11.1	0.53	0.05971	0.37	11.119	0.53	0.05829	0.49	555.2	2.8	541	11	-3	rim
012304-E-11	488	90	0.19	0.01	64.7	6.484	0.64	0.07152	0.73	6.485	0.64	0.07148	0.73	924.5	5.5	971	15	5	igneous
012304-E-11.2	6637	74	0.01	0.01	529	10.788	0.52	0.05833	0.33	10.789	0.52	0.05827	0.33	571.4	2.9	540	7	-5	rim
012304-E-13.2	3535	43	0.01	0.01	275	11.036	0.55	0.0584	0.41	11.037	0.55	0.05832	0.41	559.1	2.9	542	9	-3	rim
012304-E-15.2	5761	72	0.01	0.04	461	10.736	0.54	0.05887	0.32	10.74	0.54	0.05857	0.35	573.9	2.9	551	8	-4	rim
012304-E-17	7244	81	0.01	0.02	581	10.715	0.53	0.05866	0.3	10.717	0.53	0.05852	0.32	575.1	2.9	549	7	-4	rim
012304-E-17.2	934	244	0.27	0.06	127	6.342	0.59	0.07153	0.58	6.346	0.59	0.07105	0.63	943.3	5.2	959	13	2	igneous
012304-E-21	3902	37	0.01	0.23	305	10.978	0.54	0.06015	0.4	11.003	0.54	0.05831	0.55	560.8	2.9	541	12	-3	rim
012304-E-21.2	814	198	0.25	0.16	116	6.048	0.61	0.07347	0.6	6.058	0.61	0.0721	0.76	984.9	5.6	989	15	0	igneous
012304-E-24	4750	1164	0.25	0.01	702	5.816	0.61	0.07175	0.39	5.816	0.61	0.07169	0.4	1022.8	5.8	977	8	-4	igneous
012304-E-25	5036	53	0.01	0.01	398	10.868	0.55	0.05876	0.38	10.869	0.55	0.05871	0.38	567.4	3.0	556	8	-2	rim
012304-E-28	557	66	0.12	0.03	61.6	7.774	0.66	0.06811	0.87	7.776	0.66	0.06789	0.88	779.9	4.9	865	18	11	igneous
012304-E-28.2	4979	51	0.01	0.01	395	10.834	0.53	0.05836	0.4	10.835	0.53	0.0583	0.41	569.1	2.9	541	9	-5	rim
012304-E-30	1237	305	0.25	0.05	155	6.864	0.56	0.07012	0.48	6.868	0.56	0.06974	0.51	876.3	4.6	921	10	5	igneous
012304-E-31	770	160	0.22	--	107	6.175	0.59	0.07217	0.58	6.174	0.59	0.0723	0.59	967.7	5.3	995	12	3	igneous
012304-E-32	695	142	0.21	0.01	98.4	6.071	0.59	0.07221	0.57	6.071	0.59	0.07213	0.58	982.9	5.4	989	12	1	igneous
012304-E-36	2781	29	0.01	--	212	11.244	0.54	0.0583	0.54	11.243	0.54	0.05834	0.54	549.3	2.9	542	12	-1	rim
012304-E-36.2	641	131	0.21	0.02	85.7	6.427	0.61	0.07224	0.64	6.428	0.61	0.07211	0.66	932.2	5.3	989	13	6	igneous
012304-E-42	1362	402	0.31	0.02	190	6.173	0.55	0.07203	0.48	6.175	0.55	0.07184	0.52	967.6	5.0	981	11	1	igneous

Error in Standard calibration was 0.14%(not included in above errors but required when comparing data from different mounts).

Errors are 1-sigma; Pb_c and Pb^* indicate the common and radiogenic portions, respectively.

(1) Common Pb corrected using measured ^{204}Pb.

Table. 5.15 SHRIMP U-Pb data for zircons from the sample BC08010604A

Spot	ppm U	ppm Th	$^{232}Th/^{238}U$	% $^{206}Pb_c$	ppm $^{206}Pb^*$	Total $^{238}U/^{206}Pb$	±%	Total $^{207}Pb/^{206}Pb$	±%	(1) $^{238}U/^{206}Pb^*$	±%	(1) $^{207}Pb^*/^{206}Pb^*$	±%	(1) $^{206}Pb/^{238}U$ Age	1sigma err	(1) $^{207}Pb/^{206}Pb$ Age	1sigma err	% Dis-cor-dant	classification
010604A-03	916	184	0.21	0.02	77.4	10.175	0.68	0.06051	0.58	10.177	0.68	0.06034	0.62	604.2	3.9	616	13	2	rim
010604A-05	602	314	0.54	0.19	86.1	6.004	0.71	0.07438	0.51	6.015	0.71	0.07279	0.75	991.4	6.5	1008	15	2	core
010604A-06	863	126	0.15	0.16	73.6	10.071	0.7	0.06107	0.59	10.087	0.7	0.05973	0.81	609.3	4.1	594	18	-3	rim
010604A-06.2	762	311	0.42	0.02	109	5.995	0.68	0.07275	0.46	5.996	0.68	0.07261	0.48	994.3	6.3	1003	10	1	core
010604A-08	958	71	0.08	0.63	107	7.689	0.69	0.0704	0.56	7.737	0.69	0.06522	1	783.6	5.1	781	22	0	core
010604A-11	636	303	0.49	0.47	83.3	6.564	0.89	0.07403	1.2	6.595	0.91	0.0701	2.5	910.1	7.7	932	51	2	core
010604A-13	2254	51	0.02	0.01	245	7.895	0.65	0.06479	0.32	7.896	0.65	0.0647	0.33	768.7	4.7	765	7	-1	rim
010604A-13.2	2083	48	0.02	0.02	231	7.739	0.65	0.06571	0.33	7.74	0.65	0.06555	0.35	783.3	4.8	792	7	1	rim
010604A-15	965	187	0.20	--	81.9	10.116	0.68	0.05976	0.57	10.114	0.68	0.05991	0.59	607.8	3.9	600	13	-1	rim
010604A-17	379	154	0.42	--	49.2	6.606	0.75	0.07097	0.68	6.602	0.75	0.07143	0.73	909.2	6.4	970	15	7	core
010604A-17.2	908	186	0.21	0.01	76.7	10.174	0.7	0.06001	0.6	10.175	0.7	0.05991	0.63	604.3	4.0	600	14	-1	rim
010604A-20	346	141	0.42	--	48.3	6.141	0.75	0.0718	0.72	6.14	0.75	0.07194	0.74	972.7	6.7	984	15	1	core
010604A-21	695	402	0.60	0.02	99.3	6.014	0.69	0.07307	0.49	6.015	0.69	0.07291	0.53	991.5	6.4	1011	11	2	core
010604A-21.2	886	195	0.23	--	74.3	10.245	0.86	0.06041	0.65	10.244	0.86	0.06052	0.66	600.4	4.9	622	14	4	rim
010604A-23	491	246	0.52	0.06	69.9	6.037	0.72	0.0733	0.63	6.041	0.72	0.07279	0.74	987.5	6.6	1008	15	2	core
010604A-25	499	225	0.47	0.07	74.1	5.792	0.7	0.07275	0.55	5.796	0.7	0.07217	0.65	1026.0	6.7	991	13	-3	igneous
010604A-25.2	2520	1257	0.52	--	374	5.784	0.65	0.07286	0.25	5.784	0.65	0.07288	0.25	1028.0	6.2	1011	5	-2	igneous
010604A-27	471	223	0.49	0.03	69.3	5.834	0.87	0.07331	0.56	5.836	0.87	0.07305	0.61	1019.6	8.2	1015	12	0	igneous
010604A-28	457	199	0.45	0.28	58.3	6.725	0.71	0.07389	0.82	6.744	0.71	0.07157	1	891.3	5.9	974	20	9	core
010604A-31	395	181	0.47	0.07	55.8	6.086	0.72	0.07271	0.63	6.09	0.72	0.07211	0.73	980.1	6.5	989	15	1	core
010604A-38	632	224	0.37	0.05	81.2	6.684	0.73	0.06997	0.59	6.687	0.73	0.06952	0.63	898.4	6.1	914	13	2	core
010604A-39	1010	451	0.46	0.02	132	6.592	0.68	0.07101	0.51	6.594	0.68	0.07082	0.53	910.3	5.8	952	11	5	core
010604A-33	848	464	0.57	--	124	5.864	0.7	0.07282	0.48	5.863	0.7	0.0729	0.48	1015.2	6.6	1011	10	0	igneous
010604A-40	851	549	0.67	0.00	111	6.565	0.7	0.07147	0.54	6.565	0.7	0.07145	0.54	914.0	6.0	970	11	6	core
010604A-41	956	294	0.32	0.43	106	7.749	0.72	0.06996	0.58	7.783	0.73	0.06643	1.2	779.2	5.3	820	25	5	core
010604A-42	582	298	0.53	0.34	79.5	6.29	0.73	0.07468	0.66	6.312	0.74	0.07183	0.97	948.0	6.5	981	20	3	core
010604A-43	1034	196	0.20	0.01	87.3	10.183	0.82	0.06045	0.72	10.184	0.82	0.06034	0.75	603.8	4.7	616	16	2	rim
010604A-44	699	393	0.58	0.02	98.5	6.095	0.73	0.07224	0.63	6.096	0.73	0.07209	0.67	979.2	6.6	989	14	1	core
010604A-45	893	536	0.62	0.05	120	6.38	0.71	0.07207	0.91	6.383	0.71	0.0717	0.99	938.3	6.2	977	20	4	core
010604A-46	483	193	0.41	0.06	65.7	6.31	0.76	0.07277	0.77	6.314	0.77	0.07231	0.86	947.8	6.7	995	17	5	core
010604A-47	494	157	0.33	0.11	59.7	7.107	1.1	0.0709	0.98	7.114	1.1	0.06999	1.1	847.8	8.4	928	23	9	core
010604A-48	663	284	0.44	0.11	83.6	6.811	0.75	0.07067	0.98	6.819	0.75	0.06974	1.2	882.2	6.2	921	24	4	rim
010604A-48.2	278	115	0.43	0.19	34.1	7.008	0.91	0.07213	1.1	7.022	0.91	0.07053	1.4	858.3	7.3	944	28	10	core
010604A-49	775	439	0.59	0.02	106	6.313	0.73	0.07321	0.61	6.314	0.73	0.07304	0.65	947.8	6.4	1015	13	7	core
010604A-49.2	553	310	0.58	0.09	70.3	6.76	0.79	0.07206	0.75	6.766	0.79	0.07133	0.87	888.6	6.6	967	18	9	core
010604A-52	706	162	0.24	0.15	83.5	7.265	0.75	0.06857	0.8	7.276	0.75	0.0673	1	830.1	5.9	847	21	2	core
010604A-53	1136	218	0.20	--	96	10.162	0.7	0.05912	0.64	10.161	0.7	0.05922	0.65	605.1	4.0	575	14	-5	rim

Error in Standard calibration was 0.22%(not included in above errors but required when comparing data from different mounts).
Errors are 1-sigma; Pb_c and Pb^* indicate the common and radiogenic portions, respectively.
(1) Common Pb corrected using measured ^{204}Pb.

Table 5.16. Chemical compositions of monazites in the sample AC07121701C from Austkampane area

Analyses No.	1.1	1.2	1.3	1.4	1.5	1.6	1.7	1.8	1.9	1.10	1.11	1.12	1.13	1.14	1.15
wt%															
P2O5	29.21	29.26	29.08	29.80	29.55	29.52	29.77	29.86	29.69	29.72	29.73	29.60	29.63	29.42	29.67
SiO2	0.35	0.38	0.37	0.18	0.21	0.22	0.20	0.17	0.17	0.18	0.19	0.20	0.21	0.18	0.17
CaO	2.23	2.17	2.15	1.33	1.45	1.49	1.53	1.31	1.27	1.34	1.33	1.55	1.55	1.35	1.35
Y2O3	0.28	0.25	0.24	0.16	0.16	0.15	0.14	0.15	0.13	0.17	0.17	0.18	0.15	0.16	0.15
La2O3	9.67	10.45	10.08	12.16	11.00	11.24	11.28	11.64	11.92	11.98	11.76	11.26	11.50	11.48	11.31
Ce2O3	26.83	27.28	27.61	30.19	29.39	29.56	29.35	30.48	30.01	29.56	29.74	29.03	29.53	30.10	29.66
Pr2O3	2.98	2.81	2.78	2.91	3.01	2.98	2.91	3.05	3.01	3.27	3.12	2.89	3.01	3.09	2.82
Nd2O3	14.95	14.76	14.77	15.58	15.71	15.39	15.61	15.46	15.77	15.56	15.35	15.29	15.02	15.59	14.95
Sm2O3	1.82	1.72	1.49	1.73	1.89	1.91	1.64	1.85	1.97	1.92	1.97	1.74	1.88	1.80	1.86
Gd2O3	0.98	0.92	0.93	1.11	1.00	0.86	1.10	0.93	0.83	1.01	0.92	1.10	0.93	1.03	0.93
Dy2O3	0.11	0.05	0.03	0.13	0.11	0.11	0.04	0.08	0.02	0.10	0.11	0.07	0.06	0.12	0.10
Er2O3	–	–	0.02	–	–	0.02	0.04	0.00	–	–	–	–	–	–	–
UO2	0.49	0.34	0.34	0.27	0.29	0.28	0.29	0.26	0.27	0.26	0.27	0.28	0.28	0.27	0.25
ThO2	10.65	10.52	10.48	5.93	6.82	6.94	7.02	5.89	5.87	6.16	6.15	7.11	7.14	6.24	6.04
PbO	0.32	0.31	0.30	0.18	0.22	0.21	0.21	0.17	0.18	0.19	0.19	0.22	0.21	0.19	0.18
Total	100.95	101.34	100.78	101.77	100.83	100.99	101.22	101.36	101.19	101.51	101.08	100.55	101.15	101.14	99.52
Cation (O=4)															
P	0.97	0.97	0.97	0.98	0.98	0.98	0.99	0.99	0.99	0.98	0.99	0.99	0.98	0.98	0.99
Si	0.01	0.01	0.01	0.01	0.01	0.01	0.01	0.01	0.01	0.01	0.01	0.01	0.01	0.01	0.01
Ca	0.09	0.09	0.09	0.06	0.06	0.06	0.06	0.05	0.05	0.06	0.06	0.07	0.07	0.06	0.06
Y	0.01	0.01	0.00	0.00	0.00	0.00	0.00	0.00	0.00	0.00	0.00	0.00	0.00	0.00	0.00
La	0.14	0.15	0.15	0.17	0.16	0.16	0.16	0.17	0.17	0.17	0.17	0.16	0.17	0.17	0.16
Ce	0.39	0.39	0.40	0.43	0.42	0.43	0.42	0.44	0.43	0.42	0.43	0.42	0.42	0.43	0.43
Pr	0.04	0.04	0.04	0.04	0.04	0.04	0.04	0.04	0.04	0.05	0.04	0.04	0.04	0.04	0.04
Nd	0.21	0.21	0.21	0.22	0.22	0.22	0.22	0.22	0.22	0.22	0.21	0.21	0.21	0.22	0.21
Sm	0.02	0.02	0.02	0.02	0.03	0.03	0.02	0.02	0.03	0.03	0.03	0.02	0.03	0.02	0.03
Gd	0.01	0.01	0.01	0.01	0.01	0.01	0.01	0.01	0.01	0.01	0.01	0.01	0.01	0.01	0.01
Dy	0.00	0.00	0.00	0.00	0.00	0.00	0.00	0.00	0.00	0.00	0.00	0.00	0.00	0.00	0.00
Er	–	–	0.00	–	–	0.00	0.00	0.00	–	–	–	–	–	–	–
U	0.00	0.00	0.00	0.00	0.00	0.00	0.00	0.00	0.00	0.00	0.00	0.00	0.00	0.00	0.00
Th	0.10	0.09	0.09	0.05	0.06	0.06	0.06	0.05	0.05	0.05	0.05	0.06	0.06	0.06	0.05
Pb	0.00	0.00	0.00	0.00	0.00	0.00	0.00	0.00	0.00	0.00	0.00	0.00	0.00	0.00	0.00
Total	2.01	2.01	2.01	2.01	2.01	2.01	2.01	2.01	2.01	2.01	2.01	2.01	2.01	2.01	2.00
ThO2*	11.98	11.36	11.33	6.65	7.61	7.68	7.79	6.58	6.60	6.87	6.86	7.83	7.86	6.98	6.71
Th/U	27.31	42.39	42.20	28.19	29.58	31.70	31.07	29.19	27.43	29.68	29.48	33.60	33.78	28.80	30.68
Nd/La	0.81	0.74	0.76	0.67	0.75	0.71	0.72	0.69	0.69	0.68	0.68	0.71	0.68	0.71	0.69
Gd/Nd	0.15	0.14	0.15	0.17	0.15	0.13	0.16	0.14	0.12	0.15	0.14	0.17	0.14	0.15	0.14
Age (Ma)	634	652	648	667	684	647	641	634	665	653	654	669	645	670	658
+/− (Ma)	26	28	28	47	41	41	40	48	48	46	46	40	40	45	47

–: below detection limit

Table 5.16. Continued

1.16	2.1	2.2	2.3	2.4	2.5	2.6	2.7	2.8	2.9	2.10	2.11	2.12	2.13	2.14	3.1	3.2
29.72	29.22	29.52	29.31	29.61	29.70	29.62	29.40	29.39	29.50	29.72	29.14	29.50	28.93	28.90	29.42	29.30
0.20	0.35	0.31	0.30	0.28	0.23	0.25	0.27	0.32	0.25	0.23	0.43	0.30	0.51	0.55	0.47	0.45
1.42	1.70	1.56	1.65	1.66	1.53	1.48	1.47	1.57	1.45	1.46	1.59	1.51	2.26	2.24	2.04	2.02
0.19	0.16	0.19	0.13	0.15	0.16	0.19	0.22	0.24	0.21	0.16	0.20	0.18	0.19	0.19	0.18	0.22
11.84	11.29	11.08	11.41	11.51	11.58	11.42	11.57	11.51	11.68	11.71	11.10	11.11	10.00	10.00	10.40	10.68
29.23	28.73	28.73	29.73	29.50	29.41	29.50	29.31	29.35	29.84	29.66	29.05	29.54	26.99	26.60	27.42	27.72
3.23	2.91	2.96	3.15	2.88	3.15	3.00	3.14	3.13	3.28	3.30	3.03	3.27	2.95	2.92	2.97	2.92
15.49	15.25	15.56	14.59	15.22	15.52	15.29	15.53	15.03	14.99	15.33	15.39	15.60	14.45	13.95	15.02	14.58
1.78	1.53	1.86	1.57	1.78	1.95	1.91	2.01	1.86	2.01	1.68	1.48	1.72	1.59	1.78	1.78	1.83
1.16	0.89	0.95	0.84	0.83	1.02	1.18	1.10	0.96	0.99	0.82	0.99	1.05	0.72	0.91	0.83	0.82
0.14	0.13	0.09	0.03	0.07	0.05	0.10	0.06	0.02	0.17	0.06	0.12	–	0.12	0.05	0.09	0.19
–	–	–	–	0.03	–	–	–	–	–	–	–	0.01	–	–	–	–
0.25	0.27	0.25	0.26	0.26	0.27	0.26	0.25	0.23	0.27	0.26	0.27	0.25	0.36	0.37	0.28	0.27
6.49	8.57	7.74	8.09	8.14	7.43	7.18	7.31	7.97	7.17	7.00	7.70	7.60	11.85	11.68	10.68	10.33
0.20	0.24	0.22	0.23	0.23	0.22	0.20	0.21	0.23	0.21	0.20	0.23	0.22	0.34	0.33	0.30	0.29
101.41	101.33	101.07	101.39	102.23	102.29	101.62	101.92	101.91	102.12	101.65	100.78	101.91	101.34	100.51	101.99	101.69
0.98	0.97	0.98	0.98	0.98	0.98	0.98	0.97	0.97	0.98	0.98	0.97	0.98	0.97	0.97	0.97	0.97
0.01	0.01	0.01	0.01	0.01	0.01	0.01	0.01	0.01	0.01	0.01	0.02	0.01	0.02	0.02	0.02	0.02
0.06	0.07	0.07	0.07	0.07	0.06	0.06	0.06	0.07	0.06	0.06	0.07	0.06	0.10	0.10	0.09	0.08
0.00	0.00	0.00	0.00	0.00	0.00	0.00	0.00	0.00	0.00	0.00	0.00	0.00	0.00	0.00	0.00	0.00
0.17	0.16	0.16	0.17	0.17	0.17	0.16	0.17	0.17	0.17	0.17	0.16	0.16	0.15	0.15	0.15	0.15
0.42	0.41	0.41	0.43	0.42	0.42	0.42	0.42	0.42	0.43	0.42	0.42	0.42	0.39	0.39	0.39	0.40
0.05	0.04	0.04	0.05	0.04	0.04	0.04	0.04	0.04	0.05	0.05	0.04	0.05	0.04	0.04	0.04	0.04
0.22	0.21	0.22	0.20	0.21	0.22	0.21	0.22	0.21	0.21	0.21	0.22	0.22	0.20	0.20	0.21	0.20
0.02	0.02	0.03	0.02	0.02	0.03	0.03	0.03	0.03	0.03	0.02	0.02	0.02	0.02	0.02	0.02	0.02
0.01	0.01	0.01	0.01	0.01	0.01	0.02	0.01	0.01	0.01	0.01	0.01	0.01	0.01	0.01	0.01	0.01
0.00	0.00	0.00	0.00	0.00	0.00	0.00	0.00	0.00	0.00	0.00	0.00	–	0.00	0.00	0.00	0.00
–	–	–	–	0.00	–	–	–	–	–	–	–	0.00	–	–	–	–
0.00	0.00	0.00	0.00	0.00	0.00	0.00	0.00	0.00	0.00	0.00	0.00	0.00	0.00	0.00	0.00	0.00
0.06	0.08	0.07	0.07	0.07	0.07	0.06	0.07	0.07	0.06	0.06	0.07	0.07	0.11	0.11	0.09	0.09
0.00	0.00	0.00	0.00	0.00	0.00	0.00	0.00	0.00	0.00	0.00	0.00	0.00	0.00	0.00	0.00	0.00
2.01	2.01	2.01	2.01	2.01	2.01	2.01	2.01	2.01	2.01	2.01	2.01	2.01	2.01	2.01	2.01	2.01
7.14	9.22	8.35	8.74	8.76	8.10	7.84	7.94	8.52	7.86	7.66	8.37	8.22	12.73	12.58	11.32	10.92
34.50	45.21	43.22	42.44	44.35	37.48	37.15	39.86	48.75	35.29	36.10	39.33	42.46	46.01	44.60	56.47	58.90
0.68	0.70	0.73	0.67	0.69	0.70	0.70	0.70	0.68	0.67	0.68	0.72	0.73	0.75	0.73	0.75	0.71
0.17	0.14	0.14	0.13	0.13	0.15	0.18	0.16	0.15	0.15	0.12	0.15	0.16	0.12	0.15	0.13	0.13
669	634	625	635	626	650	619	630	649	636	637	672	658	645	634	649	633
44	34	38	36	36	39	40	39	37	40	41	37	38	25	25	28	29

Table 5.16. Continued

3.3	3.4	3.5	3.6	3.7	3.8	3.9	3.10	3.11	3.12	3.13	3.14	3.15	3.16	4.1	4.2	4.3
29.38	29.31	29.35	29.66	29.44	29.58	29.41	29.45	29.42	29.35	29.68	29.37	29.66	29.70	28.62	28.97	29.13
0.38	0.44	0.43	0.35	0.37	0.29	0.39	0.38	0.42	0.43	0.31	0.28	0.30	0.41	0.35	0.32	0.22
1.79	2.04	1.96	1.72	1.75	1.59	1.87	1.85	1.93	1.93	1.66	1.57	1.62	1.90	1.93	1.80	1.36
0.23	0.25	0.24	0.22	0.17	0.19	0.22	0.24	0.25	0.25	0.23	0.19	0.24	0.26	0.59	0.63	0.50
10.65	10.88	10.77	10.68	10.77	11.69	10.68	11.22	10.93	10.35	11.61	11.24	11.50	11.18	10.70	10.91	13.44
28.32	27.89	28.28	28.72	28.70	29.17	28.84	28.51	28.07	28.01	28.82	29.23	28.76	28.05	27.43	28.08	30.12
3.09	3.05	3.18	3.18	3.31	3.04	2.90	3.24	3.07	3.14	3.10	3.27	3.07	2.80	3.02	3.15	3.02
14.99	14.78	14.41	15.25	15.27	14.96	14.38	14.57	14.91	14.83	14.87	15.27	15.18	14.54	14.76	14.72	13.69
2.01	1.65	1.81	1.81	1.84	1.63	1.86	1.91	1.70	1.91	1.79	1.89	1.68	1.64	1.64	1.75	1.42
0.70	0.81	0.85	0.99	0.96	0.97	1.02	0.86	0.78	0.85	0.96	0.90	1.02	0.92	1.21	1.16	0.85
0.12	0.12	0.10	0.17	0.06	0.15	0.11	0.19	0.17	–	0.12	0.04	0.04	0.11	0.08	0.09	0.03
–	–	–	0.03	0.02	0.00	–	–	–	–	0.00	0.04	–	0.03	–	–	–
0.24	0.28	0.28	0.24	0.25	0.23	0.26	0.26	0.29	0.29	0.27	0.28	0.25	0.28	0.73	0.63	0.41
9.38	10.37	10.12	8.69	8.83	7.87	9.51	9.42	9.76	9.92	8.23	7.67	7.91	9.68	9.13	8.67	6.28
0.26	0.29	0.29	0.26	0.25	0.21	0.27	0.26	0.26	0.27	0.24	0.22	0.22	0.28	0.32	0.28	0.19
101.63	102.29	102.10	102.02	102.05	101.67	101.87	102.45	102.01	101.65	102.02	101.51	101.55	101.86	100.56	101.25	100.74
0.97	0.97	0.97	0.98	0.97	0.98	0.97	0.97	0.97	0.97	0.98	0.98	0.98	0.98	0.97	0.97	0.98
0.01	0.02	0.02	0.01	0.01	0.01	0.02	0.01	0.02	0.02	0.01	0.01	0.01	0.02	0.01	0.01	0.01
0.08	0.09	0.08	0.07	0.07	0.07	0.08	0.08	0.08	0.08	0.07	0.07	0.07	0.08	0.08	0.08	0.06
0.00	0.01	0.01	0.00	0.00	0.00	0.00	0.01	0.01	0.01	0.00	0.00	0.00	0.01	0.01	0.01	0.01
0.15	0.16	0.16	0.15	0.16	0.17	0.15	0.16	0.16	0.15	0.17	0.16	0.17	0.16	0.16	0.16	0.20
0.41	0.40	0.40	0.41	0.41	0.42	0.41	0.41	0.40	0.40	0.41	0.42	0.41	0.40	0.40	0.41	0.44
0.04	0.04	0.05	0.05	0.05	0.04	0.04	0.05	0.04	0.04	0.04	0.05	0.04	0.04	0.04	0.05	0.04
0.21	0.21	0.20	0.21	0.21	0.21	0.20	0.20	0.21	0.21	0.21	0.21	0.21	0.20	0.21	0.21	0.19
0.03	0.02	0.02	0.02	0.02	0.02	0.03	0.03	0.02	0.03	0.02	0.03	0.02	0.02	0.02	0.02	0.02
0.01	0.01	0.01	0.01	0.01	0.01	0.01	0.01	0.01	0.01	0.01	0.01	0.01	0.01	0.02	0.02	0.01
0.00	0.00	0.00	0.00	0.00	0.00	0.00	0.00	0.00	–	0.00	0.00	0.00	0.00	0.00	0.00	0.00
–	–	–	0.00	0.00	0.00	–	–	–	–	0.00	0.00	–	0.00	–	–	–
0.00	0.00	0.00	0.00	0.00	0.00	0.00	0.00	0.00	0.00	0.00	0.00	0.00	0.00	0.01	0.00	0.00
0.08	0.09	0.09	0.08	0.08	0.07	0.08	0.08	0.09	0.09	0.07	0.07	0.07	0.09	0.08	0.08	0.06
0.00	0.00	0.00	0.00	0.00	0.00	0.00	0.00	0.00	0.00	0.00	0.00	0.00	0.00	0.00	0.00	0.00
2.01	2.01	2.01	2.01	2.01	2.01	2.01	2.01	2.01	2.01	2.01	2.01	2.01	2.01	2.02	2.02	2.01
9.92	11.01	10.79	9.25	9.41	8.43	10.11	10.03	10.44	10.62	8.90	8.38	8.53	10.36	11.30	10.54	7.45
59.54	54.97	52.02	52.86	51.65	47.95	53.68	52.71	48.67	48.37	42.11	36.88	43.10	48.86	14.35	15.82	18.23
0.73	0.71	0.70	0.74	0.74	0.67	0.70	0.68	0.71	0.75	0.67	0.71	0.69	0.68	0.72	0.70	0.53
0.11	0.13	0.14	0.15	0.15	0.15	0.17	0.14	0.12	0.13	0.15	0.14	0.16	0.15	0.19	0.18	0.14
639	626	643	682	652	611	634	619	607	624	643	631	612	646	671	628	614
31	28	29	34	33	37	31	31	30	29	35	37	37	30	28	30	43

Table 5.16. Continued

5	6	7	10.1	10.2	10.3
30.33	29.87	30.10	29.66	29.81	29.24
0.09	0.20	0.16	0.22	0.16	0.40
1.12	0.72	1.08	1.66	0.94	2.07
1.84	0.97	1.43	1.19	2.25	0.15
12.29	15.51	14.14	13.14	12.04	11.25
29.22	32.26	30.53	28.98	29.55	28.08
3.01	2.96	2.90	2.98	3.12	3.27
14.53	12.65	13.27	12.89	14.16	13.53
2.10	1.69	1.89	1.56	1.68	1.66
1.54	1.04	1.33	1.02	1.48	0.89
0.38	0.26	0.31	0.30	0.69	0.14
–	0.02	0.06	–	–	–
0.31	0.51	0.36	0.67	0.64	0.39
3.88	2.98	4.12	7.37	4.17	10.35
0.11	0.13	0.13	0.26	0.20	0.27
100.86	101.88	101.95	102.04	100.99	101.72
0.99	0.98	0.99	0.98	0.98	0.97
0.00	0.01	0.01	0.01	0.01	0.02
0.05	0.03	0.04	0.07	0.04	0.09
0.04	0.02	0.03	0.02	0.05	0.00
0.18	0.22	0.20	0.19	0.17	0.16
0.41	0.46	0.43	0.41	0.42	0.40
0.04	0.04	0.04	0.04	0.04	0.05
0.20	0.18	0.18	0.18	0.20	0.19
0.03	0.02	0.03	0.02	0.02	0.02
0.02	0.01	0.02	0.01	0.02	0.01
0.00	0.00	0.00	0.00	0.01	0.00
–	0.00	0.00	–	–	–
0.00	0.00	0.00	0.01	0.01	0.00
0.03	0.03	0.04	0.07	0.04	0.09
0.00	0.00	0.00	0.00	0.00	0.00
2.01	2.01	2.01	2.01	2.01	2.01
4.80	4.60	5.21	9.40	6.20	11.35
14.19	6.27	12.78	12.44	7.09	35.02
0.62	0.43	0.49	0.51	0.61	0.63
0.25	0.19	0.23	0.18	0.24	0.15
565	669	612	661	758	564
66	71	61	34	53	28

Table 5.17. Chemical compositions of monazites in the sample AC07121801M from Austkampane area

Analyses No.	1.1	1.2	1.3	1.4	1.5	1.6	1.7	1.8	1.9	1.10	1.11	1.12	1.13	1.14	1.15	1.16
wt%																
P2O5	28.34	28.18	28.25	28.40	28.11	28.39	27.95	28.42	28.32	28.23	28.44	27.88	28.08	28.18	28.14	27.53
SiO2	0.42	0.49	0.43	0.41	0.46	0.40	0.45	0.39	0.46	0.40	0.44	0.55	0.58	0.58	0.57	0.90
CaO	1.83	1.87	1.84	1.81	1.77	1.79	1.76	1.76	1.77	1.73	1.77	1.83	1.83	1.84	1.83	1.62
Y2O3	0.31	0.28	0.29	0.30	0.28	0.28	0.27	0.30	0.25	0.30	0.26	0.27	0.26	0.26	0.26	0.19
La2O3	9.84	10.04	10.04	9.98	10.14	10.09	10.29	10.39	9.85	9.97	10.39	9.98	9.76	9.97	9.84	9.95
Ce2O3	27.04	27.83	27.20	27.65	27.86	28.06	27.69	27.44	27.81	27.91	27.75	27.41	26.95	27.29	27.33	27.28
Pr2O3	3.20	2.93	2.83	3.01	3.03	3.09	3.12	3.12	3.26	3.13	3.18	3.16	3.20	3.03	3.09	3.15
Nd2O3	15.71	15.56	15.83	16.13	15.40	15.96	15.11	15.99	15.59	15.78	15.83	16.01	15.83	15.76	15.33	15.84
Sm2O3	2.01	1.76	1.99	2.10	1.88	1.80	1.85	1.91	1.83	1.97	1.99	1.83	2.01	1.78	2.13	1.91
Gd2O3	0.94	0.87	0.89	1.18	0.90	0.96	0.88	1.01	0.93	0.91	1.03	0.96	1.04	0.83	0.79	0.88
Dy2O3	0.09	0.07	0.14	0.07	0.10	0.13	0.09	0.11	0.08	0.09	–	0.09	0.10	0.04	0.07	0.05
Er2O3	0.06	–	–	–	0.08	–	–	0.02	–	–	–	–	–	0.03	0.01	–
UO2	0.43	0.43	0.41	0.42	0.39	0.40	0.38	0.40	0.38	0.40	0.39	0.35	0.35	0.35	0.37	0.32
ThO2	9.97	10.17	9.86	9.71	9.72	9.44	9.73	9.45	9.73	9.43	9.61	10.28	10.55	10.51	10.47	11.17
PbO	0.28	0.28	0.28	0.27	0.26	0.26	0.28	0.27	0.27	0.27	0.28	0.27	0.29	0.29	0.29	0.30
Total	100.56	100.81	100.33	101.50	100.39	101.15	99.97	100.98	100.59	100.59	101.44	100.95	100.89	100.77	100.62	101.17
Cation (O=4)																
P	0.96	0.96	0.96	0.96	0.96	0.96	0.96	0.96	0.96	0.96	0.96	0.95	0.95	0.96	0.96	0.94
Si	0.02	0.02	0.02	0.02	0.02	0.02	0.02	0.02	0.02	0.02	0.02	0.02	0.02	0.02	0.02	0.04
Ca	0.08	0.08	0.08	0.08	0.08	0.08	0.08	0.08	0.08	0.07	0.08	0.08	0.08	0.08	0.08	0.07
Y	0.01	0.01	0.01	0.01	0.01	0.01	0.01	0.01	0.01	0.01	0.01	0.01	0.01	0.01	0.01	0.00
La	0.15	0.15	0.15	0.15	0.15	0.15	0.15	0.15	0.15	0.15	0.15	0.15	0.14	0.15	0.15	0.15
Ce	0.40	0.41	0.40	0.40	0.41	0.41	0.41	0.40	0.41	0.41	0.40	0.40	0.40	0.40	0.40	0.40
Pr	0.05	0.04	0.04	0.04	0.04	0.04	0.05	0.05	0.05	0.05	0.05	0.05	0.05	0.04	0.05	0.05
Nd	0.22	0.22	0.23	0.23	0.22	0.23	0.22	0.23	0.22	0.23	0.23	0.23	0.23	0.23	0.22	0.23
Sm	0.03	0.02	0.03	0.03	0.03	0.02	0.03	0.03	0.03	0.03	0.03	0.03	0.03	0.02	0.03	0.03
Gd	0.01	0.01	0.01	0.02	0.01	0.01	0.01	0.01	0.01	0.01	0.01	0.01	0.01	0.01	0.01	0.01
Dy	0.00	0.00	0.00	0.00	0.00	0.00	0.00	0.00	0.00	0.00	–	0.00	0.00	0.00	0.00	0.00
Er	0.00	–	–	–	0.00	–	–	0.00	–	–	–	–	–	0.00	0.00	–
U	0.00	0.00	0.00	0.00	0.00	0.00	0.00	0.00	0.00	0.00	0.00	0.00	0.00	0.00	0.00	0.00
Th	0.09	0.09	0.09	0.09	0.09	0.09	0.09	0.09	0.09	0.09	0.09	0.09	0.10	0.10	0.10	0.10
Pb	0.00	0.00	0.00	0.00	0.00	0.00	0.00	0.00	0.00	0.00	0.00	0.00	0.00	0.00	0.00	0.00
Total	2.02	2.02	2.02	2.02	2.02	2.02	2.02	2.02	2.02	2.02	2.02	2.02	2.02	2.02	2.02	2.02
ThO2*	11.12	11.30	10.94	10.83	10.74	10.51	10.74	10.50	10.74	10.48	10.64	11.16	11.42	11.38	11.39	11.93
Th/U	29.44	30.62	31.10	29.50	32.35	29.81	32.94	30.52	33.04	30.52	31.66	39.88	41.78	41.22	38.63	50.29
Nd/La	0.83	0.81	0.82	0.84	0.79	0.82	0.77	0.80	0.83	0.83	0.79	0.84	0.85	0.82	0.81	0.83
Gd/Nd	0.14	0.13	0.13	0.17	0.14	0.14	0.14	0.15	0.14	0.13	0.15	0.14	0.15	0.12	0.12	0.13
Age (Ma)	606	588	624	606	591	599	631	627	607	629	628	587	612	614	619	614
+/− (Ma)	28	28	29	29	29	30	29	30	29	30	30	28	27	28	28	26

−: below detection limit

Table 5.17. Continued

1.17	1.18	1.19	1.20	1.21	1.22	1.23	1.24	1.25	1.26	1.27	2.1	2.2	2.3	2.4	2.5	2.6
27.12	27.21	26.99	27.23	27.19	27.33	27.15	27.25	27.34	27.69	27.71	29.18	29.10	29.18	28.96	29.37	29.02
1.26	1.20	1.29	1.25	1.20	1.31	1.29	1.20	1.23	1.07	0.91	0.15	0.12	0.13	0.15	0.08	0.18
1.42	1.43	1.42	1.44	1.48	1.42	1.37	1.42	1.36	1.41	1.62	1.30	1.22	1.21	1.29	0.87	1.33
0.15	0.16	0.17	0.16	0.15	0.14	0.16	0.16	0.15	0.13	0.17	0.22	0.22	0.24	0.21	0.25	0.21
9.61	9.70	9.42	9.81	9.70	9.90	9.75	9.58	9.82	10.21	9.97	9.97	9.66	10.05	9.97	10.08	9.69
27.81	27.91	27.37	27.71	27.61	27.77	27.69	28.00	28.08	28.17	27.83	30.18	30.31	30.20	30.09	31.11	29.75
2.81	3.41	3.40	3.49	3.10	3.07	3.23	3.08	3.20	3.26	3.25	3.57	3.46	3.87	3.66	3.77	3.87
16.49	16.33	16.33	16.29	16.35	16.69	16.49	16.45	16.29	16.48	15.74	18.00	17.90	18.27	17.50	18.93	17.92
1.89	1.72	1.70	1.63	1.70	1.74	1.74	1.62	1.75	1.74	1.76	1.96	1.82	2.07	1.74	2.38	1.87
0.67	0.76	0.74	0.83	0.77	0.66	0.66	0.78	0.86	0.77	0.64	0.64	0.77	0.68	0.93	0.72	0.77
0.11	0.11	0.06	0.06	0.06	0.06	0.08	0.09	0.07	0.09	0.04	0.09	0.06	0.05	0.09	0.18	0.03
–	0.02	–	–	–	–	–	0.05	–	0.04	–	–	–	–	0.01	–	–
0.27	0.27	0.27	0.25	0.26	0.26	0.24	0.26	0.26	0.26	0.27	0.27	0.26	0.26	0.27	0.26	0.25
11.66	11.44	11.67	11.43	11.71	11.69	11.43	11.11	11.22	10.74	10.75	6.25	5.77	5.67	6.31	3.96	6.70
0.31	0.31	0.32	0.29	0.30	0.31	0.29	0.30	0.30	0.28	0.29	0.17	0.16	0.16	0.18	0.12	0.19
101.71	102.06	101.18	101.93	101.62	102.43	101.68	101.40	102.02	102.43	100.99	102.03	100.93	102.11	101.46	102.13	101.85
0.92	0.92	0.92	0.92	0.93	0.92	0.92	0.93	0.93	0.93	0.94	0.97	0.98	0.97	0.97	0.98	0.97
0.05	0.05	0.05	0.05	0.05	0.05	0.05	0.05	0.05	0.04	0.04	0.01	0.00	0.00	0.01	0.00	0.01
0.06	0.06	0.06	0.06	0.06	0.06	0.06	0.06	0.06	0.06	0.07	0.05	0.05	0.05	0.05	0.04	0.06
0.00	0.00	0.00	0.00	0.00	0.00	0.00	0.00	0.00	0.00	0.00	0.00	0.00	0.01	0.00	0.01	0.00
0.14	0.14	0.14	0.15	0.14	0.15	0.14	0.14	0.15	0.15	0.15	0.14	0.14	0.15	0.15	0.15	0.14
0.41	0.41	0.40	0.41	0.41	0.41	0.41	0.41	0.41	0.41	0.41	0.43	0.44	0.43	0.44	0.45	0.43
0.04	0.05	0.05	0.05	0.05	0.04	0.05	0.05	0.05	0.05	0.05	0.05	0.05	0.06	0.05	0.05	0.06
0.24	0.23	0.24	0.23	0.23	0.24	0.24	0.24	0.23	0.23	0.23	0.25	0.25	0.26	0.25	0.27	0.25
0.03	0.02	0.02	0.02	0.02	0.02	0.02	0.02	0.02	0.02	0.02	0.03	0.02	0.03	0.02	0.03	0.03
0.01	0.01	0.01	0.01	0.01	0.01	0.01	0.01	0.01	0.01	0.01	0.01	0.01	0.01	0.01	0.01	0.01
0.00	0.00	0.00	0.00	0.00	0.00	0.00	0.00	0.00	0.00	0.00	0.00	0.00	0.00	0.00	0.00	0.00
–	0.00	–	–	–	–	–	0.00	–	0.00	–	–	–	–	0.00	–	–
0.00	0.00	0.00	0.00	0.00	0.00	0.00	0.00	0.00	0.00	0.00	0.00	0.00	0.00	0.00	0.00	0.00
0.11	0.10	0.11	0.10	0.11	0.11	0.10	0.10	0.10	0.10	0.10	0.06	0.05	0.05	0.06	0.04	0.06
0.00	0.00	0.00	0.00	0.00	0.00	0.00	0.00	0.00	0.00	0.00	0.00	0.00	0.00	0.00	0.00	0.00
2.02	2.02	2.02	2.02	2.02	2.02	2.02	2.02	2.02	2.02	2.02	2.02	2.01	2.02	2.02	2.02	2.02
12.24	12.01	12.25	11.95	12.25	12.24	11.93	11.66	11.77	11.29	11.34	6.97	6.48	6.39	7.02	4.72	7.33
68.12	68.49	68.56	74.46	74.13	72.07	79.04	68.98	68.77	66.70	62.57	29.53	27.62	26.78	30.32	17.76	35.89
0.90	0.88	0.90	0.87	0.88	0.88	0.88	0.90	0.87	0.84	0.82	0.94	0.97	0.95	0.92	0.98	0.97
0.09	0.11	0.11	0.12	0.11	0.09	0.09	0.11	0.12	0.11	0.09	0.08	0.10	0.09	0.12	0.09	0.10
609	614	622	594	589	613	579	627	621	600	627	602	581	597	615	633	626
25	26	25	26	25	25	26	27	26	28	28	45	49	49	45	67	43

Table 5.17. Continued

2.7	2.8	2.9	2.10	2.11	2.12	2.13	2.14	2.15	2.16	2.17	2.18	2.19	2.20	2.21	2.22	2.23
28.95	29.03	29.30	28.82	29.16	28.87	28.15	28.10	28.43	28.77	28.51	28.38	28.36	28.49	28.37	29.13	28.19
0.21	0.17	0.16	0.20	0.18	0.16	0.38	0.66	0.41	0.25	0.42	0.39	0.53	0.39	0.34	0.26	0.42
1.38	1.35	1.32	1.36	1.30	1.31	1.52	1.30	1.83	1.68	1.82	1.95	1.86	1.98	1.90	1.69	1.94
0.20	0.20	0.20	0.19	0.21	0.21	0.33	2.47	0.29	0.66	0.31	0.47	0.28	0.47	0.56	0.66	0.34
10.02	9.48	10.20	9.58	9.86	9.76	10.34	9.19	9.78	10.26	9.90	9.89	9.90	9.80	9.83	10.09	9.65
30.21	29.81	29.68	30.09	30.20	29.73	28.10	25.83	27.38	27.38	27.99	26.88	27.80	26.42	26.65	27.27	27.51
3.54	3.66	3.32	3.61	3.90	3.80	3.23	3.21	3.30	3.17	3.14	2.90	3.16	3.10	3.29	3.24	3.16
17.98	18.09	17.89	18.04	18.17	17.66	15.37	14.78	15.75	15.88	15.92	15.27	16.25	15.59	15.41	15.80	15.84
1.95	1.92	2.08	1.95	2.00	1.99	1.95	2.47	2.05	2.24	2.19	2.18	2.03	2.12	2.02	2.21	2.01
0.55	0.66	0.74	0.70	0.70	0.87	1.14	2.57	0.95	1.24	1.07	1.32	1.19	1.43	1.37	1.42	0.97
0.07	–	0.12	0.13	0.02	–	0.18	0.75	0.10	0.25	0.10	0.19	0.13	0.26	0.13	0.19	0.12
–	–	–	–	0.06	–	0.01	0.00	–	0.05	–	–	–	0.05	–	0.02	0.07
0.27	0.24	0.27	0.25	0.26	0.26	0.38	0.35	0.40	0.53	0.41	0.50	0.37	0.50	0.53	0.56	0.43
6.80	6.62	6.37	6.77	6.55	6.47	9.37	8.43	9.83	8.23	9.92	10.35	10.31	10.18	9.69	8.34	9.85
0.19	0.20	0.19	0.20	0.19	0.19	0.26	0.20	0.28	0.24	0.28	0.30	0.29	0.28	0.28	0.26	0.28
102.39	101.54	101.89	101.97	102.84	101.38	100.77	100.36	100.86	100.89	102.03	101.03	102.55	101.11	100.41	101.20	100.86
0.97	0.97	0.97	0.97	0.97	0.97	0.96	0.95	0.96	0.97	0.96	0.96	0.95	0.96	0.96	0.97	0.96
0.01	0.01	0.01	0.01	0.01	0.01	0.02	0.03	0.02	0.01	0.02	0.02	0.02	0.02	0.01	0.01	0.02
0.06	0.06	0.06	0.06	0.05	0.06	0.07	0.06	0.08	0.07	0.08	0.08	0.08	0.08	0.08	0.07	0.08
0.00	0.00	0.00	0.00	0.00	0.00	0.01	0.05	0.01	0.01	0.01	0.01	0.01	0.01	0.01	0.01	0.01
0.15	0.14	0.15	0.14	0.14	0.14	0.15	0.14	0.14	0.15	0.14	0.15	0.14	0.14	0.15	0.15	0.14
0.44	0.43	0.43	0.44	0.43	0.43	0.41	0.38	0.40	0.40	0.41	0.39	0.40	0.39	0.39	0.39	0.40
0.05	0.05	0.05	0.05	0.06	0.05	0.05	0.05	0.05	0.05	0.05	0.04	0.05	0.04	0.05	0.05	0.05
0.25	0.26	0.25	0.25	0.25	0.25	0.22	0.21	0.22	0.23	0.23	0.22	0.23	0.22	0.22	0.22	0.23
0.03	0.03	0.03	0.03	0.03	0.03	0.03	0.03	0.03	0.03	0.03	0.03	0.03	0.03	0.03	0.03	0.03
0.01	0.01	0.01	0.01	0.01	0.01	0.02	0.03	0.01	0.02	0.01	0.02	0.02	0.02	0.02	0.02	0.01
0.00	–	0.00	0.00	0.00	–	0.00	0.01	0.00	0.00	0.00	0.00	0.00	0.00	0.00	0.00	0.00
–	–	–	–	0.00	–	0.00	0.00	–	0.00	–	–	–	0.00	–	0.00	0.00
0.00	0.00	0.00	0.00	0.00	0.00	0.00	0.00	0.00	0.00	0.00	0.00	0.00	0.00	0.00	0.00	0.00
0.06	0.06	0.06	0.06	0.06	0.06	0.09	0.08	0.09	0.07	0.09	0.09	0.09	0.09	0.09	0.07	0.09
0.00	0.00	0.00	0.00	0.00	0.00	0.00	0.00	0.00	0.00	0.00	0.00	0.00	0.00	0.00	0.00	0.00
2.02	2.02	2.01	2.02	2.02	2.02	2.02	2.02	2.02	2.02	2.02	2.02	2.02	2.02	2.02	2.01	2.02
7.50	7.25	7.09	7.42	7.23	7.14	10.39	9.36	10.89	9.77	11.01	11.73	11.27	11.57	11.20	9.98	11.01
32.96	35.94	30.39	35.28	33.02	32.95	31.39	30.65	31.69	18.23	30.96	25.49	36.83	24.88	21.89	17.34	28.84
0.94	1.00	0.91	0.98	0.96	0.94	0.78	0.84	0.84	0.81	0.84	0.81	0.86	0.83	0.82	0.82	0.86
0.07	0.08	0.10	0.09	0.09	0.11	0.17	0.41	0.14	0.18	0.16	0.20	0.17	0.21	0.21	0.21	0.14
596	662	630	650	624	656	607	512	629	596	609	607	619	590	605	620	614
42	43	44	42	43	44	30	33	29	32	29	27	28	27	28	32	29

Table 5.17. Continued

2.24	2.25	2.26	2.27	2.28	2.29	2.30	2.31	2.32	3.2	3.4	3.5	3.6	3.7	3.8	3.9	3.10
28.82	28.68	27.70	27.76	27.13	28.48	28.67	27.91	27.43	28.65	29.26	29.11	28.54	29.08	27.22	26.73	27.05
0.24	0.38	1.01	0.85	1.21	0.26	0.16	0.91	0.91	0.02	0.02	0.03	0.04	0.02	1.11	1.12	1.11
1.69	1.74	1.37	1.56	1.35	1.97	1.47	1.66	1.63	0.47	0.50	0.52	0.37	0.54	1.47	1.43	1.45
0.63	0.31	0.17	0.19	0.17	0.74	0.79	0.18	0.19	0.98	0.88	0.82	0.74	0.60	0.15	0.17	0.18
10.29	10.56	10.00	10.41	9.38	9.77	10.51	9.64	9.69	14.53	14.85	14.78	13.35	14.32	9.81	9.62	9.54
27.14	28.25	28.43	28.11	27.51	26.06	26.94	27.24	27.35	31.51	32.54	31.71	31.18	31.73	26.96	27.23	26.92
3.30	3.28	3.22	3.37	3.41	3.22	3.18	3.03	3.22	3.06	2.99	3.47	3.05	3.43	3.24	3.07	3.11
15.99	15.96	15.96	16.39	16.27	14.90	15.83	16.22	15.99	14.90	14.74	14.59	15.51	15.68	16.23	15.90	15.88
2.08	2.12	1.75	2.11	1.86	2.10	2.44	1.99	2.08	1.72	1.57	1.75	1.70	1.89	1.76	1.68	1.74
1.53	1.09	0.83	0.79	0.67	1.76	1.54	0.94	0.87	1.26	1.05	1.03	1.30	1.04	0.83	0.72	0.75
0.18	–	0.06	0.08	0.10	0.36	0.28	–	0.02	0.28	0.23	0.26	0.33	0.22	0.09	0.06	0.06
–	–	0.03	–	0.11	–	–	0.01	0.08	0.06	0.07	–	–	0.00	0.00	0.04	–
0.53	0.41	0.25	0.28	0.28	0.65	0.66	0.32	0.28	0.45	0.53	0.54	0.60	0.61	0.27	0.29	0.27
8.19	9.41	10.54	10.57	11.46	9.59	6.66	11.35	11.09	1.65	1.45	1.65	1.97	1.94	11.19	11.21	11.10
0.24	0.27	0.28	0.28	0.30	0.28	0.23	0.30	0.29	0.10	0.10	0.11	0.11	0.10	0.30	0.29	0.29
100.91	102.51	101.70	102.81	101.31	100.19	99.41	101.79	101.17	99.73	100.87	100.50	98.83	101.28	100.72	99.61	99.51
0.97	0.96	0.94	0.93	0.93	0.97	0.98	0.94	0.94	0.97	0.98	0.98	0.98	0.97	0.93	0.93	0.94
0.01	0.02	0.04	0.03	0.05	0.01	0.01	0.04	0.04	0.00	0.00	0.00	0.00	0.00	0.04	0.05	0.05
0.07	0.07	0.06	0.07	0.06	0.08	0.06	0.07	0.07	0.02	0.02	0.02	0.02	0.02	0.06	0.06	0.06
0.01	0.01	0.00	0.00	0.00	0.02	0.02	0.00	0.00	0.02	0.02	0.02	0.02	0.01	0.00	0.00	0.00
0.15	0.15	0.15	0.15	0.14	0.14	0.16	0.14	0.14	0.22	0.22	0.22	0.20	0.21	0.15	0.15	0.14
0.39	0.41	0.42	0.41	0.41	0.38	0.40	0.40	0.40	0.46	0.47	0.46	0.46	0.46	0.40	0.41	0.40
0.05	0.05	0.05	0.05	0.05	0.05	0.05	0.04	0.05	0.04	0.04	0.05	0.04	0.05	0.05	0.05	0.05
0.23	0.22	0.23	0.23	0.23	0.21	0.23	0.23	0.23	0.21	0.21	0.21	0.22	0.22	0.23	0.23	0.23
0.03	0.03	0.02	0.03	0.03	0.03	0.03	0.03	0.03	0.02	0.02	0.02	0.02	0.03	0.02	0.02	0.02
0.02	0.01	0.01	0.01	0.01	0.02	0.02	0.01	0.01	0.02	0.01	0.01	0.02	0.01	0.01	0.01	0.01
0.00	–	0.00	0.00	0.00	0.00	0.00	–	0.00	0.00	0.00	0.00	0.00	0.00	0.00	0.00	0.00
–	–	0.00	–	0.00	–	–	0.00	0.00	0.00	0.00	–	–	0.00	0.00	0.00	–
0.00	0.00	0.00	0.00	0.00	0.01	0.01	0.00	0.00	0.00	0.00	0.00	0.01	0.01	0.00	0.00	0.00
0.07	0.08	0.10	0.10	0.11	0.09	0.06	0.10	0.10	0.02	0.01	0.01	0.02	0.02	0.10	0.10	0.10
0.00	0.00	0.00	0.00	0.00	0.00	0.00	0.00	0.00	0.00	0.00	0.00	0.00	0.00	0.00	0.00	0.00
2.02	2.02	2.02	2.02	2.02	2.02	2.01	2.02	2.02	2.02	2.02	2.02	2.01	2.02	2.02	2.02	2.02
9.74	10.52	11.07	11.21	12.07	11.48	8.69	12.09	11.72	3.13	3.19	3.42	3.92	3.93	11.77	11.87	11.69
17.99	29.00	67.63	56.20	63.76	17.25	11.20	51.87	60.07	3.83	2.89	3.19	3.44	3.32	65.38	57.68	64.60
0.81	0.79	0.83	0.82	0.90	0.80	0.79	0.88	0.86	0.53	0.52	0.51	0.61	0.57	0.86	0.86	0.87
0.22	0.16	0.12	0.11	0.10	0.27	0.23	0.13	0.13	0.20	0.17	0.16	0.19	0.15	0.12	0.10	0.11
603	608	605	602	600	593	621	606	589	759	750	727	635	603	617	595	603
33	30	28	28	26	28	37	26	27	108	107	99	86	85	26	26	27

Table 5.17. Continued

3.11	3.12	3.13	3.14	3.15	3.16	3.17	3.18	3.19	3.20	3.21	3.22	3.23	3.24	3.25	3.26	3.27
26.81	27.14	27.37	28.78	28.65	28.19	28.52	28.76	28.97	28.48	28.75	28.18	27.97	27.55	27.08	27.51	26.54
1.12	1.15	1.19	0.19	0.20	0.20	0.23	0.26	0.16	0.21	0.27	0.26	0.36	0.51	0.72	0.70	1.13
1.40	1.44	1.42	1.49	1.50	1.56	1.52	1.67	1.19	1.32	1.52	1.81	1.78	1.67	1.61	1.57	1.43
0.17	0.19	0.17	1.46	0.84	0.82	0.71	1.27	0.86	1.14	0.86	1.11	1.13	0.95	0.63	0.58	0.22
9.59	9.53	9.67	10.02	10.23	10.41	10.53	9.71	11.43	10.80	10.72	9.88	9.71	9.62	9.74	9.65	9.77
27.32	27.56	27.01	25.80	27.62	27.42	27.27	26.15	28.35	28.21	28.03	25.82	25.79	26.16	26.37	26.93	26.75
3.13	3.18	3.15	2.72	2.93	3.09	3.08	2.91	3.26	3.22	2.89	2.52	2.90	2.89	3.06	2.90	3.19
15.78	15.76	15.72	14.52	15.29	14.92	15.50	15.07	15.69	15.12	15.21	14.39	14.79	14.75	15.02	15.31	16.06
1.83	1.80	1.55	2.55	2.34	2.14	2.12	2.37	2.31	2.29	1.96	2.15	2.26	1.84	2.04	1.90	1.72
0.61	0.79	0.91	2.66	1.52	1.64	1.59	2.05	1.72	1.91	1.52	1.89	1.76	1.34	1.14	1.13	0.58
0.08	0.08	0.08	0.47	0.29	0.23	0.19	0.35	0.31	0.41	0.28	0.51	0.39	0.34	0.19	0.14	0.10
–	–	–	0.02	0.01	–	–	–	0.00	–	–	–	0.04	–	0.00	0.02	0.06
0.26	0.26	0.26	0.49	0.64	0.66	0.52	0.73	0.55	0.60	0.61	0.50	0.44	0.44	0.43	0.41	0.27
11.13	11.15	11.33	7.30	7.13	7.51	7.66	7.92	5.74	6.44	7.40	9.23	9.42	9.72	10.32	10.00	11.39
0.30	0.30	0.29	0.21	0.24	0.23	0.25	0.27	0.18	0.20	0.23	0.26	0.26	0.27	0.30	0.28	0.30
99.64	100.39	100.21	98.71	99.52	99.06	99.81	99.63	100.81	100.39	100.30	98.62	99.05	98.15	98.72	99.07	99.60
0.93	0.93	0.94	0.98	0.97	0.97	0.97	0.97	0.97	0.97	0.97	0.97	0.96	0.96	0.94	0.95	0.93
0.05	0.05	0.05	0.01	0.01	0.01	0.01	0.01	0.01	0.01	0.01	0.01	0.01	0.02	0.03	0.03	0.05
0.06	0.06	0.06	0.06	0.06	0.07	0.07	0.07	0.05	0.06	0.07	0.08	0.08	0.07	0.07	0.07	0.06
0.00	0.00	0.00	0.03	0.02	0.02	0.02	0.03	0.02	0.02	0.02	0.02	0.02	0.02	0.01	0.01	0.00
0.14	0.14	0.14	0.15	0.15	0.16	0.16	0.14	0.17	0.16	0.16	0.15	0.15	0.15	0.15	0.15	0.15
0.41	0.41	0.40	0.38	0.41	0.41	0.40	0.38	0.41	0.41	0.41	0.38	0.38	0.39	0.40	0.40	0.40
0.05	0.05	0.05	0.04	0.04	0.05	0.05	0.04	0.05	0.05	0.04	0.04	0.04	0.04	0.05	0.04	0.05
0.23	0.23	0.23	0.21	0.22	0.22	0.22	0.22	0.22	0.22	0.22	0.21	0.21	0.22	0.22	0.22	0.24
0.03	0.03	0.02	0.04	0.03	0.03	0.03	0.03	0.03	0.03	0.03	0.03	0.03	0.03	0.03	0.03	0.02
0.01	0.01	0.01	0.04	0.02	0.02	0.02	0.03	0.02	0.03	0.02	0.03	0.02	0.02	0.02	0.02	0.01
0.00	0.00	0.00	0.01	0.00	0.00	0.00	0.00	0.00	0.01	0.00	0.01	0.01	0.00	0.00	0.00	0.00
–	–	–	0.00	0.00	–	–	–	0.00	–	–	–	0.00	–	0.00	0.00	0.00
0.00	0.00	0.00	0.00	0.01	0.01	0.00	0.01	0.00	0.00	0.00	0.00	0.00	0.00	0.00	0.00	0.00
0.10	0.10	0.10	0.07	0.07	0.07	0.07	0.07	0.05	0.06	0.07	0.09	0.09	0.09	0.10	0.09	0.11
0.00	0.00	0.00	0.00	0.00	0.00	0.00	0.00	0.00	0.00	0.00	0.00	0.00	0.00	0.00	0.00	0.00
2.02	2.02	2.01	2.01	2.01	2.02	2.01	2.01	2.01	2.02	2.01	2.01	2.02	2.02	2.02	2.02	2.02
11.69	11.71	11.88	8.73	9.06	9.49	9.19	10.14	7.42	8.26	9.21	10.64	10.61	10.91	11.47	11.09	11.96
67.50	67.76	70.31	17.38	12.64	12.89	17.11	12.15	11.60	12.00	13.89	22.30	26.84	27.99	30.75	31.48	67.59
0.86	0.86	0.85	0.76	0.78	0.75	0.77	0.81	0.72	0.73	0.74	0.76	0.79	0.80	0.80	0.83	0.86
0.09	0.12	0.14	0.43	0.23	0.26	0.24	0.32	0.25	0.29	0.23	0.31	0.28	0.21	0.18	0.17	0.08
619	610	599	585	631	587	665	627	582	575	587	580	591	595	621	601	603
27	27	26	36	35	34	35	32	43	39	35	30	30	29	27	28	26

Table 5.17. Continued

4.1	4.2	4.3	4.4	4.5	4.6	4.7	4.8	4.9	4.10	4.11	4.12	4.13	4.14	4.15	4.16	4.17
29.08	28.95	29.12	29.02	28.23	29.19	29.04	28.89	28.15	28.99	28.85	28.44	28.87	29.11	27.14	27.00	27.82
0.11	0.09	0.09	0.10	0.41	0.10	0.09	0.09	0.50	0.08	0.26	0.27	0.26	0.31	1.08	1.06	0.76
1.01	0.96	0.95	1.00	1.01	0.99	0.99	0.99	1.08	0.89	1.03	1.04	1.04	1.08	1.06	1.07	1.07
0.38	0.31	0.36	0.40	2.13	0.20	0.20	0.23	0.12	0.39	0.20	0.19	0.19	0.17	0.07	0.08	0.09
11.22	12.12	12.05	12.01	10.33	9.66	9.93	9.52	11.55	12.21	12.01	11.54	11.87	11.87	11.39	11.63	11.68
31.78	32.04	31.64	31.47	27.91	30.71	29.04	30.09	30.40	32.37	31.27	30.98	31.22	31.80	29.84	29.75	30.19
3.22	3.47	3.60	3.58	3.15	3.60	3.94	3.66	3.21	3.33	3.34	3.30	3.27	3.44	3.11	3.34	3.17
15.38	15.00	15.88	15.27	15.23	19.71	19.22	19.30	15.89	15.70	15.23	15.42	15.40	16.16	15.67	15.62	15.53
1.93	1.84	2.01	1.92	2.03	2.17	2.12	2.20	1.73	2.01	1.85	1.84	1.54	1.85	1.54	1.44	1.64
1.03	0.99	1.04	1.11	1.78	0.85	1.04	0.92	0.66	0.88	0.86	0.70	0.79	0.81	0.67	0.47	0.66
0.09	0.09	0.18	0.18	0.56	–	0.05	0.15	–	0.05	0.06	0.04	0.12	0.15	–	0.06	0.08
–	–	–	0.08	–	–	–	0.03	–	0.00	–	0.02	–	0.03	0.07	–	0.08
0.46	0.42	0.51	0.54	0.37	0.24	0.25	0.27	0.24	0.53	0.29	0.28	0.28	0.26	0.20	0.23	0.23
4.23	4.31	4.01	4.33	5.93	4.64	4.55	4.70	6.86	3.74	5.51	5.51	5.57	5.78	9.14	9.05	7.85
0.15	0.14	0.15	0.16	0.14	0.14	0.13	0.12	0.18	0.15	0.15	0.16	0.16	0.16	0.26	0.23	0.22
100.10	100.85	101.63	101.25	99.25	102.29	100.68	101.29	100.59	101.38	100.99	99.85	100.63	103.01	101.27	101.10	101.11
0.98	0.97	0.97	0.97	0.96	0.97	0.98	0.97	0.96	0.97	0.97	0.97	0.97	0.96	0.93	0.93	0.95
0.00	0.00	0.00	0.00	0.02	0.00	0.00	0.00	0.02	0.00	0.01	0.01	0.01	0.01	0.04	0.04	0.03
0.04	0.04	0.04	0.04	0.04	0.04	0.04	0.04	0.05	0.04	0.04	0.04	0.04	0.05	0.05	0.05	0.05
0.01	0.01	0.01	0.01	0.05	0.00	0.00	0.00	0.00	0.01	0.00	0.00	0.00	0.00	0.00	0.00	0.00
0.16	0.18	0.18	0.18	0.15	0.14	0.15	0.14	0.17	0.18	0.18	0.17	0.17	0.17	0.17	0.17	0.17
0.46	0.47	0.46	0.46	0.41	0.44	0.42	0.44	0.45	0.47	0.45	0.46	0.45	0.46	0.44	0.44	0.44
0.05	0.05	0.05	0.05	0.05	0.05	0.06	0.05	0.05	0.05	0.05	0.05	0.05	0.05	0.05	0.05	0.05
0.22	0.21	0.22	0.22	0.22	0.28	0.27	0.27	0.23	0.22	0.22	0.22	0.22	0.23	0.23	0.23	0.22
0.03	0.03	0.03	0.03	0.03	0.03	0.03	0.03	0.02	0.03	0.03	0.03	0.02	0.02	0.02	0.02	0.02
0.01	0.01	0.01	0.01	0.02	0.01	0.01	0.01	0.01	0.01	0.01	0.01	0.01	0.01	0.01	0.01	0.01
0.00	0.00	0.00	0.00	0.01	–	0.00	0.00	–	0.00	0.00	0.00	0.00	0.00	–	0.00	0.00
–	–	–	0.00	–	–	–	0.00	–	0.00	–	0.00	–	0.00	0.00	–	0.00
0.00	0.00	0.00	0.00	0.00	0.00	0.00	0.00	0.00	0.00	0.00	0.00	0.00	0.00	0.00	0.00	0.00
0.04	0.04	0.04	0.04	0.05	0.04	0.04	0.04	0.06	0.03	0.05	0.05	0.05	0.05	0.08	0.08	0.07
0.00	0.00	0.00	0.00	0.00	0.00	0.00	0.00	0.00	0.00	0.00	0.00	0.00	0.00	0.00	0.00	0.00
2.01	2.02	2.02	2.02	2.02	2.02	2.01	2.02	2.02	2.02	2.01	2.02	2.01	2.02	2.02	2.02	2.02
5.64	5.60	5.59	6.03	6.98	5.32	5.25	5.47	7.46	5.40	6.32	6.29	6.36	6.47	9.56	9.56	8.39
10.21	11.36	8.66	8.73	18.92	23.40	21.96	20.75	39.12	7.66	22.92	23.99	24.12	28.47	73.46	60.50	48.91
0.71	0.65	0.69	0.66	0.77	1.06	1.01	1.06	0.72	0.67	0.66	0.70	0.68	0.71	0.72	0.70	0.69
0.16	0.15	0.15	0.17	0.27	0.10	0.13	0.11	0.10	0.13	0.13	0.11	0.12	0.12	0.10	0.07	0.10
616	612	621	643	487	616	615	547	568	642	561	628	599	601	645	592	619
57	57	58	54	45	59	60	58	42	60	50	50	50	49	33	33	37

Table 5.17. Continued

4.18	4.19	4.20	4.21	4.22	4.23	4.24	4.25	4.26	4.27	4.28	4.29	4.30	4.31	4.32	4.33	4.34
29.02	29.03	29.10	29.00	29.21	28.81	29.24	28.85	28.88	28.69	28.25	27.67	28.40	28.17	27.72	28.67	27.96
0.10	0.07	0.08	0.09	0.08	0.14	0.08	0.09	0.11	0.16	0.45	0.61	0.42	0.43	0.53	0.20	0.48
1.06	0.99	0.95	1.00	0.98	1.08	1.03	1.03	0.96	1.06	1.75	1.76	1.76	1.77	1.76	1.50	1.78
0.21	0.32	0.41	0.37	0.37	0.57	0.38	0.34	0.22	0.20	0.28	0.25	0.37	0.29	0.27	0.66	0.27
9.85	12.13	11.40	11.67	11.81	11.19	11.40	11.48	10.05	10.40	9.94	10.03	9.75	10.12	9.99	10.50	10.07
30.06	31.48	30.99	31.43	31.06	30.00	31.42	31.00	30.18	29.48	26.98	26.97	27.08	27.46	27.25	27.96	27.25
3.98	3.56	3.53	3.21	3.39	3.43	3.44	3.38	3.51	3.78	3.05	3.11	2.95	3.32	3.15	3.44	3.01
19.07	15.59	15.57	15.79	15.63	16.38	15.69	15.71	18.96	17.28	16.06	15.52	15.65	16.15	15.53	16.06	15.93
2.00	1.60	1.97	2.22	2.24	2.09	1.88	2.21	2.12	2.06	1.97	2.00	2.19	2.07	1.97	2.18	1.92
0.78	0.84	0.97	1.07	1.11	1.18	0.87	0.93	0.89	0.81	1.08	1.03	1.09	0.97	0.87	1.50	0.93
0.07	0.11	0.15	0.12	0.18	0.14	0.08	0.12	0.09	0.07	0.10	0.06	0.18	0.06	0.14	0.15	0.08
–	–	–	–	–	0.03	0.00	–	–	–	–	0.01	–	–	–	–	0.04
0.25	0.46	0.47	0.48	0.51	0.52	0.50	0.48	0.24	0.26	0.39	0.35	0.44	0.38	0.38	0.52	0.40
4.84	4.22	4.22	4.50	4.51	5.31	4.51	4.56	4.72	5.94	9.62	10.46	9.43	9.59	10.21	7.22	10.00
0.14	0.14	0.13	0.14	0.15	0.16	0.15	0.17	0.14	0.17	0.27	0.29	0.27	0.27	0.29	0.21	0.28
101.47	100.61	100.01	101.18	101.32	101.08	100.77	100.45	101.13	100.46	100.26	100.21	100.04	101.10	100.14	100.88	100.45
0.97	0.98	0.98	0.97	0.98	0.97	0.98	0.97	0.97	0.97	0.96	0.95	0.96	0.95	0.95	0.97	0.95
0.00	0.00	0.00	0.00	0.00	0.01	0.00	0.00	0.00	0.01	0.02	0.02	0.02	0.02	0.02	0.01	0.02
0.04	0.04	0.04	0.04	0.04	0.05	0.04	0.04	0.04	0.05	0.08	0.08	0.08	0.08	0.08	0.06	0.08
0.00	0.01	0.01	0.01	0.01	0.01	0.01	0.01	0.00	0.00	0.01	0.01	0.01	0.01	0.01	0.01	0.01
0.14	0.18	0.17	0.17	0.17	0.16	0.17	0.17	0.15	0.15	0.15	0.15	0.14	0.15	0.15	0.15	0.15
0.44	0.46	0.45	0.46	0.45	0.44	0.46	0.45	0.44	0.43	0.40	0.40	0.40	0.40	0.40	0.41	0.40
0.06	0.05	0.05	0.05	0.05	0.05	0.05	0.05	0.05	0.06	0.04	0.05	0.04	0.05	0.05	0.05	0.04
0.27	0.22	0.22	0.22	0.22	0.23	0.22	0.22	0.27	0.25	0.23	0.22	0.22	0.23	0.22	0.23	0.23
0.03	0.02	0.03	0.03	0.03	0.03	0.03	0.03	0.03	0.03	0.03	0.03	0.03	0.03	0.03	0.03	0.03
0.01	0.01	0.01	0.01	0.01	0.02	0.01	0.01	0.01	0.01	0.01	0.01	0.01	0.01	0.01	0.02	0.01
0.00	0.00	0.00	0.00	0.00	0.00	0.00	0.00	0.00	0.00	0.00	0.00	0.00	0.00	0.00	0.00	0.00
–	–	–	–	–	0.00	0.00	–	–	–	–	0.00	–	–	–	–	0.00
0.00	0.00	0.00	0.00	0.00	0.00	0.00	0.00	0.00	0.00	0.00	0.00	0.00	0.00	0.00	0.00	0.00
0.04	0.04	0.04	0.04	0.04	0.05	0.04	0.04	0.04	0.05	0.09	0.10	0.09	0.09	0.09	0.07	0.09
0.00	0.00	0.00	0.00	0.00	0.00	0.00	0.00	0.00	0.00	0.00	0.00	0.00	0.00	0.00	0.00	0.00
2.02	2.02	2.01	2.02	2.01	2.02	2.01	2.02	2.02	2.01	2.02	2.02	2.01	2.02	2.02	2.02	2.02
5.52	5.62	5.66	5.95	6.10	6.89	6.05	6.04	5.37	6.64	10.66	11.31	10.65	10.58	11.18	8.74	11.07
23.97	10.27	9.99	10.52	9.69	11.37	10.00	10.55	24.69	28.77	31.53	41.58	26.44	32.85	36.10	16.11	31.96
1.01	0.67	0.71	0.71	0.69	0.76	0.72	0.71	0.98	0.87	0.84	0.81	0.84	0.83	0.81	0.80	0.82
0.09	0.13	0.14	0.16	0.17	0.17	0.13	0.14	0.11	0.11	0.16	0.15	0.16	0.14	0.13	0.22	0.14
628	580	563	544	601	560	610	667	607	610	618	621	621	614	627	586	613
57	57	57	54	53	46	53	53	59	47	29	28	30	30	28	36	28

Table 5.17. Continued

4.35	4.36	4.37	4.38	4.39	4.40	4.41	4.42	4.43	4.44	4.45	5.1	5.2	5.3	5.4	5.5	5.6
28.00	28.55	27.99	27.83	28.05	27.82	28.75	27.98	28.14	28.61	28.44	29.10	28.67	28.61	28.57	28.54	28.90
0.46	0.19	0.45	0.47	0.35	0.36	0.22	0.42	0.49	0.23	0.44	0.12	0.11	0.09	0.08	0.10	0.10
1.78	1.49	1.85	1.76	1.84	1.80	1.52	1.82	1.83	1.47	1.59	0.85	0.79	0.71	0.81	0.82	0.87
0.27	1.47	0.29	0.28	0.63	0.53	0.82	0.33	0.28	1.34	0.65	0.30	0.28	0.30	0.30	0.27	0.23
10.15	9.77	10.24	10.24	9.64	9.80	10.33	10.13	10.12	9.77	9.78	13.12	12.58	13.34	12.53	12.70	12.88
27.35	26.39	27.04	27.15	26.59	26.92	27.91	26.96	26.86	26.96	27.34	30.30	31.51	31.23	30.89	31.23	31.02
3.21	2.94	3.09	3.26	3.10	3.13	3.00	2.97	3.00	3.28	3.36	3.40	3.40	3.50	3.41	3.24	3.29
15.42	15.94	15.30	15.37	15.15	15.30	15.71	15.60	15.97	15.65	15.70	15.82	15.57	15.37	15.28	15.61	15.58
1.87	2.50	1.95	1.82	2.08	2.03	2.31	1.94	2.09	2.49	2.16	2.02	2.15	1.96	2.08	2.09	2.30
0.96	2.09	1.16	0.83	1.26	1.19	1.37	1.02	0.89	1.84	1.54	1.14	1.20	1.22	1.47	1.07	1.26
0.12	0.44	–	0.09	0.14	0.07	0.27	0.08	0.08	0.33	0.21	–	0.05	0.07	0.12	0.07	0.09
–	0.00	–	0.00	–	–	0.03	–	0.02	–	0.02	0.06	0.07	–	0.02	0.01	–
0.40	0.85	0.44	0.43	0.52	0.50	0.56	0.41	0.40	0.87	0.51	0.50	0.50	0.50	0.58	0.48	0.47
9.65	6.50	10.14	10.07	9.82	9.58	7.37	10.02	10.05	6.87	9.64	3.59	3.39	3.19	3.48	3.64	3.96
0.28	0.24	0.29	0.28	0.26	0.26	0.23	0.28	0.28	0.25	0.29	0.14	0.13	0.13	0.14	0.14	0.15
99.99	99.44	100.30	99.97	99.49	99.33	100.45	100.00	100.57	100.03	101.72	100.54	100.43	100.28	99.77	100.08	101.19
0.96	0.97	0.96	0.95	0.96	0.96	0.97	0.96	0.96	0.97	0.96	0.98	0.97	0.97	0.97	0.97	0.97
0.02	0.01	0.02	0.02	0.01	0.01	0.01	0.02	0.02	0.01	0.02	0.00	0.00	0.00	0.00	0.00	0.00
0.08	0.06	0.08	0.08	0.08	0.08	0.07	0.08	0.08	0.06	0.07	0.04	0.03	0.03	0.03	0.04	0.04
0.01	0.03	0.01	0.01	0.01	0.01	0.02	0.01	0.01	0.03	0.01	0.01	0.01	0.01	0.01	0.01	0.00
0.15	0.14	0.15	0.15	0.14	0.15	0.15	0.15	0.15	0.14	0.14	0.19	0.19	0.20	0.19	0.19	0.19
0.40	0.39	0.40	0.40	0.39	0.40	0.41	0.40	0.39	0.39	0.40	0.44	0.46	0.46	0.46	0.46	0.45
0.05	0.04	0.05	0.05	0.05	0.05	0.04	0.04	0.04	0.05	0.05	0.05	0.05	0.05	0.05	0.05	0.05
0.22	0.23	0.22	0.22	0.22	0.22	0.22	0.23	0.23	0.22	0.22	0.22	0.22	0.22	0.22	0.22	0.22
0.03	0.03	0.03	0.03	0.03	0.03	0.03	0.03	0.03	0.03	0.03	0.03	0.03	0.03	0.03	0.03	0.03
0.01	0.03	0.02	0.01	0.02	0.02	0.02	0.01	0.01	0.02	0.02	0.01	0.02	0.02	0.02	0.01	0.02
0.00	0.01	–	0.00	0.00	0.00	0.00	0.00	0.00	0.00	0.00	–	0.00	0.00	0.00	0.00	0.00
–	0.00	–	0.00	–	–	0.00	–	0.00	–	0.00	0.00	0.00	–	0.00	0.00	–
0.00	0.01	0.00	0.00	0.00	0.00	0.00	0.00	0.00	0.01	0.00	0.00	0.00	0.00	0.00	0.00	0.00
0.09	0.06	0.09	0.09	0.09	0.09	0.07	0.09	0.09	0.06	0.09	0.03	0.03	0.03	0.03	0.03	0.04
0.00	0.00	0.00	0.00	0.00	0.00	0.00	0.00	0.00	0.00	0.00	0.00	0.00	0.00	0.00	0.00	0.00
2.02	2.02	2.02	2.02	2.02	2.02	2.02	2.02	2.02	2.02	2.02	2.01	2.02	2.02	2.02	2.02	2.02
10.71	9.16	11.31	11.21	11.26	10.98	9.04	11.11	11.09	9.57	11.07	5.17	4.96	4.76	5.31	5.15	5.43
31.35	8.34	29.48	30.18	23.23	23.18	15.07	31.47	32.87	8.67	23.03	7.76	7.40	6.93	6.49	8.20	9.18
0.79	0.85	0.78	0.78	0.82	0.81	0.79	0.80	0.82	0.84	0.84	0.63	0.65	0.60	0.64	0.64	0.63
0.15	0.31	0.18	0.13	0.19	0.18	0.20	0.15	0.13	0.27	0.23	0.17	0.18	0.18	0.22	0.16	0.19
629	630	612	599	546	578	604	611	618	615	636	647	636	652	643	645	648
29	35	28	28	28	29	35	28	28	34	29	63	66	69	62	63	60

Table 5.17. Continued

5.7	5.8	5.9	5.10	5.11	5.12	5.13	5.14	5.16	5.17	5.18	5.19	5.20	5.21	5.22	5.23	5.24
28.56	28.74	26.17	26.50	26.72	26.59	26.83	26.94	26.56	27.13	26.68	27.05	27.05	27.67	26.43	28.62	28.27
0.08	0.10	1.38	1.32	1.18	1.20	0.94	1.09	0.92	0.85	0.89	0.82	0.76	0.50	1.02	0.18	0.19
0.83	0.83	1.11	1.27	1.46	1.39	1.60	1.51	1.60	1.63	1.63	1.67	1.73	1.74	1.51	1.52	1.53
0.33	0.30	0.05	0.17	0.16	0.16	0.21	0.18	0.23	0.20	0.20	0.23	0.23	0.32	0.20	0.81	0.81
12.47	12.83	9.92	9.48	9.70	9.76	9.83	9.61	9.33	9.43	9.97	9.76	9.78	10.01	9.82	10.03	10.43
30.93	31.04	27.34	27.36	25.70	27.24	26.34	27.02	26.17	26.46	26.69	26.41	26.79	27.38	26.68	27.17	26.94
3.19	3.24	3.30	3.19	3.49	3.39	3.18	3.15	3.02	3.07	3.24	3.13	3.13	3.30	3.09	3.07	2.93
15.25	15.72	16.75	16.24	15.70	15.76	15.34	15.75	15.46	15.00	14.60	15.51	14.86	15.27	15.30	15.00	15.23
2.07	2.15	1.44	1.62	2.03	1.82	1.93	1.91	2.04	1.99	1.92	1.85	1.92	2.09	1.81	2.31	2.37
1.31	1.17	0.44	0.62	0.66	0.65	0.65	0.63	0.87	1.01	0.89	0.94	1.14	1.14	0.82	1.62	1.51
0.16	0.10	–	0.03	0.09	0.10	0.04	0.12	0.05	–	0.07	0.09	0.13	0.10	0.07	0.16	0.23
–	0.02	0.01	–	–	–	–	–	–	0.00	–	–	–	–	0.01	–	0.02
0.57	0.55	0.20	0.27	0.29	0.28	0.33	0.29	0.30	0.33	0.33	0.34	0.34	0.38	0.31	0.67	0.65
3.42	3.51	10.81	11.26	11.44	11.37	11.29	11.29	11.24	11.11	11.25	11.08	11.10	10.01	11.29	7.37	7.42
0.14	0.14	0.29	0.29	0.32	0.30	0.30	0.31	0.30	0.30	0.30	0.30	0.29	0.26	0.29	0.25	0.23
99.39	100.49	99.27	99.63	99.01	100.07	98.88	99.85	98.19	98.57	98.73	99.24	99.36	100.20	98.75	98.83	98.80
0.98	0.97	0.92	0.92	0.93	0.92	0.94	0.93	0.93	0.94	0.93	0.94	0.94	0.95	0.93	0.98	0.97
0.00	0.00	0.06	0.05	0.05	0.05	0.04	0.04	0.04	0.03	0.04	0.03	0.03	0.02	0.04	0.01	0.01
0.04	0.04	0.05	0.06	0.06	0.06	0.07	0.07	0.07	0.07	0.07	0.07	0.08	0.08	0.07	0.07	0.07
0.01	0.01	0.00	0.00	0.00	0.00	0.00	0.00	0.01	0.00	0.00	0.01	0.01	0.01	0.00	0.02	0.02
0.19	0.19	0.15	0.14	0.15	0.15	0.15	0.14	0.14	0.14	0.15	0.15	0.15	0.15	0.15	0.15	0.16
0.46	0.45	0.41	0.41	0.39	0.41	0.40	0.40	0.40	0.40	0.40	0.40	0.40	0.41	0.41	0.40	0.40
0.05	0.05	0.05	0.05	0.05	0.05	0.05	0.05	0.05	0.05	0.05	0.05	0.05	0.05	0.05	0.05	0.04
0.22	0.22	0.25	0.24	0.23	0.23	0.23	0.23	0.23	0.22	0.22	0.23	0.22	0.22	0.23	0.22	0.22
0.03	0.03	0.02	0.02	0.03	0.03	0.03	0.03	0.03	0.03	0.03	0.03	0.03	0.03	0.03	0.03	0.03
0.02	0.02	0.01	0.01	0.01	0.01	0.01	0.01	0.01	0.01	0.01	0.01	0.02	0.02	0.01	0.02	0.02
0.00	0.00	–	0.00	0.00	0.00	0.00	0.00	0.00	–	0.00	0.00	0.00	0.00	0.00	0.00	0.00
–	0.00	0.00	–	–	–	–	–	–	0.00	–	–	–	–	0.00	–	0.00
0.00	0.00	0.00	0.00	0.00	0.00	0.00	0.00	0.00	0.00	0.00	0.00	0.00	0.00	0.00	0.01	0.01
0.03	0.03	0.10	0.11	0.11	0.11	0.11	0.10	0.11	0.10	0.11	0.10	0.10	0.09	0.11	0.07	0.07
0.00	0.00	0.00	0.00	0.00	0.00	0.00	0.00	0.00	0.00	0.00	0.00	0.00	0.00	0.00	0.00	0.00
2.02	2.02	2.02	2.02	2.02	2.02	2.02	2.02	2.02	2.02	2.02	2.02	2.02	2.02	2.02	2.01	2.02
5.21	5.25	11.18	11.84	12.09	11.97	12.07	11.92	11.91	11.90	12.05	11.89	11.92	11.00	12.01	9.39	9.38
6.49	6.89	99.48	66.44	60.35	64.45	49.32	60.36	57.32	47.99	48.06	46.46	46.39	34.24	53.14	12.47	12.84
0.64	0.64	0.88	0.89	0.84	0.84	0.81	0.86	0.86	0.83	0.76	0.83	0.79	0.80	0.81	0.78	0.76
0.20	0.17	0.06	0.09	0.10	0.10	0.10	0.09	0.13	0.16	0.14	0.14	0.18	0.17	0.12	0.25	0.23
627	627	630	597	634	606	599	625	613	604	596	602	589	573	592	632	596
63	62	28	26	26	26	26	26	26	26	26	26	26	28	26	34	34

Table 5.17. Continued

5.25	5.26	5.27	6.1	6.2	6.3	6.4	6.7	6.8	7.2	7.3	7.4	7.5	7.6	7.7	7.8	7.9
28.34	28.23	28.29	29.08	29.17	28.94	28.83	29.16	29.24	29.46	29.53	29.54	29.72	29.42	28.88	28.72	28.98
0.20	0.20	0.19	0.05	0.06	0.06	0.06	0.05	0.06	0.07	0.07	0.08	0.06	0.23	0.32	0.27	0.26
1.51	1.54	1.49	0.65	0.62	0.65	0.69	0.58	0.63	1.01	0.98	0.95	0.91	1.66	1.85	1.81	1.81
0.78	0.77	0.76	0.41	0.43	0.41	0.37	0.41	0.36	0.38	0.34	0.35	0.34	0.41	0.36	0.35	0.35
10.43	10.52	10.33	14.52	14.44	14.40	14.14	14.72	14.91	12.50	12.74	12.54	12.73	10.83	10.00	10.24	9.92
27.19	27.40	27.41	32.02	32.24	32.19	32.34	32.28	32.86	30.81	30.95	31.41	31.05	27.87	27.17	28.00	28.46
3.04	3.07	3.17	3.18	3.25	3.13	3.28	3.32	3.08	3.16	3.40	3.33	3.27	3.19	3.23	2.97	3.33
14.96	15.25	14.94	15.11	14.81	15.23	15.17	15.39	15.00	15.73	15.75	15.95	15.89	15.91	15.76	15.37	15.53
2.47	2.49	2.18	1.78	1.80	1.58	1.78	1.59	1.48	2.32	2.15	2.26	2.16	1.93	1.98	1.99	1.98
1.73	1.60	1.63	1.07	1.00	0.93	1.16	1.05	0.85	1.29	1.39	1.26	1.19	1.26	1.06	1.14	0.87
0.21	0.25	0.23	0.03	0.09	0.21	0.01	0.18	–	0.17	0.15	0.09	0.11	0.11	0.08	–	0.09
–	–	–	0.03	–	–	–	0.11	–	–	–	–	–	–	–	–	–
0.65	0.64	0.64	0.37	0.37	0.35	0.34	0.38	0.38	0.91	0.88	0.90	0.92	0.51	0.52	0.49	0.50
7.46	7.55	7.37	2.62	2.56	2.58	2.90	2.30	2.54	3.73	3.78	3.52	3.27	8.01	9.21	8.75	8.75
0.23	0.23	0.24	0.12	0.10	0.10	0.11	0.11	0.11	0.17	0.18	0.17	0.18	0.24	0.28	0.25	0.26
99.28	99.78	98.96	101.12	100.97	100.79	101.21	101.69	101.55	101.75	102.35	102.36	101.84	101.68	100.79	100.40	101.13
0.97	0.96	0.97	0.98	0.98	0.97	0.97	0.97	0.98	0.98	0.98	0.98	0.98	0.98	0.97	0.97	0.97
0.01	0.01	0.01	0.00	0.00	0.00	0.00	0.00	0.00	0.00	0.00	0.00	0.00	0.01	0.01	0.01	0.01
0.07	0.07	0.06	0.03	0.03	0.03	0.03	0.02	0.03	0.04	0.04	0.04	0.04	0.07	0.08	0.08	0.08
0.02	0.02	0.02	0.01	0.01	0.01	0.01	0.01	0.01	0.01	0.01	0.01	0.01	0.01	0.01	0.01	0.01
0.16	0.16	0.15	0.21	0.21	0.21	0.21	0.21	0.22	0.18	0.18	0.18	0.18	0.16	0.15	0.15	0.14
0.40	0.40	0.41	0.46	0.47	0.47	0.47	0.47	0.47	0.44	0.44	0.45	0.44	0.40	0.39	0.41	0.41
0.04	0.05	0.05	0.05	0.05	0.05	0.05	0.05	0.04	0.05	0.05	0.05	0.05	0.05	0.05	0.04	0.05
0.22	0.22	0.22	0.21	0.21	0.22	0.22	0.22	0.21	0.22	0.22	0.22	0.22	0.22	0.22	0.22	0.22
0.03	0.03	0.03	0.02	0.02	0.02	0.02	0.02	0.02	0.03	0.03	0.03	0.03	0.03	0.03	0.03	0.03
0.02	0.02	0.02	0.01	0.01	0.01	0.02	0.01	0.01	0.02	0.02	0.02	0.02	0.02	0.01	0.02	0.01
0.00	0.00	0.00	0.00	0.00	0.00	0.00	0.00	–	0.00	0.00	0.00	0.00	0.00	0.00	–	0.00
–	–	–	0.00	–	–	–	0.00	–	–	–	–	–	–	–	–	–
0.01	0.01	0.01	0.00	0.00	0.00	0.00	0.00	0.00	0.01	0.01	0.01	0.01	0.00	0.00	0.00	0.00
0.07	0.07	0.07	0.02	0.02	0.02	0.03	0.02	0.02	0.03	0.03	0.03	0.03	0.07	0.08	0.08	0.08
0.00	0.00	0.00	0.00	0.00	0.00	0.00	0.00	0.00	0.00	0.00	0.00	0.00	0.00	0.00	0.00	0.00
2.02	2.02	2.01	2.02	2.01	2.02	2.02	2.02	2.02	2.01	2.01	2.02	2.01	2.01	2.01	2.02	2.01
9.42	9.45	9.29	3.79	3.74	3.66	3.97	3.51	3.74	6.67	6.61	6.41	6.24	9.48	10.67	10.12	10.18
12.89	13.48	13.14	7.73	7.42	8.15	9.30	6.57	7.30	4.32	4.56	4.16	3.76	18.49	21.47	21.63	20.94
0.75	0.76	0.75	0.54	0.53	0.55	0.56	0.55	0.52	0.66	0.64	0.66	0.65	0.77	0.82	0.78	0.82
0.27	0.24	0.25	0.17	0.16	0.14	0.18	0.16	0.13	0.19	0.20	0.18	0.17	0.18	0.16	0.17	0.13
591	575	615	725	652	654	658	721	702	616	637	626	665	614	630	595	604
34	34	34	86	87	89	82	94	87	50	50	52	54	33	30	31	31

Table 5.17. Continued

7.10	8.1	8.2	8.3	8.5	8.7	8.8	8.9	8.10	8.11	8.12	9.2	9.3	9.5	9.6	9.7	9.8
28.92	29.54	29.58	29.34	29.75	28.17	28.16	28.06	28.28	28.23	28.11	28.35	28.58	28.47	27.93	26.77	26.79
0.27	0.02	0.03	0.03	0.04	0.47	0.79	0.52	0.44	0.47	0.48	0.02	0.02	0.05	0.28	1.16	1.16
1.82	0.57	0.60	0.60	0.56	1.83	1.78	1.88	1.87	1.85	1.86	0.55	0.54	0.78	1.57	1.44	1.43
0.34	0.71	0.77	1.11	0.75	0.30	0.22	0.28	0.31	0.30	0.30	1.89	1.85	0.64	0.70	0.17	0.15
10.65	14.15	14.45	14.16	14.33	9.98	9.69	9.66	9.69	9.84	9.40	14.04	14.01	12.95	10.85	9.23	9.79
28.45	31.70	31.32	30.99	31.64	27.36	27.67	27.42	27.22	27.02	26.92	29.97	29.85	31.17	27.19	27.25	27.21
3.20	3.43	3.06	3.27	3.24	3.25	3.24	3.23	3.21	3.47	3.12	2.98	3.10	3.32	3.36	3.32	3.12
15.56	15.83	15.02	15.91	16.10	15.49	15.54	15.86	16.12	15.82	15.67	14.68	14.74	15.33	15.23	15.79	15.58
2.06	1.80	1.87	1.79	1.93	1.99	1.90	1.96	1.97	2.16	2.03	1.64	1.62	2.30	2.16	1.62	1.69
1.12	1.30	1.16	1.40	1.25	1.16	0.85	0.91	1.08	1.09	1.04	1.37	1.29	1.46	1.30	0.70	0.63
0.06	0.16	0.19	0.31	0.21	–	0.11	0.08	0.11	–	0.03	0.44	0.46	0.27	0.32	0.07	0.11
–	–	–	0.01	–	0.07	–	0.02	–	0.03	–	–	0.08	–	–	0.05	0.00
0.51	0.62	0.70	0.71	0.62	0.45	0.34	0.44	0.44	0.42	0.45	0.61	0.62	0.73	0.65	0.30	0.28
8.78	1.93	2.08	2.08	1.91	10.08	10.67	10.45	9.97	10.01	10.26	1.87	1.78	2.64	7.74	11.47	11.44
0.27	0.11	0.12	0.12	0.12	0.28	0.28	0.28	0.27	0.28	0.28	0.11	0.11	0.14	0.24	0.30	0.30
102.08	101.92	101.06	101.89	102.57	100.91	101.31	101.11	101.11	101.10	100.04	98.60	98.67	100.27	99.60	99.70	99.77
0.97	0.98	0.98	0.98	0.98	0.96	0.95	0.95	0.96	0.96	0.96	0.97	0.98	0.97	0.96	0.93	0.93
0.01	0.00	0.00	0.00	0.00	0.02	0.03	0.02	0.02	0.02	0.02	0.00	0.00	0.00	0.01	0.05	0.05
0.08	0.02	0.03	0.03	0.02	0.08	0.08	0.08	0.08	0.08	0.08	0.02	0.02	0.03	0.07	0.06	0.06
0.01	0.01	0.02	0.02	0.02	0.01	0.00	0.01	0.01	0.01	0.01	0.04	0.04	0.01	0.02	0.00	0.00
0.15	0.20	0.21	0.20	0.21	0.15	0.14	0.14	0.14	0.15	0.14	0.21	0.21	0.19	0.16	0.14	0.15
0.41	0.45	0.45	0.45	0.45	0.40	0.40	0.40	0.40	0.40	0.40	0.44	0.44	0.46	0.40	0.41	0.41
0.05	0.05	0.04	0.05	0.05	0.05	0.05	0.05	0.05	0.05	0.05	0.04	0.05	0.05	0.05	0.05	0.05
0.22	0.22	0.21	0.22	0.22	0.22	0.22	0.23	0.23	0.23	0.23	0.21	0.21	0.22	0.22	0.23	0.23
0.03	0.02	0.03	0.02	0.03	0.03	0.03	0.03	0.03	0.03	0.03	0.02	0.02	0.03	0.03	0.02	0.02
0.01	0.02	0.02	0.02	0.02	0.02	0.01	0.01	0.01	0.01	0.01	0.02	0.02	0.02	0.02	0.01	0.01
0.00	0.00	0.00	0.00	0.00	–	0.00	0.00	0.00	–	0.00	0.01	0.01	0.00	0.00	0.00	0.00
–	–	–	0.00	–	0.00	–	0.00	–	0.00	–	–	0.00	–	–	0.00	0.00
0.00	0.01	0.01	0.01	0.01	0.00	0.00	0.00	0.00	0.00	0.00	0.01	0.01	0.01	0.01	0.00	0.00
0.08	0.02	0.02	0.02	0.02	0.09	0.10	0.10	0.09	0.09	0.09	0.02	0.02	0.02	0.07	0.11	0.11
0.00	0.00	0.00	0.00	0.00	0.00	0.00	0.00	0.00	0.00	0.00	0.00	0.00	0.00	0.00	0.00	0.00
2.02	2.01	2.01	2.02	2.01	2.02	2.02	2.02	2.02	2.02	2.02	2.02	2.02	2.02	2.02	2.02	2.02
10.23	3.95	4.38	4.38	3.93	11.29	11.51	11.64	11.14	11.13	11.48	3.85	3.80	4.99	9.68	12.15	12.04
20.79	3.27	3.10	3.09	3.24	28.20	43.42	30.00	28.77	30.48	28.77	3.23	3.00	3.84	13.63	57.28	65.04
0.76	0.58	0.54	0.59	0.59	0.81	0.84	0.86	0.87	0.84	0.87	0.55	0.55	0.62	0.73	0.89	0.83
0.17	0.19	0.18	0.20	0.18	0.17	0.13	0.13	0.16	0.16	0.16	0.22	0.20	0.22	0.20	0.10	0.09
629	636	627	632	717	605	597	589	581	609	591	701	654	641	603	604	599
31	85	77	77	86	28	27	27	28	28	27	88	89	67	33	26	26

Table 5.17. Continued

9.9	9.10	9.11	9.12	9.13	9.14	9.15	9.16	9.17	9.18	9.19	9.20	9.21	9.22	9.23	9.24	9.25
26.89	26.97	27.12	27.01	27.60	27.37	27.76	28.06	28.04	27.92	28.17	28.46	27.88	27.46	28.39	28.45	29.07
1.13	1.05	1.12	1.09	0.42	0.40	0.39	0.41	0.39	0.40	0.30	0.39	0.41	0.38	0.32	0.29	0.30
1.50	1.52	1.48	1.51	1.86	1.73	1.82	1.79	1.78	1.78	1.75	1.79	1.88	1.88	1.68	1.72	1.76
0.16	0.18	0.16	0.16	0.42	0.36	0.41	0.43	0.36	0.36	0.35	0.34	0.42	0.44	0.65	0.58	0.58
9.57	9.96	9.68	9.80	9.55	10.07	9.90	9.79	10.16	10.03	10.05	9.95	9.92	9.63	10.54	9.74	10.13
27.22	27.56	27.26	26.75	26.73	27.14	26.86	26.63	26.59	27.40	27.66	27.25	26.36	26.29	27.18	26.85	27.09
3.41	3.41	3.26	3.34	3.36	3.05	2.82	3.26	3.12	3.13	3.12	3.12	3.32	2.93	3.03	3.25	3.11
15.89	15.70	15.85	15.52	14.87	15.33	15.27	15.67	15.00	15.42	15.49	15.48	15.38	15.04	15.04	15.24	15.55
1.74	1.81	1.76	1.83	1.86	1.95	2.11	1.88	2.08	2.07	2.12	2.25	1.90	1.96	2.06	2.13	2.24
0.62	0.76	0.64	0.87	1.28	1.01	1.16	1.06	1.15	1.14	1.17	1.21	1.01	1.11	1.24	1.39	1.27
0.04	0.08	0.08	0.09	0.18	0.08	0.13	0.17	0.14	0.14	0.15	0.08	0.17	0.16	0.24	0.23	0.20
–	–	–	–	–	–	–	–	–	–	–	–	–	–	–	–	0.01
0.29	0.30	0.29	0.32	0.45	0.43	0.46	0.45	0.45	0.45	0.48	0.46	0.46	0.52	0.49	0.53	0.53
11.51	11.44	11.51	11.50	10.10	9.63	9.73	9.81	9.65	9.63	9.15	9.72	10.15	10.18	8.54	8.69	8.72
0.31	0.31	0.31	0.29	0.29	0.27	0.27	0.27	0.27	0.28	0.26	0.28	0.29	0.29	0.24	0.26	0.26
100.43	101.17	100.55	100.16	99.06	98.92	99.18	99.74	99.24	100.24	100.31	100.87	99.63	98.34	99.70	99.45	100.84
0.93	0.93	0.93	0.93	0.96	0.95	0.96	0.96	0.96	0.96	0.96	0.96	0.96	0.96	0.97	0.97	0.97
0.05	0.04	0.05	0.04	0.02	0.02	0.02	0.02	0.02	0.02	0.01	0.02	0.02	0.02	0.01	0.01	0.01
0.07	0.07	0.06	0.07	0.08	0.08	0.08	0.08	0.08	0.08	0.08	0.08	0.08	0.08	0.07	0.07	0.07
0.00	0.00	0.00	0.00	0.01	0.01	0.01	0.01	0.01	0.01	0.01	0.01	0.01	0.01	0.01	0.01	0.01
0.14	0.15	0.14	0.15	0.14	0.15	0.15	0.15	0.15	0.15	0.15	0.15	0.15	0.15	0.16	0.14	0.15
0.41	0.41	0.40	0.40	0.40	0.41	0.40	0.39	0.39	0.41	0.41	0.40	0.39	0.40	0.40	0.40	0.39
0.05	0.05	0.05	0.05	0.05	0.05	0.04	0.05	0.05	0.05	0.05	0.05	0.05	0.04	0.04	0.05	0.04
0.23	0.23	0.23	0.23	0.22	0.22	0.22	0.23	0.22	0.22	0.22	0.22	0.22	0.22	0.22	0.22	0.22
0.02	0.03	0.02	0.03	0.03	0.03	0.03	0.03	0.03	0.03	0.03	0.03	0.03	0.03	0.03	0.03	0.03
0.01	0.01	0.01	0.01	0.02	0.01	0.02	0.01	0.02	0.02	0.02	0.02	0.01	0.02	0.02	0.02	0.02
0.00	0.00	0.00	0.00	0.00	0.00	0.00	0.00	0.00	0.00	0.00	0.00	0.00	0.00	0.00	0.00	0.00
–	–	–	–	–	–	–	–	–	–	–	–	–	–	–	–	0.00
0.00	0.00	0.00	0.00	0.00	0.00	0.00	0.00	0.00	0.00	0.00	0.00	0.00	0.00	0.00	0.00	0.00
0.11	0.11	0.11	0.11	0.09	0.09	0.09	0.09	0.09	0.09	0.08	0.09	0.09	0.10	0.08	0.08	0.08
0.00	0.00	0.00	0.00	0.00	0.00	0.00	0.00	0.00	0.00	0.00	0.00	0.00	0.00	0.00	0.00	0.00
2.02	2.02	2.02	2.02	2.02	2.02	2.02	2.02	2.02	2.02	2.02	2.02	2.02	2.02	2.02	2.01	2.01
12.15	12.12	12.15	12.23	11.33	10.81	10.99	11.03	10.88	10.85	10.49	10.97	11.41	11.64	9.93	10.19	10.24
60.89	57.69	61.86	53.35	28.07	27.99	26.31	27.37	26.67	26.97	23.34	26.56	27.47	23.74	20.93	19.65	19.62
0.87	0.82	0.85	0.83	0.81	0.79	0.80	0.83	0.77	0.80	0.80	0.81	0.81	0.81	0.74	0.82	0.80
0.09	0.11	0.09	0.13	0.20	0.15	0.18	0.16	0.18	0.17	0.18	0.18	0.15	0.17	0.19	0.21	0.19
611	617	610	578	624	594	599	584	603	623	600	618	605	595	590	607	614
26	26	26	26	28	29	29	29	29	29	30	29	28	27	32	31	31

Table 5.17. Continued

9.26	10.18	10.19	10.20	10.21	10.22	10.23	10.24	10.25	10.26	10.27	10.28	10.29	10.30	10.31	10.32	10.33
27.95	28.17	28.22	28.24	28.28	28.41	27.80	27.28	27.94	27.57	27.69	27.72	28.02	27.85	28.36	27.83	27.99
0.43	0.25	0.13	0.24	0.22	0.24	0.68	0.84	0.61	0.74	0.75	0.78	0.56	0.54	0.46	0.45	0.48
1.26	1.31	1.58	1.35	1.32	1.37	1.56	1.57	1.69	1.63	1.70	1.67	1.73	1.71	1.72	1.71	1.81
1.32	0.65	1.59	0.45	0.47	0.47	0.58	0.20	0.26	0.21	0.22	0.26	0.28	0.30	0.32	0.36	0.31
9.71	11.33	9.94	11.07	11.40	11.32	9.84	9.78	9.93	9.87	9.68	9.86	9.89	9.84	10.03	10.19	9.39
25.71	28.30	26.31	29.03	28.30	28.18	27.01	27.16	27.16	27.86	27.64	27.15	27.45	26.95	27.42	27.78	27.07
2.94	2.94	3.09	3.12	3.26	2.90	3.15	3.25	3.23	3.32	3.19	3.29	3.04	3.11	3.18	3.18	3.34
15.20	15.43	14.23	15.21	15.48	15.42	15.37	15.60	15.40	15.69	15.61	15.72	15.60	15.50	15.58	15.88	15.72
2.18	2.08	2.60	2.17	2.14	2.34	2.13	1.92	2.02	1.77	1.91	1.99	2.17	2.04	2.01	2.04	1.97
1.90	1.56	2.26	1.35	1.03	1.08	1.05	0.98	1.08	0.72	0.91	0.84	1.06	1.03	1.10	1.04	1.02
0.50	0.16	0.62	0.23	0.14	0.09	0.14	0.01	0.11	0.06	0.10	0.02	0.10	0.05	0.27	0.07	0.15
0.08	0.03	–	–	0.00	0.03	–	–	0.02	–	–	–	0.00	–	–	–	–
0.54	0.47	0.41	0.51	0.50	0.52	0.27	0.30	0.36	0.32	0.32	0.33	0.35	0.35	0.39	0.41	0.41
8.39	6.76	6.97	6.81	6.77	6.75	10.07	10.69	10.27	10.49	10.62	10.78	10.09	10.02	9.52	9.41	9.99
0.24	0.20	0.18	0.22	0.22	0.21	0.27	0.29	0.28	0.29	0.28	0.28	0.28	0.26	0.27	0.25	0.28
98.43	99.70	98.16	100.10	99.64	99.43	100.04	99.99	100.44	100.65	100.69	100.72	100.71	99.67	100.70	100.65	99.99
0.96	0.96	0.97	0.96	0.97	0.97	0.95	0.94	0.95	0.94	0.94	0.94	0.95	0.96	0.96	0.95	0.96
0.02	0.01	0.01	0.01	0.01	0.01	0.03	0.03	0.02	0.03	0.03	0.03	0.02	0.02	0.02	0.02	0.02
0.06	0.06	0.07	0.06	0.06	0.06	0.07	0.07	0.07	0.07	0.07	0.07	0.07	0.07	0.07	0.07	0.08
0.03	0.01	0.03	0.01	0.01	0.01	0.01	0.00	0.01	0.00	0.00	0.01	0.01	0.01	0.01	0.01	0.01
0.15	0.17	0.15	0.16	0.17	0.17	0.15	0.15	0.15	0.15	0.14	0.15	0.15	0.15	0.15	0.15	0.14
0.38	0.42	0.39	0.43	0.42	0.42	0.40	0.40	0.40	0.41	0.41	0.40	0.40	0.40	0.40	0.41	0.40
0.04	0.04	0.05	0.05	0.05	0.04	0.05	0.05	0.05	0.05	0.05	0.05	0.04	0.05	0.05	0.05	0.05
0.22	0.22	0.21	0.22	0.22	0.22	0.22	0.23	0.22	0.23	0.22	0.23	0.22	0.22	0.22	0.23	0.23
0.03	0.03	0.04	0.03	0.03	0.03	0.03	0.03	0.03	0.02	0.03	0.03	0.03	0.03	0.03	0.03	0.03
0.03	0.02	0.03	0.02	0.01	0.01	0.01	0.01	0.01	0.01	0.01	0.01	0.01	0.01	0.01	0.01	0.01
0.01	0.00	0.01	0.00	0.00	0.00	0.00	0.00	0.00	0.00	0.00	0.00	0.00	0.00	0.00	0.00	0.00
0.00	0.00	–	–	0.00	0.00	–	–	0.00	–	–	–	0.00	–	–	–	–
0.00	0.00	0.00	0.00	0.00	0.00	0.00	0.00	0.00	0.00	0.00	0.00	0.00	0.00	0.00	0.00	0.00
0.08	0.06	0.06	0.06	0.06	0.06	0.09	0.10	0.09	0.10	0.10	0.10	0.09	0.09	0.09	0.09	0.09
0.00	0.00	0.00	0.00	0.00	0.00	0.00	0.00	0.00	0.00	0.00	0.00	0.00	0.00	0.00	0.00	0.00
2.01	2.02	2.02	2.02	2.02	2.02	2.02	2.02	2.02	2.02	2.02	2.02	2.02	2.02	2.02	2.02	2.02
9.95	8.14	8.14	8.32	8.25	8.30	10.67	11.38	11.19	11.26	11.38	11.58	10.99	10.91	10.57	10.49	11.06
18.31	16.70	20.18	15.34	15.67	14.76	56.75	52.73	37.93	46.89	47.70	46.04	38.48	38.42	31.01	29.53	31.61
0.82	0.71	0.75	0.72	0.71	0.71	0.81	0.83	0.81	0.83	0.84	0.83	0.82	0.82	0.81	0.81	0.87
0.29	0.24	0.37	0.21	0.15	0.16	0.16	0.15	0.16	0.11	0.14	0.12	0.16	0.15	0.16	0.15	0.15
576	585	527	630	635	617	616	606	598	621	603	589	618	583	614	569	617
32	39	39	38	39	38	29	27	28	28	27	27	29	29	30	30	28

Table 5.17. Continued

10.34	10.35	10.36	10.37	10.38	10.39	10.40	10.41	10.42	10.43	10.44	10.45	10.46	10.47	10.48	10.49	10.50
27.91	26.98	27.31	27.63	27.66	26.91	27.10	27.46	28.04	27.51	27.69	27.66	27.93	28.65	28.43	27.95	28.07
0.44	0.90	0.89	0.86	0.86	0.85	0.85	0.59	0.66	0.86	0.89	0.89	0.20	0.17	0.17	0.26	0.25
1.78	1.61	1.61	1.58	1.62	1.57	1.60	1.67	1.75	1.64	1.57	1.60	1.54	1.44	1.42	1.32	1.37
0.32	0.22	0.21	0.21	0.22	0.22	0.21	0.27	0.29	0.21	0.20	0.20	0.77	0.82	0.84	0.49	0.51
9.83	9.41	10.39	9.97	10.17	9.72	9.85	9.83	9.94	9.67	9.57	9.80	10.70	10.73	10.79	11.28	11.25
27.49	27.28	26.81	27.25	27.24	27.59	27.24	27.37	27.31	27.08	27.25	27.40	27.61	27.94	28.09	28.28	28.35
3.27	3.14	3.02	3.24	3.20	3.06	3.24	3.26	3.20	3.21	3.08	3.19	3.13	3.17	3.21	3.01	3.12
15.42	16.07	15.68	15.64	15.56	15.89	16.30	15.55	15.23	15.62	15.32	15.58	14.92	15.03	15.12	15.42	15.53
1.91	2.10	1.92	1.83	1.91	1.88	2.03	1.79	1.92	2.00	1.97	2.01	2.23	2.23	2.49	1.94	2.02
1.16	0.78	0.98	0.88	0.77	0.85	0.77	1.03	1.02	0.76	1.04	0.86	1.60	1.55	1.75	1.11	1.17
0.12	0.01	0.11	0.10	0.06	0.12	0.15	0.07	0.10	0.06	0.06	–	0.26	0.28	0.21	–	0.03
–	–	–	–	–	–	0.01	–	–	–	–	0.02	–	–	–	0.01	–
0.43	0.30	0.31	0.30	0.30	0.32	0.30	0.36	0.35	0.32	0.31	0.29	0.64	0.65	0.68	0.55	0.53
9.82	10.86	10.89	10.69	10.85	10.65	10.83	10.13	10.43	10.96	10.91	10.88	7.29	6.83	6.61	6.72	6.77
0.27	0.28	0.30	0.29	0.29	0.29	0.28	0.27	0.28	0.29	0.29	0.29	0.23	0.23	0.23	0.21	0.22
100.25	99.99	100.51	100.58	100.79	100.00	100.83	99.72	100.61	100.22	100.26	100.80	99.14	99.79	100.13	98.60	99.24
0.95	0.93	0.94	0.94	0.94	0.93	0.93	0.95	0.95	0.94	0.95	0.94	0.96	0.97	0.97	0.97	0.96
0.02	0.04	0.04	0.03	0.03	0.03	0.03	0.02	0.03	0.03	0.04	0.04	0.01	0.01	0.01	0.01	0.01
0.08	0.07	0.07	0.07	0.07	0.07	0.07	0.07	0.08	0.07	0.07	0.07	0.07	0.06	0.06	0.06	0.06
0.01	0.00	0.00	0.00	0.00	0.00	0.00	0.01	0.01	0.00	0.00	0.00	0.02	0.02	0.02	0.01	0.01
0.15	0.14	0.16	0.15	0.15	0.15	0.15	0.15	0.15	0.14	0.14	0.15	0.16	0.16	0.16	0.17	0.17
0.41	0.41	0.40	0.40	0.40	0.41	0.41	0.41	0.40	0.40	0.40	0.40	0.41	0.41	0.41	0.42	0.42
0.05	0.05	0.04	0.05	0.05	0.05	0.05	0.05	0.05	0.05	0.05	0.05	0.05	0.05	0.05	0.04	0.05
0.22	0.23	0.23	0.23	0.22	0.23	0.24	0.23	0.22	0.23	0.22	0.22	0.22	0.22	0.22	0.22	0.23
0.03	0.03	0.03	0.03	0.03	0.03	0.03	0.03	0.03	0.03	0.03	0.03	0.03	0.03	0.03	0.03	0.03
0.02	0.01	0.01	0.01	0.01	0.01	0.01	0.01	0.01	0.01	0.01	0.01	0.02	0.02	0.02	0.01	0.02
0.00	0.00	0.00	0.00	0.00	0.00	0.00	0.00	0.00	0.00	0.00	–	0.00	0.00	0.00	–	0.00
–	–	–	–	–	–	0.00	–	–	–	–	0.00	–	–	–	0.00	–
0.00	0.00	0.00	0.00	0.00	0.00	0.00	0.00	0.00	0.00	0.00	0.00	0.01	0.01	0.01	0.00	0.00
0.09	0.10	0.10	0.10	0.10	0.10	0.10	0.09	0.10	0.10	0.10	0.10	0.07	0.06	0.06	0.06	0.06
0.00	0.00	0.00	0.00	0.00	0.00	0.00	0.00	0.00	0.00	0.00	0.00	0.00	0.00	0.00	0.00	0.00
2.02	2.02	2.02	2.02	2.02	2.02	2.02	2.02	2.02	2.02	2.01	2.02	2.02	2.01	2.02	2.02	2.02
10.99	11.55	11.60	11.40	11.54	11.41	11.52	11.05	11.31	11.70	11.62	11.55	9.23	8.82	8.70	8.37	8.36
28.65	53.73	52.17	51.28	53.12	47.43	52.97	37.42	40.35	50.25	52.30	55.75	12.82	11.75	10.81	13.86	14.55
0.82	0.89	0.79	0.82	0.80	0.85	0.86	0.83	0.80	0.84	0.84	0.83	0.73	0.73	0.73	0.71	0.72
0.17	0.11	0.15	0.13	0.12	0.12	0.11	0.15	0.16	0.11	0.16	0.13	0.25	0.24	0.27	0.17	0.18
598	583	623	619	599	604	580	597	603	602	599	610	609	623	631	606	629
29	27	27	27	27	27	27	28	28	27	27	27	35	36	37	38	38

Table 5.17. Continued

10.51	10.52	10.53	10.54	10.55
28.26	28.05	28.20	27.66	27.78
0.25	0.45	0.55	0.82	0.81
1.35	1.74	1.75	1.61	1.54
0.49	0.68	0.44	0.27	0.79
10.96	10.63	9.76	10.01	10.24
28.73	27.32	26.93	27.46	26.74
3.21	3.03	3.08	3.13	3.05
15.49	14.50	15.46	15.58	15.29
2.22	1.74	2.07	1.93	1.95
1.28	1.17	1.03	0.74	1.03
0.00	0.15	0.11	0.10	0.22
–	–	–	–	0.04
0.63	0.40	0.40	0.30	0.38
6.47	9.29	10.28	10.73	9.68
0.23	0.24	0.28	0.29	0.25
99.60	99.51	100.42	100.69	99.85
0.97	0.96	0.96	0.94	0.95
0.01	0.02	0.02	0.03	0.03
0.06	0.08	0.08	0.07	0.07
0.01	0.01	0.01	0.01	0.02
0.16	0.16	0.14	0.15	0.15
0.42	0.40	0.40	0.41	0.39
0.05	0.04	0.05	0.05	0.04
0.22	0.21	0.22	0.22	0.22
0.03	0.02	0.03	0.03	0.03
0.02	0.02	0.01	0.01	0.01
0.00	0.00	0.00	0.00	0.00
–	–	–	–	0.00
0.01	0.00	0.00	0.00	0.00
0.06	0.09	0.09	0.10	0.09
0.00	0.00	0.00	0.00	0.00
2.02	2.02	2.01	2.02	2.02
8.41	10.37	11.33	11.44	10.66
11.44	29.14	33.41	51.30	33.36
0.74	0.71	0.83	0.81	0.78
0.19	0.19	0.16	0.11	0.16
653	564	603	603	560
38	30	28	27	29

Table 5.18. Chemical compositions of monazites in the sample 07120402A from Brattnipene area

Analysis No.	1.1	1.2	1.3	1.4	1.5	1.6	1.7	1.8	1.9	1.1	1.11	1.12	1.13	1.14	1.15
wt%															
P2O5	28.52	28.66	28.47	27.93	28.41	28.47	27.44	28.43	28.40	28.55	28.38	28.38	28.67	28.83	29.24
SiO2	0.28	0.50	0.60	0.81	0.39	0.51	1.10	0.46	0.53	0.25	0.54	0.45	0.48	0.25	0.27
CaO	1.39	1.13	1.28	1.36	1.07	1.15	1.69	1.18	1.16	1.40	1.22	1.16	1.08	1.42	1.43
Y2O3	0.27	0.33	0.20	0.13	0.43	0.21	0.12	0.48	0.25	0.30	0.24	0.32	0.32	0.27	0.27
La2O3	11.16	10.47	10.15	9.69	10.25	10.52	8.62	10.08	10.22	10.59	10.21	10.40	10.31	11.37	11.50
Ce2O3	29.09	29.21	28.96	28.16	28.45	29.65	27.05	28.62	28.91	28.94	29.29	28.47	29.06	29.19	29.28
Pr2O3	3.38	3.41	3.37	3.46	3.36	3.42	3.37	3.31	3.52	3.30	3.25	3.29	3.32	3.04	3.18
Nd2O3	15.77	16.58	16.61	16.88	16.26	16.13	16.26	16.37	17.03	15.57	16.91	16.84	16.38	15.16	15.47
Sm2O3	1.88	1.79	1.70	1.46	2.38	1.81	1.43	2.11	1.81	1.87	1.90	2.00	2.12	1.69	1.77
Gd2O3	0.84	1.21	0.76	0.53	1.51	0.91	0.42	1.28	0.97	0.89	0.91	1.15	1.14	0.94	0.94
Dy2O3	0.10	0.13	0.06	0.13	0.21	0.14	0.05	0.04	0.08	0.15	0.08	0.23	0.17	0.12	0.18
Er2O3	–	–	–	–	–	–	0.01	–	–	–	–	–	0.07	0.00	0.03
UO2	0.24	0.27	0.24	0.26	0.23	0.26	0.26	0.29	0.26	0.23	0.26	0.27	0.22	0.25	0.22
ThO2	7.17	6.95	8.02	9.38	6.32	7.03	11.91	7.16	7.22	7.24	7.51	6.75	6.76	7.12	6.99
PbO	0.19	0.19	0.22	0.25	0.18	0.20	0.31	0.20	0.21	0.19	0.21	0.19	0.19	0.18	0.18
Total	100.37	100.86	100.74	100.47	99.54	100.46	100.12	100.02	100.63	99.54	101.00	100.01	100.36	99.88	101.04
Cation (O=4)															
P	0.97	0.96	0.96	0.95	0.97	0.96	0.94	0.97	0.96	0.97	0.96	0.96	0.97	0.98	0.98
Si	0.01	0.02	0.02	0.03	0.02	0.02	0.04	0.02	0.02	0.01	0.02	0.02	0.02	0.01	0.01
Ca	0.06	0.05	0.05	0.06	0.05	0.05	0.07	0.05	0.05	0.06	0.05	0.05	0.05	0.06	0.06
Y	0.01	0.01	0.00	0.00	0.01	0.00	0.00	0.01	0.01	0.01	0.01	0.01	0.01	0.01	0.01
La	0.16	0.15	0.15	0.14	0.15	0.16	0.13	0.15	0.15	0.16	0.15	0.15	0.15	0.17	0.17
Ce	0.43	0.43	0.42	0.41	0.42	0.43	0.40	0.42	0.42	0.43	0.43	0.42	0.42	0.43	0.42
Pr	0.05	0.05	0.05	0.05	0.05	0.05	0.05	0.05	0.05	0.05	0.05	0.05	0.05	0.04	0.05
Nd	0.23	0.24	0.24	0.24	0.23	0.23	0.23	0.23	0.24	0.22	0.24	0.24	0.23	0.22	0.22
Sm	0.03	0.02	0.02	0.02	0.03	0.02	0.02	0.03	0.02	0.03	0.03	0.03	0.03	0.02	0.02
Gd	0.01	0.02	0.01	0.01	0.02	0.01	0.01	0.02	0.01	0.01	0.01	0.02	0.02	0.01	0.01
Dy	0.00	0.00	0.00	0.00	0.00	0.00	0.00	0.00	0.00	0.00	0.00	0.00	0.00	0.00	0.00
Er	–	–	–	–	–	–	0.00	–	–	–	–	–	0.00	0.00	0.00
U	0.00	0.00	0.00	0.00	0.00	0.00	0.00	0.00	0.00	0.00	0.00	0.00	0.00	0.00	0.00
Th	0.07	0.06	0.07	0.09	0.06	0.06	0.11	0.07	0.07	0.07	0.07	0.06	0.06	0.06	0.06
Pb	0.00	0.00	0.00	0.00	0.00	0.00	0.00	0.00	0.00	0.00	0.00	0.00	0.00	0.00	0.00
Total	2.02	2.01	2.01	2.01	2.01	2.01	2.01	2.01	2.01	2.01	2.02	2.01	2.01	2.01	2.01
ThO2*	7.75	7.65	8.60	9.98	6.89	7.68	12.44	7.91	7.88	7.79	8.16	7.46	7.30	7.74	7.54
Th/U	41.95	33.57	46.40	53.19	37.57	36.68	76.66	32.26	37.02	44.54	39.41	32.33	42.63	38.89	43.55
Nd/La	0.74	0.83	0.85	0.91	0.83	0.80	0.98	0.85	0.87	0.77	0.86	0.84	0.83	0.70	0.70
Gd/Nd	0.12	0.17	0.11	0.07	0.22	0.13	0.06	0.18	0.13	0.13	0.13	0.16	0.16	0.15	0.14
Age (Ma)	587	612	624	616	624	613	594	595	634	574	622	622	635	562	581
+/− (Ma)	40	41	36	31	46	41	25	40	40	40	38	42	43	40	41

−: below detection limit

Table 5.18. Continued

1.16	1.17	1.18	1.19	1.20	1.21	1.22	1.23	2.1	2.2	2.3	2.4	2.5	2.6	2.7	2.8	2.9
28.81	28.92	28.74	28.57	28.94	28.83	28.43	28.57	29.25	29.21	29.31	29.23	29.08	28.76	29.06	29.18	29.39
0.17	0.26	0.37	0.92	0.26	0.23	0.50	0.24	0.17	0.52	0.27	0.23	0.37	0.49	0.23	0.18	0.17
1.48	1.39	1.09	1.15	1.35	1.43	1.16	1.41	1.47	1.39	1.49	1.44	1.48	1.35	1.38	1.35	1.34
0.95	0.26	0.47	1.11	0.22	0.32	0.25	0.33	1.28	0.15	1.20	0.34	0.18	0.19	0.31	0.24	0.33
11.05	11.22	10.43	9.41	10.14	11.30	10.27	11.35	10.21	10.35	10.28	10.66	10.39	10.32	11.20	11.04	11.31
28.36	29.31	28.51	26.49	29.01	29.07	29.27	28.82	28.21	29.74	28.18	29.88	28.83	29.63	29.49	30.05	29.10
2.93	3.14	3.18	3.07	3.53	3.35	3.08	3.12	2.98	3.53	3.21	2.95	3.43	3.61	3.40	3.28	3.23
14.14	15.52	16.27	16.07	17.26	15.19	15.79	15.12	15.56	16.90	15.81	15.91	16.45	16.84	16.09	15.71	16.10
2.11	1.79	2.30	2.57	1.95	1.88	1.99	1.84	2.20	1.57	1.94	1.74	2.12	1.45	1.71	2.13	1.90
1.41	0.78	1.66	2.04	1.11	0.93	1.27	1.12	1.30	0.40	1.06	0.80	1.00	0.56	0.89	0.88	1.09
0.44	0.08	0.25	0.41	0.04	0.12	0.19	0.18	0.35	0.06	0.26	0.01	0.03	0.05	0.09	0.13	0.09
0.06	0.04	–	–	–	–	0.01	–	0.09	–	0.03	–	–	–	0.03	–	–
0.34	0.23	0.22	0.41	0.26	0.29	0.20	0.25	0.42	0.24	0.37	0.27	0.36	0.25	0.27	0.31	0.34
6.77	6.92	6.05	5.81	6.70	7.09	6.83	6.87	6.84	8.25	7.36	7.17	7.68	7.95	6.88	6.36	6.37
0.20	0.19	0.16	0.18	0.20	0.18	0.20	0.18	0.18	0.20	0.19	0.18	0.21	0.21	0.17	0.19	0.17
99.27	100.11	99.80	98.32	100.99	100.31	99.46	99.51	100.55	102.61	101.00	100.87	101.65	101.70	101.23	101.13	101.00
0.98	0.98	0.97	0.97	0.97	0.97	0.97	0.97	0.98	0.97	0.98	0.98	0.97	0.96	0.97	0.98	0.98
0.01	0.01	0.01	0.04	0.01	0.01	0.02	0.01	0.01	0.02	0.01	0.01	0.01	0.02	0.01	0.01	0.01
0.06	0.06	0.05	0.05	0.06	0.06	0.05	0.06	0.06	0.06	0.06	0.06	0.06	0.06	0.06	0.06	0.06
0.02	0.01	0.01	0.02	0.00	0.01	0.01	0.01	0.03	0.00	0.03	0.01	0.00	0.00	0.01	0.01	0.01
0.16	0.16	0.15	0.14	0.15	0.17	0.15	0.17	0.15	0.15	0.15	0.16	0.15	0.15	0.16	0.16	0.16
0.42	0.43	0.42	0.39	0.42	0.42	0.43	0.42	0.41	0.43	0.41	0.43	0.42	0.43	0.43	0.43	0.42
0.04	0.05	0.05	0.04	0.05	0.05	0.05	0.05	0.04	0.05	0.05	0.04	0.05	0.05	0.05	0.05	0.05
0.20	0.22	0.23	0.23	0.24	0.22	0.23	0.22	0.22	0.24	0.22	0.22	0.23	0.24	0.23	0.22	0.23
0.03	0.02	0.03	0.04	0.03	0.03	0.03	0.03	0.03	0.02	0.03	0.02	0.03	0.02	0.02	0.03	0.03
0.02	0.01	0.02	0.03	0.01	0.01	0.02	0.01	0.02	0.01	0.01	0.01	0.01	0.01	0.01	0.01	0.01
0.01	0.00	0.00	0.01	0.00	0.00	0.00	0.00	0.00	0.00	0.00	0.00	0.00	0.00	0.00	0.00	0.00
0.00	0.00	–	–	–	–	0.00	–	0.00	–	0.00	–	–	–	0.00	–	–
0.00	0.00	0.00	0.00	0.00	0.00	0.00	0.00	0.00	0.00	0.00	0.00	0.00	0.00	0.00	0.00	0.00
0.06	0.06	0.06	0.05	0.06	0.06	0.06	0.06	0.06	0.07	0.07	0.06	0.07	0.07	0.06	0.06	0.06
0.00	0.00	0.00	0.00	0.00	0.00	0.00	0.00	0.00	0.00	0.00	0.00	0.00	0.00	0.00	0.00	0.00
2.01	2.01	2.01	2.01	2.01	2.01	2.01	2.01	2.01	2.01	2.01	2.01	2.01	2.01	2.01	2.01	2.01
7.70	7.50	6.62	7.00	7.38	7.84	7.31	7.52	8.04	8.81	8.36	7.88	8.65	8.55	7.60	7.23	7.31
24.81	40.70	36.12	16.57	33.28	31.72	49.02	35.80	19.36	49.70	24.82	34.30	26.95	45.12	32.57	25.06	23.16
0.67	0.72	0.81	0.89	0.89	0.70	0.80	0.69	0.79	0.85	0.80	0.78	0.83	0.85	0.75	0.74	0.74
0.23	0.12	0.24	0.30	0.15	0.14	0.19	0.17	0.19	0.06	0.16	0.12	0.14	0.08	0.13	0.13	0.16
617	603	599	632	647	555	661	572	525	560	546	564	580	597	541	631	558
41	42	47	45	43	40	43	42	39	35	38	40	36	37	41	44	43

Table 5.18. Continued

2.10	2.11	2.12	2.13	2.14	3.1	3.2	3.3	4.1	4.2	4.3	5.1	5.2	5.3	6.1	6.2	6.3
29.75	28.66	29.19	28.80	28.85	29.59	29.43	29.40	29.58	29.82	29.93	29.97	29.67	29.77	29.78	30.12	30.02
0.40	0.54	0.24	2.23	0.11	0.12	0.19	0.23	0.18	0.14	0.15	0.17	0.18	0.14	0.21	0.20	0.21
1.51	1.41	1.42	1.45	1.49	0.75	1.05	1.28	1.10	0.88	1.11	0.94	1.14	0.90	1.62	1.54	1.62
0.20	0.11	0.25	0.66	2.03	1.41	1.19	0.26	0.65	1.39	0.51	1.38	0.34	1.58	0.24	0.23	0.24
10.78	10.16	11.15	10.65	10.44	12.86	12.85	13.02	12.61	13.12	12.31	12.69	12.55	13.12	10.15	9.77	10.08
28.43	29.27	29.37	27.39	26.94	30.33	30.47	30.37	30.05	30.27	29.98	29.89	29.85	30.06	28.56	28.97	28.48
3.40	3.73	3.45	3.29	3.22	3.11	3.04	3.12	3.27	3.13	2.95	3.01	2.98	2.74	3.53	3.62	3.48
16.58	17.29	16.03	15.76	14.69	14.25	14.20	14.34	15.04	14.18	15.50	14.51	15.42	14.15	17.47	16.77	17.26
2.30	1.39	1.98	2.00	2.14	1.88	1.83	1.53	1.78	1.73	1.70	1.62	1.64	1.62	1.90	1.98	2.02
0.81	0.44	0.81	0.99	1.77	1.43	1.43	0.90	0.90	1.19	0.85	0.96	0.88	1.38	0.70	0.80	0.71
–	0.03	0.02	0.10	0.58	0.37	0.40	0.07	0.05	0.43	0.10	0.32	0.11	0.62	0.17	0.15	0.05
–	–	–	–	–	0.03	–	–	–	0.06	–	–	–	–	0.01	–	0.01
0.29	0.24	0.26	0.37	0.51	0.53	0.70	0.68	0.51	0.49	0.46	0.79	0.46	0.60	0.30	0.30	0.32
7.08	8.08	6.83	6.30	6.61	3.16	4.66	5.95	4.91	3.91	4.87	4.05	5.23	3.75	7.58	7.23	7.85
0.20	0.22	0.17	0.16	0.18	0.16	0.18	0.20	0.18	0.16	0.17	0.19	0.17	0.16	0.21	0.20	0.22
101.78	101.67	101.28	100.25	99.63	100.08	101.63	101.44	100.88	101.03	100.66	100.58	100.66	100.67	102.52	101.94	102.72
0.98	0.96	0.97	0.94	0.97	0.99	0.98	0.98	0.98	0.99	0.99	0.99	0.99	0.99	0.98	0.99	0.98
0.02	0.02	0.01	0.09	0.00	0.00	0.01	0.01	0.01	0.01	0.01	0.01	0.01	0.01	0.01	0.01	0.01
0.06	0.06	0.06	0.06	0.06	0.03	0.04	0.05	0.05	0.04	0.05	0.04	0.05	0.04	0.07	0.06	0.07
0.00	0.00	0.01	0.01	0.04	0.03	0.02	0.01	0.01	0.03	0.01	0.03	0.01	0.03	0.00	0.00	0.00
0.15	0.15	0.16	0.15	0.15	0.19	0.19	0.19	0.18	0.19	0.18	0.18	0.18	0.19	0.15	0.14	0.14
0.40	0.42	0.42	0.39	0.39	0.44	0.44	0.44	0.43	0.43	0.43	0.43	0.43	0.43	0.41	0.41	0.40
0.05	0.05	0.05	0.05	0.05	0.04	0.04	0.04	0.05	0.04	0.04	0.04	0.04	0.04	0.05	0.05	0.05
0.23	0.24	0.23	0.22	0.21	0.20	0.20	0.20	0.21	0.20	0.22	0.20	0.22	0.20	0.24	0.23	0.24
0.03	0.02	0.03	0.03	0.03	0.03	0.02	0.02	0.02	0.02	0.02	0.02	0.02	0.02	0.03	0.03	0.03
0.01	0.01	0.01	0.01	0.02	0.02	0.02	0.01	0.01	0.02	0.01	0.01	0.01	0.02	0.01	0.01	0.01
–	0.00	0.00	0.00	0.01	0.00	0.00	0.00	0.00	0.01	0.00	0.00	0.00	0.01	0.00	0.00	0.00
–	–	–	–	–	0.00	–	–	–	0.00	–	–	–	–	0.00	–	0.00
0.00	0.00	0.00	0.00	0.00	0.00	0.01	0.01	0.00	0.00	0.00	0.01	0.00	0.00	0.00	0.00	0.00
0.06	0.07	0.06	0.06	0.06	0.03	0.04	0.05	0.04	0.03	0.04	0.04	0.05	0.03	0.07	0.06	0.07
0.00	0.00	0.00	0.00	0.00	0.00	0.00	0.00	0.00	0.00	0.00	0.00	0.00	0.00	0.00	0.00	0.00
2.01	2.02	2.01	2.01	2.02	2.01	2.01	2.01	2.01	2.01	2.00	2.00	2.01	2.01	2.01	2.01	2.01
7.83	8.66	7.51	7.33	8.11	4.86	6.86	8.06	6.48	5.44	6.28	6.60	6.60	5.67	8.38	8.02	8.70
32.08	47.76	34.32	20.56	14.90	6.45	7.21	9.65	10.77	8.75	11.80	5.46	13.00	6.70	32.26	31.02	31.61
0.80	0.89	0.75	0.77	0.73	0.58	0.58	0.57	0.62	0.56	0.66	0.60	0.64	0.56	0.90	0.90	0.89
0.11	0.06	0.12	0.15	0.28	0.23	0.23	0.15	0.14	0.19	0.13	0.15	0.13	0.23	0.09	0.11	0.10
605	614	551	533	525	785	640	598	659	717	653	675	608	690	602	614	613
40	36	42	43	39	68	47	40	50	60	51	50	48	58	37	39	36

Table 5.18. Continued

6.4	6.5	6.6	6.7	6.8	6.9	6.10	6.11	6.12	6.13	6.14	6.15	8	9.1	9.2	11
29.91	29.83	29.96	30.09	30.08	29.96	29.99	30.13	29.63	29.91	30.25	29.97	29.32	28.83	29.97	28.93
0.19	0.20	0.21	0.21	0.20	0.19	0.20	0.20	0.21	0.17	0.17	0.19	0.38	0.64	0.27	0.33
1.55	1.62	1.60	1.63	1.60	1.61	1.47	1.59	1.58	1.56	1.53	1.52	0.99	1.12	0.74	1.09
0.22	0.26	0.22	0.25	0.25	0.26	0.23	0.23	0.18	0.23	0.17	0.23	0.89	0.21	0.04	0.82
10.29	10.25	10.26	9.76	10.13	10.04	10.65	10.33	10.13	10.41	10.50	9.90	12.56	12.01	12.60	11.02
28.51	28.43	28.50	28.29	28.28	28.12	29.38	28.23	28.67	29.03	29.19	28.61	30.32	30.28	32.18	29.11
3.42	3.27	3.49	3.58	3.53	3.34	3.37	3.59	3.65	3.42	3.68	3.55	3.27	3.34	3.62	3.06
17.34	17.07	17.18	17.53	17.60	16.68	16.74	16.82	17.18	17.20	16.77	17.22	14.61	15.34	15.81	15.80
1.95	2.02	2.01	2.24	2.12	2.13	1.99	1.94	2.23	2.03	2.08	2.08	1.46	1.70	1.87	1.93
0.79	0.80	0.86	0.96	0.95	1.15	0.82	1.00	0.73	0.86	0.87	0.82	0.60	0.84	0.59	1.06
0.04	0.11	0.09	0.09	0.07	0.17	0.12	0.11	0.11	0.03	0.09	0.11	0.04	0.05	–	–
–	–	–	0.01	–	–	–	–	–	–	–	–	–	0.07	–	0.02
0.29	0.33	0.30	0.30	0.33	0.30	0.32	0.32	0.32	0.29	0.31	0.30	0.33	0.39	0.27	0.34
7.33	7.64	7.52	7.73	7.58	7.63	6.91	7.42	7.47	7.23	7.14	7.11	5.37	7.18	4.07	5.45
0.22	0.21	0.21	0.23	0.23	0.20	0.18	0.21	0.21	0.21	0.20	0.21	0.16	0.21	0.13	0.15
102.13	102.18	102.52	103.00	103.01	101.85	102.44	102.16	102.38	102.64	103.06	101.88	100.38	102.28	102.23	99.19
0.98	0.98	0.98	0.98	0.98	0.99	0.98	0.99	0.98	0.98	0.99	0.99	0.98	0.96	0.98	0.98
0.01	0.01	0.01	0.01	0.01	0.01	0.01	0.01	0.01	0.01	0.01	0.01	0.01	0.03	0.01	0.01
0.06	0.07	0.07	0.07	0.07	0.07	0.06	0.07	0.07	0.06	0.06	0.06	0.04	0.05	0.03	0.05
0.00	0.01	0.00	0.01	0.01	0.01	0.00	0.00	0.00	0.00	0.00	0.00	0.02	0.00	0.00	0.02
0.15	0.15	0.15	0.14	0.14	0.14	0.15	0.15	0.15	0.15	0.15	0.14	0.18	0.17	0.18	0.16
0.41	0.40	0.40	0.40	0.40	0.40	0.42	0.40	0.41	0.41	0.41	0.41	0.44	0.44	0.46	0.43
0.05	0.05	0.05	0.05	0.05	0.05	0.05	0.05	0.05	0.05	0.05	0.05	0.05	0.05	0.05	0.04
0.24	0.24	0.24	0.24	0.24	0.23	0.23	0.23	0.24	0.24	0.23	0.24	0.21	0.22	0.22	0.23
0.03	0.03	0.03	0.03	0.03	0.03	0.03	0.03	0.03	0.03	0.03	0.03	0.02	0.02	0.02	0.03
0.01	0.01	0.01	0.01	0.01	0.01	0.01	0.01	0.01	0.01	0.01	0.01	0.01	0.01	0.01	0.01
0.00	0.00	0.00	0.00	0.00	0.00	0.00	0.00	0.00	0.00	0.00	0.00	0.00	0.00	–	–
–	–	–	0.00	–	–	–	–	–	–	–	–	–	0.00	–	0.00
0.00	0.00	0.00	0.00	0.00	0.00	0.00	0.00	0.00	0.00	0.00	0.00	0.00	0.00	0.00	0.00
0.06	0.07	0.07	0.07	0.07	0.07	0.06	0.07	0.07	0.06	0.06	0.06	0.05	0.06	0.04	0.05
0.00	0.00	0.00	0.00	0.00	0.00	0.00	0.00	0.00	0.00	0.00	0.00	0.00	0.00	0.00	0.00
2.01	2.01	2.01	2.01	2.01	2.01	2.01	2.01	2.01	2.01	2.01	2.01	2.01	2.01	2.01	2.01
8.10	8.53	8.32	8.52	8.48	8.41	7.78	8.26	8.33	8.00	7.96	7.91	6.31	8.26	4.86	6.42
32.53	29.18	32.22	33.50	28.90	33.22	26.97	30.01	29.82	32.11	29.67	30.52	19.41	22.54	17.60	19.15
0.88	0.87	0.87	0.94	0.91	0.87	0.82	0.85	0.88	0.86	0.83	0.91	0.61	0.67	0.65	0.75
0.11	0.11	0.12	0.13	0.13	0.16	0.11	0.14	0.10	0.12	0.12	0.11	0.10	0.13	0.09	0.16
647	597	618	637	654	577	553	619	603	625	610	641	610	618	628	570
39	37	38	37	37	37	40	38	38	39	39	40	50	38	65	49

Chapter 6 Implication for tectonic process of the Sør Rondane Mountains

6.1 Combining metamorphic evolution with tectonic process in the central Sør Rondane Mountains

As the results of previous chapters, following interpretations are obtained;

・The metamorphic rocks in Austkampane area show the signature of decompression near peak condition, ca. 800 °C and 0.4-0.5 GPa, at 640-600 Ma. Although the timing has not been well-constrained, subsequent hydration caused retrogression. Finally the rocks were re-heated by granite intrusion at ca. 500 Ma in the andalusite stability field. (Hereafter, the rocks, which experienced decompression near peak granulite-facies condition at 640-600 Ma are referred to as "**A-type**" rock, Table 6.1.)

・The metamorphic rocks in Brattnipene area and Menipa area have experienced granulite-facies metamorphism of which P-T conditions were estimated as at ca. 800 °C and 0.7-0.8 GPa accompanying pressure increase at 640-600 Ma and subsequent retrograde hydration at ca. 570-550 Ma during isobaric cooling. Finally the rocks were hydrated in andalusite stability field. (Hereafter, the rocks, which experienced pressure increase near peak

granulite-facies condition at 640-600 Ma are referred to as “**B-type**” rock)

・Whereas the rocks occurring in the areas described above, the rocks in Lunckeryggen area preserve prograde signatures and they have not experienced 640-600 Ma event. (Hereafter, the rocks, which preserve prograde signatures and demonstrate amphibolite-facies at ca. 550 Ma are referred to as “**L-type**” rock.) Distribution of each type is shown in Fig. 6.1.

Compared A-type rocks with B-type rocks, although mode of pressure change near peak condition is different, they show similarity on the temperature condition and the timing of peak metamorphism. Such similarity implies that A-type and B-type units originally behaved as single geological unit. Garnet grains in pelitic gneisses from both types commonly include spinel with 5-12 wt% of ZnO and sillimanite inclusions. The paragenesis of these mineral inclusions can be interpreted as the products of staurolite break down in the sillimanite stability field. This probably supports the previous unity of the two type units. Difference of pressure variation between A-type rocks and B-type rocks near peak condition is explained as that B-type unit thrust up on A-type unit, as an intra-plate phenomenon, during 640-600 Ma event.

L-type rocks record quite different nature from A- and B-type rocks in

terms of metamorphism and geochronology. L-type rocks have been subjected to up to amphibolite facies metamorphism at ca. 550 Ma, however have not experienced 640-600 Ma event. Lack of signature of 640-600 Ma event in L-type rocks indicates that L-type rocks and the other type rocks do not share the geological event at 640-600 Ma. This strongly suggests that L-type unit would be separate geological unit from A- and B-type units. However three types of rocks shear signatures of geological events around/after ca. 550 Ma; retrograde hydration and pegmatite intrusion in A- and B-type units and metamorphism in L-type unit. This age consistency implies the possibility that A- and B-type units and L-type unit joined together around ca. 550 Ma.

Structural relationship between B-type unit and L-type unit can be observed at Menipa area and the boundary area between Brattnipene area and Lunckeryggen area (Fig .6.2). At both localities, L-type unit is apparently overlain by B-type unit. Especially at Menipa area, the boundary between B-type unit and L-type unit seems nearly-horizontal and parallel to the foliation observed in both units. This implies that nappe-like structure is essentially prevailing in the central Sør Rondane Mountains. Such structure can explain complex distribution of the metamorphic grade and metamorphic ages as klippe and fenster due to various

degree of denudation.

Nappe structure also can explain the geological events in A- and B-type units and L-type unit at ca. 550 Ma (Fig. 6.3). Accompanied by A- and B-type units thrusting up on L-type unit, L-type unit should be heated and dehydrated (and might be partially molten). Then A- and B-type units probably are subjected to hydration and pegmatite intrusion under extensional tectonics. Thus, nappe structure is compatible to interpret field relation and geological event between A- and B- type units and L-type unit.

Field observations that all three units are intruded by ca. 500 Ma undeformed granites indicate that thrusting must be before ca. 500 Ma. From Walnumfjella and to the west, relatively high-angle structure is dominantly observed, indicating low-angle nappe structure seems to be not consistent in those areas. However meta-tonalite in Lunckeryggen is geochemically different from that in Walnumfjella (Kamei, personal communication). It indicates that Lunckeryggen and Walnumfjella are geologically discontinuous, that is, Walnumfjella and to the west area might be structurally modified after forming nappe structure. High-angle structure in Walnumfjella area should be highly associated with an activity of Main Shear Zone, therefore timing of deformation

is probably a key to resolve this issue.

6.2 Comparison of tectonic process between the Sør Rondane Mountains and “EAAO” related terranes at Gondwana assembly

Since the Sør Rondane Mountains is located within collision zone inferred between East Africa and Antarctica, so-called East Africa-Antarctic Orogen (EAAO; Jacobs & Thomas, 2004), tectonic process is required to be correlated with Mozanbique, central Dronning Maud Land in East Antarctica, Sri Lanka and so on.

Mozambique is divided into two dominant blocks, Namuno Block and Nampula Block, by the Lurio Belt. Namuno Block comprises an accretionary complex which is subjected to high-grade metamorphism. Nampula Block is dominated by medium-grade tonalitic gneisses and paragneisses (e.g. Viola et al., 2006). At least two high-grade klippens, Monapo Complex and Mugeba Complex, are recognized overlying the Nampula Block (Pinna et al., 1993). These klippens contain granulite-facies ortho- and para-gneisses and have been regarded as remnants of a larger thrust sheet. Age distributions of igneous and metamorphic events in Namuno and Nampula Blocks are compiled by Grantham

et al (2008). They suggested that a significant difference is that Namuno Block is characterized by ca. 650-900 Ma, which is absent from Nampula Block. ca. 630 Ma is recognized only from Monapo and Mugeba klippens in Nampula Block, which is clearly demonstrate these klippens have age characteristics similar to rocks in Namuno Blocks. Based on these age distributions, Namuno Block and Nampula Block should be different geological units, and they juxtaposed as low-angle nappe structure (e.g. Grantham et al., 2008).

Such geological relations are also observed in western and central Dronning Maud Land and Sri Lanka (Fig. 6.4). In Dronning Maud Land, granulite-facies rocks are distributed in Schirmacher Hills and eastern Mühlig-Hofmanfjella and they commonly record 600-900 Ma events. On the other hand, Sverdrupfjella, Kirwanveggen and Gjelsvikfjella in western Dronning Maud Land lack 600-900 Ma ages (e.g. Bisnath & Frimmel, 2005; Granttham et al., 1995). In Sri Lanka, granulite-facies Highland Complex is interpreted as to be overlying amphibolite-facies Vijayan Complex (Kleinschrodt, 1994). Ages 600-900 Ma are obtained from only in Highland Complex, these ages are absent in Vijayan Complex (Grantham et al., 2008). Based on such broaden observation, Grantham et al. (2008) proposed mega-nappe structure as dominant tectonics in

the EAAO region. Whereas, several possible problems with this model has been also pointed out. Jacobs et al. (2008) pointed out following problems: (1) the high-grade klippens overlying 600-900 Ma absent blocks are never seen to be intruded by the late-tectonic granites as might be expected, (2) the granitoids are typically charnockitic A-types and not the minimum-melt granitoids and (3) timing of shearing along the Lurio Belt should be ca. 530-500 Ma (Bingen et al., 2006a,b) which is significantly younger than 620-550 Ma of main movement on the structure. In Sør Rondane Mountains, two distinct granitoid activities are recognized; ca. 550 Ma pegmatite and ca. 500 Ma granite. That all three units are intruded by ca. 500 Ma undeformed granites indicate piling-up before ca. 500 Ma. 550 Ma pegmatites intrude hanging-wall A- and B-type units. Pegmatite generation should be nearly simultaneous with juxtaposition of A- and B-type units and L-type unit, therefore pegmatites are probably products resulted in thrusting. Such pegmatites are undeformed, which implies that thrust movement had finished around ca. 550 Ma. These observations in the Sør Rondane Mountains resolve the previously described problems on mega-nappe model in EAAO areas. However If such large-scale nappe structure is dominant in the EAAO region, the following problems are remained;

・ thermal process causing widespread high-grade metamorphism at ca. 600 Ma

・ exhumation process of such broad high-grade metamorphic terranes at ca. 550 Ma

To clarify these problems, comprehensive analyses of coeval metamorphism, magmatism and fluid activity should be required.

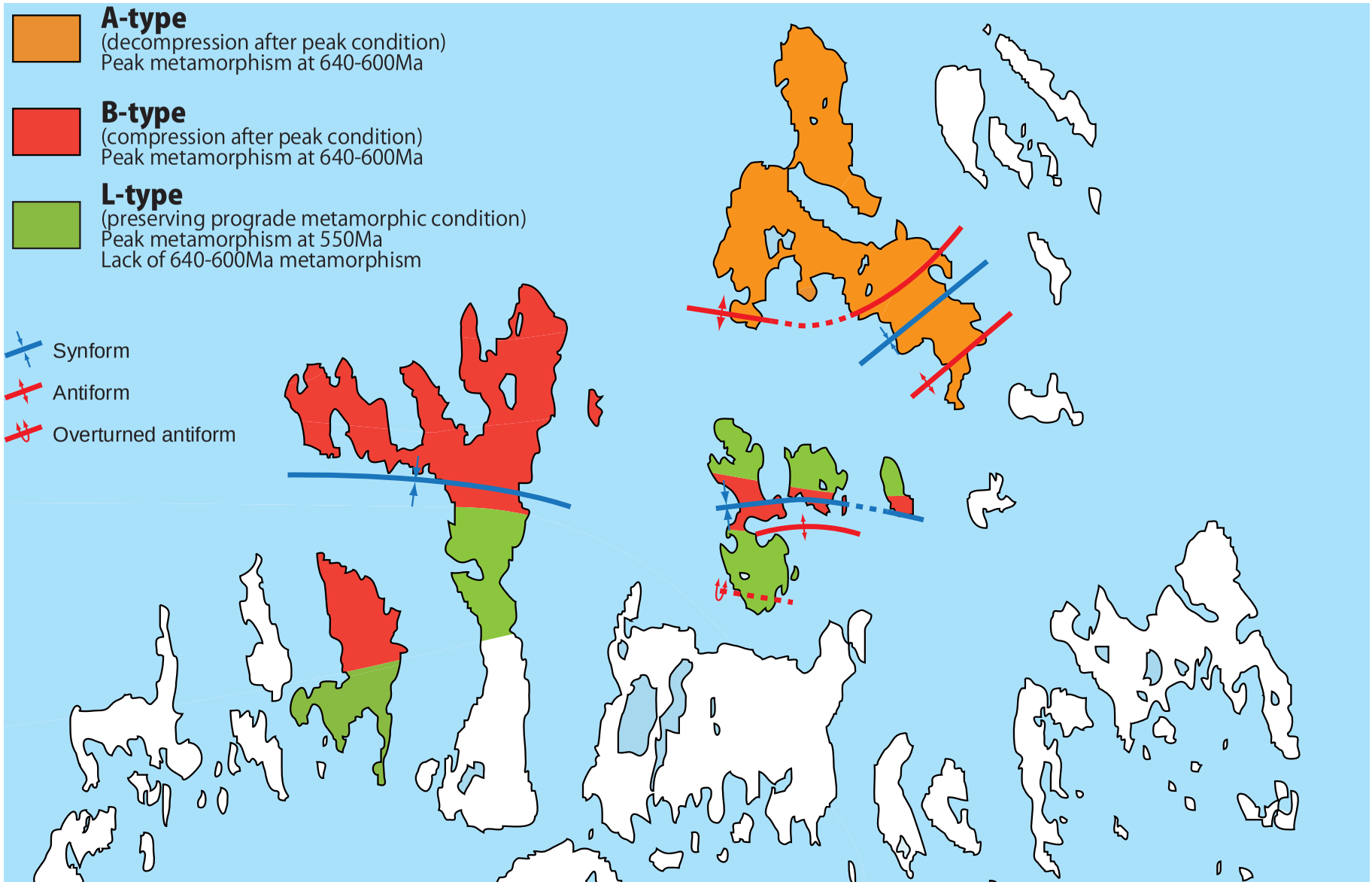

Fig. 6.1. Distributin of Brattnipene type, Austkampane type and Lunckeryggen type rocks in the central Sør Rondane Mountains.

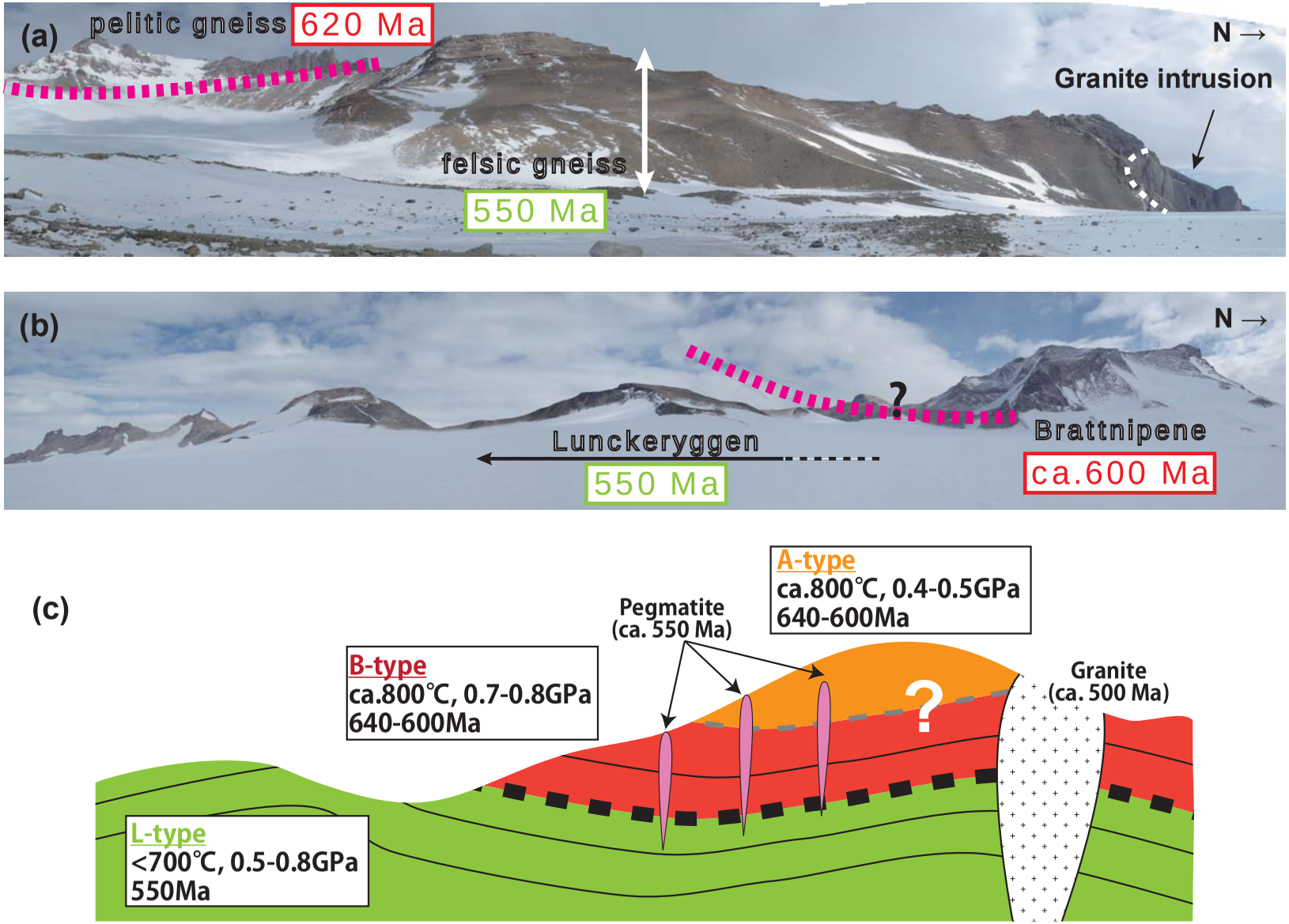

Fig. 6.2. structural relations between B-type and L-type. (a) Field relation observed at the northern part of Menipa area. The lithological boundary appears almost horizonrtal. L-type is apparently overlain by B-type. (b) Field relation observed at the boundary area between Lunckeryggen area and Brattnipene area. (c) Simplified schematic of structural relationship among A-type, B-type and L-type.

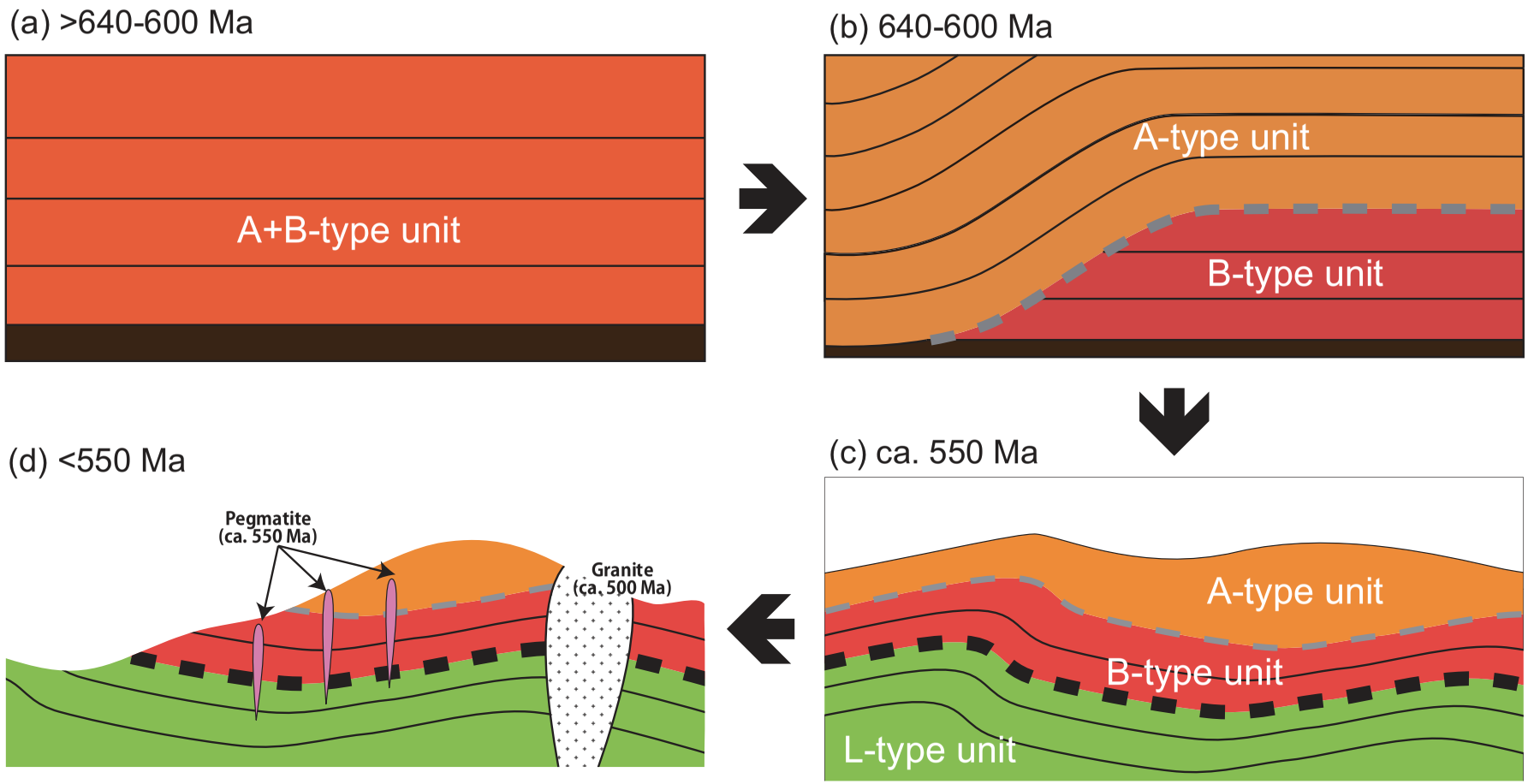

Fig. 6.3. Schematic tectonic history of the central Sør Rondane Mountains. (a) > 640-600 Ma. A- and B-type units behaved as a sigle geological unit. (b) At 640-600 Ma. A-type unit thrusted onto B-type unit during granulite-facies metamorphic event. (c) At ca. 550 Ma. A- and B-type units thrusted onto L-type unit. L-type unit was subjected to amphibolite-facies metamorphism. (d) < 550 Ma. Pegmatites intruded into A- and B-type units slightly after pile-up. Finally granites intruded into all three units at ca. 500 Ma.

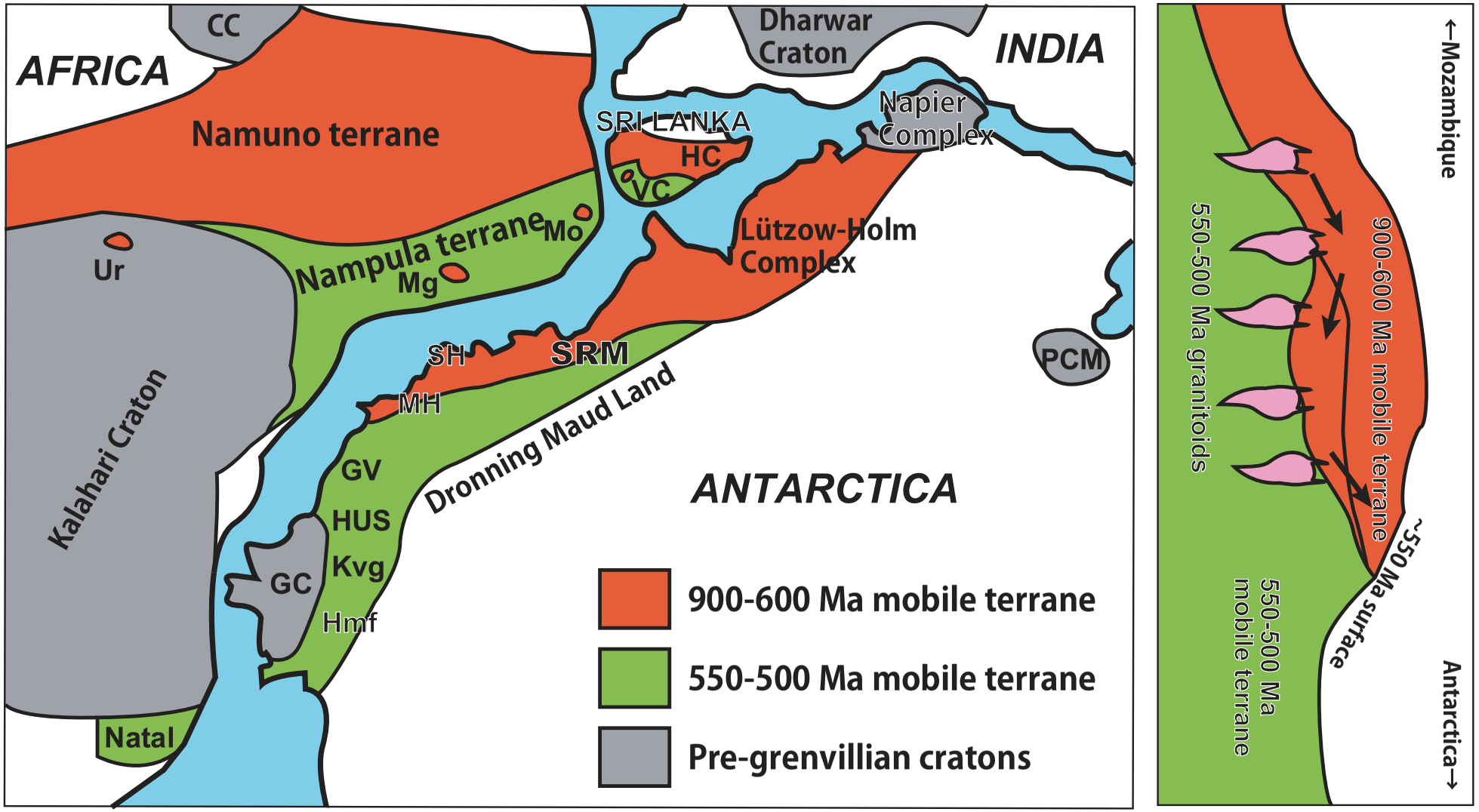

Fig. 6.4. Schematic map of the various crustal blocks “EAAO” related terranes and schematic cross-section. (After Grantham et al., 2008) VC, Vijayan Complex; HC, Highland Complex; Mo, Monapo Klippen; Mg, Mugeba Klippen; L, Lurio Belt; CC, Congo Craton; SH, Schirmacher Hills; MH, Mühlig-Hofmannfjella; GV, Gjelsvikfjella; HUS, Sverdrupfjella; Kvg, Kirwanveggen; Hmf, Heimefrontfjella; GC, Grunehogna Craton; Ur, Urungwe Klippen; PCM, Prince Charles Mountain.

Table 6.1. Classification of the metamorphic rocks in the central Sør Rondane Mountains.

Area	sample No.	Mineral assemblage	Peak/prograde									Retrograde					Reaction texture	Rt Exs.	Ti phase	T range (°C) Ti-in-Qtz		T_{other} (°C)	Method	U-Pb ages		Classification
			Grt	Opx	Cpx	Hbl	Bt	Sil	Crd	Ep	Other	And	Bt	Ms	Ep	Other				F	D			igneous	metamorphic	
Brattnipene	07120402A	Grt-Bt-Sil	○				○	○					○	○			Grt⇒Bt+Pl	-	Rt	~670					620-550 (M)	B type
	07121003A	Opx-Cpx-Hbl-Bt		○	○	○	○										Opx+Pl ⇒Hbl+Bt+Qtz	-	Ilm	820~760	830~760	850	OC	1000-950	600	B type
	07121003B	Hbl-Bt-Ep											○		○	Hbl		○	Ilm	690~640	820~750	700	HP			B type
	07121003D	Pegmatite																						550		intrusion
	A07123001E	Grt-Opx-Bt	○	○			○											-	Ilm			770	GO			B type
	A07123001F	Grt-Opx-Bt	○	○			○											-	Ilm	770~710						B type
	A07123001I	Grt-Opx-Hbl	○	○		○												-	Ilm			750	GO			B type
	A07123001N	Opx-Cpx-Hbl		○	○	○												-	Ilm			810	OC			B type
	A07123001P	Grt-Crn-Bt	○				○	○			Crn,Spl		○				Sil+Spl⇒Grt+Crn	-	Ilm							B type
	A07123001R	Grt-Opx-Bt	○	○			○											-	Ilm	750~690		750	GO			B type
	A07123001AC	Hbl-Bt				○	○											-	Ilm							other
	A07123001AF	Grt-Bt	○				○						○				Grt⇒Bt+Pl	-	Ilm	710~660		770	GB			other
	B07121703A	Pegmatite																						550		intrusion
	BC08010302A	Grt-Bt	○				○						○	○			Grt⇒Bt+Pl	○	Rt	~670	~800					B type
	BC08010302B	Grt-Crn-Bt	○				○	○			Crn,Spl						Sil+Spl⇒Grt+Crn	-	Rt			780	GB			B type
	BC08010302C	Grt-Bt-Sil	○				○	○				○	○	○			Grt⇒Bt+Pl	○	Rt	~630	~730			1000	670-580	B type
	BC08010401B	Grt-Bt-Sil	○				○	○					○				Grt⇒Bt+Pl	-	Rt							B type
	BC08010502B	Grt-Bt	○				○											-	Ttn	600~560				780	690	other
	BC08010504A	Hbl-Bt-Ep				○	○			○								-	Ttn	500~470						L type
	84021904B	Grt-Bt-Sil	○				○	○					○			Ky/Sil	Grt⇒Bt+Ky/Sil	-	Rt							B type
	85011501B	Grt-Bt-Sil	○				○	○					○			Ky/Sil	Grt⇒Bt+Ky/Sil	-	Rt							B type
Menipa	AC08011301M	Grt-Bt	○				○											○	Rt	~650	~860	750	GB	~1080	620	B type
	AC08011601A	Hbl-Bt				○	○											-	-	570~530						L type
	AC08012001A	Hbl-Bt				○	○											○	Ttn	480~450		620	HP		560	L type
Austkampane	AC07121302B	Grt-Bt-Sil	○				○	○					○	○			Grt⇒Bt+Sil	○	Rt	~620	~850					A type
	AC07121303E	Grt-Crd-Bt	○				○	○								Crd	Grt+Sil+Bt⇒Crd	○	Rt							A type
	AC07121501U	Granite																						500		intrusion
	AC07121601A	Granite																						520		intrusion
	AC07121701C	Grt-Crd-Bt	○				○		○									○	Rt	~670	~830	760	GCrd		640 (M)	A type
	AC07121702B	Grt-Bt, Grt-Crn-Bt	○				○	○			Crn,Spl		○	○			Sil+Spl⇒Grt+Crn Grt⇒Bt+Pl	-	-	710~660		550	GB			A type
	AC07121801H	Grt-Crd-Bt	○				○	○								Crd	Grt+Sil+Bt⇒Crd	○	Rt							A type
	AC07121801M	Grt-Crd-Oam	○				○		○		Oam							○	Rt	~590	~830	780	GCrd		610 (M)	A type
	BC07122801C	Grt-Bt	○				○						○	○			Grt⇒Bt+Pl	○	Rt	~590	~760					A type
	BC07122801D	Grt-Bt-Sil	○				○	○					○	○			Grt⇒Bt+Pl	-	Rt			550	GB			A type
	BC07122804A	Grt-Bt-Sil	○				○	○						○			Grt⇒Bt+Sil	○	Rt							A type
	BC07122804	Pegmatite																						640, 520 (Hokada et al)		intrusion (2types)
	BC07122805C	Grt-Bt	○				○											-	Ttn	530~490				640		other
	BC07122903A	Grt-Bt	○				○						○	○			Grt⇒Bt+Pl	○	Ilm	620~570	900~820					A type
	AC07121901A	Hbl-Bt				○	○			○								-	-	590~550		700	HP	890	600-550	other
Walnumfjella	BC08010602J	Grt-Bt	○				○											-	-	600~560						L type ?
	BC08010604A	Grt-Hbl-Bt	○			○	○											-	Ilm					1080	600	B type ?
	BC08010604E	Grt-Hbl-Bt	○			○	○										Grt⇒Bt+Pl	○	Ilm	650~600	720~660	610	GH			B type ?
Lunckeryggen	B08012201I	Grt-Hbl-Bt	○			○	○											-	-	550~510		660-550	GH	990		L type
	B08012203A	Grt-Bt	○				○											-	Ilm	540~500						L type
	B08012204	Grt-Hbl-Bt	○			○	○			○								-	Ilm	520~480		710-650	GH			L type
	B08012302A	Hbl-Bt				○	○			○								-	Ttn	480~450						L type
	B08012304C	Grt-Hbl-Bt	○			○	○			○								-	Ilm							L type
	B08012304D	Grt-Hbl-Bt	○			○	○											-	Ttn							L type
	B08012304E	Grt-Hbl-Bt	○			○	○											-	-	480~450		650-590	GH	1000	550	L type

$T_{Ti\text{-}in\text{-}Qtz}$: based on Wark & Watson (2006). D: with 100 μm of probe diameter and 25 kV of accerelating voltage, F: with 2 μm and 15 kV. GB:Grt-Bt thermometer (Holldaway, 2000), GCrd: Grt-Crd thermometer (Perchuk&Lavrent'eva, 1983), GO: Grt-Opx thermometer (Harley. 1984), OC: Opx-Cpx thermometer (Taylor, 1998), GH: Grt-Hbl thermometer (Graham&Powell, 1984), HP: Hbl-Pl thermometer (Holland&Blundy, 1994). B type: P increase near peak T at 650-600Ma. A type: P decrease near peak T at 650-600Ma. L type: amphibolite-facies peak metamorphism at 550Ma.

Table 6.2. Metamorphic conditions and their ages in EAAO related areas.

	Locality	P-T path	Peak condition	Peak age	Retrograde condition	Retrograde age
Mozanbique	Muguba&Monapo klipper	ITD→IBC	900-1000ºC, >1.0GPa	640-610Ma	700ºC, 0.6-0.7GPa	590-570Ma
	Nampula Block	Heating	>700 ºC, <0.7-0.8GPa	530-495Ma		
cDML	Shirmacher Hills	ITD→IBC	950-1050ºC, 0.9-1.0GPa	770Ma	700ºC, 0.6-0.7GPa	ca. 550Ma
	Gjelsvikfjella	ITD→IBC	700-800℃, 1.0GPa	1090-1030Ma	650℃, 0.5GPa	ca. 550Ma
	Muhlig-Hofmannfjella	Heating	?	ca. 550Ma		
	Kirwanveggen	Heating	700℃, 0.65GPa	～530Ma		
Sri Lanka	Highland Complex	ITD→IBC	1100℃, 1.2GPa	ca. 550Ma?	600-700ºC, 0.6-0.7GPa	ca. 550Ma?
Sør Rondane	B type	ITC→IBC	800℃, 0.7-0.8GPa	640-600Ma		570-550Ma
	A type	ITD→IBC	800℃, 0.4-0.5GPa	640-600Ma		ca. 550Ma
	L type	Heating	600-700℃, 0.5-0.8GPa	550Ma		

Data from Grantham et al. (2008) and Baba et al. (2008). cDML: central Dronning Maud Land, ITD: isothermal decompression, ITC: isothermal compression, IBC: isobaric cooling

Chapter 7 Conclusions

1. Metamorphic rocks in the central Sør Rondane Mountains can be divided into three types based on petrological characteristics including presence/absence of signatures of granulite-facies condition, signature of retrograde hydration, mode of compositional zoning of garnet and so on. Rocks in Austkampane preserve ca. 800 °C and 0.4-0.5 GPa of peak metamorphic condition with decompression and subsequent intense hydration (A-type), Rocks in Brattnipene and part of Menipa indicates ca. 800 °C and 0.7-0.8 GPa of peak metamorphic condition with compression and subsequent intense hydration (B-type), Rocks mainly from Lunckeryggen show signatures of prograde metamorphism and amphibolite-facies peak condition (L-type).

2. Rutile exsolution in quartz was found from the retrograde hydrated gneisses in widespread central Sør Rondane Mountains. On the basis of the pre-exsolution Ti concentration in quartz integrated using EPMA with defocused beam, pre-hydration (near peak condition) temperature condition can be estimated with Ti-in-quartz thermometer (Wark & Watson, 2006). As the result of application of this method for the central Sør Rondane Mountains, high-grade (700-800 °C) metamorphism should be pervasive event in the NE terrane

(Austkampane, Brattnipene and Menipa areas). On the other hand, <600 °C of the metamorphic condition is recognized in the SW terrane (mainly Lunckeryggen area). Such distributions of temperature condition estimated with Ti-in-quartz thermometer support the distributions of each rock types.

3. U-Pb zircon SHRIMP and U-Th-Pb monazite EPMA datings indicate that the timing of peak granulite-facies metamorphism of A- and B-type rocks is ca. 640-600 Ma. Ages of ca. 570-550 Ma are also detected and interpreted as timing of hydration. Contact metamorphism caused by minor granite intrusion is locally found in A-type rocks occurs at ca. 500 Ma. Timing of amphibolite-facies metamorphism of L-type rocks is ca. 550 Ma. L-type rocks lack ca. 640-600 Ma events, indicating that A- and B-type rocks and L-type rocks do not share the geological event before 550 Ma. This strongly suggests that L-type rocks would belong to separate geological unit from A- and B-type rocks.

4. L-type unit is structurally apparently overlain by B-type unit. The boundary between B-type unit and L-type unit seems nearly-horizontal and parallel to the foliation observed in both units. This implies that nappe-like structure, A- and B-type units thrust up onto L-type unit, is essentially prevailing in the central Sør Rondane Mountains. Such structure can explain complex

distribution of A-, B- and L-type rocks as klippe and fenster due to various degree of denudation.

5. Nappe-like structure has been proposed in EAAO related areas including Mozambique, central Dronning Maud Land and Sri Lanka (e.g. Grantham et al., 2008). This commonality indicates that nappe structure should be dominant tectonics in the EAAO region.

Acknowledgments

This thesis has been conducted at the National Institute of Polar Research (Department of Polar Science, the Graduate University for Advanced Studies) under the supervision of Prof. Yoichi Motoyoshi, Prof. Kazuyuki SHiraishi and Dr. Tomokazu Hokada. I would like to express my appreciation to them for discussion, support and encouragement.

Geological survey in Antarctica was carried out as part of 49th Japanese Antarctic Research Expedition (JARE) led by S. Imura and S. Ushio. I would like to thank members of 48th and 49th Japan Antarctic Research Expedition and the crew of the icebreaker *Shirase* for their support. I am also grateful to A. Hubert, G. Johnson-Amin and members of Belgian Antarctic Research Station 2007–2008 for supporting our fieldwork. I appreciate the members of Geology team of JARE 49 including Prof. Y. Osanai, Dr. T. Toyoshima, Prof. S. Baba, Dr. T Hokada, Dr. N. Nakano and Mr. M. Abe. Field work with them has been amazing and beautiful experience for me. The cost to conducting field work in Antarctica was offset in part by grants-in-aid from the Graduate University for Advanced Studies and the Japan Polar Research Association. I appreciate their financial support.

Prof. Y. Hiroi, Prof. H. Ishizuka, Prof. T. Kawasaki,Prof. Y. Osanai, Prof.

M. Owada, Prof. N. Tsuchiya and other JARE geology members are thanked for lively discussion and encouragement.

Laboratory work conducted at NIPR has been supported by staffs and students in NIPR, especially Dr. D.J. Dunkley for SHRIMP, Dr. A. Yamaguchi for EPMA and Mr. H. Sasaki for making thin sections. Ms. K. Arai, Ms F. Matsushita, Prof. K. Shibuya, Dr. Y. Nogi and Dr. Y. Aoyama gave me dairy support and encouragement. Thanks are due to them.

References

Adams, C.J., Höhndorf, A. 1984. Age of the metamorphic basement of the Salamander and Lanterman ranges, northern Victoria Land, Antarctica. Geological Evolution of Antarctica, 149-153.

Asami, M., Shiraishi, K. 1987. Kyanite from the western part of the Sør Rondane Mountains, East Antarctica. Proceedings of the NIPR Symposium on Antarctic Geosciences 1, 150–168.

Asami, M., Grew, E.S., Makimoto, H. 1990. A staurolite-bearing corundum-garnet gneiss from the eastern Sør Rondane Mountains, Antarctica. Proceedings of the NIPR Symposium on Antarctic Geosciences, 4, 22–40.

Asami, M., Grew, E.S., Makimoto, H. 2007. Relict sapphirine+kyanite and spinel+kyanite associations in pyrope garnet from the eastern Sør Rondane Mountains, East Antarctica. Lithos, 93, 107-125.

Asami, M., Makimoto, H., Grew, E.S., Osanai, Y., Takahashi, Y., Tsuchiya, N., Tainosho, Y., Shiraishi, K. 1991. Geological map of Balchenfjella, Sør Rondane Mountains, Antarctica. Antarctic Geological Map Series, sheet 31, scale 1 : 100,000. National Institute of Polar Research, Tokyo.

Asami, M., Osanai, Y., Shiraishi, K., Makimoto, H. 1992. Metamorphic evolution of the Sør Rondane Mountains, East Antarctica. In: Yoshida, Y., Kaminuma, K., Shiraishi, K., (eds) Recent Progress in Antarctic Earth Science, TERRAPUB, Tokyo, 7-15.

Asami, M., Suzuki, K., Grew, E.S. 2005. Monazite and zircon dating by the chemical Th–U–total Pb isochron method (CHIME) from Alasheyev Bight to the Sør Rondane Mountains, East Antarctica: a reconnaissance study of the Mozambique suture in eastern Queen Maud Land. Journal of Geology, 113, 59–82.

Asami, M., Suzuki, K., Adachi, M. 1989. Geology of the eastern Sør Rondane Mountains, East Antarctica. Proceedings of the NIPR Symposium on Antarctic Geosciences,3, 81-99.

Asami, M., Suzuki, K., Adachi, M. 1996. Monazite ages by the chemical Th-U-total Pb isochron method for pelitic gneisses from the eastern Sør Rondane Mountains, East Antarctica. Proceedings of the NIPR Symposium on Antarctic Geosciences, 9, 49–64.

Asami, M., Suzuki, K., Adachi, M. 1997. Th, U and Pb data and CHIME dating of monazites from metamorphic rocks of the Rayner, Lützow-Holm,

Yamato-Belgica and Sør Rondane Complexes, East Antarctica. Proceedings of the NIPR Symposium on Antarctic Geosciences,10, 130–152.

Baba, S., Toyoshima, T., Osanai, Y., Nakano, N., Adachi, T., Hokada, T. 2008. Mode of occurrence of sapphirine, corundum and staurolite in Brattnipene, Sør Rondane Mountains, East Antarctica. The 28 th Symposium on Polar Geosciences Program and Abstracts, 24.

Bingen, B., Viola, G., Henderson, I.H.C., et al. 2006a. Geochronology of Pan-African terrain assembly in the NE Mozambique. In: 21st Colloquium of African Geology, Maputo, Mozambique. Abstracts, 12-14.

Bingen, B., Boyd, R., Thomas, R.J. et al. 2006b. Crustal architecture in Northern Mazambique: results from a regional bedrock mapping project. In: EGU General Assembly, Vienna, Geophysical Research Abstracts, Vol. 8, 06049.

Bisnath, A., Frimmel, H.E. 2005. Metamorphic evolution of the Maud Belt: P-T-t path for high-grade gneisses in Gjelsvikfjella, Dronning Maud Land, East Antarctica. Precambrian Research, 43, 505-524.

Bohlen, S.R., Essene, E.J. 1977. Feldspar and oxide thermometry of granulites

in the Adirondack Highlands. Contributions to Mineralogy and Petrology. 62, 153–169.

Breton, N.L., Thompson, A.B. 1988. Fluid-absent (dehydration) melting of biotite in metapelites in the early stages of crustal anatexis. Contributions to Mineralogy and Petrology 99, 226-237

Ellis, D.J., Thompson, A.B., 1986. Subsolidus and partial melting reactions in the quartz excess CaO+MgO+Al2O3+SiO2+H2O system under water-excess and water-deficient conditions to 1.0 GPa: some implications for the origin of peraluminous melts from mafic rocks. Journal of Petrology. 27, 91–121.

Fitzsimons, I.C.W. 2000. A review of tectonic events in the east antarctic shield and their implications for gondwana and earlier supercontinents. Journal of African Earth Sciences, 31, 3-23.

Graham, C.M., Powell, R. 1984. Garnet-hornblende geothermometer: Calibration, testing, and application to the Pelona Schist, southern California. Journal of Metamorphic Geology. 2, 13 – 31.

Grantham, G.H., Maboko, M., Eglington, B.M. 2003. A review of the evolution of the Mozambique Belt and implications for the amalgamation of

Rodinia and Gondwana. In: Yoshida, M., B. F. Windley & S., Dasgupta (eds.) Proterozoic East Gondwana, Supercontinent Assembly and Breakup. Geological Society, London, Special Publications, 206, 401 – 426.

Grantham, G. H., Macey, P. H., Ingram, B. A., Roberts, M. P., Armstrong, R. A., Hokada, T., Shiraishi, K., Bisnath, A., Manhica, V. 2007. Terrane correlation between Antarctica, Mozambique and Sri Lanka: Comparisons of geochronology, lithology, structure and metamorphism. In COOPER A.K., Raymond, C.R., ISAES Editorial Team. (eds) A Keystone in a Changing World-Online Proceedings of the 10 th international Symposium on Antarctic Earth Sciences. US Geological Society Open File Report, 2007-1047, Extended Abstract 004.

Grantham, G.H., Macey, B.A. Ingram, M.P., Roberts, Armstrong, R.A., Hokada, T., Shiraishi, K., Jackson, C., Bisnath, A., Manhica, V. 2008. Terrane Correlation between Antarctica, Mozambique and Sri Lanka; Comparisons of Geochronology, Lithology, Structure and Metamorphism and possible implications for the geology of southern Africa and Antarctica. In Satish-Kumar, M., Motoyoshi, Y., Osanai, Y., Hiroi, Y.,

Shiraishi, K. (eds) Geodynamic evolution of East Antarctica: a key to the East–West Gondwana connection Geological Society of London Special Publication, 308, 91-120.

Grantham, G.H., Jackson, C., Moyes, A.B., Groenewald, G.H., Harris, P.D., Ferrar, G., Krynauw, J.R. 1995. The tectonothermal evolution of the Kirwanveggen-H.U. Sverdrupfjella areas, Dronning Maud Land, East Antarctica. Precambrian Research, 75, 209-230.

Grew, E.S., Asami, M., Makimoto, H. 1989. Preliminary petrological studies of the metamorphic rocks of the eastern Sør Rondane Mountains, East Antarctica. Proceedings of the NIPR Symposium on Antarctic Geosciences, 3, 100-127.

Grew, E.S., Manton, W.I., Asami, M., Makimoto, H. 1992. Geochronologic data on Proterozoic polymetamorphic rocks of the eastern Sør Rondane Mountains, East Antarctica. In: Yoshida, Y., Kaminuma, K. & Shiraishi, K., (eds) Recent Progress in Antarctic Earth Science, TERRAPUB, Tokyo; 37-44.

Harley, S.L. 1986. A sapphirine-cordierite-garnet-sillimanite granulite from Enderby Land, Antarctica: implications for FMAS petrogenetic grids in

the granulite facies. Contributions to Mineralogy and Petrology. 94, 452–460.

Hoffman, P.F. 1991. Did the breakout of Laurentia turn Gondwanaland inside-out? Science, 252, 1409-1412.

Hokada, T., Adachi, T., Osanai, Y., Nakano, N., Baba, S., Toyoshima, T. 2009. Metamorphic records inferred for the high-grade rocks from Austkampane in the central Sør Rondane Mountains, East Antarctica. Abstracts of Japan Geoscience Union Meeting 2009. G123-017.

Hokada, T., Motoyoshi, Y. 2006. Electron microprobe technique for U-Th-Pb and REE chemistry of monazite, and its implications for pre-, peak- and post-metamorphic events of the Lützow-Holm Complex and the Napier Complex, East Antarctica. Polar Geoscience, 19, 118-151.

Hokada, T. 2001. Feldspar thermometry in ultrahigh-temperature metamorphic rocks: Evidence of crustal metamorphism attaining ~1100°C in the Archean Napier Complex, East Antarctica. American Mineralogist. 86, 932–938.

Holdaway, M.J. 2000. Application of new experimental and garnet Margules data to the garnet-biotite geothermometer. American Mineralogist

85,881-892

Holdaway, M.J., Lee, S.M. 1977. Fe-Mg cordierite stability in high-grade pelitic rocks based on experimental, theoretical, and natural observations. Contributions to Mineralogy and Petrology 63, 175-198

Holland, T., Blundy, J., 1994. Non-ideal interactions in calcic amphiboles and their bearing on amphibole-plagioclase thermometry. Contributions to Mineralogy and Petrology. 116, 433–447.

Ikeda, Y., Shiraishi, K. 1998. Petrogenesis of the tonalitic rocks from the Sør Rondane Mountains, East Antarctica. Polar Geoscience, 11, 143-153.

Ishizuka, H., Asami, M., Grew, E.S., Kojima, S., Makimoto, H., Moriwaki, K.,Osanai, Y., Owada, M., Sakiyama, T., Shiraishi, K., Tainosho, Y., Takahashi, Toyoshima, T.,Y., Tsuchiya, N. 1993. Geological map of Bergersenfjellet, Sør Rondane Mountains, Antarctica. Antarctic Geological Map Series, sheet 33, scale 1 : 100,000. National Institute of Polar Research, Tokyo.

Ishizuka, H., Kojima, H. 1987. A preliminary report on the geology of the central part of the Sør Rondane Mountains, East Antarctica. Proceedings of the NIPR Symposium on Antarctic Geosciences, 1, 113-128.

Ishizuka, H., Suzuki, S., Kojima, H. 1995. Mineral paragenesis of the sapphirine-bearing rock from Austkampane area of the Sør Rondane Mountains, East Antarctica. Proceedings of the NIPR Symposium on Antarctic Geosciences, 8, 65-74

Ishizuka, H., Suzuki, S., Kojima, H. 1996. Meta-ultramafic rock from the Austkampane area of the Sør Rondane Mountains, East Antarctica. Proceedings of the NIPR Symposium on Antarctic Geosciences, 9, 40-48.

Jacobs, J., Bauer, W., Fanning, C.M., 2003. Late Neoproterozoic/Early Paleozoic events in central Dronning Maud Land and significance for the southern extension of the East African Orogen into East Antarctica. Precambrian Research. 126, 27–53.

Jacobs, J., Bingen, B., Thomas, R.J., Bauer, W., Wingate, M.T.D., Feitio, P. 2008. Early Paleozoic orogenic collapse and voluminous late-tectonic magmatism in Dronning Mard Land and Mozambique: insights into the partially delaminated orogenic root of the East African Antarctic Orogen? In Satish-Kumar, M., Motoyoshi, Y., Osanai, Y., Hiroi, Y., Shiraishi, K. (eds) Geodynamic evolution of East Antarctica: a key to the

East–West Gondwana connection Geological Society of London Special Publication, 308, 69-90.

Jacobs, J., Klemd, J. R., Fanning, C.M., Bauer, W., Colombo, F. 2003. Extensional collapse of the Late Neoproterozic-Early Palaeozoic East African-Antarctic Orogen in central Dronning Maud Land, East Antarctica. In: Yoshida, M., Windley, B.F. & Dasgupta, S. (eds). Proterozoic East Gondwana: supercontinent Assembly and Breakup. Geological Society of London Special Publication., 206, 271-287.

Jacobs, J., Thomas, R.J. 2002. The Mozambique Belt from an East Antarctic perspective. In: Gamble, J.A., Skinner, D.N.B. & Henrys, S. (eds) Antarctica at the close of a Millennium. The Royal Society of New Zealand Bulletin, 35, 3-18.

Jacobs, J., Thomas, R.J. 2004. A Himalayan-type indenter-escape tectonic model for the southern part of the Late Neoproterozoic/Early Paleozoic East African-Antarctic Orogen. Geology, 32, 721-724.

Kawasaki, T., Motoyoshi, Y., 2007. Solubility of TiO2 in garnet and orthopyroxene: Ti thermometer for ultra high temperature granulites. In: Cooper, A., Raymond, C. (Eds.), Antarctica: A Keystone in a Changing

World. US Geological Survey Open-File Report 2007-1047; Short Research Paper 038.

Kawasaki, T., Osanai, Y., 2008. Empirical thermometer of TiO2 in quartz for ultrahigh-temperature granulites of East Antarctica. In Satish-Kumar, M., Motoyoshi, Y., Osanai, Y., Hiroi, Y., Shiraishi, K. (Eds.). Geodynamic Evolution of East Antarctica: A Key to the East-West Gondwana Connection. Geological Society, London, Special Publication 308,139–146.

Kleinschrodt, R. 1994. Large-scale thrusting in the lower crustal basement of Sri Lanka. Precambrian Research, 66, 39-57.

Kohn, M.J., Spear, F.S. 1990. Two new geobarometers for garnet amphibolites, with applications to southern Vermont. American Mineralogist 75, 9-96.

Kojima, S., Shiraishi, K., 1986. Note on the geology of the western part of the Sør Rondane Mountains, East Antarctica. Memoir of National Institute of Polar Research, Special Issue 43, 116–131.

Kretz, R., 1983. Symbols for rock-forming minerals. American Mineralogist. 68, 277–279.

Leake, B.E., Woolley, A.R., Arps, C.E.S., Birch, W.D., Gilbert, M.C., Grice, J.D.,

Hawthorne, F.C., Kato, A., Kisch, H.J., Krivovichev, V.G., Linthout, K., Laird, J., Mandarino, J.A., Maresch, W.V., Nickel, E.H., Rock, N.M.S., Schumacher, J.C., Smith, D.C., Stephenson, N.C.N., Ungaretti, L., Whittaker, E.J.W., Youzhi, G., 1997. Nomenclature of amphiboles: Report of the Subcommittee on Amphiboles of the International Mineralogical Association, Commission on New Minerals and Mineral Names. Canadian Mineralogist. 35, 219–246.

Liou, J.G. 1973. Synthesis and Stability Relations of Epidote, Ca2Al2FeSi3O12 (OH). Journal of Petrology, 14, 381-413

Liou, J.G., Kim, H.S., Maruyama, S. 1983. Prehnite-epidote equilibria and their petrologic applications. Journal of Petrology 24, 321-342

Ludwig, K.R. 2001. SQUID 1.00 User's Manual. Berkeley Geochronology Center, Special Publication 2, 17 pp. Berkley, California.

Ludwig, K.R. 2003. Isoplot/Ex 3.0 User's Manual. Berkeley Geochronology Center, Special Publication 4, 55 pp, Berkley, California.

McWilliams, M.O. 1981. Palaeomagnetism and Precambrian tectonic evolution of Gondwana. Precambrian Plate Tectonics, 649-687.

Meert J. G. 2003. A synopsis of events related to the assembly of eastern

Gondwana. Tectonophysics. 362, 1-40.

Member of the Sør Rondane Reconnaissance Party. 1985. Report on the reconnaissance survey of the Sør Rondane Mountains, 1984. Nankyoku Shiryo (Antarctic Research), 82, 46-70 (in Japanese with English abstract).

Michot, J. 1961. Etude petrologique des echantillons preleves dans les monts Sør Rondane, (Antactique). Expedition Antarctique Belge 1957-1958. I. Les roches a caractere intrusive. Ann. Soc. Geol. Belg., 85, B87-99.

Newton, R.C., Perkins, D. 1982. Thermodynamic calibration of geobarometers based on the assemblage garnel-plagioclase-orthopyroxene-(clinopyoxene)-quartz. American Mineralogist. 67, 268-286

Norconsult Consortium. 2007. Mineral resources management capacity building project, Republic of Mozambique, component 2: Geological infrastructure development project, Geological Mapping Lot 1, Report B6.f.

Osanai, Y., Shiraishi, K., Takahashi, Y., Ishizuka, H., Moriwaki, K., Tainosho, Y., Tsuchiya, N., Sakiyama, T., Toyoshima, T., Owada, M., Kojima, H. 1996.

Geological map of Brattnipene, Sør Rondane Mountains, Antarctica. Antarctic Geological Map Series, sheet 34, scale 1 : 100,000. National Institute of Polar Research, Tokyo.

Osanai, Y., Shiraishi, K., Takahashi, Y., Ishizuka, H., Tainosho, Y., Tsuchiya, N., Sakiyama, T., Kodama, S., 1992. Geochemical characteristics of metamorphic rocks from the central Sør Rondane Mountains, East Antarctica. In Yoshida, Y., Kaminuma, K., Shiraishi, K. (Eds.). Recent Progress in Antarctic Earth Science. Terra, Tokyo, 17–27.

Osanai, Y., Toyoshima, T., Baba, S., Hokada, T., Nakano, N., Adachi, T. 2008. Metamorphic evolution of ultramafic complex from the Sør Rondane Mountains, Dronning Maud Land, East Antarctica. Abstracts of the 115 th annual meeting of the Geological Society of Japan, 132.

Osanai, Y., Toyoshima, T., Owada, M., Tsunogae, T., Hokada, T., Crowe, W.A., Kusachi, I., 2001. Ultrahigh temperature sapphirine-osumilite and sapphirine-quartz granulites from Bunt Island in the Napier Complex, East Antarctica-Reconnaissance estimation of P-T evolution. Polar Geoscience. 14, 1–24.

Osanai, Y., Yoshimura, Y., 2002. High-temperature limit of crustal

metamorphism: a perspective of ultra-high temperature metamorphism. Chishitsu News 573, 10–26. (in Japanese)

Owada, M., Osanai, Y., Toyoshima, T., Shiraishi, K. 2008. Metamorphic process of pelitic rocks at the deeper part of continental collision zone, Sør Rondane Mountains, East Antarctica. 2008 Japan Association of Mineralogical Sciences Annual Meeting abstract, 83

Paces, J. B., Miller, J. D. Jr. 1993. Precise U-Pb ages of Duluth Complex and related mafic intrusions, northeastern Minnesota: Geochronological insights to physical, petrogenetic, paleomagnetic, and tectonomagmatic processes associated with the 1.1 Ga Midcontinent Rift System. Journal of Geophysical Research. 98, 13997–14013.

Perchuk, L.L., Lavrent'eva, I.V. 1983. Experimental investigation of exchange equilibria in the system cordierite-garnet-biotite. in Saxena, S.K. (ed) Kinetics and Equilibrium in Mineral Reactions, Springer-Verlag, Berlin pp. 199-239

Picciotto, E., Deutch, S., Pasteels, P. 1964. Isotopic ages from the Sør Rondane Mountains, Dronning Maud Land. In: Adie, R.J. (ed), Antarctic Geology. North-Holland, Amsterdam; 570-578.

Pinna, P., Jourde., G., Calvez, J.Y., Mroz, J.P., Marques, J.M. 1993. The Mozambique Belt in northern Mozambique: Neoproterozoic (1100-850 Ma) crustal growth and tectogenesis, and superimposed Pan-African (800-550 Ma) tectonism. Precambrian Research, 62, 1-59.

Raase, P. 1998. Feldspar thermometry: a valuable tool for deciphering the thermal history of granulite-facies rocks, as illustrated with metapelites from Sri Lanka. Canadian Mineralogist. 36, 67–86.

Rogers, J.J.W., Unrug, R., Sultan, M. 1995. Tectonic assembly of Gondwana. Journal of Geodynamics, 19, 1-34.

Sakiyama, T., Takahashi, Y., Osanai, Y. 1988. Geological and petrological characters of the plutonic rocks in the Lunckeryggen-Brattnipane region, Sør Rondane Mountains, East Antarctica. Proceedings of the NIPR Symposium on Antarctic Geosciences. 2, 85-90.

Seno, K., Ishizuka, H., Motoyoshi, Y., Shiraishi, K. 2002. Quantitative chemical analyses of rocks with X-ray fluorescence analyzer: (3) Rare earth elements. Ant. Rec. 46, 15–33. (in Japanese with English abstract)

Shiraishi, K., Kojima, S. 1987. Basic and intermediate gneisses from the western part of the Sør Rondane Mountains, East Antarctica. Proceedings of the

NIPR Symposium on Antarctic Geosciences. 1, 129-149.

Shiraishi, K., Asami, M., Ishizuka, H., Kojima, H, Kojima, S., Osanai, Y. Sakiyama, T., Takahashi, Y., Yamazaki, M., Yoshikura, S. 1991. Geology and metamorphism of the Sør Rondane Mountains, East Antarctica. In Thomson, M.R.A., Crame, J.A., Thomson, J.W. (eds). Geological Evolution of Antarctica. Cambridge University Press, Cambridge, 77-82.

Shiraishi, K., Dunkley, D.J., Hokada, T., Fanning, C.M., Kagami, H., Hamamoto, T. 2008. Geochronological constraints on the Late Proterozoic to Cambrian crustal evolution of eastern Dronning Maud Land, East Antarctica: a synthesis of SHRIMP U-Pb age and Nd model age data. In Satish-Kumar, M., Motoyoshi, Y., Osanai, Y., Hiroi, Y., Shiraishi, K. (eds) Geodynamic evolution of East Antarctica: a key to the East–West Gondwana connection Geological Society of London Special Publication, 308, 21-67.

Shiraishi, K., Ellis, D., Hiroi, Y., Fanning, C.M., Motoyoshi, Y., Nakai, Y. 1994. Cambrian Orogenic Belt in East Antarctica and Sri Lanka: Implications for Gondwana Assembly. Journal of Geology, 102, 47-65.

Shiraishi, K., Kagami, H., 1992. Sm-Nd and Rb-Sr ages of the metamorphic

rocks from the Sør Rondane Mountains, East Antarctica. In Yoshida, Y., Kaminuma, K., Shiraishi, K. (Eds.), Recent Progress in Antarctic Earth Science. Terra, Tokyo, pp. 29–35.

Shiraishi, K., Kojima, S., 1987. Basic and intermediate gneisses from the western part of the Sør Rondane Mountains, East Antarctica. Proceedings of NIPR Symposium on Antarctic Geoscience 1, 129–149.

Shiraishi, K., Osanai, Y., Ishizuka, H., Asami, M., 1997. Geological Map of the Sør Rondane Mountains, Antarctica. Antarctic Geological Map Series, Sheet 35, scale 1:250 000. National institute of Polar Research, Tokyo.

Shiraishi, K., Osanai, Y., Tainosho, Y.,Takahashi, Y., Tsuchiya, N., Kojima, S., Yanai, K., Moriwaki, K. 1992. Geological map of Widerøefjellet, Sør Rondane Mountains, Antarctica. Antarctic Geological Map Series, sheet 32, scale 1 : 100,000. National Institute of Polar Research, Tokyo.

Shulters, J.C., Bohlen, S.R. 1989. The stability of hercynite and hercynite-gahnite spinels in corundum- or quartz-bearing assemblages. Journal of Petrology 30, 1017-1031

Stacey, J. C., Kramers, J., 1975. Approximation of terrestrial lead isotope evolution by a two-stage model. Earth and Planetary Science Letters,

26, 207–221.

Stern, R.J. 1994. Arc assembly and continental collision in the Neoproterozoic East African Orogen: implications for the consolidation of Gondwanaland. Annual Review of Earth & Planetary Sciences, 22, 319-351.

Tainosho, Y., Takahashi, Y., Arakawa, Y., Osanai, Y., Tsuchiya, N., Sakiyama, T. 1992. Petrochemical character and Rb-Sr isotopic investigation of the granitic rocks from the Sør Rondane Mountains, East Antarctica. In Yoshida, Y., Kaminuma, K., Shiraishi, K., (eds) Recent Progress in Antarctic Earth Science, TERRAPUB, Tokyo, 17-27.

Takahashi, Y., Arakawa, Y., Sakiyama, T., Osanai, Y., Makimoto, H. 1990. Rb-Sr and K-Ar whole rock ages of the plutonic bodies from the Sør Rondane Mountains, East Antarctica. Proceedings of the NIPR Symposium on Antarctic Geosciences, 4, 1-8.

Takigami, Y., Funaki, M. 1991. 40Ar-39Ar and K-Ar ages for igneous and metamorphic rocks from the Sør Rondane Mountains, East Antarctica. Proceedings of NIPR Symposium on Antarctic Geosciences, 5, 122-135.

Taylor, W.R., 1998. An experimental test of some geothermometer and geobarometer formulations for upper mantle peridotites with application to the thermobarometry of fertile lherzolite and garnet websterite. Neues Jahrbuch fur Mineralogie-Abhandlungen 172, 381–408.

Tingey, R.J. 1991. The regional geology of Archaean and Proterozoic rocks in Antarctica. The Geology of Antarctica, 1-73.

Van Autenboer, T. 1964. The geomorphology and glacial geology of the Sør Rondane, Dronning Maud Land. In Adie, R.J. (ed). Antarctic Geology. Amsterdam, North-Holland, 81-103.

Van Autenboer, T. 1969. Geology of the Sør Rondane Mountains. Geologic Maps of Antarctica, ed. by C. Craddock et al., New York, Am. Geogr. Soc., Pl. VIII (Antarct. Map Folio Ser., Folio 12).

Viola, G., Henderson, I., Bingen, B., Feitio, P., Thomas, R.J., Hollick, L., Jacobs, J. 2006. A new tectonic framework for northern Mozambique. In: Abstracts CAG 21, 3-5 July, Maputo, Mozambique, 168.

Wark, D.A., Hildreth, W., Spear, F.S., Cherniak, D.J., Watson, E.B., 2007. Pre-eruption recharge of the Bishop magma system. Geology 35, 235–238.

Wark, D.A., Watson, E.B., 2006. TitaniQ: a titanium-in-quartz geothermometer. Contributions to Mineralogy and Petrology. 152, 743–754.

Wegener, A. 1966. The Origin of Continents and Oceans. Dover Publications.

Wells, P.R.A., 1977. Pyroxene thermometry in simple and complex systems. Contributions to Mineralogy and Petrology. 62, 129–139.

Yoshida, M. 1995. Assembly of East Gondwanaland during the Mesoproterozoic and its rejuvenation during the Pan-African period India and Antarctica during the Precambrian, 34, 22-45.

Zhang, R.Y., Zhai, S.M., Fei, Y.W., Liou, J.G., 2003. Titanium solubility in coexisting garnet and clinopyroxene at very high pressure: the significance of exsolved rutile in garnet. Earth and Planetary Science Letters. 216, 591–601.

Appendix. Mineral parageneses in the central Sør Rondane Mountains

◎:abundant ○:common △:poor ×:rare ():inc/symp

	Major Minerals												Minor Minerals							Rock type
sample No.	Qtz	Pl	Kfs	Hbl	Bt	Grt	Opx	Cpx	Als	Spl	Ms	etc	Opq	Ap	Zrn	Ttn	Mnz	Gr	etc	
07120201A	○exs	○		○	○									○	○	○			Aln ×	intermediate
07120201B		○		○	△			○						△						mafic
07120201C1	△	○		○	○								×	○						intermediate
07120201C2	○exs	○		○								Ep × Chl △	△	○	△					mafic
07120402A	○	○	△		○	○			○Sil	(×)Grt			△	△	○		○		Rt △	pelitic
07120402B		○		○	△							Ep ×	△	○		△				mafic
07120402C		○		○	△	○						Cc △	△	○exs						mafic
07120403A1	○exs	○	△	○	○			×					△	○exs	△	○				intermediate
07120404A1	○	○	○	△	○								△	○	○				Aln △	felsic
07120901A	○exs	○		○	△			×			×	Chl ×	△	○	×	×				felsic
07120901B		○		◎		○		○					○	○	△					calc
07120902A	○	○		○	○			△			×		○	○exs	△					felsic
07120902B		○		○	△		○	△					○	△	×					mafic
07120903A	×	○		△			○	○					○	○						mafic
07120903B	×	○		○	×	○	(×)Hbl	○					○	○						mafic
07120903C		○			×								△	×		○				mafic
07120903D	○exs	○	◎	◎	○								△	○	○	○			Aln ×	felsic
07121001A	△	○		○		△	○	△					△	△	×					felsic
07121001B		○		◎	△		△						×	×	○					mafic
07121001C	○	○		△	△		Pseudo	P					△	○	△					felsic
07121001D	×	○		○	×	△exs	(×)Hbl						×	○	○					mafic
07121001F1	○	○		○	△		○							○exs	○					felsic
07121001F2	○			△	○	○	Pseudo						○	×	×					psam
07121001H	○exs	○	○	△	△								×	○	×					felsic
07121002A	△	○		○	△		○	○					○	○	○					felsic
07121003A	○	○		△	×		○	△					○	○exs	○					felsic
07121003B	○exs	○		○	○							Ep △	△	○	△	△	△			felsic
07121003C	○	○		○	○		△							○exs						mafic
07121004A	○	○		△	△		○						○	○exs	○					felsic
07121004B	△	○		○			△	○						○						mafic
A07122602E	×	○			○	○exs	○			(×)Mag			○	○exs	○					felsic
A07122602F	×	◎			◎	◎exs				(×)Grt			○	○			○			pelitic
A07123001B		○		○	△	◎	○			×			○	○exs						mafic
A07123001E	×	◎			△	△	○exs			(×)			○	○exs						felsic
A07123001E		◎							○ Sil	(×)Sil	△	Crn △	○							aluminous
A07123001F	△	○		×	○	○exs	△						○	○exs	○		○			felsic
A07123001I		○		△		◎	○	△		(×)Grt			○	○						mafic
A07123001L	△	○		◎	×		○						△	○exs						mafic
A07123001N		○		○			○	○		(×)Mag			○	○						mafic
A07123001P		○	○		○	○			△Sil	(×)Mag		Crn △	○		×		×			pelitic
A07123001R	○	○			△	○	○			(×)			○	△						felsic
A07123001AC	○	○		○	○								○	○						intermediate
A07123001AF	○	○	○		○	△					×	Chl ×	△		△		△			felsic
A08010401A	○	○	△	△	○							Ep		△	×	○				intermediate
A08010401B	△	○		○	○								(△)Ttn	◎		○				mafic
A08010401D	○	○	△	○	△									○	△	○				intermediate
A08010401E	△	○		◎	○								(○)Ttn	○		○				mafic
A08010401F	○	○		○	○								(○)Ttn	○	△	○				mafic
A08010402A		○		○	○	○	○	○					○	◎						mafic
A08010402B	○	○		○	○	△							○	◎		△				mafic
A08010402C	△exs	○		◎	○	○							○	◎						mafic
A08010402D	△	○		○	△	○		○					○	◎						mafic
A08010402E	△	○		○	○	○exs						Ep	○	◎		×				mafic
A08010402F	○	○		○	○	○						Ep	○	◎		△				mafic
A08010402G	○	○		○	○	○		○					○	◎						mafic
A08010402I	○	○	△		△								○	◎		◎				felsic
A08010402J	○exs	○			○	○exs			△Sil				○	○	○		○		Rt	pelitic
A08010402K	○exs	△			○	○exs						Chl	○	×	○		◎		Rt	pelitic
A08010402L		○		○	△	○	○symp						○	△	△		△		Rt	mafic
A08010402M	○	○		○	×	△		△					○	○	△	○	△		(Rt)	mafic
A08010402N	△	○		○	○	○							○	○		×	○			mafic
A08010402O	○	○	○	×	○	△						Ep ×	△	○			○		Aln △	felsic
A08010402P	○	◎		○	△							Ep ×	×	○		○			Rt ×	felsic
A08010402Q		○		○	○							Ep ×		×		△				intermediate
A08010402U	○	△	◎	(×)	(×)						×		△	×	×					felsic
A08010402V	○	○	○	○	○								△	○		○			Aln ×	felsic
AC07121302A	○exs				○	○exs			○Sil/And				○	○	△	△	○			pelitic
AC07121302B	○exs	○			○	○exs			○Sil	(×)	×		○	△	△		○			pelitic
AC07121302C	○exs	○	◎		○						△		×		×		○			felsic
AC07121302D	○exs	△			○	○exs							○	○	△				Rt ×	
AC07121302E	◎exs	△			○	○exs	Pseudo						○	○	△		△			pelitic
AC07121302F	◎exs	○			○	○exs					×		○	○	○		○			pelitic
AC07121302G	○	○		○Oam	○	○exs	Pseudo				△	Crd ○	○	○	○					pelitic
AC07121302H	○	○			○						×		△	○	△		○			pelitic
AC07121303A	○exs	○			○	○exs			○Sil		△	Crd ○	○	○	○			△	Rt ×	pelitic
AC07121303B	○exs	○			○	○exs						Crd △	○	×	○		△	△		pelitic
AC07121303C	○exs	○			○	○exs					×	Crd △	○	×	○		○	△		pelitic
AC07121303D	○				◎	○exs			◎Sil			Crd △	○		○			△	Rt ×	pelitic
AC07121303E		△			○	○exs			◎Sil			Crd ○	○		○					pelitic
AC07121303F	◎exs				○				○Sil			Crd ×	×		○			×	Rt ×	psam
AC07121303G	○	○			○	×					×		×		△					felsic
AC07121303G		○		○exs	○	○	Pseudo						○	△						mafic
AC07121303H		○		○OamHb	×		△exs	△					○	△						mafic
AC07121402C		○		◎	○	◎	Pseudo						◎	△	△					mafic
AC07121501I		△			◎	○				(×)			○	◎	△		△			micaceous
AC07121501J		△		◎exs	○	○							○	○						mafic
AC07121501K		○		◎	×	○	Pseudo			(△)			○	○						mafic
AC07121701A	○exs	○exs			○	○exs			○Sil		△		○	×	△		△			pelitic
AC07121701B	△exs	○			○	△exs			○Sil	(×)Sil		Crd	○	×	△		○			pelitic
AC07121701C	○exs	◎			◎	○exs						Crd ×	○	○	△		○			pelitic
AC07121701C	○exs	◎			◎	○exs				(×)		Crd △	○	○	△		○			pelitic
AC07121701C	○exs	○			○	○exs			○Sil		○	Chl △	○	×	○		○			pelitic
AC07121701D	○exs	○			○	○exs						Chl ×	○	×	△		○		Rt ×	psam
AC07121701E	◎exs	△exs			○	○exs							△	×	△		△			psam
AC07121701F	×exs	○			○	○exs			○Sil	(×)Grt,Sil			△	×	○		○			pelitic
AC07121701G	△	△			◎	○exs							○	○	△		△			pelitic

Appendix. Continued

◎:abundant ○:common △:poor ×:rare ():inc/symp

	Major Minerals												Minor Minerals							Rock type
sample No.	Qtz	Pl	Kfs	Hbl	Bt	Grt	Opx	Cpx	Als	Spl	Ms	etc	Opq	Ap	Zrn	Ttn	Mnz	Gr	etc	
AC07121701I	◎exs	△			○	△exs			○Sil		△		△	×	△		○			pelitic
AC07121701J		○		◎oam	○	△	Pseudo						○	○	△					mafic
AC07121701K	◎	○		○OamHb	△	○	Pseudo	×					○	○	○				Rt×	psam
AC07121701L	○	○		○Oam	○	○	○						×	○	○					mafic
AC07121701M		○		○OamHb	○								○	○						mafic
AC07121701N	○	◎		○Oam	○		△						△	○						mafic
AC07121701O	△	◎		△Oam	○		○exs						○	○						mafic
AC07121701P		○		△Oam	○		○exs						○	○					Rt×	mafic
AC07121701Q	×	○		◎	×								△	△						mafic
AC07121702A	○exs	○	○		○	○exs			○Sil/And	(×)Grt	△		○	×	○		◎			pelitic
AC07121702B	○exs	○	○		○	○exs			(×)Grt,Sil	(○)Pl,Grt		Crn	△	×	×		○			pelitic
AC07121702C	○	○	○		○	△exs					△		×	×	○		○			felsic
AC07121702D	○	○	△		○	○exs			○Sil	(×)Sil	△		△	×	△		○			pelitic
AC07121702E	◎exs		△			×					○		△	×	×					psam
AC07121702F	○exs				○	△exs			○Sil	(×)Grt,Sil	○		○	×	△		○			pelitic
AC07121702G		○		○	○		Pseudo						○	○	○					mafic
AC07121702H		○		○			Pseudo						○	○	○					mafic
AC07121702I	○	○	○		△	×							○	○	○					felsic
AC07121702J	○		○	○	◎	○							○	○	×	×				mafic
AC07121702K	○	○			○	○exs				(×)Grt	×		○	○	○		○			felsic
AC07121702L	○	○	○		△	○exs							○	○	△					felsic
AC07121702M	○	○	○		△						×		○	○	△					felsic
AC07121801A	○	△			○	○exs			○Sil					○	○		△			pelitic
AC07121801B	○	△			○				○Sil		○			○	○					pelitic
AC07121801C	○exs	○pth	○exs		○	○exs			○Sil				○	○	○				Rt×	pelitic
AC07121801D	○exs				○green	○			○Sil,Fib		○		△		○				Rt△	pelitic
AC07121801E																				
AC07121801F	○exs				○	○exs			△Sil	△(Grt)	○	○Crd	○		○		○			pelitic
AC07121801G	○exs				△	△exs						◎Tur △Chl				×	○	○		TurQtz rock
AC07121801H	△exs				○	○exs			○Sil	×(×)		○Crd	○		○		○		Rt(×)	pelitic
AC07121801I																				
AC07121801J	○				◎	△(Bt)			○Sil			△Crd	×							pelitic
AC07121801K																				
AC07121801L	○exs	△symp			◎	○exs						○Crd	○				○			
AC07121801M	△			△	○	◎exs						◎Crd	○		○		◎		Rt(×)	pelitic
AC07121801M				△	○	◎exs						◎Crd	○		○		◎		(Rt)	MgAl
AC07121801N	○exs	○			○	○exs			△Fib			○Crd	○		○		○		Rt×	pelitic
AC07121801O	○				○	△			○Sil	×(Grt)		○Crd	△		○					pelitic
AC07121801P	○exs	○			○				△Fib					○			○			pelitic
AC07121801Q		○		○brown	△								△							
AC07121801R		○		○brown	○										△					
AC07121801S	○	△	△		○				○Sil		△		△	△	○				Rt(×)	pelitic
AC07121801T	○exs				○	△exs			○Sil,Fib				×	×					Rt×	pelitic
AC07121801U	○exs				○	△			○Fib				×		○					pelitic
AC07121901A	◎	◎	△	△	△							Ep	×	○	○					felsic
AC07121901B	○	○		○	△									×	×	△				intermediate
AC08011301M	◎exs	○			○	○exs							△		○				Rt ○	psam
AC08011302A	○	○			◎	○				(×)	×		△		○					pelitic
AC08011302H		○		○		○	○	○					○	△	△					mafic
AC08011501A	○	○		×	○						×	Ep ×	△	△	○	○	△			felsic
AC08011501E	○	○		◎	○							Ep ×	×	×		○			Aln ×	intermediate
AC08011501G		○		◎	○								△	○		◎				mafic
AC080115T01A	◎	△			○	○						Chl	×	×	○					psam
AC080115T01B	◎	○		○	○	○							○	○	○					intermediate
AC08011601A	◎	○	△		◎								○	△	○					felsic
AC08011601B	○	○		◎	○							Ep ×	(×)Ttn	△		○				intermediate
AC08011601G				◎Act									○							Actrock
AC08011602H	◎	○			○	○			○				△	△	△				Rt	pelitic
AC08012001A1	○exs	○pth		○agg	○	○					△	Cc	△	○	○					felsic
AC08012001A2	○exs	○pth		○brown	○						△		△	○	○	△	○		Aln	felsic
AC08012001B		○		○	○		○	○					×	○		○				mafic
AC08012001C	○	○	○	○	○	△							○	○		○			Aln	intermediate
AC08012001D		○zone		○		○symp	○Pig	○					△(symp)			○				mafic
AC08012001E	○exs	○pth			○								×	△		○				felsic
AC08012001F	○	△	○		△	△							△							pegmatite
B07121705C																				
B08012001A	○	◎		×	◎							Ep ○	×	○exs	△		○		Aln(△	intermediate
B08012001B	○	○	△		△						△		×		×		×			felsic
B08012001C	○	○	○		△						×		△		×					felsic
B08012002A		○		◎		○						LowCaAmp	△	○						mafic
B08012003C	○	○	○		△						×		△	○	△	○			Aln ×	felsic
B08012101A	(○)	○exs	○	○	○			(△)P					△	○		×	○			felsic
B08012101B	○	○	○		○									◎		○			Aln ×	felsic
B08012101C	○	○	○		○						×	Cc ×	△	○		○			Aln ○	felsic
B08012102A	○exs	○		○	○			×					○	○	△					intermediate
B08012102C	△exs	△		◎	△			○				Cc △								mafic
B08012102G	○	○	○		○						△		○	○	×					felsic
B08012104A	△	○		○	○			P					○	○	○	×				intermediate
B08012104B	○	○exs	○	(△)symp	○								△	○	○				Aln △	intermediate
B08012104C	△	○exs		○	○			(△)			△		○	◎						intermediate
B08012104F				◎	○									△	△					mafic
B08012105A	○	○			○						Cc △		△	○		○				shale
B08012105A	○exs	○	○	○	○			×					○	○	○	○				felsic
B08012105C		○		◎	△			P					○	○						mafic
B08012105C		○		◎	○			P					○	○		×				mafic
B08012105D	○	◎			○	○							○	○exs	△		○			psam
B08012105D	○	○	○		○	○								○exs	○	×				felsic
B08012105E	○	○	△		○	○							△	○exs	△		○			pelitic
B08012105E	○	○	○		○	○							○	○	○					pelitic
B08012106A	○	○		○	○			△					△	○exs	○					pelitic
B08012106B	○	○	○	△	○		○	△					△	○	○					pelitic
B08012106C	○	○	○		○		○	○					○	○	○					felsic
B08012106C	○	○	○		○		×	×						○	○	○				felsic
B08012106D	○	○			○	○								○	○		○			pelitic
B08012106E	○	○	○	△	△	○		△				Cc ×	△	○	○					felsic
B08012106F		○		○	○		○						○	○	○					pelitic

Appendix. Continued

◎:abundant ○:common △:poor ×:rare ():inc/symp

	Major Minerals												Minor Minerals							Rock type
sample No.	Qtz	Pl	Kfs	Hbl	Bt	Grt	Opx	Cpx	Als	Spl	Ms	etc	Opq	Ap	Zrn	Ttn	Mnz	Gr	etc	
B08012201A	○	○		○	○							Ep △	○	○	×	△			Aln (×	intermediate
B08012201G	△	○		○	×	○							△	×	×					mafic
B08012201H	○	◎		◎	○									×	△					mafic
B08012201I	○	◎		○	○	○							◎	○	△					intermediate
B08012202A		○		◎	○								×	×						mafic
B08012202C	○	○	○		○						×	Ep ×	○	△					Aln ○	felsic
B08012202D	×	○		○								Ep △	×	○						intermediate
B08012203A	◎	◎			○	×					×		○	△	×					psam
B08012204	○	○		○	△	○						Ep △	○	○	×					intermediate
B08012302A	○	○		○								Ep △	○	○		○				intermediate
B08012302E		○			○			×				Ep ×		○		○			Aln ×	mafic
B08012304B		○		◎	△								○	×						mafic
B08012304C	◎	○		×	○	△						Ep △	○	○		△			Aln ×	felsic
B08012304D	○	○		○	△	×								△						intermediate
B08012304E	○	○		△	△	△								○						felsic
B08012304F	○	○		○	○	△							△	○					Aln ×	intermediate
B08012305C	◎	○	○		○	△					×	Ep ×	△	△	○				Aln ×	intermediate
B08012305D	○	○		○	○							Ep ○	△	△	△					intermediate
B08012305F	△	○		◎	×							Ep ×		×						mafic
B08012401A	○	○	○	△	△						×		△	○	○	○				felsic
B08012401A	○	○	○	×	×									○	○	○				felsic
B08012401B	○	○	○		○								×	○	○	○			Aln △	felsic
B08012401B	○	○	△		○								×	○		○			Aln △	felsic
B08012401C	○	○		○	○							Ep △	△	○	○	○				felsic
B08012401D	○	○		○	○								△	○	○	○				mafic
B08012401D	○	○		○	○							Ep ×	△	○	○				Aln △	felsic
B08012401E	○	○		○	○							Ep ○	○	○	△	○				intermediate
B08012401E	○	○		○								Ep ○		○	○	◎			Aln △	mafic
B08012401F		○		○	△								×	○exs	×					mafic
B08012401G	△	○		◎	△								×	×						mafic
B08012401G	△	○		○	△								○	○	△	△				mafic
B08012401H	○	○		○	○							Ep ×	△	○					Aln ×	felsic
B08012401I	○	○			○	△					×	Chl		○	○					psam
B08012401I	○	○	△		○	△					△	Cc △		○	○				Aln △	felsic
B08012401J	○	○		○	○	○						Chl △ (St)grt	○	○	△					felsic
B08012402C	△	◎		△				◎						○		○				calc
B08012402D		△		◎	○							Cc×		×						mafic
B08012402D	△	○		◎	△			○				Cc×		○		×				calc
B08012402E	○exs	○		○retro	○			○					×	△	×	×				calc
B08012402F	○		×		◎							Crd ○			○					pelitic
B08012402G		△			◎							Crd ○ Crn(△)			○				Rt ×	aluminous
B08012402G	×	○exs			◎				△And/Sil		△				○				Rt ×	pelitic
BC07122801A	○exs	○mylm			○	○exs					△		○		○	○	○			pelitic
BC07122801B	○exs	○exs	○	×	○symp	○exs			(△)Pl		○		○		△		○			pelitic
BC07122801C	○exs	○exs	○		○symp	○exs			(△)Pl		△	Chl△	○		○		○			pelitic
BC07122801C2	○	○pth	○		○symp	×P			△		△		×		○		○		Rt ×	pelitic
BC07122801D	○	○pth	△		○symp	○exs			△Sil	(×)Grt	△		○		○		○			pelitic
BC07122801E	○exs	○			○						○				△					felsic
BC07122801F		○		○exs	○			○					○	○						mafic
BC07122802A	○	○mylm	○		○2type	○exs					△				○		○			pelitic
BC07122802C		○		○exs	○		○ ?						×							mafic
BC07122804A	○	○			○	○exs			○Sil	(×)Grt	○		○		○		○			pelitic
BC07122805B	○	○	△		○	○								○	○					felsic
BC07122805C	○	○	△		○	○					×		○	○	○		○			felsic
BC07122805D	○	○	○	○agg	○symp	○							×	○	○		○			intermediate
BC07122901A	○	○	○	×	○									○	○					felsic
BC07122901B	○	○	○	○	○									○	◎	○				felsic
BC07122901C	○	○		○	○								△	○		○				intermediate
BC07122901D	○	○		○zone	○								○	○exs	○					intermediate
BC07122901E	○	○	○		△	△zone									×					felsic
BC07122902A																				marble
BC07122902D																				
BC07122902J	○		○		○								△	○	○	○				felsic
BC07122902K	○	○		○zone	○			○						○	○	○				intermediate
BC07122903A1	○	○			○	(×)qtz					△		×	○	○					felsic
BC07122903A2	○exs	○	○		○2type	(×)bt,exs					○		×	△	○		○			pelitic
BC07122903B	○	○pth	○		○						×			○	○		◎			pelitic
BC07122903C	○	○		○	○								○	○	△	○				intermediate
BC07122903D	○	○		○	○									○		○				intermediate
BC07122903E	○	○exs,pt	○	○agg	○symp	×Pseudo							○	○						intermediate
BC07122903F	○	○		○	○									○						mafic
BC07122903G	○exs	○	○		○								○	△	○				Rt ×	felsic
BC071229T01	○	○	○		○2type	×Pseudo								○	○		△			psammitic
BC08010302A2	○exs	○			○	△exs				(×)	△		○		△		△		Rt ×	psam
BC08010302B	△exs	○			◎	○			○Sil	△		Crn △	○		△				Rt ×	pelitic
BC08010302C	△exs	△	×		○	○exs			○And/Sil	(×)		Sid ×	○		△					pelitic
BC08010302I	○	○	○		△								△	○	△		○			felsic
BC08010302J	○	○	○		○	○				(×)	×		(×)	△	△					pelitic
BC08010401A	○	○			○	○exs			○Sil		△		△	○	○		○		Rt ×	pelitic
BC08010401B	○	○			○	○exs			○Sil				△	○	○				Rt ×	pelitic
BC08010401C	○	○			○	○			○Sil				○	○	○		○			pelitic
BC08010401K	○exs	○	○		△	△					△		×	△	△					felsic
BC08010501A	○	○	○	△	△							Cc × Ep △	○	○	×	○				felsic
BC08010501B	○exs	○	○	○								Ep ○	○	○		×			Aln ○	felsic
BC08010501C	○	○	○	○	○							Ep ×	○	○		◎				mafic
BC08010501D	○	○	○		△						×		○	○	△	○				felsic
BC08010502A	○	○			○	×							×	○	○	△				felsic
BC08010502B	○	○	○		○	△							△	○	○	×				psam
BC08010503A	○	○	△		○						×		○	○	○	○			Aln △	felsic
BC08010503B	△	○		○	○							Ep ×	○	○		○				mafic
BC08010504A	○	○	△	○	○							Ep ○	○	○	△	○			Aln △	felsic
BC08010504B	○	○		○	○							Ep ○	△	○	△	○				mafic
BC08010505A	○	○	△	○	○								△	○	△	○			Aln ×	intermediate
BC08010505D	○	○	○	○	○	△								○	△	○			Aln △	psam
BC08010601A	○	○		○	○	△					△	Ep/Zo △	△	○	○					felsic
BC08010601B	◎	○		△	△	×					△	Ep, Chl △	△	△	△					felsic

Appendix. Continued

	◎:abundant ○:common △:poor ×:rare ():inc/symp																			
	Major Minerals												Minor Minerals							Rock type
sample No.	Qtz	Pl	Kfs	Hbl	Bt	Grt	Opx	Cpx	Als	Spl	Ms	etc	Opq	Ap	Zrn	Ttn	Mnz	Gr	etc	
BC08010602B				◎								Ep ○	△							mafic
BC08010602C	△			◎	△							Ep △	×							mafic
BC08010602J	○	○			○	△						Ep △	△	○	○					psam
BC08010604A	○exs	○		△	○	△						Ep ×	△	△	△					psam
BC08010604D	○	○exs		△	△	○						Ep ×	○	×	×					psam
BC08010604E	○exs	○		○	○	○							○	△	△					felsic
BC08010604F	△	△		◎	○															felsic

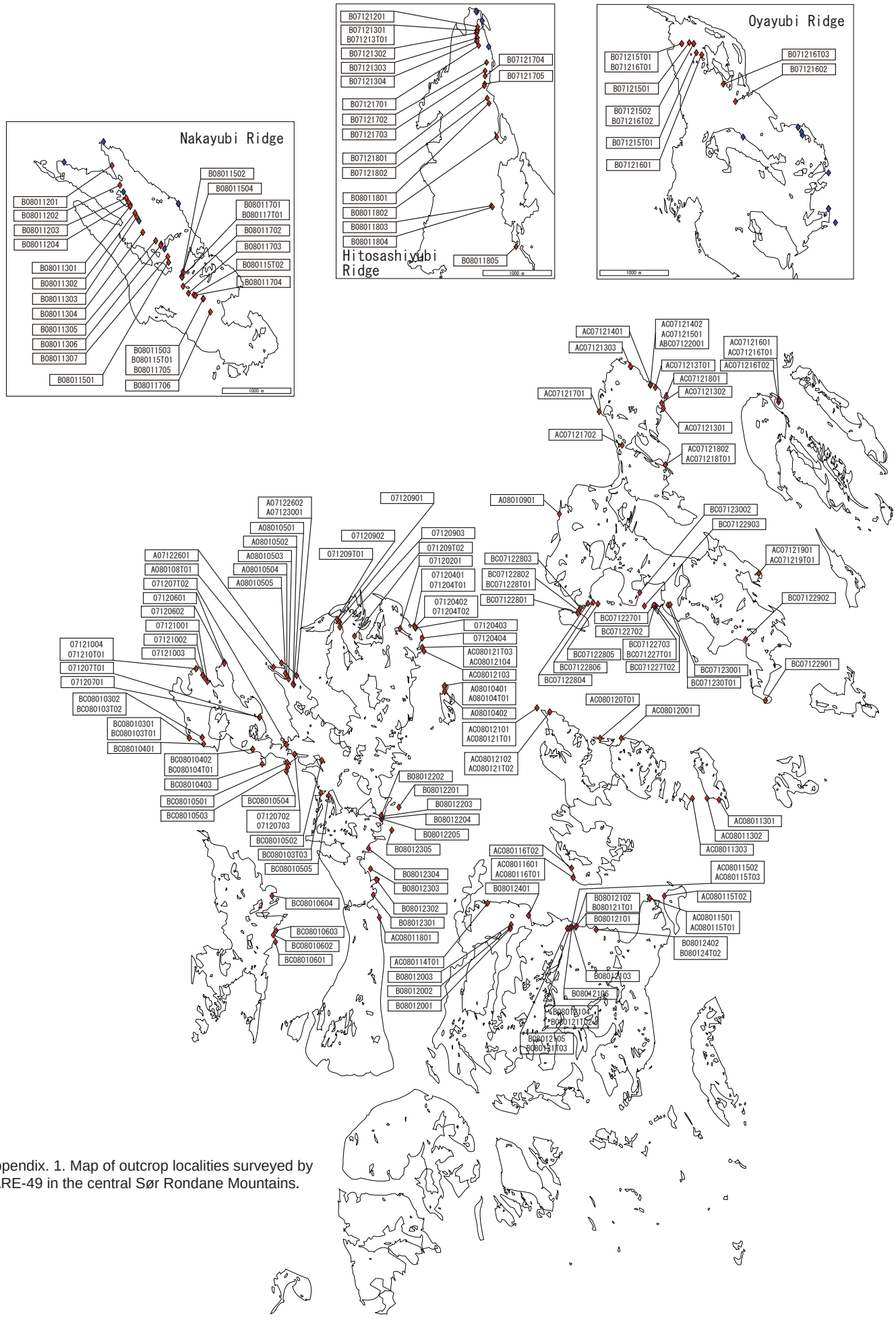

Appendix. 1. Map of outcrop localities surveyed by JARE-49 in the central Sør Rondane Mountains.

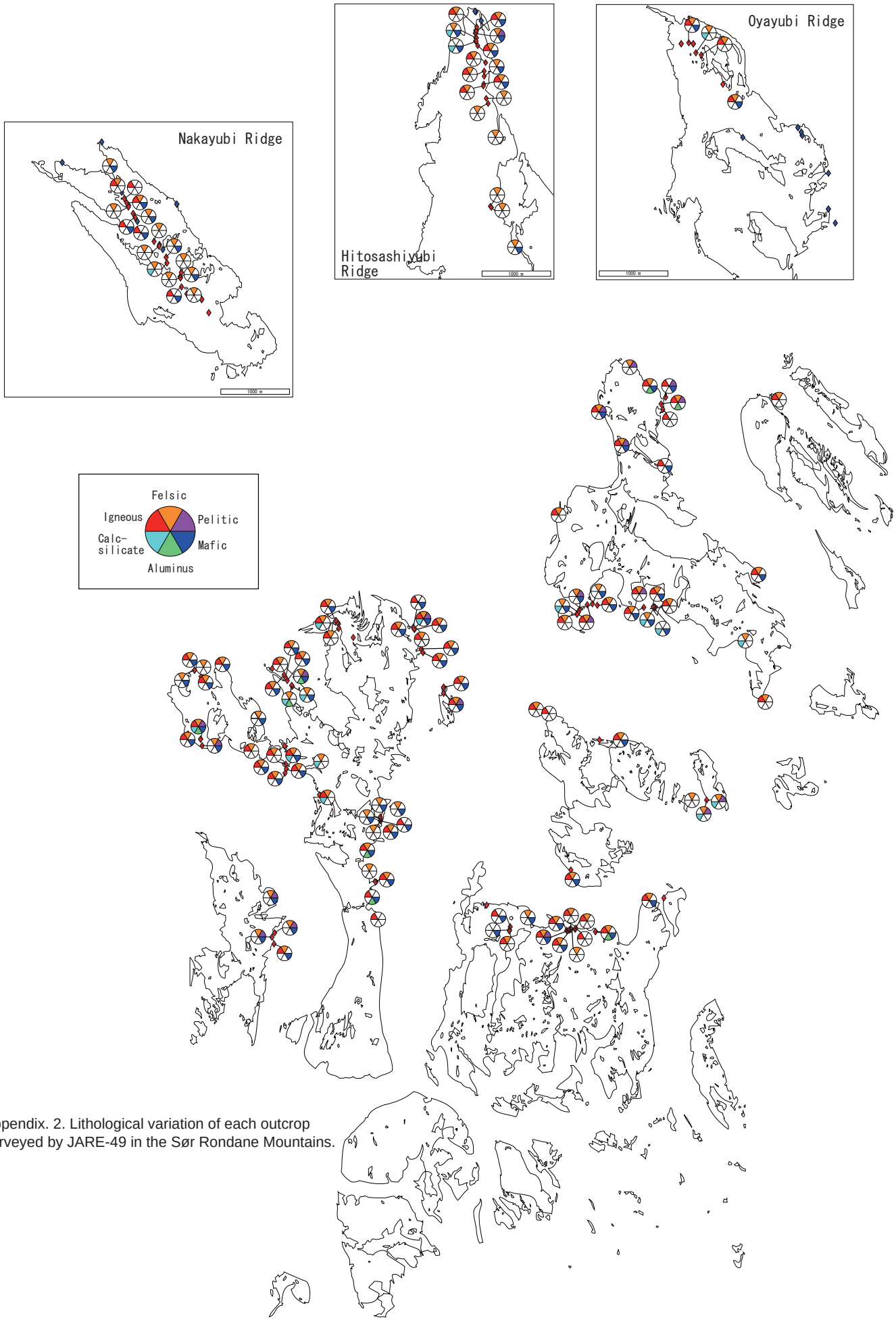

Appendix. 2. Lithological variation of each outcrop surveyed by JARE-49 in the Sør Rondane Mountains.